Alma Mater Studiorum – Università di Bologna

DOTTORATO DI RICERCA IN

Scienze e Biotecnologie degli Alimenti

Ciclo XXV

Settore Concorsuale di afferenza: 07/F1

Settore Scientifico disciplinare. AGR/15

PHYSIOLOGICAL AND STRUCTURAL ASPECTS OF FRUIT AND VEGETABLE MILD PROCESSING

Presentata da: Valentina Panarese

Coordinatore Dottorato **Relatore**

Prof. Claudio Cavani **Dr. Pietro Rocculi**

Esame finale anno 2013

DIPARTIMENTO DI SCIENZE E TECNOLOGIE AGRO-ALIMENTARI

Giudizio di ammissione all'esame finale per il titolo di Dottore di Ricerca in Scienze e Biotecnologie degli Alimenti

Dott.ssa Valentina PANARESE

La Dottoranda ha concentrato parte del lavoro di ricerca sullo studio di due tecniche impiegate nel settore della trasformazione alimentare. Inoltre ha applicato e sviluppato tecniche di analisi finalizzate alla valutazione delle principali modificazioni strutturali, chimico-fisiche e metaboliche a carico di tessuti vegetali assoggettati a tali trattamenti. Le tecnologie studiate sono state:

- Trattamenti di disidratazione osmotica su differenti specie di kiwifruit (*Actinidia deliciosa*) a diversi stati di maturazione mediante soluzioni osmotiche a diverse temperature. In particolare sono stati studiati sui tessuti vegetali i fenomeni di trasporto di massa ed i cambiamenti strutturali, dello stato dell'acqua e dei compartimenti cellulari (Tylewicz *et al*., 2011; Dalla Rosa *et al*., 2011; Panarese *et al.*, 2012 *a*; Panarese *et al.*, 2012 *b*; Santagapita *et al.*, 2012);
- Trattamenti di impregnazione sottovuoto mediante diverse soluzioni zuccherine su materie prime a differente porosità (mela e spinacio). In particolare sono stati studiati i fenomeni di trasporto di massa (Panarese *et al.*, 2013) e gli effetti metabolici (Panarese *et al.*, *manuscript*) a carico dei tessuti vegetali.

Lo studio si è basato sull'applicazione di un approccio multianalitico, all'interno del quale misurazioni di tipo macro- (risonanza magnetica nucleare), micro- (microscopia ottica) ed ultrastrutturali (microscopia elettronica a trasmissione) sono state affiancate ad analisi di *texture* e di calorimetria a scansione differenziale. A seguito di individuali trattamenti di disidratazione osmotica o di impregnazione sottovuoto sono stati valutati i principali effetti sui tessuti vegetali riguardanti le interazioni aria-liquido in reali condizioni, lo stato dell'acqua del tessuto ed i compartimenti cellulari. Misurazioni di calorimetria in isoterma parallele a valutazioni dell'attività respiratoria e fotosintetica hanno permesso un'indagine dei cambiamenti metabolici a seguito dell'applicazione dei processi tecnologici.

La Dottoranda ha trascorso un periodo di 8 mesi in Svezia, presso il *Department of Food Technology, Engineering and Nutrition* dell'Università di Lund dove sono stati approfonditi i temi delle tecniche di impregnazione e della valutazione metabolica dei tessuti vegetali.

La candidata ha partecipato a congressi nazionali ed esteri e ad eventi di divulgazione e promozione della ricerca, presentando poster, comunicazioni orali e progetti sui temi trattati nel corso di Dottorato.

La Dottoranda ha svolto attività di correlazione di una tesi triennale e di una tesi specialistica.

Il Collegio dei Docenti unanime ritiene la Dott.ssa Valentina Panarese idonea a sostenere l'esame finale per il conseguimento del titolo di Dottore di Ricerca in Scienze e Biotecnologie degli Alimenti.

Cesena, 15 Febbraio 2013

Il Coordinatore del Dottorato di Ricerca
in Scienze e Biotecnologie degli Alimenti

DIPARTIMENTO DI SCIENZE E TECNOLOGIE AGRO-ALIMENTARI

Assessment for admission to the final examination
for the degree of PhD in Food and Biotechnology Science

Dr. Valentina PANARESE

The Ph.D. student investigated two innovative food processing technologies currently used in the food sector. Furthermore, analytical and sensory techniques have been developed in order to evaluate the principal structural, physico-chemical and metabolic changes of plant tissues upon the application of technological processes. The studied technologies were:

- Osmotic dehydration treatments on different kiwifruit species (*Actinidia deliciosa*) at different ripening stages by means of osmotic solutions at different temperature. The transport phenomena and the structural changes, the effects on water state and cellular compartments and the metabolic consequences have been studied on the vegetable tissues (Tylewicz *et al*., 2011; Dalla Rosa *et al*., 2011; Panarese *et al.*, 2012 *a*; Panarese *et al.*, 2012 *b*; Santagapita *et al.*, 2012);
- Vacuum impregnation treatments by means of different sugar solutions on raw materials with different porosity (apple and spinach). The mass transfer phenomena (Panarese *et al.*, 2013) and the metabolic effects (Panarese *et al.*, *manuscript*) have been studied on the vegetable tissues.

The study has been carried out by following a multianalytical approach. Macro (low-frequency nuclear magnetic resonance), micro (light microscopy) and ultrastructural (transmission electron microscopy) measurements combined with textural and differential scanning calorimetry analysis allowed evaluating the effects of individual osmotic dehydration or vacuum impregnation processes on the interaction between air and liquid in real plant tissues, the plant tissue water state and the cell compartments. Isothermal calorimetry, respiration and photosynthesis determinations led to investigate the metabolic changes upon the application of osmotic dehydration or vacuum impregnation.

The Ph.D. student spent about 8 months in Sweden at the Department of Food Technology, Engineering and Nutrition of Lund University, where impregnation techniques and metabolic measurements have been studied.

The candidate participated to national and international congresses (presenting posters and oral communications) and to dissemination events involving the topics treated during the Ph.D. project.

The Ph.D. student has been co-tutor of Bachelor of Science and Master of Science theses.

The Board unanimously agrees that Dr. Valentina Panarese is qualified to sit the final exam for the doctorate degree in Food and Biotechnology Science.

Cesena, February 15th 2013

Coordinator of PhD Course
in Food and Biotechnology Science

Abstract

Over the past years fruit and vegetable industry has become interested in the application of both osmotic dehydration and vacuum impregnation as mild technologies because of their low temperature and energy requirements.

Osmotic dehydration is a partial dewatering process by immersion of cellular tissue in hypertonic solution. The diffusion of water from the vegetable tissue to the solution is usually accompanied by the simultaneous solutes counter-diffusion into the tissue.

Vacuum impregnation is a unit operation in which porous products are immersed in a solution and subjected to a two-steps pressure change. The first step (vacuum increase) consists of the reduction of the pressure in a solid-liquid system and the gas in the product pores is expanded, partially flowing out. When the atmospheric pressure is restored (second step), the residual gas in the pores compresses and the external liquid flows into the pores. This unit operation allows introducing specific solutes in the tissue, *e.g.* antioxidants, pH regulators, preservatives, cryoprotectancts.

Fruit and vegetable interact dynamically with the environment and the present study attempts to enhance our understanding on the structural, physico-chemical and metabolic changes of plant tissues upon the application of technological processes (osmotic dehydration and vacuum impregnation), by following a multianalytical approach. Macro (low-frequency nuclear magnetic resonance), micro (light microscopy) and ultrastructural (transmission electron microscopy) measurements combined with textural and differential scanning calorimetry analysis allowed evaluating the effects of individual osmotic dehydration or vacuum impregnation processes on (i) the interaction between air and liquid in real plant tissues, (ii) the plant tissue water state and (iii) the cell compartments. Isothermal calorimetry, respiration and photosynthesis determinations led to investigate the metabolic changes upon the application of osmotic dehydration or vacuum impregnation. The proposed multianalytical approach should enable both better designs of processing technologies and estimations of their effects on tissue.

Abstract

Negli ultimi anni l'industria di trasformazione al minimo ha mostrato un crescente interesse verso i trattamenti di disidratazione osmotica e di impregnazione sottovuoto per le loro caratteristiche basse temperature di processo e per le relativamente contenute esigenze energetiche.

La disidratazione osmotica, che consiste nell'immersione di tessuti vegetali in soluzioni ipertoniche, consente all'acqua presente nei tessuti di diffondere nella soluzione osmotica ed ai soluti in soluzione di diffondere, in direzione opposta, all'interno dei tessuti.

L'impregnazione sottovuoto prevede l'immersione del tessuto vegetale in una soluzione di processo e consiste di due fasi successive. Durante la prima fase, la riduzione della pressione agente sul sistema solido-liquido provoca l'espansione ed il parziale rilascio nella soluzione del gas contenuto nei pori del tessuto. La seconda fase di ripristino della pressione atmosferica determina l'espansione del gas residuo nel tessuto con conseguente richiamo della soluzione esterna all'interno dei pori. L'impregnazione sottovuoto rappresenta un'interessante operazione tecnologica poiché può permette l'introduzione nei tessuti di specifiche molecole quali antiossidanti, regolatori di pH, stabilizzanti o crioprotettori.

Il presente studio si è proposto di valutare, seguendo un approccio multianalitico di indagine, le principali modificazioni a carico di tessuti vegetali assoggettati a trattamenti di disidratazione osmotica o impregnazione sottovuoto. Misurazioni di tipo macro- (risonanza magnetica nucleare), micro- (microscopia ottica) ed ultrastrutturali (microscopia elettronica a trasmissione) sono state affiancate ad analisi di texture e di calorimetria a scansione differenziale. Sono stati valutati i principali effetti sulle interazioni aria-liquido in reali condizioni, sullo stato dell'acqua del tessuto e sui compartimenti cellulari. Misurazioni di calorimetria in isoterma e determinazioni dell'attività respiratoria e fotosintetica hanno infine permesso un'indagine dei cambiamenti metabolici. Tale approccio multianalitico, permettendo una valutazione complessiva delle modificazioni a carico della materia prima, può essere applicato nell'ottimizzazione dei parametri di processo sulla base delle caratteristiche ricercate nel prodotto finito.

List of Papers

This thesis is based on the following Papers, referred to in the text by their Roman numerals. The Papers are attached as appendixes at the end of the thesis.

I Tylewicz U, **Panarese V**, Laghi L, Rocculi P, Nowacka M, Placucci G, & Dalla Rosa M (2011) NMR and DSC water study during osmotic dehydration of *Actinidia deliciosa* and *Actinidia chinensis. Food Biophysics*, 6: 327-333.

II Dalla Rosa M, Tylewicz U, **Panarese V**, Laghi L, Pisi A, Santagapita P, & Rocculi P (2011) Effect of osmotic dehydration on kiwifruit: Results of a multianalytical approach to structural study. *Journal on Processing and Energy in Agriculture,* 15: 113-117.

III **Panarese V**, Laghi L, Pisi A, Tylewicz U, Dalla Rosa M, & Rocculi P (2012) Effect of osmotic dehydration on *Actinidia deliciosa* kiwifruit: a combined NMR and ultrastructural study. *Food Chemistry,* 132:1706–1712.

IV **Panarese V**, Tylewicz U, Santagapita P, Rocculi P, & Dalla Rosa M (2012) Isothermal and differential scanning calorimetries to evaluate structural and metabolic alterations of osmo-dehydrated kiwifruit as a function of ripening stage. *Innovative Food Science and Emerging Technologies*, 15: 66-71.

V Santagapita P, Laghi L, **Panarese V**, Tylewicz U; Rocculi P, & Dalla Rosa M (2012) Modification of T_2 relaxation times and water diffusion coefficients of kiwifruit pericarp tissue subjected to osmotic dehydration. *Food and Bioprocess Technology,* DOI 10.1007/s11947-012-0818-5.

VI **Panarese V**, Dejmek P, Rocculi P, & Gómez Galindo F (2013) Microscopic study providing insight into the mechanisms of mass transfer phenomena in vacuum impregnation. *Innovative Food Science and Emerging Technologies*, http://dx.doi.org/10.1016/j.ifset.2013.01.008.

VII **Panarese V**, Rocculi P, Baldi E, Wadsö L, Rasmusson A G, & Gómez Galindo F (2012) Exploring metabolic responses of spinach leaves induced by vacuum impregnation, Manuscript in progress.

Contents

1 Introduction and objectives

One of the main aims of the fruit and vegetable industry is to develop new preservation technologies to efficiently respond to the exigent quality and safety consumer's perception, defining their choices and food economics. Consumers demand high quality and convenient fruit and vegetable products, with natural flavour and taste, and appreciate the freshness of minimally processed food. Besides, they require safe and natural products without additives such as preservatives and humectants.

Over the past years the industry has become interested in the application of osmotic dehydration and vacuum impregnation as mild technologies because of their energy efficiency, since the processes do not require water-phase change.

The main aim of this PhD thesis was to investigate physiological and structural aspects of different raw materials submitted to osmotic dehydration or vacuum impregnation process. In particular the research was focused on the following aspects:

- Study of structural, physicochemical changes and metabolic responses of kiwifruit induced by osmotic dehydration (***Paper I, II, III, IV, V***);
- Study of mass transfer phenomena on raw materials with different porosities during vacuum impregnation (***Paper VI***);
- Metabolic responses of spinach leaves induced by impregnation with different sugars (***Paper VII***).

2 Structure of plant tissue

Plants are biological systems constituted by living cells that are assembled in tissues and are constructed from three main types of organs: leaves, stems, and roots. Each plant organ in turn is made from three tissue systems with specialized functions: dermal, vascular and ground. Dermal tissue is the plant's protective outer covering in contact with the environment. It facilitates water and ion uptake in roots and regulates gas exchange in leaves and stems. Vascular tissue, together the phloem and the xylem, form a continuous vascular system throughout the plant. This tissue conducts water and solutes between organs and also provides mechanical support. Ground tissue is a supportive tissue which accounts for much of the bulk of the young plant. It also functions as carbohydrates manufacture and storage. The ground tissue system contains three main cell types called parenchyma, collenchyma, and sclerenchyma. Parenchyma cells are found in all plant tissue systems. They are living cells and generally capable of further division. These cells have a variety of functions. The apical and lateral meristematic cells of shoots and roots provide the new cells required for growth. Carbohydrate production and storage occur in the photosynthetic cells of the leaf and stem (called mesophyll cells) whilst storage parenchyma cells form the bulk of most fruits and vegetables. Collenchyma are living cells similar to parenchyma cells except that they have much thicker cell walls and are usually elongated and packed. They are capable of stretching and provide mechanical support. Collenchyma cells are especially common in subepidermal regions of stems. Sclerenchyma, like collenchyma, have strengthening and supporting functions. However, they are usually dead cells with thick, lignified secondary cell walls that prevent them from stretching as the plant grows (Alberts *et al*., 2009).

All plant cells have the same basic eukaryotic organization: they contain a nucleus and a cytoplasm, gel-like substance residing within the cell membrane holding all the cell's internal sub-organelles (Figure 1). Certain structures, including the nucleus, can be lost during cell maturation, but all plant cells begin with a similar complement of organelles (Taiz & Zeiger, 2010).

The cell wall

A fundamental difference between plants and animals is that each plant cell is surrounded by a rigid cell wall. In animals, embryonic cells can migrate from one location to another, resulting in the development of tissues and organs containing cells that originated in different parts of the organism. In plants, such cell migrations are prevented because each walled cell and its neighbour are cemented together by a middle lamella. As a consequence, plant development unlike animal development, depends solely on patterns of cell division and cell enlargement. Plant cells have two types of walls: primary and secondary. Primary cell wall (Figure 1) is typically thin (less than 1 μm) whilst the secondary cell wall is thicker and owes its strength and toughness to lignin. The secondary cell wall is absent in young cells (Figure 1) and is deposited when most cell enlargement has ended. The middle lamella (Figure 1), the outermost layer found in between cells, is rich in pectin cementing the primary cell walls of adjacent cells together (Gunning & Steer, 1996).

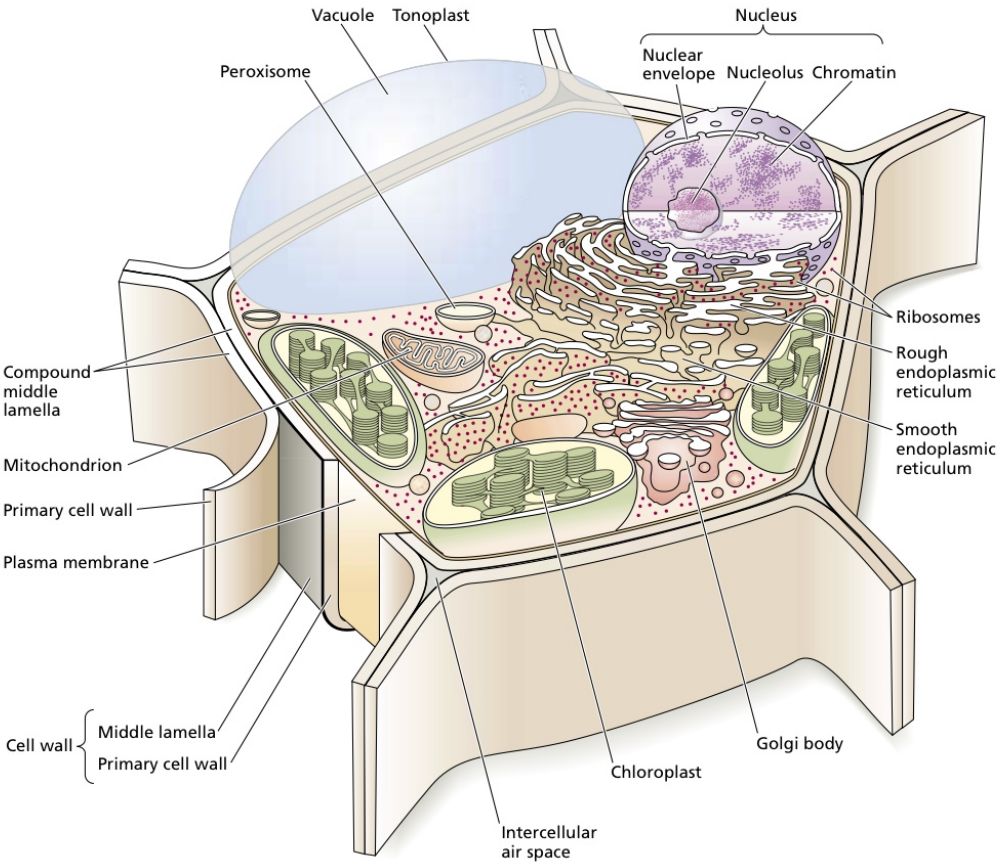

Figure 1. Diagrammatic representation of a young plant cell. Various intracellular compartments are defined by their respective membranes, such as the tonoplast, the nuclear envelope, and the membranes of the other organelles. The middle lamella cements the primary cell walls of adjacent cells together (adapted from Taiz & Zeiger, 2010).

The biological membranes

All cells are enclosed in the plasma membrane (also called plasmalemma) that serves as their outer boundary, separating the cytoplasm from the external environment. This membrane allows the cell to take up and retain certain substances while excluding others. Various transport proteins embedded in the plasma membrane are responsible for this selective traffic of solutes across the membrane. Membranes also delimit the boundaries of the specialized internal organelles of the cell and regulate the fluxes of ions and metabolites into and out of these compartments. All biological membranes have the same basic molecular organization. They consist of a double layer (bilayer) of either phospholipids or, in the case of chloroplasts, glycosylglycerides, in which proteins are embedded. In most membranes, proteins make up about half of the membrane's mass. However, the composition of the lipid components and the properties of the proteins vary from membrane to membrane, conferring on each membrane its unique functional characteristics (Evert, 2006).

The nucleus and the endoplasmic reticulum

The nucleus is a membrane-enclosed organelle containing most of the cell's genetic material, organized as multiple long linear DNA molecules in complex with a large variety of proteins, such as histones, to form chromosomes. The genes within these chromosomes are the cell's nuclear genome. The function of the nucleus is to maintain the integrity of genes and to control the activities of the cell by regulating gene expression. The nucleus is primarily responsible for regulating the metabolism, growth, and differentiation of the cell.

Cells have an elaborate network of internal membranes called the endoplasmic reticulum (ER). There are two types of ER, smooth and rough, and the two types are interconnected. The structural differences between the two forms of ER are accompanied by functional differences. Smooth ER functions as a major site of lipid synthesis and membrane assembly. Rough ER is the site of synthesis of membrane proteins to be secreted outside the cell or into the vacuoles (Taiz & Zeiger, 2010).

The Golgi apparatus

The Golgi apparatus (also called Golgi complex) of plant cells is a dynamic structure consisting of one or more stacks of three to ten flattened membrane sacs, or cisternae, and an irregular network of tubules and vesicles called the trans Golgi network (TGN). Each individual stack is called a Golgi body or dictyosome. In plant cells, the Golgi body plays an important role in cell wall formation. Noncellulosic cell wall polysaccharides (hemicellulose and pectin) are synthesized, and a variety of glycoproteins are processed within the Golgi (Driouich *et al.,* 1994).

The central vacuole contains water and solutes

Mature living plant cells contain large, water-filled central vacuoles that can occupy 80 to 90% of the total volume of the cell (Figure 1). Each vacuole is surrounded by a vacuolar membrane, or tonoplast (Nobel, 1991). Many cells also have cytoplasmic strands that run through the vacuole, but each transvacuolar strand is surrounded by the tonoplast. The vacuole contains water and dissolved inorganic ions, organic acids, sugars, enzymes, and a variety of secondary metabolites, which often play roles in plant defense. Active solute accumulation provides the osmotic driving force for water uptake by the vacuole, which is required for plant cell enlargement. The turgor pressure generated by this water uptake provides the structural rigidity needed to keep herbaceous plants upright, since they lack the lignified support tissues of woody plants (Evert, 2006).

The mitochondria and the chloroplasts are sites of energy conversion

A typical plant cell has two types of energy-producing organelles: mitochondria and chloroplasts. Both types are separated from the cytosol by a double membrane. Mitochondria are the cellular sites of respiration, a process in which the energy released from sugar metabolism is used for the synthesis of ATP (adenosine triphosphate) from ADP (adenosine diphosphate) and inorganic phosphate (P_i). Mitochondria can vary in shape from spherical to tubular, but they all have a smooth outer membrane and

a highly convoluted inner membrane. The compartment enclosed by the inner membrane, the mitochondrial matrix, contains the enzymes of the pathway of intermediary metabolism called the Krebs cycle. The inner membrane is highly impermeable to the passage of H^+ and it serves as a barrier to the movement of protons. This important feature allows the formation of electrochemical gradients. Dissipation of such gradients by the controlled movement of H^+ ions through the transmembrane enzyme ATP synthase is coupled to the phosphorylation of ADP to produce ATP. ATP can then be released to other cellular sites where energy is needed to drive specific reactions.

Chloroplasts belong to another group of double membrane–enclosed organelles called plastids. Chloroplast membranes are rich in glycosylglycerides. Chloroplast membranes contain chlorophyll and its associated proteins and are the sites of photosynthesis. In addition to their inner and outer envelope membranes, chloroplasts possess a third system of membrane called thylakoids. The ATP synthases of the chloroplast are located on the thylakoid membranes. During photosynthesis, light-driven electron transfer reactions result in a proton gradient across the thylakoid membrane. As in the mitochondria, ATP is synthesized when the proton gradient is dissipated via the ATP synthase.

Plastids that contain high concentrations of carotenoid pigments rather than chlorophyll are called chromoplasts. They are one of the causes of the yellow, orange, or red colors of many fruits and flowers. Nonpigmented plastids are called leucoplasts. The most important type of leucoplast is the amyloplast, a starch-storing plastid. Amyloplasts are abundant in storage tissues of the shoot and root, and in seeds. Specialized amyloplasts in the root cap also serve as gravity sensors that direct root growth downward into the soil (Taiz & Zeiger, 2010).

3 Transport processes in plant

Plants do not have a circulatory system like animals, but they do have a sophisticated transport system for carrying water and dissolved solutes to different parts of the plant, often over large distances.

3.1 Transport barriers separate the symplast from the apoplast

Nutrient and water taken up by any cell must, at some stage, pass the plasma membrane. The plasma membrane, in principle, is impermeable to solutes, such as ions and polar molecules. A root is always enriched in nutrients compared to the surrounding soil and without a tight wrapping most of its contents would leak out of the plant and back into the growth medium. Thus, there is only one way that solutes can be transported from the outside medium, called the apoplast, into a cell, and this is by specific transport proteins that span the plasma membrane. As cells tend to accumulate nutrients, this transport is most often uphill, i.e. against a concentration gradient and/or an electrical gradient, and needs to be energised. Water and ions travel into and through the cell wall and extracellular space following the apoplastic path (Figure 2). Once inside a plant cell, a given solute can diffuse through the symplastic path (Figure 2) from cell to cell via cellular bridges called plasmodesmata (Figure 8f). Plasmodesmal transport by diffusion is not very effective, and for long-distance transport the nutrient in question might have to leave the symplast to enter from the apoplast in a neighbouring cell or in another part of the plant. Here again, uptake needs to be energized and occurs through specialised transport proteins (Sondergaard et al., 2004)

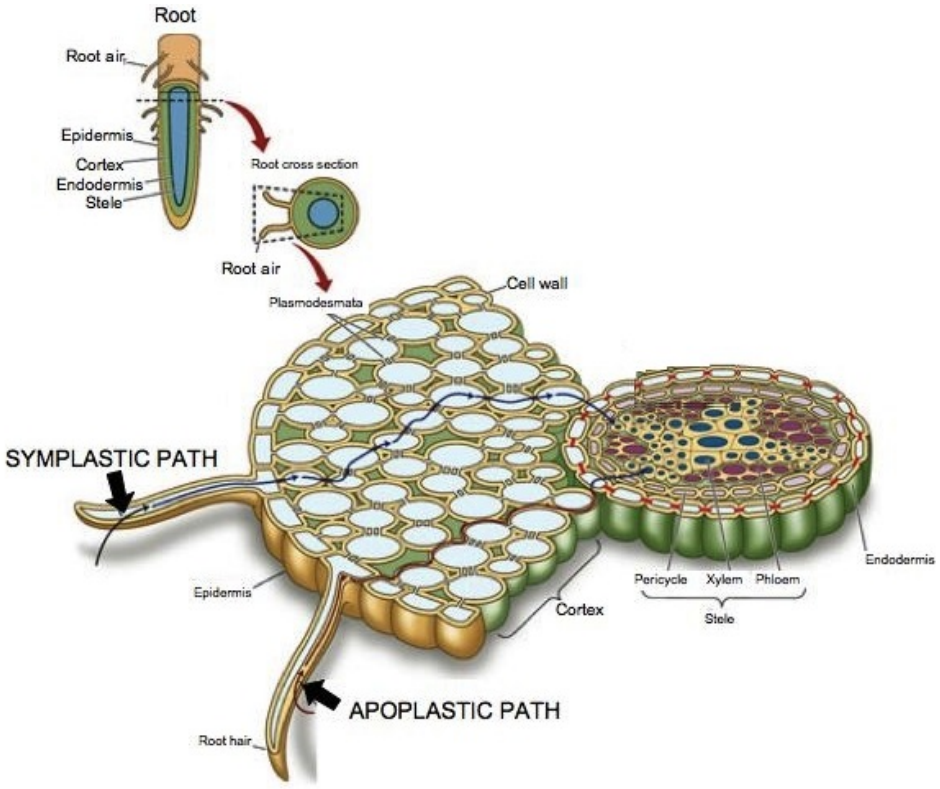

Figure 2. Symplastic and apoplastic pathway in plant tissue. In the apoplast water and ions travel into and through the cell wall and extracellular space. Water and ions cross the plasma membrane to enter the symplast (adapted from Sadava et al., 2007).

3.2 Water transport

Water Potential

The chemical potential is a quantitative expression of the free energy associated with water. In thermodynamics, free energy represents the potential for performing work. Chemical potential is a relative quantity: it is expressed as the difference between the potential of a substance in a given state and the potential of the same substance in a standard state. The unit of chemical potential is energy per mole of substance (J mol^{-1}) (Finkelstein, 1987). For historical reasons, plant physiologists have most often used a related parameter called water potential, defined as the chemical potential of water divided by the partial molal volume of water (the volume of 1 mol of water, 18×10^{-6} m^3 mol^{-1}). Water potential is a measure of the free energy of water per unit volume (J m^{-3}). This unit is equivalent to pressure units such as Pascal, which is the common measurement unit for water potential. The major factors influencing the water potential in plants are concentration, pressure, and gravity. Water potential is symbolized by Ψ_w and the water potential of solutions may be dissected into individual components (Eq. 1):

$$\Psi_w = \Psi_s + \Psi_p + \Psi_g \quad (1)$$

The terms Ψ_s and Ψ_p and Ψ_g denote the effects of solutes, pressure, and gravity, respectively, on the free energy of water. The term Ψ_s, called the solute potential or the osmotic potential, represents the effect of dissolved solutes on water potential. Solutes reduce the free energy of water by diluting the water. This is primarily an entropy effect; that is, the mixing of solutes and water increases the disorder of the system and thereby lowers free energy. The term Ψ_p is the hydrostatic pressure of the solution. Positive pressures raise the water potential; negative pressures reduce it (Friedman, 1986).

Water enters and leaves the cell along a water potential gradient

If a cell (Ψ_w= –0.732 MPa) is immersed in a sucrose solution (e.g. Ψ_w= –0.244 MPa), water will move from the sucrose solution to the cell (from high to low water potential). Because plant cells are surrounded by relatively rigid cell walls, even a slight increase in cell volume causes a large increase in the hydrostatic pressure within the cell. As water moves into the cell, the hydrostatic pressure, or turgor pressure (Ψ_p), of the cell increases. Consequently, the cell water potential (Ψ_w) increases, and the difference between inside and outside water potentials ($\Delta \Psi_w$) is reduced. Eventually, cell Ψ_p increases enough to raise the cell Ψ_w to the same value as the Ψ_w of the sucrose solution. Viceversa, water can also leave the cell by osmosis. Water flow is a passive process. That is, water moves in response to physical forces, toward regions of low water potential or low free energy. There are no metabolic "pumps" (reactions driven by ATP hydrolysis) that push water from one place to another. This rule is valid as long as water is the only substance being transported (Taiz & Zeiger, 2010). When solutes are transported, however, as occurs for short distances across membranes and for long distances in the phloem, then water transport may be coupled to solute transport and this coupling may move water against a water potential gradient (Loo *et al*. 1996).

Aquaporins facilitate the movement of water across cell membrane

For many years plant physiologist were uncertain about how water move across plasma membrane. Specifically was unclear whether water movement into plant cells was limited to the diffusion of water molecule across the plasma membrane's lipid bilayer or if it also involved diffusion through protein-lined pores (Figure 3). In 1991 aquaporins were discovered. Aquaporins are integral membrane proteins that form water-selective channels across the membrane (Maurel *et al*., 2008). Because water diffuses much faster through such channels than through lipid bilayer, aquaporins facilitate water movement into plant cells (Weig *et al*., 1997, Schäffner, 1998). Aquaporins not change the direction of transport or the driving force for water movement, however can be reversibly transferred between an open and a closed state, in response to pH or Ca^{+} levels (Tyerman *et al*., 2002). This might suggests plant actively regulate the permeability of their cell membrane to water.

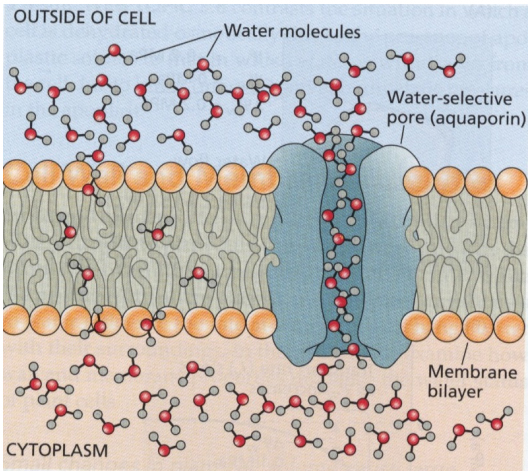

Figure 3. Water can cross plant membranes by diffusion of individual water molecules through the membrane bilayer, as shown on the left, and by linear diffusion of water molecules through water-selective pores formed by integral membrane proteins such as aquaporins (adapted from Taiz & Zeiger, 2010).

3.3 Solute transport

According to Fick's first law, the movement of molecules by diffusion always proceeds spontaneously, down a gradient of free energy or chemical potential, until equilibrium is reached. The spontaneous 'downhill' movement of molecules is termed passive transport. The extent to which a membrane allows the movement of substances is called membrane permeability (Taiz & Zeiger, 2010). Beside simple diffusion, in facilitated diffusion, the direction of net flux is also down the potential energy gradient. In contrast to simple diffusion, however, the molecule moves across the membrane by a specific carrier or channel. Since the bilayer is a formidable barrier to most hydrophilic molecules, facilitated transport substantially increases their rate of translocation. Most transport activity associated with biological membranes is mediated by specific, proteinaceous pathways (Bush, 1993).

According to chemiosmotic nomenclature, transport systems can be sorted into two classes: primary transport systems, which pump substrates by a process that directly involves the breaking of covalent bonds (e.g. ATPases), and secondary transport systems, where only non-covalent bonds are

broken. From a mechanistic point of view, the latter systems can be sorted into two classes, channels and carriers (Stein, 1990). When open, channels can be regarded as selective pores through which substrate ions move without inducing a change in the general conformation of the protein. Whereas carriers undergo a cycle of conformational changes for each molecule/ion they transport. The maximum velocity of action of carriers (in the range of 10-1000 transport events per second and carrier) is therefore much lower than that of channels (10^7 ions per second). From an energetic point of view, carriers can be classed as uniporters and cotransporters. Uniporters move their substrates down their electrochemical gradients, whereas cotransporters (symporters or antiporters) can move a substrate up its electrochemical gradient, by coupling this transport to that of another substrate that is moving down its electrochemical gradient. The putative plasma membrane transport systems identified in plants to date are illustrated in Figure 4a,b (Logan et al., 1997).

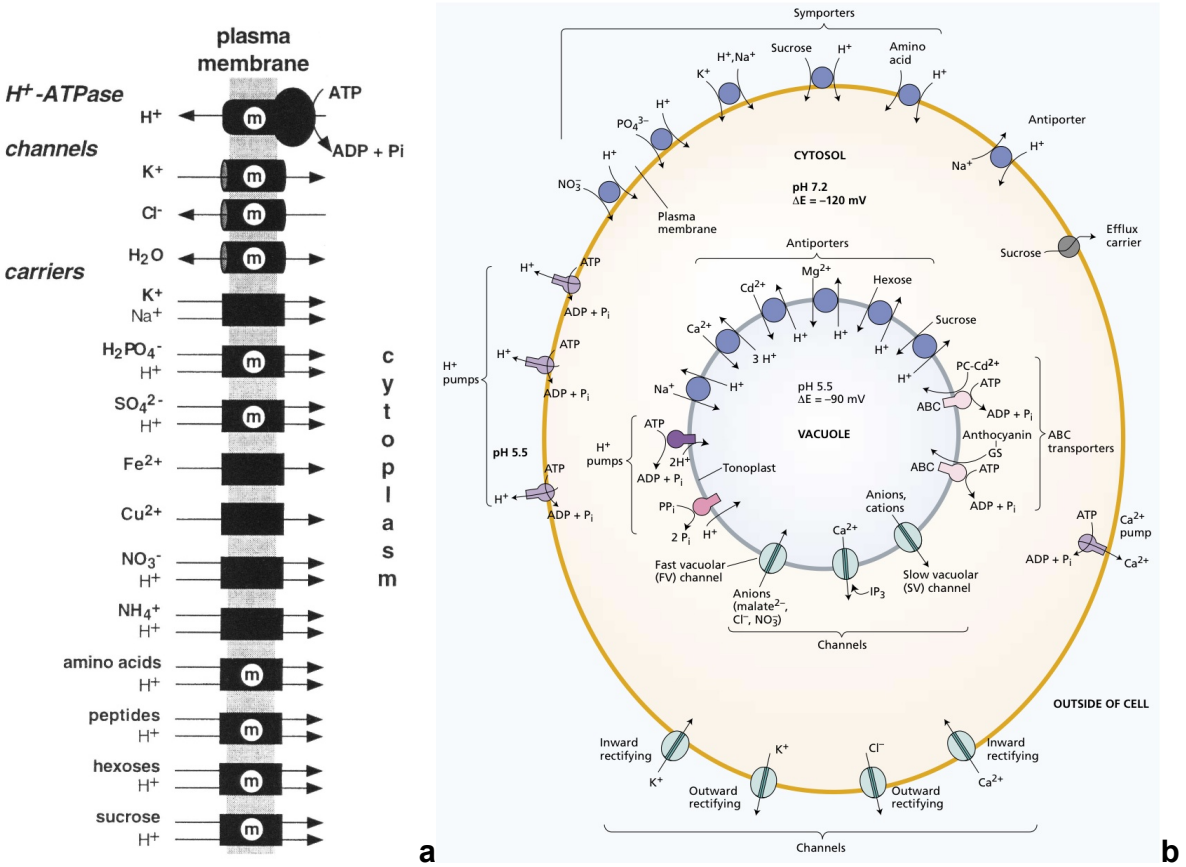

Figure 4. **a** Schematic diagram of plant plasma membrane transport systems. m: Indicates that functional evidence for a multigene family or several families is available. For carriers a single arrow indicates that it is a uniporter and two arrows a cotransporter (energized by the Na^+ or H^+ transmembrane electrochemical gradient) (Logan et al., 1997), **b** Overview of the various transport processes on the plasma membrane and tonoplast of plant cells (adapted from Taiz & Zeiger, 2010).

4. Mild unit operations affecting structure, physico-chemical properties and metabolism of fruit and vegetable tissues

The stability and safety of many traditional and novel foods is obtained by applying the 'hurdles technology', which is a combination of traditional and innovative mild preservation techniques, interacting cumulative or synergically to slow down the degradative phenomena responsible of food deterioration (Leistner, 1995). Osmotic dehydration and vacuum impregnation can be considered non-thermal mild processes, leading to retention of flavours and nutrients and a fresh-like taste of the final product. They also offer the advantages of low processing temperatures and low energy utilization (Vega-Mercado *et al*., 2007; Bressa *et al*., 1997). In the last years the osmotic dehydration and vacuum impregnation treatments have gained importance in the food industry with applications in minimal fruit processing and/or freezing, allowing developing of new products with specific innovative characteristics (Talens *et al*., 2001; Nieto *et al*., 1998; Barrera *et al*., 2009; Phoon *et al*., 2008).

4.1 Osmotic dehydration

Osmotic dehydration treatment is a partial dewatering process by immersion of cellular tissue in hypertonic solution. The driving force for the water removal is the concentration gradient between the solution and the intracellular fluid (Rahman, 2008). The diffusion of water from the vegetable tissue to the solution is usually accompanied by the simultaneous solutes counter-diffusion into the tissue (Kowalska & Lenart, 2001; Kaymak-Ertekin & Sultanoglu, 2000) and natural solutes present in the cells (vitamins, organic acids, minerals, pigments, etc.) can also be leached into the osmotic medium (Lerici *et al*., 1985; Dixon & Jen, 1977).

4.1.1 Transport phenomena and structural changes

There are two major mass transfer phenomena involved in osmotic dehydration: the movement of solute into the material and the flow of water out of the tissue. Thus, osmotic dehydration is actually a multicomponent transfer process of two simultaneous, countercurrent solution flows and one gas flow. The solution flowing out of the food material is water mixed with some solutes such as organic acids, reducing sugars, minerals, and some flavor and pigment compounds that affect the organoleptic and nutritional characteristics of the final products. Soluble solids present in the osmotic solution are taken up by the food material. Also, there may be gas flow out of the intercellular space (Shi & Le Maguer, 2003). There have been numerous studies to describe the kinetics of the two counter-current flows in osmotic dehydration. Variables such as temperature, time of treatment, concentration and composition of solutes influence the mass transfer kinetics. The kinetics of mass transfer is usually described through the terms: water loss, solids or solutes gain, and weight reduction (***Paper I***).

Water transfer in food materials immersed in osmotic solutions may be described by several different transport mechanisms, depending on the nature of the material, the type of moisture bonding, the

moisture content, the temperature, and the pressure in the capillary pores (Fish, 1958). In general, liquid diffusion occurs in nonporous solids, whereas capillary movement occurs in porous solids. In liquid solutions and gels, transport of water takes place only by molecular diffusion, a relatively simple phenomenon. In porous biological materials, the gas-filled cavities, the capillaries, the cell walls and the intercellular and extracellular spaces can influence the mass transfer properties. Water can be transported by several mechanisms simultaneously: molecular diffusion, liquid diffusion, vapor diffusion (through gas flow), hydrodynamic flow, capillary transport, and surface diffusion. Most frequently, a combination of these mechanisms occurs due to the complex structures found in foods (Shi & Le Maguer, 2003).

Mass transfer kinetics depend on both the process parameters and the structural properties of the biological tissue, e.g. cell maturity and porosity, but at the same time the osmotic process may affect tissue structure. Structural organization rather than the presence of single components dictates plant tissue textural properties (Stanley, 1987). The texture of vegetable tissue can be mainly attributed to the structural integrity of cell walls and the middle lamellae, as well as to the turgor pressure generated within cells by osmosis (Jackman & Stanley, 1995). Cell turgidity loss, deformation and/or cell wall rupture, splitting and degradation of the middle lamella, membrane lysis (plasmalemma and tonoplast), cellular collapse, plasmolysis and tissue shrinkage have been pointed out as the main effects of osmotic dehydration on the cellular structure of different plant tissues (Pereira *et al*., 2009**)**. As example, Prinzvalli *et al*. (2006) showed on strawberry tissue submitted to osmotic dehydration a significant loss of texture, which was related to the duration of the treatment. Osmotic dehydration with glucose, glycerol or sucrose hypertonic solutions decreased sharply the elasticity of the tissue (Muntada *et al*., 1998).

New findings

Transport Phenomena

Paper IV studied the mass transfer rates occurring upon osmotic dehydration using kiwifruit at different ripening stages. Along the storage time, two kiwifruit groups were selected with refractometric index values of 9±1 (called as LB, low °Brix) and 14±1 °Brix (called as HB, high °Brix). The fruits were submitted to osmotic dehydration and the increased rate of soluble solids content (SSC) during the treatment resulted similar for both kiwifruit groups, as shown in Figure 5. However the overall SSC increase of HB group was lower than that of LB group. This result may be due to the higher sugar content of ripe fruit that reduced the difference between solution and fruit osmotic potentials, which is the driving force of osmotic transport phenomena (Chiralt & Fito, 2003; Shi & Le Maguer, 2003). Furthermore the decrease of the osmotic pressure difference between solution and fruit over time led to the decrease of the rate of SCC uptake for both LB and HB kiwifruits, as shown in Figure 5.

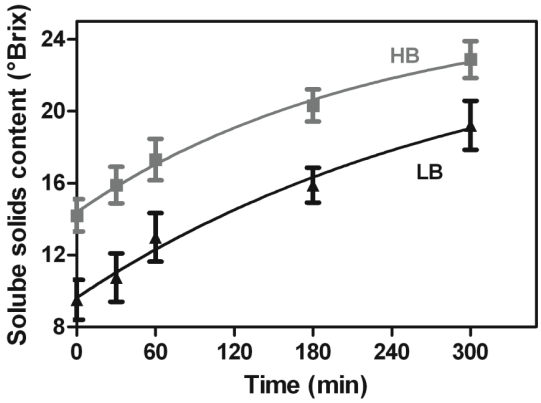

Figure 5. Solids gain expressed as soluble solids content vs. time of dehydration treatment for low (LB) and high (HB) °Brix kiwifruit slices (corresponding to Figure 1a in ***Paper IV***).

Paper I investigated mass transfer and water state changes promoted by osmotic dehydration on two kiwifruit species, *Actinidia deliciosa* and *Actinidia chinensis*. Osmotic dehydration kinetics of kiwifruit were evaluated by calculating net change of kiwifruit slices total mass, water mass and solids mass (Fito & Chiralt, 1997). The mass transfer data were modelled according to the equation proposed by Palou *et al*. (1994) and Sacchetti *et al.* (2001), using the Peleg's model (Peleg, 1988). For both *A. deliciosa* and *A. chinensis*, the osmotic solution temperature seemed to positively influence the initial water loss rate ($1/k_1^w$) as reported in Figure 6a. Higher process temperatures seemed to promote several phenomena: faster water loss through swelling and plasticizing of cell membranes; faster water diffusion within the product; lower viscosity of the osmotic medium facilitating the water transfer on the surface (Lazarides *et al.*, 1995). Kiwifruit has a porous structure and a high treatment temperature would permit a better release of trapped air from the tissue, resulting in more effective removal of water by osmotic pressure (Cao *et al.*, 2006). The initial rate of weight reduction ($1/k_1^\circ$) of *A. chinensis* was higher than the one of *A. deliciosa* at 25, 35 and 45 °C (Figure 6b); initial rate of water ($1/k_1^w$, Figure 6a) and weight ($1/k_1^\circ$) reduction reached the maximum at 45 °C for both kiwifruit species. During the initial phase of the treatment *A. chinensis* solids gain ($1/k_1^{ST}$) was modest and it seemed to be positively influenced by the temperature less than *A. deliciosa*, as shown in Figure 6c. During the second phase of the treatment all the considered mass transfer rates ($1/k_2^w$, $1/k_2^{ST}$, $1/k_2^\circ$) for both the kiwifruit species underwent a significant and very similar increase, by varying the temperature from 25 to 35 °C, as shown in Figure 6a-c.

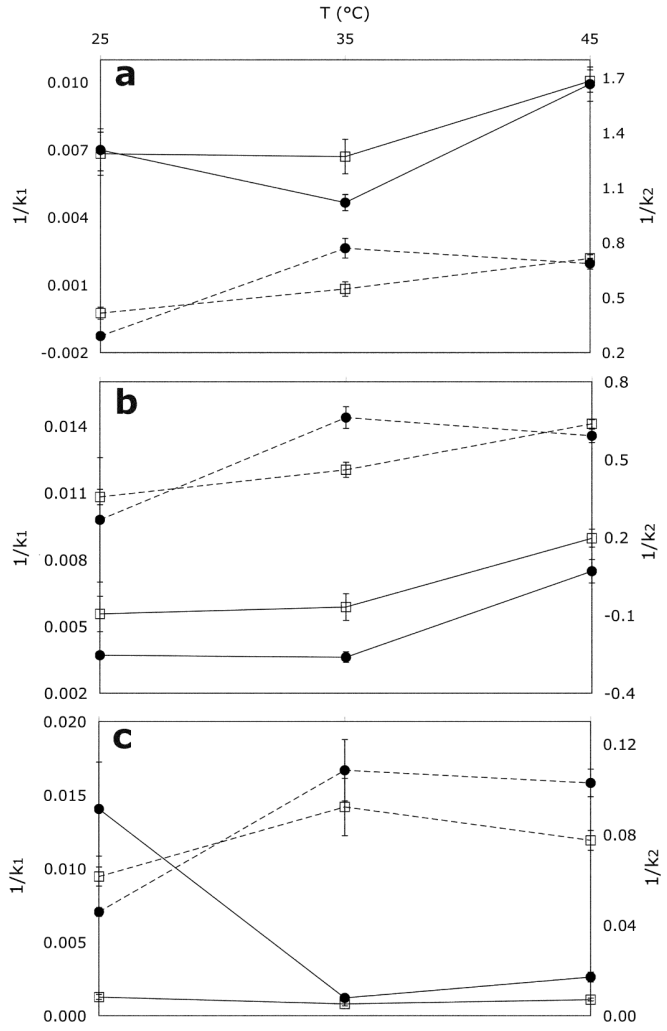

Figure 6. Effect of the temperature on mass changes kinetic parameters: $1/k_1$ (*open square-solid line*) and $1/k_2$ (*open square-dashed line*) of *A. chinensis* and $1/k_1$ (*filled circle-solid line*) and $1/k_2$ (*filled circle-dashed line*) of *A. deliciosa*. **a** Water mass change; **b** total mass change; **c** soluble solids mass change (corresponding to Figure 2 in ***Paper I***).

Structural Changes

Paper III describes the modifications on micro- and ultrastructure of *Actinidia deliciosa* during the osmotic dehydration process. At both light microscopy (LM) and transmission electron microscopy (TEM) considerable changes in size, structure and uptake of stains (Toluidine blue for LM and uranyl acetate for TEM) were observed during the treatment. Moreover cell walls showed extensive swelling, which intensity varied from cell to cell and even within the same cell. At LM the expansion of the cell walls was detected, as shown in Figure 7a and 7b, respectively obtained on raw and treated (35 °C, 120 min) kiwifruit slices.

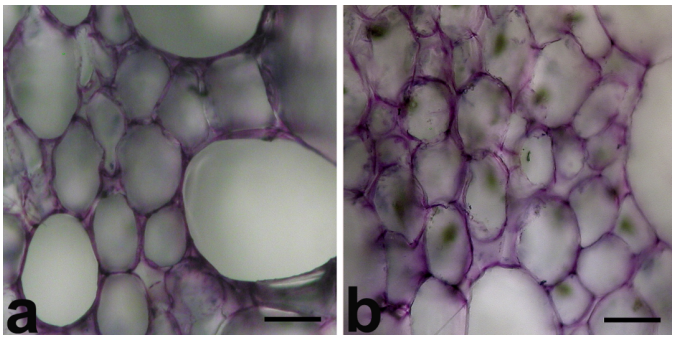

Figure 7. LM of kiwifruit outer pericarp cells: stained cell walls before **a** and after **b** 120 min of osmotic dehydration at 35 °C. Bar = 100 µm (corresponding to Figure 4 in ***Paper III***).

Tissues of raw kiwifruits observed at TEM showed cells with an apparent well-defined cell wall structure (Figure 8a). Cells were more or less regular in shape, in general isodiametric, and attached along extended contact areas. The cell wall stained intensely, exhibiting dense longitudinal fibrous or reticulate staining (Figure 8c). In treated fruits the stain became much more grainy and light and most wall material failed to stain (Figure 8d). Furthermore the cell wall showed swelling (Figure 8d) and accumulation of electron-dense deposits in intercellular spaces and wall margins (Figure 8b). Outer pericarp cells from raw kiwifruits showed at TEM numerous plasmodesmatal connections densely stained, and a slight thinning of the cell wall containing plasmodesmata (Figure 8f). In treated fruits, the plasmodesmatal region appeared as a distinct constriction of the wall, with the staining restricted to this site with a sharp difference between the lightly stained cell wall and the plasmodesmatal area (Figure 8e). These structural anomalies could result in connectivity deviations between adjacent cells. A marked reduction in staining intensity of cell wall material occurred predominantly in the treated kiwifruit tissues and might be partially accounted for by wall expansion. Thus either the material was being lost from the cell wall or there occurred chemical modifications, which reduced the reactivity of cell wall materials with the stain. Hemicellulose stains strongly, and it could be that during the osmotic dehydration there was a modification of hemicelluloses molecular size. This change might contribute to a decrease reactivity of hemicelluloses for staining by reducing the number of available staining sites. Cell wall changes promoted by the osmotic dehydration resulted similar to those promoted by fruit ripening (Redgwell *et al.,* 1991, 1989).

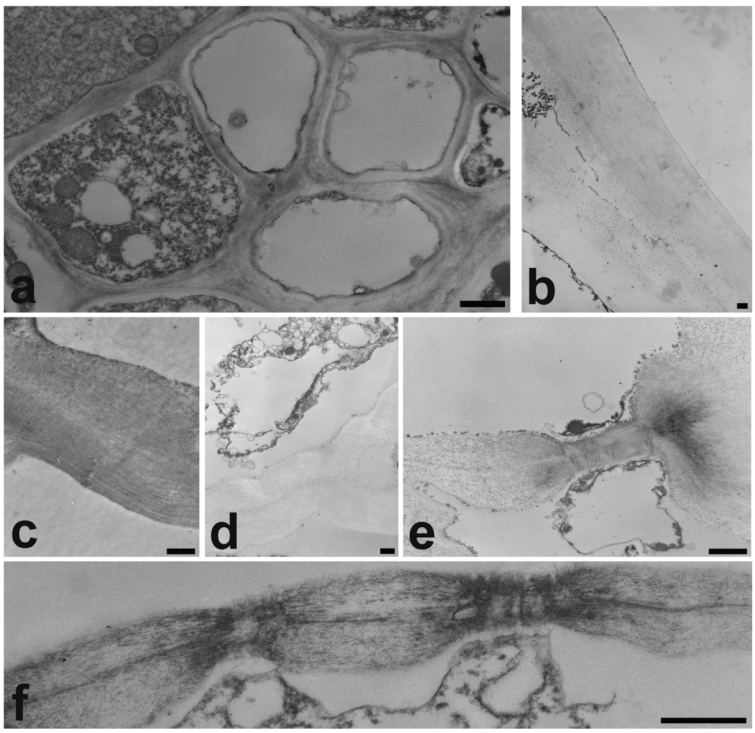

Figure 8. Transmission electron micrographs of cell wall, plasmodesmata and intercellular spaces of outer pericarp cells of raw and treated fruits. Bar = 1 μm.
a Section of the raw fruit tissue. The cells are well attached along the contact areas showing a well-preserved structure.
b Detail of cell wall from treated fruit. Wall swollen and lack of staining are apparent. Electron- dense deposits accumulated in intercellular space region and wall margins.
c Detail of cell wall from raw fruit. Wall shows intense staining of mainly longitudinal fibers. No swelling detected.
d Detail of cell wall from treated fruit. Wall is swollen, failed to show any significant staining and little details are visible within the wall.
e Plasmodesmata in cell wall from treated fruit. Plasmodesmata appear as a distinct constriction of the wall, staining is restricted to this area and there is a sharp difference between the lightly stained cell wall and the plasmodesmatal site.
f Detail of plasmodesmata in cell wall from raw fruit. Wall shows a constriction in the plasmodesmata region. Staining density is similar in wall and plasmodesmatal regions (corresponding to Figure 5 in ***Paper III***).

According to Muntada et al. (1998), firmness is one of the most important parameters since its changes could be related to structural modifications. ***Paper IV*** investigates the textural and the modification of the cell wall principal components on unripe (LB) and ripe (HB) osmodehydrated *A. deliciosa* kiwifruits. As shown in Figure 9, firmness values showed differences for LB and HB raw kiwifruits, due to the higher ripening on HB samples (Barboni *et al.*, 2010; Beirão da Costa *et al.*, 2006). Treated samples of both ripe and unripe kiwifruit displayed lower firmness than raw samples. Raw LB revealed the highest firmness values, but the firmness loss along osmotic dehydration was more marked respect to HB kiwifruit. Figure 9b shows that the major firmness loss occurred during the first hour of osmotic dehydration resulting for LB and HB respectively four and two times higher than the firmness loss recorded during the following four hours of treatment. The overall shape of the penetration curve in Figure 9a reveals for the osmotic dehydrated samples two very different slopes prior to arrive to the first peak/maximum force. In contrast raw samples (especially LB samples) showed a unique slope prior to the first peak. Since the slope of the force deformation curve before the first inflection point indicates the point of non-destructive elastic deformation (Beaulieu, 2010), it could be proposed that the LB raw material did not present this kind of deformation, which slightly appeared increasing ripening, and especially during the treatment.

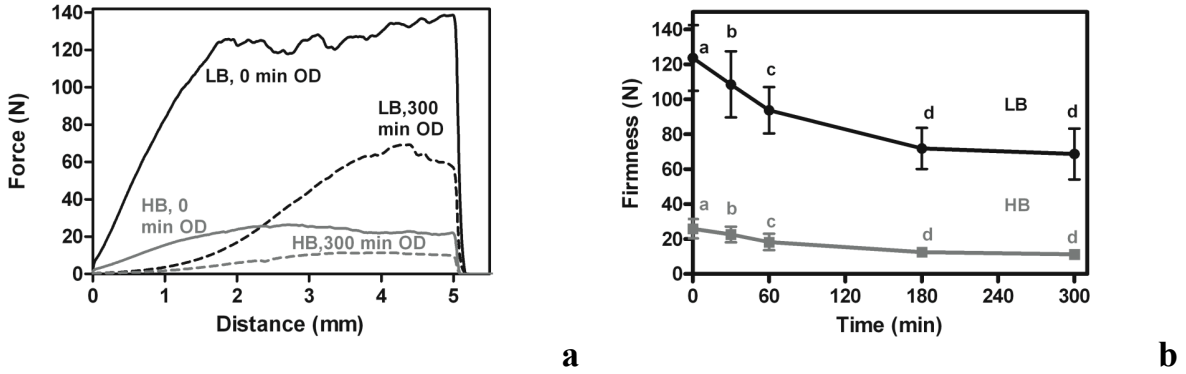

Figure 9. Overall shape of the penetration curves **a** and firmness **b** of low (LB) and high (HB) °Brix kiwifruit slices as a function of osmotic dehydration duration (corresponding to Figure 2 in ***Paper IV***).

DSC measurements reported in ***Paper IV*** allowed defining the modification promoted by osmotic dehydration on the principal components of the cell wall (pectins, cellulose, hemi-celluloses and proteins, Redgwell *et al.*, 1991) of *A. deliciosa* at two different ripening stages. Figure 10 shows the thermograms obtained for unripe (LB) and ripe (HB) kiwifruits before and after 300 min of treatment. LB thermograms show better separated peaks and higher heat flow value than HB kiwifruit. Peak 1, highlighted in Figure 10 by a squared shape, might be attributed to sucrose (Abd-Elrahman & Ahmed, 2009). The enthalpy value of peak 1 (Table 1**)** appeared higher for HB than for LB kiwifruit, following the sucrose content increase. Enthalpy values increased slowly for LB along osmotic dehydration whereas enthalpy increased up to 3 times after 3 h for HB kiwifruit.

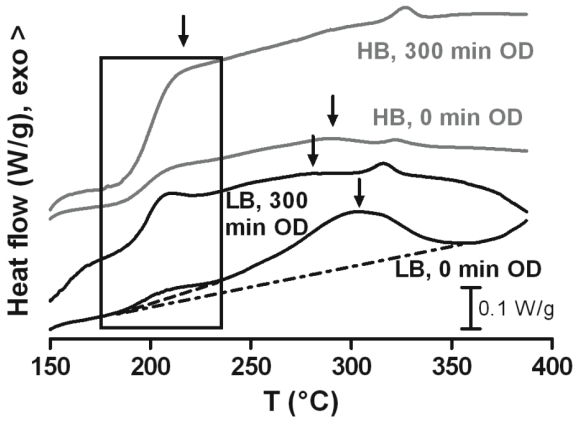

Figure 10. Thermograms obtained by differential scanning calorimetry (DSC) of low (LB) and high (HB) °Brix kiwifruit slices raw (0 min) and subjected to 300 min of osmotic dehydration. The square indicates the changes occurred to peak 1 and arrows point out the peak temperature of peak 2. The dashed lines show the two analyzed peaks, values reported in Table 1 (corresponding to Figure 3 in ***Paper IV***).

A complex peak appears (peak 2, arrow in Figure 10) for higher temperature of analysis, which is ascribable to cell wall components (e.g. pectins, hemi-celluloses and cellulose decomposition, Abd-Elrahman & Ahmed, 2009; Einhorn-Stoll *et al.*, 2007; Ray *et al.*, 2004). Peak 2 related to raw LB kiwifruit showed a higher heat flow value (W g^{-1}, Figure 10) than the corresponding peak of raw HB kiwifruit, possibly due to the differences in cell wall structure between LB and HB raw material (Bennet,

2002). Values of peak 2 associated both HB and LB kiwifruit changed similarly along the treatment. This analogy can be related to cell wall ultrastructural modifications promoted by both fruit ripening and treatment (***Paper III***), which is supported by the very similar shape of LB 300 min and HB 0 min thermograms, in the temperature range corresponding to the cell wall components decomposition. Peak 2 enthalpy values decreased during the first treatment hour and then increased in both kiwifruit groups, mainly for HB (Table 1). Hemi-cellulose depolymerization and pectin network disassembly could lead to the formation of more compounds with minor molecular mass (Bennet, 2002; Lloyd & Wyman, 2003), which might depict lower degradation temperature and overall higher enthalpy values.

Table 1.

Enthalpy values of raw (0 min) and subjected to osmotic dehydration low and high °Brix kiwifruit slices. Peak 1 and 2 correspond to those evidenced by the dashed lines in Figure 10 (corresponding to Table 1 in ***Paper IV***).

Kiwifruit ripening (°Brix)	**Time (min)**	**Peak 1** Area* (J/g)	**Peak 2** Area* (J/g)
Low °Brix	0	1.6 ± 0.2^{c}	71.4 ± 4.2^{b}
	30	4.5 ± 0.5^{a}	84 ± 11.5^{b}
	60	4.0 ± 0.4^{a}	79.0 ± 15.4^{b}
	180	2.7 ± 0.4^{b}	142.3 ± 26.4
	300	4.1 ± 0.4^{a}	104.9 ± 27.4^{ab}
High °Brix	0	10 ± 2^{c}	84 ± 6^{b}
	30	11.9 ± 0.4^{c}	62.1 ± 3.4^{b}
	60	11 ± 1^{c}	62 ± 21^{b}
	180	27 ± 2^{b}	101 ± 3^{a}
	300	37 ± 3^{a}	107 ± 17^{a}

*Values in the same column followed by different letters differ significantly at $p < 0.05$ levels.

4.1.2 Effects on water state and cellular compartments

Thermal properties

Water as a major food component affects safety, stability, quality, and physical food properties. Thermophysical properties, which depend on the chemical composition, structure of the product and temperature, but also on food processing, are *e.g.* freezing point, freezing range and unfreezable water content (Delgado *et al.,* 2012). Although there is a great debate concerning the physics of free water, which is related to water activity and the concept of bound water, progress in product development and preservation can be made by considering the unfreezable water mass fraction. This is the amount of water remaining unfrozen even at very low temperature, it includes both uncrystallised free water and water of hydration of ultrastructural components (Rahman, 2010). This portion of water content is unavailable for chemical or microbial processes (Schenz, 1995; Biliaderis, 1983).

New Findings

Paper I reports the changes of initial point of ice melting ($T_{f,onset}$) and freezable water content (x_W^F) of the outer pericarp of two kiwifruit species (*A. deliciosa* and *A. chinensis*) submitted to osmotic dehydration. During the osmotic treatment, the kiwifruit slices thermo-physical properties ($T_{f,onset}$ and x_W^F) progressively changed as shown in Table 2. In agreement with Cornillon (2000) the depletion of the initial ice melting temperature ($T_{f,onset}$) progressively increased along with the proceeding of the treatment and with the increase of the treatment temperature, following the trend of water loss and solids gain results. With the proceeding of the osmotic treatment all the samples showed a decrease of x_W^F (g g_{fw}^{-1}) particularly in samples treated at high temperatures (35, 45 °C). The results presented in ***Paper I*** are in agreement with previous studies assessing the changes of thermal properties on fruit and vegetable during storage or processing. Goñi *et al.* (2007) studied the water status in cherimoya tissues analysing the biochemical and metabolic changes occurring during ripening. The authors found, during the storage time, an increase of the unfreezable water weight fraction, possibly due to a reduction in the amount of water available in the tissues of ripe and over-ripe fruit associated with the accumulation of osmolites, *i.e.* increase of soluble solids content, which might be also related to the decrease in the freezing onset temperature recorded during storage time (Bonilla-Zavaleta *et al.*, 2006).

Table 2.
$T_{f,onset}$ and x_W^F average values obtained during the osmotic dehydration of *A. deliciosa* and *A. chinensis* kiwifruit. Statistical significance was assessed by one-way ANOVA. Different letters within the same column indicate statistical differences, $p < 0.01$ (corresponding to Table 1 in ***Paper I***).

kiwifruit species	temperature (°C)	time (min)	$T_{f,onset}$ (°C)	X_W^F ($g \cdot g_{fw}^{-1}$)
Actinidia chinensis	raw	0	- 1.8 ^{a}	0.75 ^{a}
	25	60	- 4.3 ^{bc}	0.61 ^{b}
		120	- 4.4 ^{bc}	0.62 ^{b}
		300	- 4.8 ^{c}	0.60 ^{b}
	35	60	- 4.2 ^{bc}	0.61 ^{b}
		120	- 4.6 ^{bc}	0.60 ^{b}
		300	- 8.7 ^{e}	0.42 ^{d}
	45	60	- 4.1 ^{b}	0.61 ^{b}
		120	- 6.7 ^{d}	0.59 ^{b}
		300	- 9.1 ^{e}	0.47 ^{c}
Actinidia deliciosa	raw	0	- 2.7 ^{a}	0.66 ^{a}
	25	60	- 4.9 ^{b}	0.60 ^{b}
		120	- 4.5 ^{b}	0.67 ^{a}
		300	- 5.4 ^{bc}	0.65 ^{ab}
	35	60	- 4.6 ^{b}	0.60 ^{b}
		120	- 6.6 ^{c}	0.49 ^{c}
		300	- 7.8 ^{c}	0.48 ^{de}
	45	60	- 5.2 ^{b}	0.52 ^{c}
		120	- 7.0 ^{c}	0.42 ^{de}
		300	- 12.6 ^{d}	0.36 ^{e}

Total unfreezable water is the maximum water content at which no enthalpic peak is detected (Quinn *et al.*, 1988) and, considered as the moisture content for $\Delta H=0$, can be calculated for air-drying processes as the linear regression of ΔH (J g_{dw}^{-1}) *vs* water content (g_{H2O} 100 g_{dw}^{-1}) (Venturi *et al*., 2007). This method applied to our results provided not trustable negative values of total not freezable water content, possibly because osmotic dehydration leads to both water removal and soluble solid content increase. Thus ΔH values were normalized against sample soluble solids content (°Brix), as shown in Figure 11, and from the obtained fitting equations (R^2 = 0.914 and R^2 = 0.967 respectively for *A. deliciosa* and *A. chinensis* samples) the not freezable water content of *A. deliciosa* and *A. chinensis* resulted respectively of 127.9 and 116.4 ($g_{H2O} \cdot 100\ g_{db}^{-1}$) corresponding to 56.12 and 53.79 ($g_{H2O} \cdot 100\ g_{dw}^{-1}$), in agreement with those of Tocci & Mascheroni (2008).

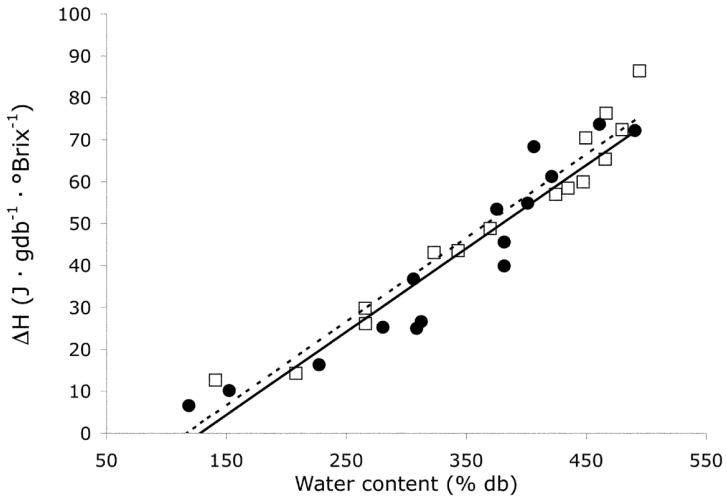

Figure 11. Regression equations of ΔH vs. water content: (*filled circle*) *A. deliciosa* and (*open square*) *A. chinensis* data; regressions: (*solid line*) *A. deliciosa*; (*dashed line*) *A. chinensis* (corresponding to Figure 3 in ***Paper I***).

Transverse NMR Relaxation Time and Water Diffusion Coefficients

A large number of nuclei, e.g., ^{1}H, ^{13}C, ^{19}F, ^{23}Na and ^{31}P, possess the property of *spin*. NMR is a spectroscopic method based on the interaction between a radio frequency (rf) magnetic field and the magnetic moments of spins of samples placed in a magnetic field. The magnetic moments of nuclei tend to precess around the magnetic field direction with a frequency called Larmor frequency. Of the NMR – measurable nuclei available in porous biosystems in natural abundance, ^{1}H is the most sensitive and has by far the highest concentration. Excitation of spins by a rf pulse disturbs the equilibrium in the nuclear spin system. A time-dependent rf signal is induced in the NMR measuring probe by the nuclear spin system as it returns to equilibrium. The NMR signals are characterised by a number of different parameters. Two relaxation-time constants describe the rate and manner at which the nuclear spin system returns to equilibrium after excitation. One time constant, the spin-lattice relaxation time T_1, describes the return to the equilibrium state in the direction of the magnetic field. The second time constant, the spin-spin relaxation time T_2, characterises the return in the plane perpendicular to the applied magnetic field. Both relaxation times depend on the physical environment (pore size and geometry, adsorbing walls, packing density) (Van As & Lens, 2001). NMR is also capable of discriminating proton spins of flowing and stationary water on the basis of the physical properties of the flow. The frequency of the signal given off by stationary spins will be constant in time, even in the presence of magnetic field gradients. However, when spins move from one position to another (diffusion, flow) in the presence of a magnetic field gradient, the frequency of these spins will change in time because of this displacement (Callaghan, 1994). Diffusion is the random translational motion of molecules or ions that is driven by internal thermal energy. Quantitative measurements of the effective diffusivity provide information on the shape and the interactions of the diffusing molecule (Nicolay *et al.* 2001).

Water in cells is compartmentalised into several major divisions, *i.e.* extracellular spaces, cytoplasm and vacuoles, and it can be conveniently monitored in large tissue samples using non-spatially resolved low frequency nuclear magnetic resonance (LF-NMR) techniques. Protons in different compartments are characterized by different transverse relaxation times (T_2), thus LF-NMR allowed to study a number of different physiological conditions in several fruits and vegetables, including changes caused by ripening, bruising, microbial infection, drying, freezing and high pressure processing (Marigheto *et al.*, 2004; Hills & Clark, 2003; Hills & Remigerau, 1997). The measurement of water self-diffusion could enrich such observations allowing the description of barriers, interfaces, and other noteworthy features inside compartmentalised structures (Hills & Clark 2003).

New Findings

Paper II, Paper III and ***Paper V*** report LF-NMR analysis to evaluate the changes on water mobility occurring at cellular level on *Actinidia deliciosa* kiwifruit, at two ripening stages during osmotic dehydration. By fitting the T_2-weighted curves to a continuous distribution of exponential curves, three proton pools were observed and ascribed (Cornillon, 2000) to cell compartments, *i.e.* vacuole, cytoplasm plus extracellular space and cell wall (Figure 12).

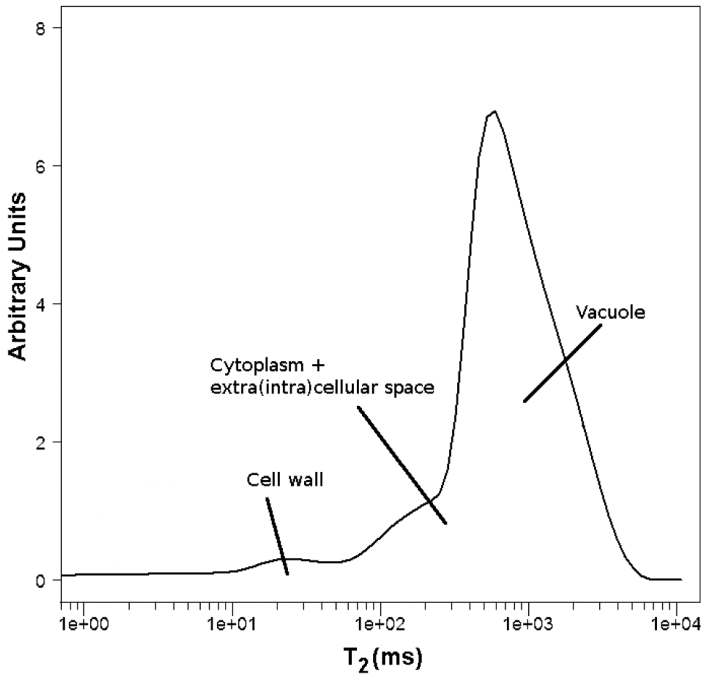

Figure 12. Example of T_2 spectrum obtained on kiwifruit treated 30 min at 25 °C (corresponding to Figure 1 in ***Paper III***).

Table 3 summarizes the cell compartment T_2 and absolute intensity values on raw and 300 min treated ripe (HB, high °Brix) and unripe (LB, low °Brix) kiwifruits along osmotic dehydration time. At t_0 LB samples, characterized by a solutes/water ratio lower than HB kiwifruits, showed higher T_2 both in the vacuole and in cytoplasm plus extracellular space. The water and solutes transfer promoted by osmosis

might modify the original kiwifruit cellular organisation and the subcellular structures. Osmotic dehydration had the effect of halving vacuole proton pool signal, with slight differences between HB and LB kiwifruits. The decrease of vacuole T_2 values might be due to vacuole water loss leading to its shrinkage (***Paper II***) causing a concentration of solutes, retained by the tonoplast. Table 3 shows, for HB kiwifruits, that the decrease of vacuole T_2 was parallel to an increase of cytoplasm plus extracellular space signal. Osmotic dehydration, by removing water from both compartments and increasing their solutes content, caused a marked T_2 decrease in both kiwifruit groups. Bowtell *et al.* (1992) found that during osmotic dehydration the cytoplasm, followed by the cellular membrane, stick to the shrinking tonoplast, allowing the formation of intracellular spaces. These last, filled with water from both the vacuoles and the osmotic solution, might contribute to the increase of the cytoplasm plus extracellular space proton pool (Table 3).

Table 3.
T_2 and absolute intensity values of the three proton pools identified through T_2-weighted curves for low (LB) and high (HB) °Brix raw (t_0) and 300 min treated kiwifruits. The intensities were scaled so that they equalled 100 in the case of raw HB fruits. (corresponding to Table 1 in ***Paper V***).

		Vacuole		Cytoplasm + extra-cell. space		Cell wall	
		t_0	300 min	t_0	300 min	t_0	300 min
LB	T_2 (ms)	$1321^{A} \pm 64$	$1009^{C} \pm 14$	$320^{A} \pm 21$	$221^{B} \pm 37$	19 ± 2	21 ± 5
	Intensity	$47^{b} \pm 9$	$25^{c} \pm 2$	$41^{a} \pm 5$	$36^{a} \pm 2$	10 ± 3	6 ± 2
HB	T_2 (ms)	$1227^{B} \pm 79$	$991^{C} \pm 92$	$303^{A} \pm 36$	$259^{AB} \pm 46$	21 ± 1	26 ± 6
	Intensity	$60^{a} \pm 8$	$31^{b} \pm 10$	$33^{b} \pm 3$	$37^{a} \pm 6$	7 ± 2	4 ± 1

$^{A\text{-}C,\ a\text{-}c.}$ The letters, capital for T_2 and low case for signal intensity, highlight the values which were found to be different with 95% confidence through a t test.

The phenomena observed through T_2 -weighted curves might be followed by determining the water self-diffusion coefficient (D_w). A first overall picture was obtained by considering the kiwifruit parenchyma, as a tissue with a homogeneous water distribution. This oversimplification allowed a quick evaluation of a single D_w value through one diffusion-weighted signal. For both LB and HB groups, D_w values of raw kiwifruits (Figure 13) resulted much lower than that of pure water ($2.3 \cdot 10^{-9}$ m^2 s^{-1} at 25 °C, Holz *et al.*, 2000). This was not unexpected, as cellular structures hinder water diffusion while solutes increase its viscosity. Indeed LB (Figure 13a), with low soluble solids content, showed higher D_w values than HB raw fruits (Figure 13b). To have a deeper insight into the consequences of the osmotic dehydration on each cell compartment of kiwifruit, the diffusion was analyzed through a multiple component model (see Materials and Methods section, ***Paper V***) leading to the estimation of the diffusion coefficient corresponding to the vacuole and cytoplasm plus extracellular space compartments. For both kiwifruit °Brix groups, Figure 13 shows water self-diffusion coefficients obtained respectively for vacuole ($D_{w,v}$), major proton population, and cytoplasm plus extracellular space ($D_{w,c}$). $D_{w,v}$ and $D_{w,c}$ values were respectively higher and lower than the D_w values calculated with the single component model for both kiwifruit °Brix groups. $D_{w,v}$ higher than $D_{w,c}$ may reflect the lower solutes/water ratio, as for T_2 values (Table 3).

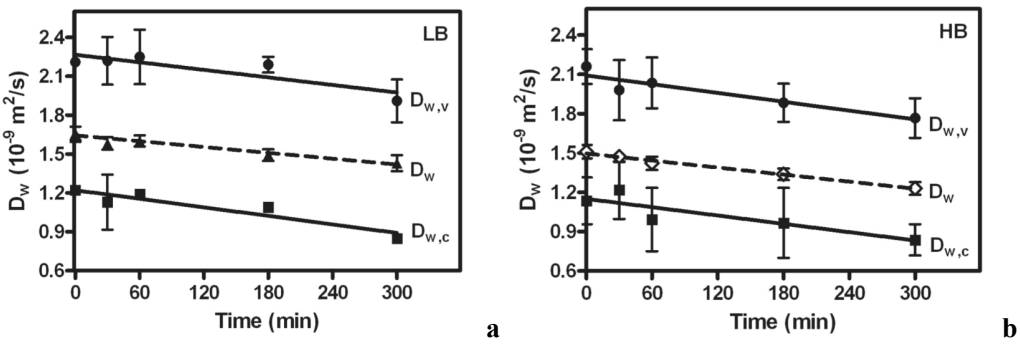

Figure 13. Water self-diffusion coefficients of **a** low (LB) and **b** high (HB) kiwifruits as a function of osmotic dehydration time. Filled symbols are average values obtained by applying the two components model, leading to two different water self-diffusion values for vacuole ($D_{w,v}$) and cytoplasm plus extra-cellular space compartment ($D_{w,c}$). Open symbols were obtained by applying the single component model (D_w). Lines show the fitting obtained using linear regression. Bars represent SD values (corresponding to Figure 4 in ***Paper V***).

4.1.3 Metabolic consequences

The mass transfer processes during osmotic treatment involve changes on the cell, *e.g.* the volume of protoplast may decrease (cellular shrinkage) and the plasma membrane may be damaged, reducing cellular viability. Ferrando & Spiess (2003) showed that osmotic stress did not affect the cellular viability of onion epidermis but significantly reduced the viability of protoplasts of strawberry in the whole range of sucrose solution concentrations tested (30 to 60% w/w). Mavroudis *et al.* (2004) found that, upon immersion of apple tissue in a 50% sucrose solution, cell death occurs and the depth of the layer of severely injured or dead cells coincides with the penetration depth of the osmotic solute. Absence of cell viability might be indicative of loss of mitochondrial activity upon osmotic dehydration (Towill & Mazur, 1975), which might negatively influence the respiration activity. Castelló *et al.* (2009) found a reduced oxygen consumption of treated sample with final soluble solids content of 20 °Brix.

New Findings

In ***Paper IV*** metabolic alterations of osmo-dehydrated kiwifruit as a function of ripening stage were studied. Kiwifruit as well as other fruit and vegetables are metabolic active tissues producing heat as a result of respiration. Figure 14 shows an example of heat production profiles of a negative control (heat treated kiwifruit), a raw and an osmodehydrated LB (low °Brix) kiwifruit sample, during 24 h at 20 °C. The thermograms evidenced a progressively decreased of the specific thermal power P (mW g_{fw}^{-1}) by increasing the treatment time. A similar behaviour was obtained for HB (high °Brix) kiwifruit.

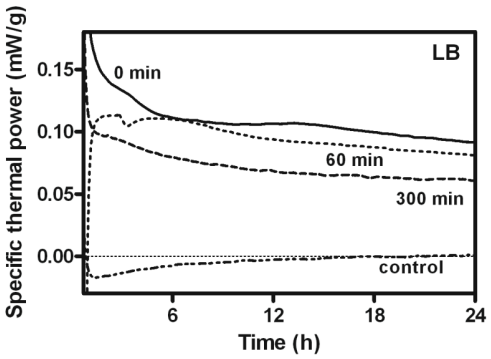

Figure 14. Specific thermal power profiles of pericarp tissue cylinders of raw (0 min), cooked (control) and selected osmo-dehydrated kiwifruit during 24 h of analysis at 20 °C. Each thermogram is an average of four replicates. The initial signal disturbance is a consequence of sample ampoule loading (corresponding to Figure 4 in ***Paper IV***).

The aerobic cell respiration produces about 455 kJ of heat per mol of O_2 consumed or mol of CO_2 produced, thus calorimetric measurements on tissue metabolism may give similar information as respiration measurements (Wadsö & Gómez Galindo, 2009). The respiration within the 24 h of analysis was considered aerobic (***Paper IV***) and the thermal power values (mJ s^{-1} g^{-1}) were expressed as heat of respiration ($RRO_{2,cal}$) (gO_2 h^{-1} kg^{-1}). Respiration measurements (RRO_2, gO_2 h^{-1} kg^{-1}) performed on HB raw and 60 min treated kiwifruit samples were compared with the heat production results. Figure 15a shows that RRO_2 values obtained by gas measurement and $RRO_{2,cal}$ values calculated from calorimetric analysis resulted positively correlated for both raw and 60 min treated samples ($r > 0.98$).

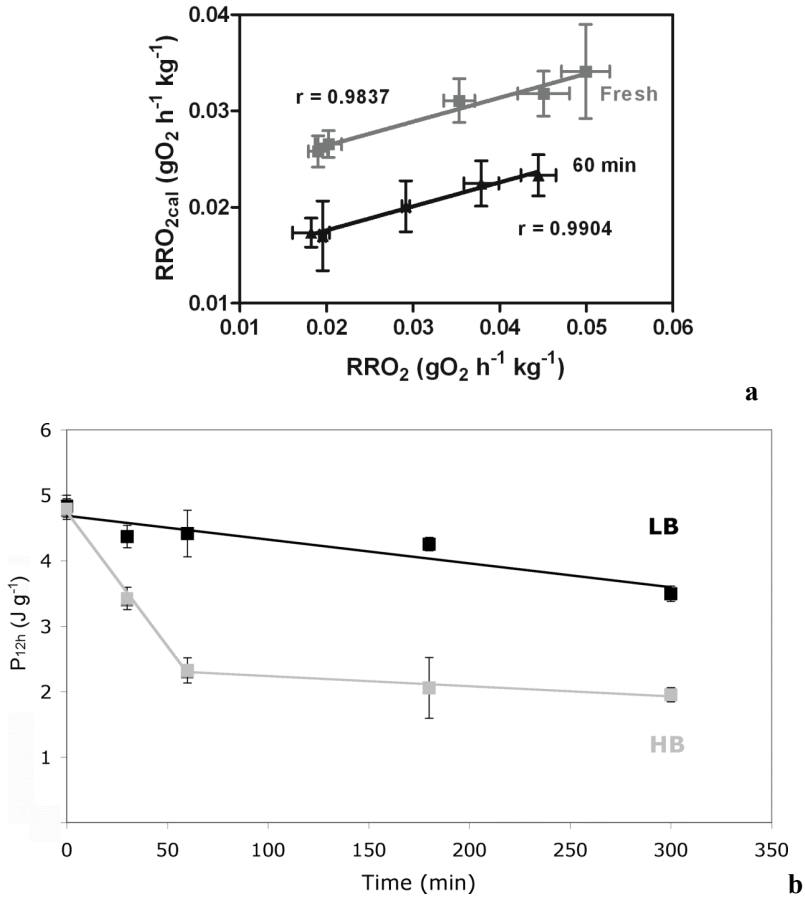

Figure 15. **a** Linear correlation between respiration rate obtained by O_2 measurement (RRO_2) or calculated from specific thermal power curves (RRO_{2cal}) for raw and 60 min treated HB samples; **b** Specific heat production (P_{12h}) (J g^{-1}) results *vs* treatment time for LB and HB samples (corresponding to Figure 5 and 6 in ***Paper IV***).

To better understand the effect of osmotic dehydration on the metabolic heat of both LB and HB samples, the thermal power curves were integrated from 1 to 13 h of analysis and the obtained specific heat production (P_{12h}) (J g^{-1}) results *vs* treatment time are reported in Figure 15b. The metabolic heat production of the raw samples appeared very similar for both the ripening stage investigated and progressively decreased with the increasing of treatment time. During osmotic dehydration tissue damage progressively occurred (***Paper III***) and, as suggested by Gómez Galindo *et al.* (2004), the decrease in thermal power might be correlated with cell membrane damage. Metabolic heat production of LB kiwifruit samples showed a linear decrease with the proceeding of OD; instead, the detected heat production for HB samples sharply decreased along the first 60 min of the treatment. These differences can be explained by the different physiological state of the fruit tissue. Cells of more ripe kiwifruit seemed more sensitive to osmotic stress possibly because of their increased membrane permeability due to the loss of membrane integrity upon kiwifruit ripening (Song *et al.*, 2009).

4.1.4 Industrial application

The use of osmotic dehydration process in the food industry has several advantages: (i) quality retention in terms of colour, flavour, and texture, (ii) energy efficiency, reduction in packaging and distribution

costs, (iii) elimination of the need for chemical treatments, (iv) increase of product stability and (v) retention of nutrients during storage (Shi & Le Maguer, 2002).

It is well established that osmotic dehydration applied as a pre-treatment in air-drying processing of fruit and vegetable using solutions of different molecules, such as of sodium chloride, sucrose, citric acid, sorbitol, glycerol, maltodextrin or corn syrup, may improve the overall acceptability of the final product (Bidaisee & Badrie, 2001; Ertekin & Cakaloz, 1996; Torreggiani, 1995, Kim & Toledo, 1987). Minerals or functional substances could be fortified in vegetables and fruits by applying the osmotic process. Calcium showed the capability of strengthening cell structure, which diminished effective diffusivities. Osmodehydrated apple showed much lower and uniform shrinkage compared to the air-dried control, at the same level of moisture content (Moreira & Sereno, 2003). Fito & Pastor (1994) explored the possibility of formulating functional, stable, and fresh-like products by incorporating minerals, vitamins, and health-beneficial functional components in the osmotic solution, in addition to water activity or pH depressors and antimicrobial components (Derossi *et al.*, 2011; Barrera *et al.*, 2004; Moreira & Sereno, 2003). Canning using high-moisture fresh fruits and vegetables is not practiced commercially as water can flow from the product to the syrup brine causing dilution. This can be avoided using the *osmocanning* process to improve product stability. Osmocanning involves the use of osmotically treated raw material in the canning process, promoting a firmer texture and improved overall quality of the product (Barrera *et al.*, 2004; Sharma *et al.*, 1991).

Osmotic dehydration is a less energy-intensive process than air- or vacuum-drying because it can be conducted at low temperatures. Lenart & Lewicki (1988) found that energy consumption in osmotic dehydration at 40°C, with syrup reconcentration by evaporation, was at least two times lower than convection air-drying at 70°C. In the frozen food industry, high energy levels are used for freezing, because a large quantity of water is present in fresh foods. A significant proportion of this energy could be saved if the plant materials is concentrated prior to freezing (Beedie, 1995; Huxsoll, 1982).

Chemical treatments to reduce enzymic browning can be avoided by the osmotic process. There are two effects of sugar in producing high-quality product: effective inhibition of polyphenol oxidase, the enzyme that catalyzes oxidative browning of many cut fruits, and prevention of the loss of volatile flavour during further air- or vacuum-drying (Ponting *et al*., 1956).

4.2 Vacuum impregnation

Vacuum impregnation is a unit operation in which porous products are immersed in a solution of different compositions and/or concentrations and subjected to a two-step pressure change. The first step (vacuum increase) consists of the reduction of the pressure in a solid-liquid system. During this step, the gas in the product pores is expanded and partially flows out until mechanical equilibrium is achieved. When the atmospheric pressure (second step) is restored, the residual gas in the pores compresses and the external liquid flows into the pores (Tylewicz *et al.*, 2011). Compared to the classical diffusion processes, such as candying, salting, soaking, osmotic dehydration, which are carried out by simple dipping or prolonged immersion of the product in the solution for several hours or days, vacuum impregnation has the advantage of a fast penetration – only few minutes – of the active substances directly into the internal structure of the product (Saurel *et al.*, 1994).

4.2.1 Transport phenomena and structural changes

Impregnation takes place due to the action of hydrodynamic mechanisms (HDM) brought about by pressure changes (Fito, 1994; Fito & Pastor, 1994). A model was constructed by regarding the pores of the plant tissue as ideal cylinders of constant diameter, facing the liquid solution. The change in pore volumetric fraction occupied by the liquid was considered to be a function of the internal pressure in the pore (p_i), the capillary pressure (p_c) and the pressure acting on the liquid (p_l) (expressed in Pa). The capillary pressure is related to the characteristics of the pores and is defined by the Young-Laplace equation (Dullien, 1992):

$$p_c = \sigma\left[\frac{1}{r_1}+\frac{1}{r_2}\right]\cos\theta \tag{2}$$

where σ is the interfacial tension (N m^{-1}), r_1 and r_2 are the principal radii of the pores in (m) and θ is the contact angle (rad).

The interaction between air and liquid during the two steps of vacuum impregnation has been studied extensively in single, ideal cylindrical pores (Fito & Pastor, 1994) and in micromodels (Badillo *et al.*, 2011; Lenormand, 1990). However, to the best of our knowledge, it has not been studied directly in plant tissues.

New Findings

Paper VI aimed at determining on raw materials with different morphological and porosity characteristics, *i.e.* apple and spinach, the pressure at which gas was released from the pores (seen as bubbles) during the application of vacuum, and the pressure at which tissue impregnation took place during the restoration of atmospheric pressure. Micrographs of tissues subjected to vacuum impregnation

were recorded as the pressure in the treatment chamber (Figure 16a and Figure 16b) was varied by using an automatic vacuum controller system.

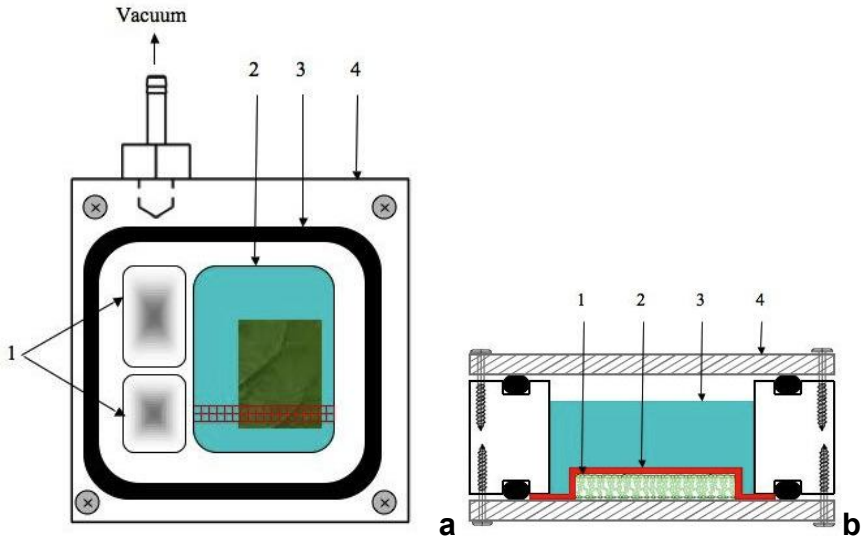

Figure 16. Scheme of the chamber used for vacuum impregnation. **a** Top view: 1. Vacuum pre-chambers, 2. Main chamber containing sample and impregnating solution, 3. O-ring, 4. Plastic frame; **b** Cross section: 1. Sample, 2. Plastic fastener, 3. Impregnating solution, 4. Upper and lower glass plates sealed to the plastic frame by the O-ring (corresponding to Figure 2 a,b in ***Paper VI***).

Bubbles were visible for the apple samples from the beginning of vacuum impregnation, indicating a pressure threshold for gas outflow of 860 ± 15 mbar. Spinach tissue, however, showed bubbling at a late stage in vacuum formation, in the range of 554 ± 56 mbar. Furthermore, the size of the bubbles leaving spinach pores was less than one-hundredth of that of the bubbles leaving the pores in apple tissue, at the respective outflow threshold.

Figure 17 shows images of apple and spinach tissues taken at: (i) 150 mbar, the minimum absolute pressure employed, (ii) during atmospheric pressure restoration, where bright regions appeared in the samples due the impregnation of the tissue, and (iii) at the end of vacuum impregnation (at atmospheric pressure), where the translucency of the sample increased in the whole area, indicating homogeneous impregnation of both the apple and spinach samples. The results regarding the change in tissue translucency obtained from image analysis revealed the pressure thresholds for pore impregnation, which were in the range of 220 ± 27 mbar for spinach and 173 ± 2 mbar for apple.

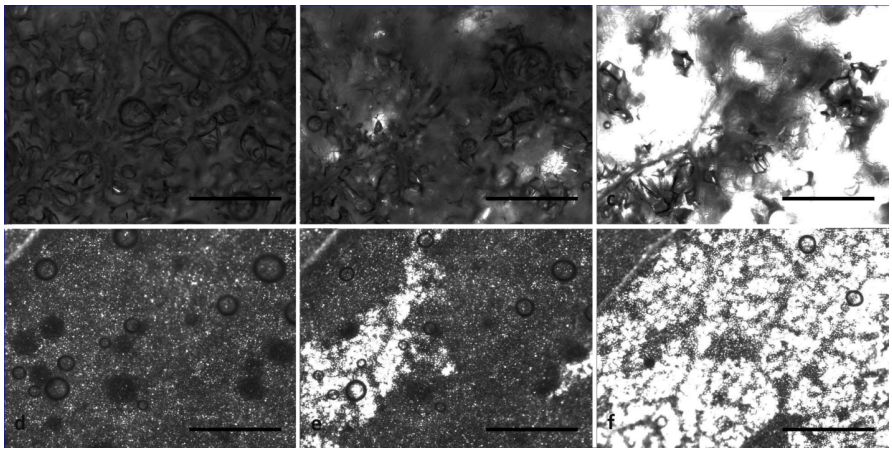

Figure 17. Examples of microscope images of apple (a, b, c) and spinach (d, e, f) samples during the restoration of atmospheric pressure. Scale bar = 1 mm. (a) and (d) were recorded at the minimum pressure (150 mbar); (b) and (e) at pressures of 330 mbar and 450 mbar, respectively, and (c) and (f) at atmospheric pressure (*i.e.* at the end of vacuum impregnation) (corresponding to Figure 6 in ***Paper VI***).

Spinach tissue showed incipient bubbling, *i.e.* the release of gas, at a much lower pressure than apple, and impregnation commenced at a much higher pressure. These differences are believed to be the result of the narrow pores, the higher porosity and possible changes in volume of the spinach leaves (*i.e.* leaf expansion during the application of vacuum and recompression during the restoration of atmospheric pressure).

4.2.2 Metabolic consequences

To the best of our knowledge, little attention has been given to the investigation of both long- and short-term tissue metabolic responses upon the application of vacuum impregnation. Castelló *et al.* (2010) reported the respiration rate during one week of storage of strawberries impregnated with a hypertonic sucrose solution. The impregnated fruits showed lower respiration rate and higher respiration quotient than the untreated fruits during the whole period, suggesting the onset of anaerobic metabolism. Regarding short-term effects of vacuum impregnation on tissue metabolism, MacDonald *et al.* (1975) showed that, immediately after impregnation with water, the photosynthetic activity of wheat leaves decreased to one fifth, however, over the first 4 h after vacuum impregnation, the effect on the respiration rate was negligible. Tylewicz *et al.* (2011) demonstrated that vacuum impregnation in the presence of different sugars (sucrose and trehalose) results in the formation of membrane vescicle inside the cells already 30 min after impregnation. As vesciculation is regarded to be a metabolic consequence of the impregnation progress, the authors suggested short-term metabolic responses provoked by vacuum impregnation.

New Findings

In ***Paper VII*** short-term gross metabolic responses of spinach leaves induced by the application of vacuum impregnation with different sugars were explored. Changes in metabolic heat rate were studied

by using isothermal calorimetry. Calorimetric measures of the heat production rate of a biological tissue is related to its metabolic rate and provides a direct indication of integrated metabolic responses, such as respiration and reaction to stress (Gómez Galindo *et al.*, 2008; Criddle *et al.*, 1991).

Calorimetric measurements provided evidence of a drastic increase of spinach leaf gross metabolism as a consequence of impregnation with trehalose and sucrose isotonic solutions (Figure 18).

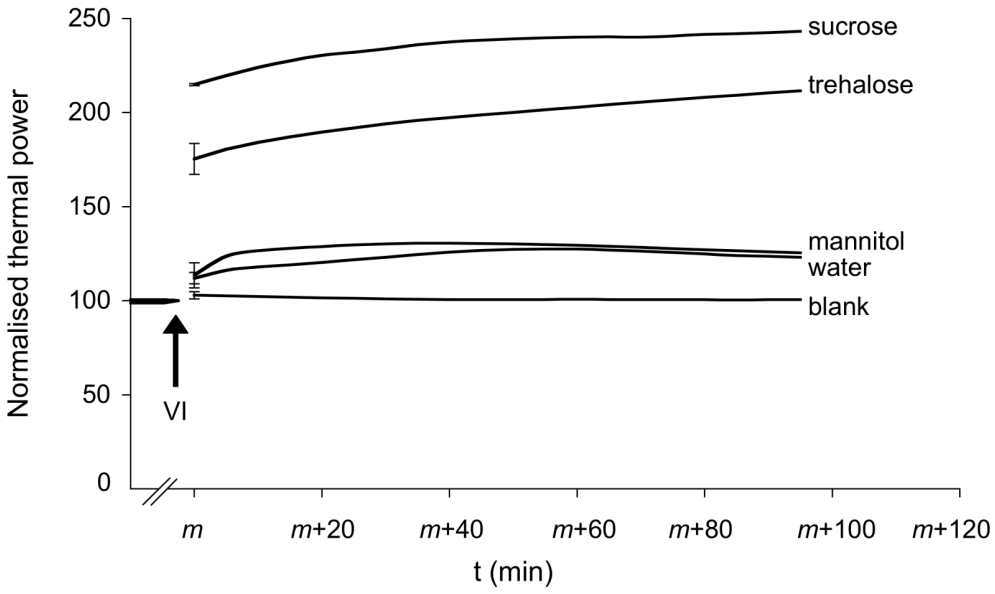

Figure 18. Calorimetric metabolic heat rate measurements of spinach samples subjected to VI. Spinach was impregnated with sucrose solution (13%), trehalose solution (11%), mannitol solution (8%), water or no solution (blank). Average curves from three replicates are shown. The variable *m* (min) in the x-scale is defined by $m = t_1 + t_2 + t_3$, where t_1 is the duration of the initial disturbance of the calorimetric measurement; t_2 is the time for the thermal power to stabilise before the application of vacuum; t_3 is the duration of the disturbance provoked by VI. For each heat production rate curve, within the time interval described by the variable *m*, the initial stable thermal power value normalised to 100 is reported. For each curve is reported the confidence limit (SEM, n=3) of the first heat rate value measured after VI.

With the application of VI, extracellular air is replaced by the impregnation solution, potentially limiting tissue respiration to any remaining volume of air in the tissue. However the fact that the impregnated leaves show photosynthetic activity (Figure 19a) strongly suggests that not all air was exhausted during VI. Therefore, in a separate experiment, KCN and SHAM were impregnated together with the sugars (Figure 19b). The results clearly demonstrate that the metabolic response responsible for the drastic increase in gross metabolism upon VI depends on the mitochondrial oxygen consuming pathways. Interestingly, the metabolic effect involving mannitol (Figure 18) was less pronounced and comparable with water impregnation, suggesting that the strong metabolic effect here reported might be influenced by sugars that can be metabolized by the cells.

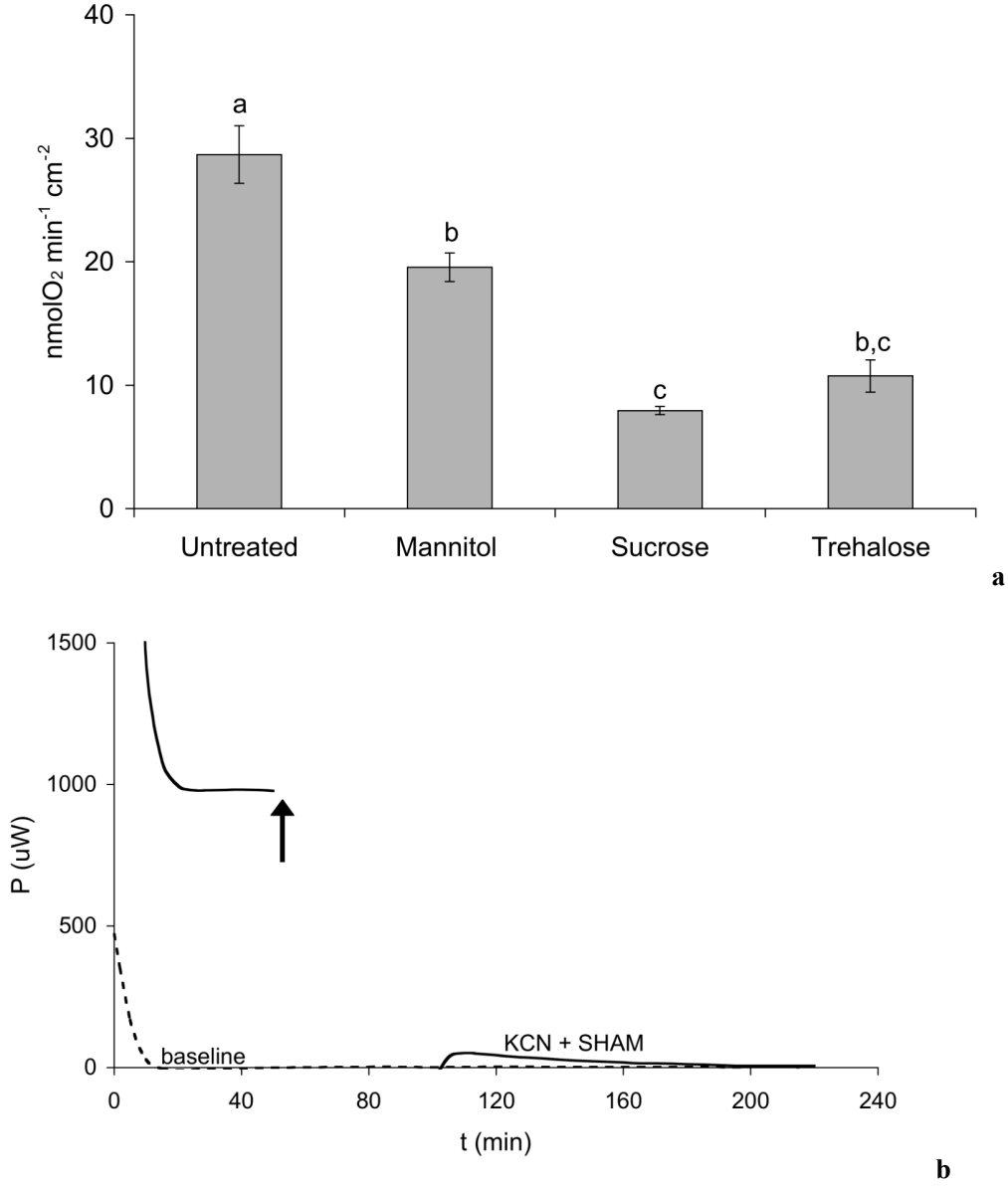

Figure 19. **a** Photosynthesis measurements in untreated, mannitol, sucrose and trehalose impregnated spinach. Average and SEM from at least three replicates is reported. Different letters indicate statistical differences ($p < 0.05$); **b** Typical calorimeter output (mW) from spinach tissue subjected to VI with sucrose or trehalose mixed with the metabolic inhibitors KCN and SHAM (continuous line). VI was applied (the time of VI application is indicated with an arrow in the continuous line). After an initial disturbance, VI was applied (the time of VI application is indicated with an arrow in the continuous line). Application of vacuum provoked a second disturbance where the thermal power values were outside the detectable range for about 50 min (gap of values in the continuous line) and, once back within the detectable range, the disturbance in the calorimetric measurements lasted about 20 more min before recording the real thermal power from the impregnated sample, which was close to the baseline of the calorimeter (dashed line).

4.2.3 Industrial application

Food industry has an increasing interest in fruit and vegetable-based products, particularly in the value-added and minimally processed market because of their significant health benefit and favourable flavour and colour. Vacuum impregnation in fruit and vegetable processing may have two important functions: formulation and dewatering. The solution used for vacuum impregnation can be enriched with different additives such as anti-browning agents, pH reducers and microbial preservatives, increasing the microbial

stability and allowing shelf-life extension (Fito *et al.*, 2001, Sapers *et al.,* 1990). Nutraceuticals may also be introduced into the porous structure of plant tissue for developing nutritionally fortified fruit and vegetable products. Betoret *et al*. (2003) studied probiotic enriched dried fruits by vacuum impregnation with commercial apple juice containing *Saccharomyces cerevisiae*, and with whole milk or apple juice containing *Lactobacillus casei*, obtaining similar concentration levels of probiotics than that in commercial dairy products. Calcium fortification of vacuum impregnated fruit and vegetables was studied by Gras *et al.* (2003) and Barrera *et al.* (2009). Vacuum impregnation applied prior freezing has been studied to improve the quality of frozen fruit and vegetable products by mainly reducing of drip loss and improving texture quality, as well as saving energy consumption during freezing (Xie & Zhao, 2003; Martinez-Monzo *et al.,* 1998).

New Findings

The mass transfer taking place during vacuum impregnation depends on the characteristics of the tissue pores. Effective vacuum impregnation requires the efficient removal of air from the tissue during vacuum treatment to obtain complete filling of the tissue during the subsequent impregnation step. The findings of the study reported in ***Paper VI*** may allow food manufacturers to optimize vacuum impregnation parameters depending on the porosity characteristics of the raw material.

5. Conclusions

The study on osmotic dehydration of kiwifruits has resulted in interesting findings. The following remarks underline important results:

- The changes of mass transfer parameters and kiwifruit thermal properties, upon the application of osmotic dehydration, depend on the processing temperature and the kiwifruit species and ripening stage;
- Osmotic dehydration alters the water distribution among the cell compartments and promotes the formation of tissue intracellular spaces;
- Osmotic dehydration promotes cell wall changes, *i.e.* wall swelling and dissolution of the middle lamella;
- Osmotic dehydration alters the tissue metabolic heat rate depending on treatment time and tissue ripening stage.

The results presented in this thesis represent a step forward in the understanding of spinach leaves vacuum impregnation mass transfer parameters and its metabolic consequences:

- A microscopic method has been developed to detect pressure thresholds for gas outflow and solution impregnation during the treatment. This method contributes to the clarification of the mechanisms of mass transfer in vacuum impregnation, as the interaction between air and liquid during the treatment is studied directly in plant tissues.
- The short-term metabolic response of spinach tissue to the application of VI involves mitochondrial oxygen consuming pathways. The increase of spinach metabolism upon VI is related to the impregnated molecule. Metabolizable molecules (*e.g.* sucrose, trehalose) seem the main stimulants of metabolic activity. The direct effects of the mechanical treatment instead appear quite low.
- Spinach impregnation appears to reach a maximum with remaining gas-filled compartments.

References

Abd-Elrahman M. I., & Ahmed S. M. (2009) Thermal degradation kinetics and geometrical stability of D-sucrose. *International Journal of Polymeric Materials*, 58: 322–335.

Aguilera J M, Chiralt A, & Fito P (2003) Food dehydration and product structure. *Trends in Food Science & Technology,* 14: 432-437.

Alberts B, Bray D, Hopkin K, Johnson A, Lewis J, Raff M, Roberts K, & Walter P (2009) *Enlarge essential cell biology*. Garland Science, Taylor & Francis Group.

Badillo G M, Segura L A, & Laurindo J B (2011) Theoretical and experimental aspects of vacuum impregnation of porous media using transparent etched networks. *International Journal of Multiphase Flow*, 37: 1219–1226

Barboni T, Cannac M, & Chiaramonti N (2010) Effect of cold storage and ozone treatment on physicochemical parameters, soluble sugars and organic acids in *Actinidia deliciosa. Food Chemistry,* 121: 946–951.

Barrera C, Betoret N, & Fito P (2004) Ca^{2+} and Fe^{2+} influence on the osmotic dehydration kinetics of apple slices *(var. Granny Smith)*. *Journal of Food Engineering*, 65: 9-14.

Barrera C, Betoret N, Corell P, & Fito P (2009) Effect of osmotic dehydration on the stabilization of calcium-fortified apple slices (var. Granny Smith): Influence of operating variables on process kinetics and compositional changes. *Journal of Food Engineering*, 92: 416–424.

Beaulieu J (2010) Factors affecting sensory quality of fresh-cut produce. In: Martin-Belloso O, & Soliva-Fortuny R, *Advances in Fresh-Cut Fruits and Vegetables Processing*, CRC Press, Boca Raton, 115–143.

Beedie M (1995) Energy saving – a question of quality. *South African Journal of Food Science and Technology,* 48: 14-16.

Beirão da Costa S, Steiner A, Correia L, Empis J, & Moldão Martins M (2006) Effects of maturity stage and mild heat treatments on quality of minimally processed kiwifruit. *Journal of Food Engineering*, 76: 616-625.

Bennett A B (2002) Biochemical and genetical determinants of cell wall disassembly in ripening fruit: a general model. *HortScience*, 37: 3–6.

Betoret N, Puente L, Diaz M J, Pagan M J, Garcia M J, Gras M L, Marto J, & Fito P (2003) Development of probiotic-enriched dried fruits by vacuum impregnation. *Journal of Food Engineering*, 56: 273–277.

Bidaisee G, & Badrie N (2001) Osmotic dehydration of cashew apples (*Anacardium occidentale L.*): quality evaluation of candied cashew apples. *International Journal of Food Science & Technology,* 36: 71-78.

Biliaderis C G (1983) Differential scanning calorimetry in food research — a review. *Food Chemistry,* 10: 239–265.

Bonilla-Zavaleta E, Vernon-Carter E J, Beristain C O (2006) Thermophysical properties of freeze-concentrated pineapple juice. *Italian Journal of Food Science,* 18: 367-376.

Bowtell R, Mansfield P, Sharp J C, Brown G D, McJury M, & Glover P M (1992) NMR microscopy at 500 MHz: Cellular resolution in biosystems. In: Blümich B, & Kuhn W*, Magnetic Resonance Microscopy*, VCH, Weinheim, Germany, 427-439.

Bressa F, Dalla Rosa M, & Mastrocola D (1997) Use of a direct osmosis treatment to produce minimally processed kiwifruit slices in a continuous pilot plant. *Acta Horticulturae*, 444: 649–654.

Bush D R (1993) Proton-coupled sugar and aminoacid transporters in plants. *Annual Review of Plant Physiology and Plant Molecular Biology*, 44: 513-542

Callaghan P (1994) *Principles of nuclear magnetic resonance microscopy*, Oxford University Press.

Cao H, Zhang M, Mujumdar A S, Du W H, & Sun J C (2006) Optimization of osmotic dehydration of kiwifruit. *Drying Technology,* 24: 89-94.

Castelló M L, Fito P J, & Chiralt A (2010) Changes in respiration rate and physical properties of strawberries due to osmotic dehydration and storage. *Journal of Food Engineering,* 97: 64-71.

Castelló M L, Igual M, Fito P J, & Chiralt A (2009) Influence of osmotic dehydration on texture, respiration and microbial stability of apple slices (*Var. Granny Smith*). *Journal of Food Engineering*, 91: 1–9.

Chiralt A, & Fito P (2003) Transport mechanisms in osmotic dehydration: The role of the structure. *Food Science and Technology International*, 9: 179–186.

Cornillon P (2000) Characterization of osmotic dehydrated apple by NMR and DSC. *LWT - Food Science & Technology*, 33: 261-267.

Criddle R S, Breindenbach R W, & Hansen L D (1991) Plant calorimetry: How to quantitatively compare apples and oranges. *Thermochimica Acta,* 193: 67-90.

Delgado A E, Sun D W, &, Rubiolo A C (2012) In: Sun D W, *Thermal Food Processing. New Technologies and Quality Issues*, Second Edition, CRC Press, Boca Raton, 3-32.

Derossi A, De Pilli T, La Penna M P, & Severini C (2011) pH reduction and vegetable tissue structure changes of zucchini slices during pulsed vacuum acidification. *LWT - Food Science and Technology*, 44: 1901-1907.

Dixon G M, & Jen J J (1977) Changes of sugars and acids of osmovac-dried apple slices. *Journal of Food Science*, 42: 1136–1140.

Driouich A, Levy S, Staehelin L A, & Faye L (1994) Structural and functional organization of the Golgi apparatus in plant cells. *Plant Physiology and Biochemistry,* 32: 731–749.

Dullien F A L (1992) *Porous media: fluid transport and pore structure*, Second edition, Academia Press, USA.

Einhorn-Stoll U, Kunzek H, & Dongowski G (2007) Thermal analysis of chemically and mechanically modified pectins. *Food Hydrocolloids*, 21: 1101-1112.

Ertekin F K, & Cakaloz T (1996) Osmotic dehydration of peas II. Influence of osmosis on drying behavior and product quality. *Journal of Food Processing and Preservation*, 20:105-119.

Evert R F (2006) *Esau's Plant Anatomy: Meristems, Cells, and Tissues of the Plant Body: Their Structure, Function, and Development*, John Wiley & Sons, Hoboken, New Jersey.

Ferrando M, & Spiess W (2003) Effect of osmotic stress on microstructure and mass transfer in onion and strawberry tissue. *Journal of Food Science and Agriculture*, 83: 951–959

Finkelstein A (1987) *Water movement through lipid bilayers, pores, and plasma membranes: theory and reality*, Wiley, New York.

Fish B P (1958) *Diffusion and thermodynamics of water in potato starch. Fundamental aspects of the dehydration of food stuffs*, Soc. Chem. Ind., London.

Fito P (1994) Modelling of vacuum osmotic dehydration of food. *Journal of Food Engineering,* 22: 313-28.

Fito P, & Chiralt A (1996) Osmotic dehydration, an approach to modelling of solid food–liquid operations. In: *Food Engineering 2000*, Chapman and Hall, London.

Fito P, Chiralt A, Betoret N, Gras M, Cháfer M, Martínez-Monzó J, Andrés A, & Vidal D (2001) Vacuum impregnation and osmotic dehydration in matrix engineering. Application in functional fresh food development. *Journal of Food Engineering,* 49: 175–183.

Fito P., & Pastor R. (1994) Non-diffusional mechanisms occurring during vacuum osmotic dehydration. *Journal of Food Engineering*, 21: 513-519

Friedman M H (1986) *Principles and models of biological transport*, Springer Verlag, Berlin.

Gómez Galindo F, Teledo R, Wadsö L, Gekas V, & Sjöholm I (2004) Isothermal calorimetry approach to evaluate tissue damage in carrot slices upon thermal processing. *Journal of Food Engineering*, 65: 165-173.

Gómez Galindo F, Wadsö L, Vicente A, & Dejmek P (2008) Exploring metabolic responses of potato tissue induced by electric pulses. *Food Biophysics,* 3: 352 -360.

Goñi O, Muñoz M, Ruiz-Cabello J, Escribano M I, & Merodio C (2007) Changes in water status of cherimoya fruit during ripening. *Postharvest Biology and Technology*, 45:147-150.

Gras M L, Vidal D, Betoret N, Chiralt A, & Fito P (2003) Calcium fortification of vegetables by vacuum impregnation. Interactions with cellular matrix. *Journal of Food Engineering*, 56: 279–284.

Gu L, Pallardy S G, Tu K, Law B E, & Wullschleger S D (2010) Reliable estimation of biochemical parameters from C3 leaf photosynthesis–intercellular carbon dioxide response curves. *Plant, Cell & Environment*, 33: 1852–1874.

Gunning E S, & Steer M W (1996) Plant Cell Biology: Structure and Function, Jones & Bartlett, Boston.

Hawlicka E. (1995) Self-diffusion in multicomponent liquid systems. *Chemical Society Reviews,* 34: 13743–13750.

Hills B P, & Clark C J (2003) Quality assessment of horticultural products by NMR. *Annual Reports on NMR Spectroscopy*, 50: 75–120

Hills B P, & Duce S L (1990) The influence of chemical and diffusive exchange on water proton transverse relaxation in plant tissue. *Magnetic Resonance Imaging*, 8: 321-331.

Hills B P, & Remigerau B (1997) NMR studies of changes in subcellular water compartmentation in parenchyma apple tissue during drying and freezing. *International Journal of Food Science and Technology*, 32: 51–61.

Holz M, Heil S R, & Sacco A (2000). Temperature-dependent self-diffusion coefficients of water and six selected molecular liquids for calibration in accurate ^{1}H NMR PFG measurements. *Physical Chemistry Chemical Physics*, 2: 4740–4742.

Huxsoll C C (1982) Reducing the refrigeration load by partial concentration of foods prior to freezing. *Food Technology*, 35: 98-102.

Jackman R L, & Stanley D W (1995) Perspectives in the textural evaluation of plant foods. *Trends in Food Science & Technology,* 6: 187-194.

Kaymak-Ertekin F, & Sultanoglu M (2000) Modelling of mass transfer during OD of apples. *Journal of Food Engineering*, 46, 243–250.

Kim M H, & Toledo R T (1987) Effect of osmotic dehydration and high temperature fluidized bed drying on properties of dehydrated blueberries. *Journal of Food Science*, 52 : 980-984.

Knight M R, Campbell A K, Smith S M, & Trewavas A J (1991) Transgenic plant aequorin reports the effects of touch and cold-shock and elicitors on cytoplasmic calcium. *Nature*, 352: 524-526.

Kowalska H, & Lenart A (2001) Mass exchange during osmotic pretreatment of vegetables. *Journal of Food Engineering*, 49, 137–140.

Lazarides H N, Katsanidis E, & Nickolaidis A (1995) Mass transfer kinetics during osmotic preconcentration aiming at minimal solid uptake. *Journal of Food Engineering*, 25: 151-166.

Lenart A, & Lewicki P P (1988) Energy consumption during osmotic and convective drying of plant tissue. *Acta Alimentaria Polonica,* 14: 65-72.

Leistner L. (1995) Principles and applications of hurdle technology. In: Gould G W, *New Methods of Food Preservation*, Ed. Blackie Academic & Professional, London.

Lenormand R (1990) Liquids in porous media. *Journal of Physics: Condensed Matter*, 2: 79–88.

Lerici C L, Pinnavaia G, Dalla Rosa M, & Bartolucci L (1985) OD of fruit: Influence of osmotic agents on drying behaviour and product quality. *Journal of Food Science,* 50: 1217–1219

Lloyd T, & Wyman C E (2003) Application of a depolymerization model for predicting thermochemical hydrolysis of hemicellulose. *Applied Biochemistry and Biotechnology*, 105–108.

Logan H, Basset, M, Very A A, & Sentenae H (1997) Plasma membrane transport systems in higher plants: From black boxes to molecular physiology. *Physiologia Plantarum,* 100: 1-15.

Loo D D F, Zeuthen T, Chandy G, & Wright E M (1996) Cotransport of water by the Na^+/glucose cotransporter. *Proceedings of the National Academy of Sciences of the United States of America*, 93: 13367–13370.

Manzoor H, Chiltz A, Madani S, Vatsa P, Schoefs B, Pugin A, & Garcia-Brugger A (2012) Calcium signatures and signaling in cytosol and organelles of tobacco cells induced by plant defense elicitors. *Cell Calcium*, 51: 434-444.

Marigheto N, Vial A, Wright K, & Hills B (2004) A combined NMR and microstructural study of the effect of high pressure processing on strawberries. *Applied Magnetic Resonance*, 26: 521-531

Marshall A G (1978) *Biophysical Chemistry. Principles, Techniques, and Applications*, Wiley, New York.

Martinez-Monzo J, Martinez-Navarrete N, Chiralt A, & Fito P (1998) Mechanical and structural change in apple (var. Granny Smith) due to vacuum impregnation with cryoprotectants. *Journal of Food Science*, 63: 499–503.

Maurel C, Verdoucq L, Luu DT, & Santoni V (2008) Plant aquaporins: membrane channels with multiple integrated functions. *Annual Review of Plant Biology,* 59: 595-624.

Mavroudis N E, Dejmek P, & Sjöholm I (2004) Studies on some raw material characteristics in different Swedish apple varieties. *Journal of Food Engineering*, 62: 121-129.

Moreira R, & Sereno A M (2003) Evaluation of mass transfer coefficients and volumetric shrinkage during osmotic dehydration of apple using sucrose solutions in static and non-static conditions. *Journal of Food Engineering*, 57: 25-31.

Muntada V, Gerschenson L N, Alazamora S M and Castro, M A (1998) Solute infusion effects on texture of minimally processed kiwifruit. *Journal of Food Science*, 63: 616–620.

Nicolay K, Braun K P J, Graaf R A, Dijkhuizen R M, & Kruiskamp M J (2001) Diffusion NMR spectroscopy. *NMR in Biomedicine*, 14: 94–111.

Nieto A B, Salvatori D M, Castro M A, & Alzamora S M (2004) Structural changes in apple tissue during glucose and sucrose osmotic dehydration: shrinkage, porosity, density and microscopic features. *Journal of Food Engineering,* 61: 269-278.

Nieto A, Salvatori D, Castro MA, & Alzamora S M (1998) Air drying behaviour of apples as affected by blanching and glucose impregnation. *Journal of Food Engineering*, 36: 63-79.

Nobel P.S. (1991) *Physicochemical and environmental plant physiology*. San Diego: Academic Press Inc.

Palou E, Lopez-Malo A, Argaiz A, & Welti J (1994) Use of Peleg's equation to osmotic concentration of papaya. *Drying Technology,* 12: 965-978.

Peleg M (1988) An empirical model for the description of moisture sorption curves. *Journal of Food Science*, 53: 1216–1217.

Pereira L M, Carmello-Guerreiro S M, & Hubinger M D (2009) Microscopic features, mechanical and thermal properties of osmotically dehydrated guavas. *LWT - Food Science & Technology*, 42: 378-384.

Phoon P Y, Gómez G F, Vicente A, & Dejmek P (2008) Pulsed electric field in combination with vacuum impregnation with trehalose improves the freezing tolerance of spinach leaves. *Journal of Food Engineering*, 88: 144–148.

Ponting J D, Watters G G, Forrey R R, Jackson R, & Stanley W L (1966) Osmotic dehydration of fruits. *Food Technology*, 20: 125-128.

Prinzivalli C, Brambilla A, Maffi D, Lo Scalzo R, & Torreggiani, D (2006) Effect of osmosis time on structure, texture and pectic composition of strawberry tissue. *European Food Research and Technology*, 224: 119-127.

Quinn F X, Kampff E, Smyth G, & McBrierty V J (1988) Water in hydrogels. 1. A study of water in poly(N-vinyl-2-pyrrolidone/methyl methacrylate) copolymer. *Macromolecules,* 21: 3191–3198.

Rahman M S (2008) Osmotic dehydration of foods. In: Rahman M S, *Handbook of food preservation,* CRC Press, Boca Raton, 403–432.

Rahman M S (2010) Food stability determination by macro-micro region concept in the state diagram and by defining a critical temperature. *Journal of Food Engineering,* 99: 402-416.

Ray D, Sarkar B K, Basak R K, & Rana A K (2004) Thermal behavior of vinyl ester resin matrix composites reinforced with alkali- treated jute fibers. *Journal of Applied Polymer Science*, 94: 123-129.

Redgwell R J, Melton L D, & Brasch D J (1989) Cell wall changes in kiwifruit following postharvest ethylene treatment. *Phytochemistry*, 29: 399-407.

Redgwell R J, Melton L D, & Brasch D J (1991) Cell wall polysaccharides of kiwifruit (*Actinidia deliciosa*): effect of ripening on the structural features of cell wall materials. *Carbohydrate Research*, 209: 191-202.

Rosnes J T, Sivertsvik M, & Skåra T (2007) MA packaging combined with other preserving factors. In: Wilson C L, *Intelligent and Active Packaging for Fruits and Vegetables*, CRC Press., Boca Raton, 113 - 149.

Sacchetti G, Gianotti A, & Dalla Rosa M (2001) Sucrose-salt combined effects on mass transfer kinetics and product acceptability. Study on apple osmotic treatments. *Journal of Food Engineering*, 49: 163–173.

Sadava D, Hillis D M, Heller H C, & Berenbaum M (2007) *Life, the science of biology* - 8th ed. Sinauer Associates and Freeman W H and Co. Sunderland, MA.

Sapers G M, Garzarella L, & Pilizota V (1990) Application of browning inhibitors to cut apple and potato by vacuum and pressure infiltration. *Journal of Food Science*, 55: 1049–1053.

Saurel R., Raoult-Wack A L, Rios G, & Guilbert S (1994) Mass transfer phenomena during osmotic dehydration of apple. I. Fresh plant tissue. *International Journal of Food Science and Technology*, 29, 531-542.

Schäffner A R (1998) Aquaporin function, structure, and expression: Are there more surprises to surface in water relations? *Planta,* 204: 131–139.

Schenz T W (1995) Glass transitions and product stability — an overview. *Food Hydrocolloids,* 9: 307–315,

Schmidt-Nielsen K (1997) *Animal Physiology: Adaptation and Environment*, Cambridge University Press, 1-40.

Schulze B, Peth S, Hubbermann E M, & Schwarz K (2012) The influence of vacuum impregnation on the fortification of apple parenchyma with quercetin derivatives in combination with pore structures X-ray analysis. *Journal of Food Engineering*, 109: 380-387.

Sharma R C, Joshi V K, Chauhan S K, Chopra S K & Lal B B (1991) Application of osmosis – osmocanning of apple rings. *Journal of Food Science and Technology,* 28: 86.

Shi J, & Le Maguer M (2003) Mass transfer flux at solid-liquid contacting interface. *Food Science and Technology International,* 9: 193-199.

Sondergaard T E, Schulz A, & Palmgren M G (2004) Energization of transport processes in plants. Roles of the plasma membrane H^+- ATPase. *Plant Physiology,* 136: 2475-2482.

Song L, Gao H, Chen H, Mao J, Zhou Y, Chen W, & Jiang Y (2009) Effects of short-term anoxic treatment on antioxidant ability and membrane integrity of postharvest kiwifruit during storage. *Food Chemistry*, 114: 1216-1221.

Stanley D W (1987) Food texture and microstructure. In: Moskowitz H R, *Food Texture. Instrumental and Sensory Measurement,* Marcel Dekker Inc., New York, 35-64.

Stein W D (1990) *Channels, carders and pumps. An introduction to membrane transport*. Academic Press, San Diego, CA, 326.

Taiz L, & Zeiger E (2010) *Plant Physiology* - Fifth Edition. Sinauer Associates, 1-40.

Talens P, Martínez-Navarrete N, Fito P, & Chiralt A (2001) Changes in optical and mechanical properties during osmodehydrofreezing of kiwi fruit. *Innovative Food Science & Emerging Technologies,* 3: 191-199.

Tocci A M, & Mascheroni R H (2008) Some thermal properties of fresh and osmotic ally dehydrated kiwifruit above and below the initial freezing temperature. *Journal of Food Engineering*, 88: 20-27.

Torreggiani D (1995) Technical aspects of osmotic dehydration in foods. In: Barbosa-Canovas G V, & Welti-Chanes J, *Food preservation by moisture control. Fundamentals and Applications*, Technomic Publishing, PA, 281–304.

Towill L E, & Mazur P (1975) Studies on the reduction of 2,3,5,triphenyltetrazolium chloride as a viability assay for plant tissue cultures. *Canadian Journal of Botany*, 53: 1097–1102.

Tyerman S. D., Niemietz C. M., & Bramley H (2002) Plant aquaporins: Multifunctional water and solute channels with expanding roles. *Plant, Cell & Environment,* 25: 173–194.

Tylewicz U, Lundin P, Cocola L, Dymek K, Rocculi P, Svanberg S, Dejmek P, & Gómez Galindo F (2012) Gas in scattering media absorption spectroscopy (GASMAS) detected persistent vacuum in apple tissue after vacuum impregnation. *Food Biophysics*, 7: 28-34.

Tylewicz U, Rocculi P, Cocci E, & Dalla Rosa M (2009) Fenomeni di trasporto di massa durante la disidratazione osmotica di Actinidia (*Actinidia chinensis* cv. Hort16A). *Industrie Alimentari,* 48: 1-5.

Tylewicz U, Romani S, Widell S, & Gómez Galindo F (2011) Induction of vesicle formation by exposing apple tissue to vacuum impregnation. *Food and Bioprocess Technology,* DOI: 10.1007/s11947-011-0644-1

Van As H, & Lens P (2001) Use of ^{1}H NMR to study transport processes in porous biosystems. *Journal Of Industrial Microbiology & Biotechnology*, 26: 43-52.

Van Buggenhout S, Grauwet T, Van Loey A, & Hendrickx M (2008) Use of pectinmethylesterase and calcium in osmotic dehydration and osmodehydrofreezing of strawberries. *European Food Research and Technology*, 226: 1145–1154.

Vega-Mercado H, Gongora-Nieto M M, Barbosa-Cánovas G V, & Swanson B G (2007) Pulsed Electric Fields in Food Preservation. In: Rahman M S, *Handbook of Food Preservation* 2nd Edition, CRC Press, Boca Raton.

Venturi L, Rocculi P, Cavani C, Placucci G, Dalla Rosa M, & Cremonini M A (2007) Water absorption of freeze-dried meat at different water activities: a multianalytical approach using sorption isotherm, differential scanning calorimetry, and nuclear magnetic resonance. *Journal of Agricultural and Food Chemistry,* 55: 10572-10578.

Wadsö L, & Gómez Galindo F (2009) Isothermal calorimetry for biological application in food science and technology. *Food Control*, 20: 956-961.

Weig A, Deswarte C, & Chrispeels M J (1997) The major intrinsic protein family of *Arabidopsis* has 23 members that form three distinct groups with functional aquaporins in each group. *Plant Physiology,* 114: 1347-1357.

Xie J, & Zhao Y (2003). Improvement of physicochemical and nutritional qualities of frozen Marionberry by vacuum impregnation pretreatment with cryoprotectants and minerals. *Journal of Horticultural Science and Biotechnology*, 78: 248–253.

Zhu L, Cai T, Huang J, Stringfellow T C, Wall M, & Yu L (2011) Water self-diffusion in glassy and liquid maltose measured by Raman microscopy and NMR. *The Journal of Physical Chemistry B*, 115: 5849-5855.

Paper I

Food Biophysics
DOI 10.1007/s11483-011-9210-7

SPECIAL ISSUE ARTICLE

NMR and DSC Water Study During Osmotic Dehydration of *Actinidia deliciosa* and *Actinidia chinensis* Kiwifruit

Urszula Tylewicz · Valentina Panarese · Luca Laghi · Pietro Rocculi · Małgorzata Nowacka · Giuseppe Placucci · Marco Dalla Rosa

Received: 6 August 2010 / Accepted: 25 January 2011

Abstract This study investigated mass transfer and water state changes promoted by osmotic dehydration on two kiwifruit species, *Actinidia deliciosa* and *Actinidia chinensis*. Osmotic treatment was performed in a 61.5% *w/v* sucrose solution at three different temperatures (25, 35 and 45 °C), with treatment time from 0 to 300 min. Treatment time positively influenced kiwifruit water loss and solid gain while temperature significantly affected only water loss. Peleg's model highlighted that the main response differences between the two species occurred during the initial phase of the osmotic treatment. Thermal properties and relaxation time measurements offered a complementary view concerning the effects of osmotic dehydration on kiwifruit. DSC parameters appeared to be sensitive to water and solid exchange between fruit and osmotic solution. LF-NMR proton T_2 revealed the consequences of the water–solid exchange on the cell compartments, namely vacuole, cytoplasm plus extracellular space and cell wall. During the osmotic treatment, the initial freezing temperature and the freezable water content decrease was dependent on time and treatment temperature, showing a similar tendency for both the kiwifruit species. They evidenced the same treatment response also concerning the reduction of vacuole and the increase of cytoplasm plus extracellular space T_2 values.

Keywords Osmo-dehydration · Kiwifruit · Mass transfer · DSC · NMR

U. Tylewicz (✉) · V. Panarese · L. Laghi · P. Rocculi · G. Placucci · M. Dalla Rosa
Department of Food Science, Alma Mater Studiorum, University of Bologna,
Campus of Food Science, Piazza Goidanich 60,
47521, Cesena (FC), Italy
e-mail: urszula.tylewicz@unibo.it

M. Nowacka
Faculty of Food Science,
Department of Food Engineering and Process Management,
Warsaw University of Life Sciences,
Warsaw, Poland

Introduction

Osmotic dehydration is a partial dewatering impregnation process usually carried out by immersion of cellular tissue in hypertonic solution.

The cells of plant tissue are characterized by semi-permeable membranes and the mass transfer phenomenon occurs because of the difference in the chemical potential of water between the food and the osmotic medium.[1,2] The diffusion of water from the plant tissue to the solution is usually accompanied by the simultaneous counter-diffusion of solutes from the concentrated solution into the tissue.[3,4] When the membrane responsible for osmotic transport is not perfectly selective, natural solutes present in the cells (vitamins, organic acids, minerals, pigments, etc.) can also leach into the osmotic solution.[5,6]

From the industrial point of view, the osmotic dehydration is mainly used as a pre-treatment for fruit and vegetables intended for further processing, like freezing and/or freeze drying.[7,8] Moreover, when mild processing conditions are applied, this treatment could be useful to increase the shelf-life of minimally processed products with relatively high moisture content.[9] In fact, the reduction of freezable water content and water activity at low temperature permits both to slow down degradative reactions and to guarantee a higher microbiological stability.[10]

Recently, the approach of combining different analytical techniques has been adopted to better investigate the status

Published online: 05 February 2011

of water in several systems.[11–13] Differential scanning calorimetry (DSC), and nuclear magnetic resonance (NMR) can offer a different but complementary point of view in studying the water mobility.[11,13,14]

The amount of unfreezable water within a sample after being cooled below zero is determined by DSC.[15] As explained by Wolfe[16], the amount of unfreezable water depends in general on three effects: (1) the presence of small solutes, for example ions, (2) the presence of macromolecules and membranes and (3) the viscosity of the solution.

The analysis of transverse relaxation time (T_2) curves obtained through LF-NMR yields an additional degree of details for the description of the embedded water. In fact, the T_2 of foodstuff reveals a multicomponent behaviour that reflects the existence of different proton pools within the sample.

The main objectives of this work were (1) to investigate the mass transfer phenomena and (2) to analyze the water status provided by DSC and NMR measurements, during osmotic dehydration of two different kiwifruit species.

Materials and Methods

Raw Materials

Two species of kiwifruit (*Actinidia deliciosa* var. Hayward and *Actinidia chinensis* var. Hort 16A) were bought on the local market and stored at 4±1 °C until they were processed. The osmotic dehydration treatment was applied on fruit hand peeled and cut into 10-mm thick slices.[17] The fruit had homogeneous size (major axis of 60±5 mm and minor axis of 45±5 mm) and refractometric index of 12.0± 0.4 °Brix.

Osmotic Dehydration Treatment

The osmotic dehydration was carried out by dipping the samples in 61.5% (*w*/*v*) sucrose solution equilibrated at three temperatures (25, 35 and 45 °C) for pre-established contact period of 0, 15, 30, 60 and 300 min, as reported by Tylewicz.[18] The product/solution ratio was about 1:4 (*w*/*w*), to avoid changes in the solution concentration during the treatment. The temperature of the solution was maintained constant by a thermo-controlled water bath. Three slices from the central part of each kiwifruit (about 180 g) were placed in mesh baskets and immersed in osmotic solution. The baskets were continuously stirred with a propeller. The rotational speed was experimentally determined to assure negligible resistance to mass transfer. After that, the slices were taken from the osmotic solution and each slice face was rinsed with distilled water for 3 s and placed on blotting paper for 2 s.

Analytical Determinations

Kiwifruit slices were weighted before and after osmotic dehydration process by means of technical balance (precision 0.01 g).

The moisture content of kiwifruit samples was determined gravimetrically by vacuum drying (pressure≤ 100 mmHg) at 70 °C until a constant weight was achieved (AOAC 920.15, 2002).[19]

Soluble solids content was determined at 20 °C by measuring the refractive index with a digital refractometer (PR1, Atago, Japan).

Mass Transfer Parameters

Osmotic dehydration kinetics of kiwifruit were evaluated by calculating net change (Δ) of kiwifruit slices total mass (M°), water mass (M^W) and solids mass (M^{ST}) adopting the following equations:[20]

$$\Delta M_t^\circ = M_t^\circ - M_0^\circ = \frac{m_t - m_0}{m_0} \tag{1}$$

$$\Delta M_t^W = M_t^W - M_0^W = \frac{m_t x_{wt} - m_0 x_{w0}}{m_0} \tag{2}$$

$$\Delta M_t^{ST} = M_t^{ST} - M_0^{ST} = \frac{m_t x_{STt} - m_0 x_{ST0}}{m_0} \tag{3}$$

where:

m_0 Initial weight before osmotic treatment (kg)
m_t Weight after a time t (kg)
x_w Water mass fraction (kg kg^{-1})
x_{ST} Total solids mass fraction (kg kg^{-1})

Kinetic Model

Mass transfer data were modelled according to the equation proposed by Palou[21] and Sacchetti[22], using the Peleg[23]'s model:

$$M_t^W - M_0^W = -\frac{t}{k_1^W + k_2^W \times t} \tag{4}$$

$$M_t^{ST} - M_0^{ST} = +\frac{t}{k_1^{ST} + k_2^{ST} \times t} \tag{5}$$

In this work, the same equation rewritten as:

$$M_t^\circ - M_0^\circ = -\frac{t}{k_1^\circ + k_2^\circ \times t} \tag{6}$$

was also used in order to model total mass change kinetics.

As reported by Sacchetti[22] at the equilibrium condition ($t\rightarrow\infty$) the value for mass transfer parameters could be calculated as:

$$P_t^J = P_0^J \pm \frac{t}{k_2^J} \quad (7)$$

where P^J could be respectively: M°; M^w; $M_\cdot^{ST}$

Similarly, the initial rate (t=0) of mass transfer parameters is:

$$\frac{1}{k_1^J}$$

This kinetic model offers the advantage that by calculating the inverse of the constant (k_1 and k_2) it is possible to obtain the initial rate value of mass transfer parameters and the one at the equilibrium condition.[22]

DSC Measurements

DSC analysis was carried out on a Pyris 6 DSC (Perkin-Elmer Corporation, Wellesley, USA). The DSC was equipped with a low-temperature cooling unit Intacooler II (Perkin-Elmer Corporation, Wellesley, USA). Temperature and melting enthalpy calibrations were performed with ion exchanged distilled water (mp 0.0 °C), indium (mp 156.60 °C), and zinc (mp 419.47 °C); heat flow was calibrated using the heat of fusion of indium (ΔH=28.71 J g^{-1}). For the calibration, the same heating rate, as used for sample measurements, was applied under a dry nitrogen gas flux of 20 mL min^{-1}. Samples of about 20–30 mg were encapsulated in 50 μl hermetic aluminium pans prior to measurements. An empty pan was used as a reference. DSC curves were obtained by cooling samples to −60 °C and then heating at 5 °C min^{-1} to 110 °C after an isothermal hold for 5 min at −60 °C.

According to Quinn[24] the amount of freezable water (g g_{fw}^{-1}) was determined as following reported:

$$x_w^F = \frac{\Delta H}{\Delta H_{ice}} \quad (8)$$

where ΔH (g g_{fw}^{-1}) is the measured latent heat of melting of water for gram of sample obtained by the integration of the melting endothermic peak; ΔH_{ice} (334 J g^{-1}) is the latent heat of melting of pure water at 0 °C.

NMR Measurements

Samples of about 400 mg of kiwifruit were placed inside 10 mm outer diameter NMR tubes so that they did not exceed the active region of the radio frequency coil, and they were analyzed at 24 °C with the Carr–Purcell–Meiboom–Gill (CPMG) pulse sequence using a Bruker Minispec PC/20 spectrometer operating at 20 MHz. Each measurement comprised 30,000 echoes, with a 2τ interpulse spacing of 80 μs and a recycle delay of 3.5 s. The number of scans was varied depending on moisture content, to obtain a *S/N* ratio in the range 900–1,400. The CPMG decays were normalized to the sample weight, and analyzed with the UPEN program, which inverts the CPMG signal using a continuous distribution of exponential curves, according to Eq. 9:

$$I(2\tau n) = \sum_{i=1}^{M} I_0(T_{2,i}) \exp(-2\tau n / T_{2,i}) \quad (9)$$

where 2τ is the CPMG interpulse spacing, n is the index of a CPMG echo, and $I_0(T_{2,i})$ provides a distribution of signal intensities for each T_2 component extrapolated at τ=0 (the relaxogram), sampled logarithmically in the interval $T_{2,\ min}$–$T_{2,\ max}$ set by the user. Default values for all UPEN parameters were used throughout this work.

Statistical Analysis

The osmotic dehydration process was performed once for each time–temperature treatment condition. Analytical determinations were performed in triplicates. Mass transfer, DSC, and NMR samples were collected from three kiwifruit slices for each treatment condition. Significance of the osmotic dehydration effects was evaluated by means of one- and two-way analyses of variance (ANOVA, 95% significance level) using the software STATISTICA 6.0 (Statsoft Inc., Tulsa, UK). In order to estimate the kinetic model constants, non-linear regression was carried out by means of the quasi-Newton calculus algorithm using STATISTICA 6.0.

Result and Discussion

Water Loss, Weight Reduction and Solid Gain Kinetic Model

The kinetic model was used to fit mass transfer parameter data over processing time ($0.83<R^2<0.99$). The predictive capability of the model can be observed in Figure 1, where, by way of example, the Eqs. 4, 5 and 6 were used to model the mass transfer parameters of *A. deliciosa* treated at 35 °C.

For both *A. chinensis* and *A. deliciosa* kiwifruit species, the highest water loss rates occurred during the first treatment hour as shown in the example in Figure 1. During that time water loss in *A. chinensis* was 18%, 20% and 35% of the initial fresh weight and in *A. deliciosa* 15%, 21% and 29% respectively, for 25, 35 and 45 °C. After 300 min of osmotic treatment, the percentage of water loss varied on average close to 38%, 45% and 62% in

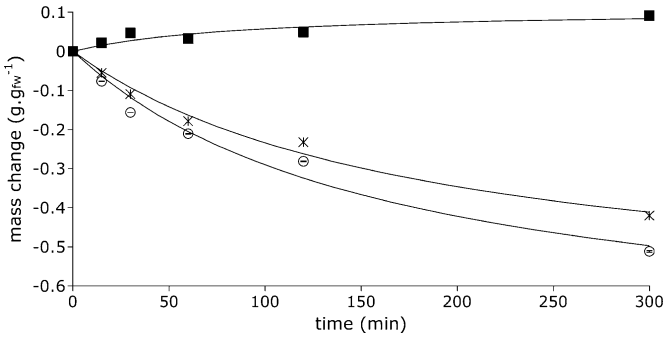

Fig. 1 Application of the Peleg's model to mass transfer data of *A. deliciosa* at 35 °C: total mass change ($\Delta M°_t$; *asterisk*); water mass change (ΔM_t^W; *open circle*); soluble solids mass change (ΔM_t^{ST}; *filled square*)

A. chinensis and 27%, 50% and 58% in *A. deliciosa* at 25, 35 and 45 °C. This agrees with the literature; in fact, Kowalska and Lenart[4] showed noteworthy water content decreasing during the first 30 min of the osmotic process (30 °C, 61.5% sugar solution). After this period, the dehydration of carrots, apples and pumpkins appears slower. Besides kiwifruit, dehydration rate presented by Vial[25] seems to decrease dramatically between 30 and 90 min of processing. The water loss rate was the highest at the beginning of the process because the dehydration driving force was the greatest. For both *A. deliciosa* and *A. chinensis*, the osmotic solution temperature seemed to positively influence the initial water loss rate as suggested by the behaviour of $1/k_1^W$ reported in Figure 2a. This displays the initial water loss rate and water loss rate at equilibrium of both the kiwifruit varieties as a function of temperature. Higher process temperatures seem to promote several phenomena: faster water loss through swelling and plasticizing of cell membranes; faster water diffusion within the product; lower viscosity of the osmotic medium facilitating the water transfer on the surface.[26] Kiwifruit has a porous structure; therefore, high temperature would release trapped air from the tissue, resulting in more effective removal of water by osmotic pressure.[27]

The initial weight reduction rate of *A. chinensis* was higher than the one of *A. deliciosa* at 25, 35 and 45 °C (Figure 2b); water and weight loss initial rates of both kiwifruit species reached the maximum at 45 °C (Figure 2a,b).

In agreement with Vial's findings[25,] *A. deliciosa* solid gain was minimally influenced by the increase of osmo-dehydration treatment temperature and time (Figure 2c). In fact during the first hour of osmotic treatment the solid gain in *A. chinensis* was about 2.5%, 2.5% and 3.6% and in *A. deliciosa* 3.6%, 3.2% and 6.1% for 25, 35 and 45 °C, respectively. After 300 min of osmotic treatment, the percentage of solid gain reached 5.6%, 6.5% and 6.3% in *A. chinensis* and 5.1, 8.8 and 9.6% in *A. deliciosa* for 25, 35 and 45 °C. These results disagree with those found by

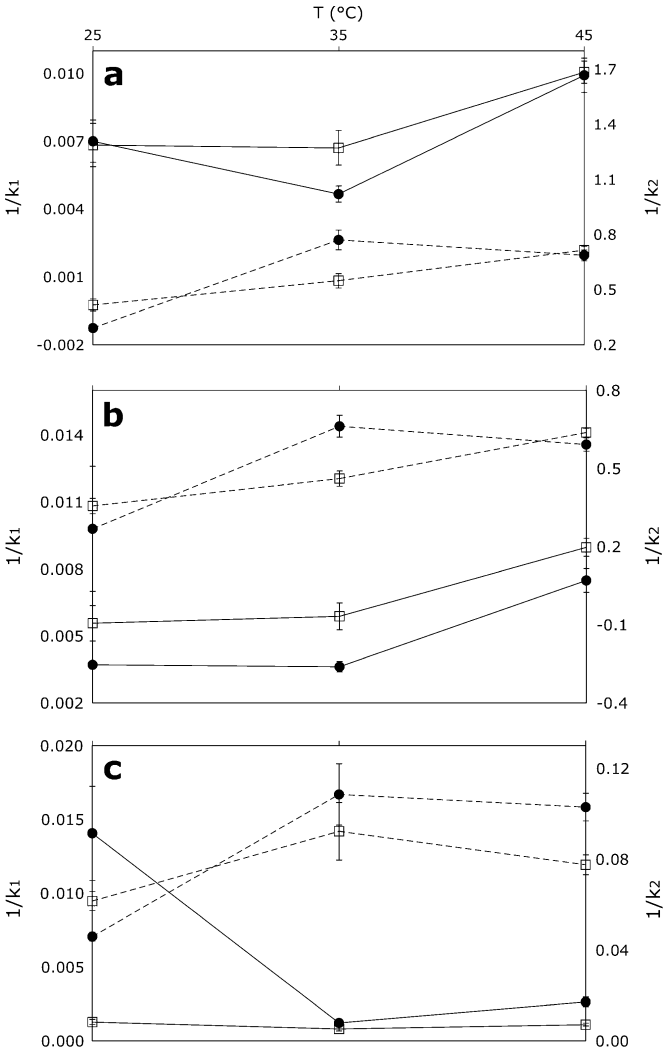

Fig. 2 Effect of the temperature on mass changes kinetic parameters: $1/k_1$ (*open square–solid line*) and $1/k_2$ (*open square–dashed line*) of *A. chinensis* and $1/k_1$ (*filled circle–solid line*) and $1/k_2$ (*filled circle–dashed line*) of *A. deliciosa*. **a** Water mass change; **b** total mass change; **c** soluble solids mass change

Bchir[28] and Cao.[27] Bchir[28] found a significant temperature effect during the first 20 min of osmotic treatment on pomegranate seeds (55 °Brix solution; 30, 40 and 50 °C). Cao[27] observed in kiwifruit a remarkable solid gain rising by varying the osmotic dehydration temperature (15–75 °C) and time (60–420 min) at different solution concentration (20–80% $w_{sucrose}/w_{solution}$). During the osmotic treatment, *A. chinensis* solid gain was modest and it seemed to be positively influenced by the temperature less than *A. deliciosa*, as shown in Figure 2c. These results are consistent with the higher weight reduction rate of *A. chinensis* and with Tylewicz[18] results.

During the second phase of the treatment, described by the parameter $1/k_2$, all the considered mass transfer rates ($1/k_2^W$, $1/k_2^{ST}$, $1/k_2°$) for both the kiwifruit species, underwent a significant and very similar increase by varying the temperature from 25 to 35 °C.

DSC Measurements

DSC measurements permitted to evaluate the changes of initial point of ice melting ($T_{f,onset}$) and freezable water content (x_W^F), that are related to product stability. The freezable water is water having enough mobility to freeze, as weakly bound to the macromolecular matrix.

During the osmotic treatment, the kiwifruit slices thermo-physical properties ($T_{f,onset}$ and x_W^F) progressively changed as shown in Table 1. In agreement with Cornillon[12] the depletion of the initial ice melting temperature ($T_{f,onset}$) progressively increased along with the proceeding of the osmotic treatment and with the increase of the treatment temperature, following the trend of water loss and solids gain results. For $T_{f,onset}$ two-way ANOVA analysis evidenced a strong effect of both time ($p<0.001$) and temperature ($p<0.01$). With the proceeding of the osmotic treatment, all the samples showed a tendentious decrease of x_W^F (g g_{fw}^{-1}); this behaviour was particularly evident for samples treated at high temperatures (35, 45 °C). Even for x_W^F two-way ANOVA analysis evidenced significant effects of both time ($p<0.001$) and temperature ($p<0.01$).

Table 1 $T_{f,onset}$ and x_w^F average values obtained during the osmotic dehydration of *A. deliciosa* and *A. chinensis* kiwifruit

Kiwifruit species	Temperature (°C)	Time (min)	$T_{f,onset}$ (°C)	X_W^F (g g_{fw}^{-1})
Actinidia chinensis	Raw	0	−1.8a	0.75a
	25	60	−4.3bc	0.61b
		120	−4.4bc	0.62b
		300	−4.8c	0.60b
	35	60	−4.2bc	0.61b
		120	−4.6bc	0.60b
		300	−8.7e	0.42d
	45	60	−4.1b	0.61b
		120	−6.7d	0.59b
		300	−9.1e	0.47c
Actinidia deliciosa	Raw	0	−2.7 a	0.66a
	25	60	−4.9 b	0.60b
		120	−4.5b	0.67a
		300	−5.4bc	0.65ab
	35	60	−4.6b	0.60b
		120	−6.6c	0.49c
		300	−7.8c	0.48de
	45	60	−5.2b	0.52c
		120	−7.0c	0.42de
		300	−12.6d	0.36e

Statistical significance was assessed by one-way ANOVA. Different letters within the same column and species indicate statistical differences ($p<0.01$)

According to Quinn[24], total non-freezable water corresponds to the maximum water content for which no enthalpic peak is detected. In previous dehydration studies[13,24], this value has been considered as the moisture content when $\Delta H=0$ and thus calculated through the linear regression of ΔH (J g_{dw}^{-1}) vs. water content (WC; $g_{H2O}100\ g_{dw}^{-1}$). This method applied to our results provided not trustable negative values of total non-freezable water content, but it is important to consider that the previous mentioned researches were focused on dehydration studies. During osmotic dehydration, in addition to water removal, a contemporaneous qualitative modification of the dry matter occurs, that in our experiments was promoted by sucrose soaking. In order to consider the latter phenomenon, ΔH values were normalized against soluble solids content (°Brix). Linear regressions of normalized ΔH (J g_{dw}^{-1} °$Brix^{-1}$) data vs. WC are reported in Figure 3. Obtained fitting equations ($\Delta H=0.199\times WC-25.453$, $R^2=0.914$ and $\Delta H=0.200\times WC-23.279$, $R^2=0.967$, respectively, for *A. deliciosa* and *A. chinensis* samples) showed that in our experimental conditions, the not freezable water content of *A. deliciosa* and *A. chinensis* was, respectively, 127.9 and 116.4 ($g_{H2O}100\ g_{dw}^{-1}$) or 56.12 and 53.79 (g_{H2O} $100\ g_{fw}^{-1}$). These last results are in agreement with those of Tocci[29] that found disappearance of freezable water between 58.1 and 50.6 ($g_{H2O}100\ g_{fw}^{-1}$) for *A. deliciosa* kiwifruit treated at 20 °C in sucrose solution (60% *w*/*w*). However, this result needs to be confirmed by further experiments enabling to reach lower water content values.

NMR Measurements

The CPMG decays registered during the present investigation, when inverted to a continuous distribution of exponential curves, allowed the identification of three proton pools in both

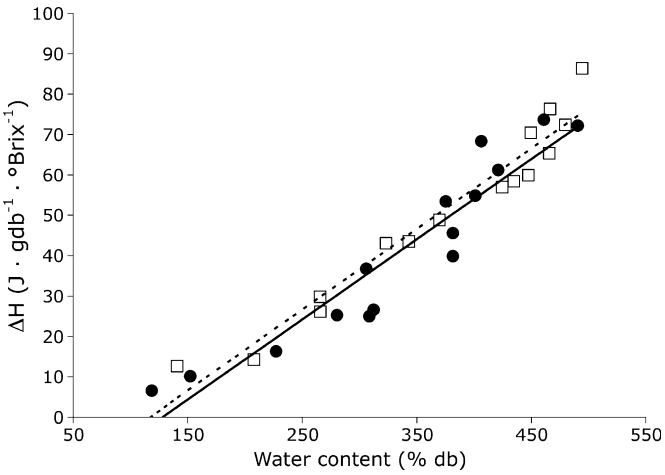

Fig. 3 Regression equations of ΔH vs. water content: (*filled circle*) *A. deliciosa* and (*open square*) *A. chinensis* data; regressions: (*full line*) *A. deliciosa*; (*dotted line*) *A. chinensis*

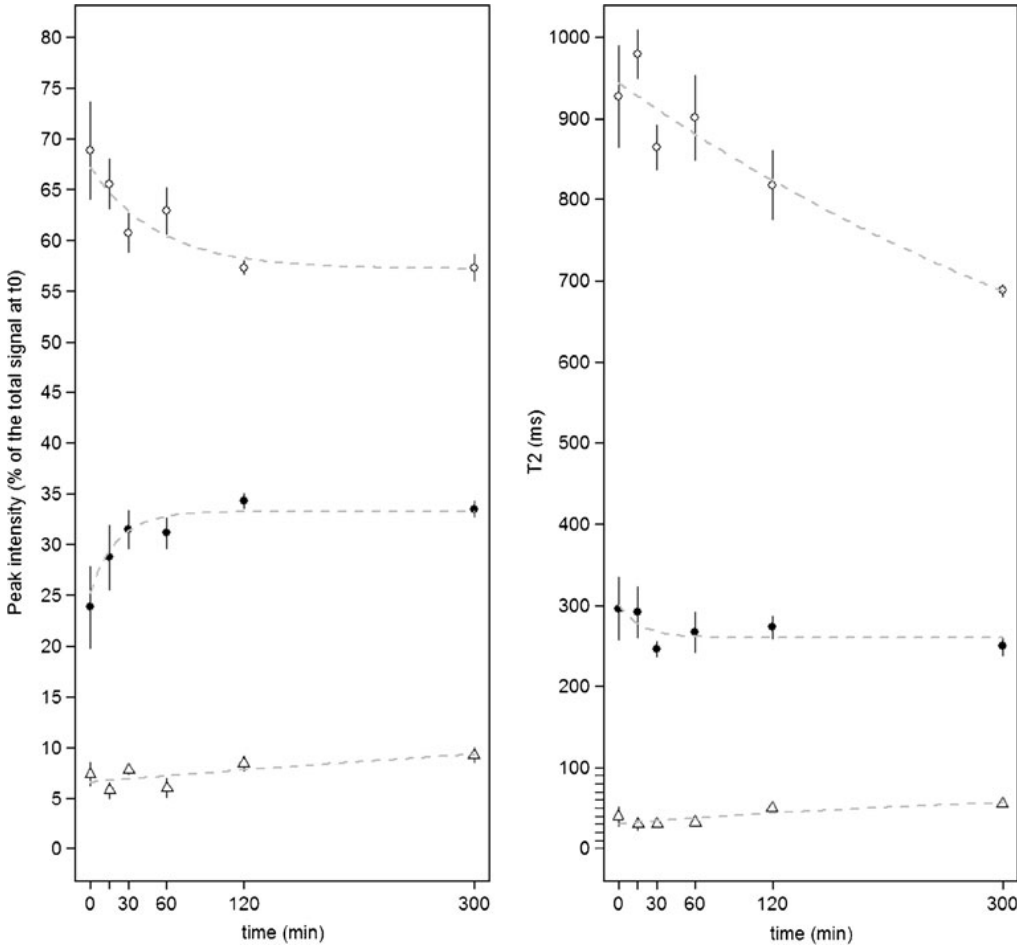

Fig. 4 Intensities and T_2 of *A. chinensis* kiwifruit proton pools during the osmotic treatment at 25 °C: vacuole (*open circle*), cytoplasm and extracellular spaces (*filled circle*), cell walls (*open upright triangle*). To help in visualizing the value trends, the points are fitted to monoexponential curves presented as *dashed lines*

kiwifruit varieties, with T_2 for raw fruits around 40, 300 and 950 ms, respectively. Through a comparison with the results obtained on apples and carrots by Hills[30,31], such pools were ascribed to cell wall, cytoplasm plus extracellular space and vacuole, respectively. Figure 4 shows the typical effect of osmotic dehydration on the intensity and T_2 of the named pools, considered separately by fitting the raw T_2 decays to the sum of three exponentials. Table 2 summarizes the proton pool values obtained on raw and 300 min osmo-dehydrated fruits at 25, 35, and 45 °C.

In raw kiwifruits, the protons located inside the vacuole represented the 61% of the total protons in *A. deliciosa*, and an even greater portion in *A. chinensis* (70%). During the osmotic treatment, the T_2 value and amount of vacuole protons of *A. deliciosa* decreased proportionally to the temperature. The reduction could be observed also in *A.*

Table 2 Proton pool intensity and T_2 values of raw and 300 min osmo-dehydrated kiwifruits

Kiwifruit species	Temperature	Vacuole		Cytoplasm/extracellular space		Cell wall	
	(°C)	T_2 (ms)	Peak intensity (a.u.)	T_2 (ms)	Peak intensity (a.u.)	T_2 (ms)	Peak intensity (a.u.)
A. deliciosa	Raw	1061±100	61±4	302±23	32±5	42±4	6±1
	25	847±77	42±4	237±12	45±3	48±6	13±2
	35	640±125	35±3	196±3	47±2	49±5	19±1
	45	375±123	23±3	123±20	58±4	34±6	20±1
A. chinensis	Raw	964±89	70±6	298±14	23±5	36±5	6±1
	25	696±63	57±4	262±15	33±3	54±6	9±2
	35	784±141	53±2	260±8	39±3	38±4	7±1
	45	463±141	27±3	171±24	63±5	30±6	8±1

The intensity values are scaled to the raw fruit, set to 100. The errors are expressed as standard deviation among the replicates

chinensis, resulting higher than *A. deliciosa* at 45 °C and lower at 25 and 35 °C. This behaviour can be explained considering that, at 20 MHz radiofrequency, T_2 value (ms) shorter than the one of pure water (≈1,600 ms) mainly reflects the proton exchange between water and solutes.[30] Thus, the T_2 of the water protons pertaining to a certain compartment can decrease when the (solutes+biopolymers)/water ratio increases. The decrease of signal values from vacuole protons suggests that this compartment can undergo shrinkage during the dehydration due to water leakage[32]; consequent solutes concentration caused a shortening of the T_2. As far as the cytoplasm/extracellular space proton pool is concerned, with the proceeding of the treatment time, the proton pool intensity increased together with a T_2 reduction, because the extracellular space was filled with the osmotic solution.[33]

Conclusions

The present work shows the effect of osmotic dehydration on two kiwifruit species, *A. deliciosa* and *A. chinensis*, in terms of mass transfer and water state behaviours.

Treatment time positively influenced water loss and solid gain of both the studied species, while temperature significantly affected only water loss. Peleg's model highlighted that the main response differences between the two species occurred during the initial phase of osmotic treatment.

Thermal properties and relaxation time measurements offered a complementary view concerning the effects of osmotic dehydration on kiwifruit. DSC parameters appeared to be sensitive to water and solid exchange between fruits and osmotic solution. LF-NMR proton T_2 revealed the consequences of the water–solid exchange on the cell compartments, namely vacuole, cytoplasm plus extracellular space and cell wall. During the osmotic treatment, the initial freezing temperature and the freezable water content decrease was dependent on treatment time and temperature, showing a similar tendency for both the kiwifruit species. The two species evidenced the same treatment response also concerning the reduction of vacuole and the increase of cytoplasm plus extracellular space T_2 values.

This study confirms that DSC analysis could give key information about macroscopic water changes of vegetable tissue consequent to a technological process, whereas NMR analysis enables to assess the microscopic modifications of cell compartmentation.

To obtain a better understanding of the tissue changes promoted by osmotic treatment, microscopic studies and metabolic consequences determination are in progress in our laboratories.

Acknowledgements The authors acknowledge Dr. Patricio Santagapita, of the *Departamento de Industrias*, *Facultad de Ciencias Exactas y Naturales*, *Universidad de Buenos Aires*, for his critical reading of the manuscript and highlighting suggestions, and Dr. Emiliano Cocci of our department for his help in the set up of the osmosis pilot plant.

References

1. C. Ratti, A.S. Mujumadar, *Processing Fruit Science and Technology* eds. by D.M. Barrett, L.P. Somogyi, H.S. Ramaswamy (CRC, 2005)
2. M.M. Khin, W. Zhou, C.O. Perera, J. Food Eng. **77**, 84–95 (2006)
3. F. Kaymak-Ertekin, M. Sultanoğlu, J. Food Eng. **46**, 243–250 (2000)
4. H. Kowalska, A. Lenart, J. Food Eng. **49**, 137–140 (2001)
5. G.M. Dixon, J.J. Jen, J. Food Sci. **42**, 1136–1140 (1977)
6. C.L. Lerici, G. Pinnavaia, M. Dalla Rosa, L. Bartolucci, J. Food Sci. **50**, 1217–1219 (1985)
7. M. Robbers, R.P. Singh, L.M. Cunha, J. Food Sci. **62**, 1039–1042 (1997)
8. A. Chiralt, N. Martínez-Navarrete, J. Martínez-Monzó, P. Talens, G. Moraga, A. Ayala, P. Fito, J. Food Eng. **49**, 129–135 (2001)
9. M. Dalla Rosa, D. Torreggiani, *Industrial application of osmotic dehydration/treatments of food*, eds. M. Dalla Rosa, W.E.L. Spiess, Forum, (2000)
10. A. Gianotti, G. Sacchetti, M.E. Guerzoni, M. Dalla Rosa, J. Food Eng. **49**, 265–270 (2001)
11. S. Li, L.C. Dickinson, P. Chinachoti, J. Agric, Food Chem. **46**, 62–71 (1998)
12. P. Cornillon, Lebensm. Wiss. Technol. **33**, 261–267 (2000)
13. L. Venturi, P. Rocculi, C. Cavani, G. Placucci, M. Dalla Rosa, M. A. Cremonini, J. Agric, Food Chem. **55**, 10572–10578 (2007)
14. N. Aktaş, Y. Tülek, H.Y. Gökalp, J. Therm, Anal. Calorim. **50**, 617–624 (1997)
15. D. Simatos, M. Faure, E. Bonjour, M. Couach, in *Water relation in foods*, ed. by R.D. Duckworth (Academic, London, 1975)
16. J. Wolfe, G. Bryant, K.L. Koster, Cryoletters **23**, 157–166 (2002)
17. I. Escriche, R. Garcia-Pinchi, A. Andrés, P. Fito, J. Food Process Eng. **23**, 191–205 (2000)
18. U. Tylewicz, P. Rocculi, E. Cocci, M. Dalla Rosa, Ind. Aliment. **48**, 1–5 (2009)
19. AOAC International. *Official Methods of Analysis of AOAC International*, 17th edn. 920.15 (2002)
20. P. Fito, A. Chiralt, in *Food Engineering 2000*, ed. by P. Fito, E. Ortega, G. Barbosa (Chapman & Hall, New York, 1997), pp. 231–252
21. E. Palou, A. Lopez-Malo, A. Argaiz, J. Welti, Dry. Technol. **12**, 965–978 (1994)
22. G. Sacchetti, A. Gianotti, M. Dalla Rosa, J. Food Eng. **49**, 163–173 (2001)
23. M. Peleg, J. Food Sci. **53**, 1216–1217 (1988)
24. F.X. Quinn, E. Kampff, G. Smyth, V.J. McBrierty, Macromol. **21**, 3191–3198 (1988)
25. C. Vial, S. Guilbert, J.L. Cuq, Sci. Aliment. **11**, 63–84 (1991)
26. H.N. Lazarides, E. Katsanidis, A. Nickolaidis, J. Food Eng. **25**, 151–166 (1995)
27. H. Cao, M. Zhang, A. Mujumdar, W. Du, J. Sun, Dry. Technol. **24**, 89–94 (2006)
28. B. Bchir, S. Besbes, H. Attia, C. Blecker, Int. J. Food Sci. Technol. **44**, 2208–2217 (2009)
29. A.M. Tocci, R.H. Mascheroni, J. Food Eng. **88**, 20–27 (2008)
30. B.P. Hills, B. Remigereau, Int. J. Food Sci. Technol. **32**, 51–61 (1997)
31. B.P. Hills, K.P. Nott, Appl. Magn. Reson. **17**, 521–535 (1999)
32. W.G. Hopkins, *Introduction to plant physiology* (Wiley, New York, 2008), pp. 23–38
33. J.M. Aguilera, A. Chiralt, P. Fito, Trends Food Sci. Technol. **14**, 432–437 (2003)

Paper II

Biblid: 1821-4487 (2011) 15; 3; p.113-117
UDK: 542.934.8

Original Scientific Paper
Originalni naučni rad

EFFECT OF OSMOTIC DEHYDRATION ON KIWIFRUIT: RESULTS OF A MULTIANALYTICAL APPROACH TO STRUCTURAL STUDY
UTICAJ OSMOTSKE DEHIDRACIJE NA KIVI: REZULTATI MULTIANALITIČKOG PRISTUPA PROUČAVANJA STRUKTURE

Marco DALLA ROSA, Urszula TYLEWICZ*, Valentina PANARESE*, Luca LAGHI*, Annamaria PISI**, Patricio SANTAGAPITA***, Pietro ROCCULI**

**Alma Mater Studiorum University of Bologna, Department of Food Science, P.zza Goidanich 60, 47521 Cesena (Italy)*
***Alma Mater Studiorum University of Bologna, Department of Agroenvironmental Science and Technologies, University of Bologna, Viale G. Fanin 44, 40127 Bologna, Italy*
**** University of Buenos Aires, Faculty of Exact and Natural Sciences, Industry Department - National Council of Scientific and Technical Research (CONICET), Buenos Aires, Argentina*
e-mail: marco.dallarosa@unibo.it

ABSTRACT

This paper presents the results of the comparison of different analytical techniques (Differential Scanning Calorimetry - DSC, Low Field Nuclear Magnetic Resonance - LF-NMR, Light Microscopy - LM and Transmission Electron Microscopy – TEM) in order to evaluate the mass transfer, water status and cellular compartment modifications of the kiwifruit outer pericarp tissue during osmotic dehydration treatment (OD). Two kiwifruit species, A. deliciosa and A. chinensis were submitted to OD. OD was performed in a 61.5 % w/v sucrose solution at three different temperatures (25, 35 and 45 °C), with treatment time from 0 to 300 min. Peleg's model highlighted that the main response differences between the two kiwifruit species occurred during the initial phase of the osmotic treatment. DSC parameters appeared to be sensitive to water and solid exchange between fruits and osmotic solution. LF-NMR proton T_2 revealed the consequences of the water-solid exchange on the cell compartments, namely vacuole, cytoplasm plus extracellular space and cell wall. During OD, the reduction of the vacuole proton pool, detected by LF-NMR, suggested a shrinkage of such compartment, confirmed by LM. Cell walls of outer pericarp showed considerable changes in size, structure and stain uptake during OD observed at TEM. The proposed multianalytical approaches should enable better design of combined processing technologies permitting the evaluation of their effects on tissue response.

Key words: *osmotic dehydration, cell compartments, DSC, NMR, TEM.*

REZIME

U ovom radu su prikazani rezultati poređenja različitih analitičkih tehnika (Diferencijalna skeniranja Kalorimetrija – DSC, Niska Polje nuklearna magnetna rezonanca - LF-NMR, svetlost mikroskopije - LM i Prenos elektronsku mikroskopiju - TEM), u cilju određivanja prenosa mase, statusa vode i modifikacije ćelija tkiva perikarpa kivija tokom osmotske dehidratacije tretmana (OD). Dve sorte kivija su bile izložene osmotskom tretmanu, A. deliciosa i A. chinensis. Osmotsko sušenje obavljeno je u 61,5% rastvoru saharoze na tri različite temperature (25, 35 i 45°C), sa vremenom trajanja sušenja od 0 do 300 minuta. Pelegovim modelom naglašene su glavne razlike između dve sorte kivija koje se događaju tokom početne faze osmotskog tretmana. DSC parametri osetljivi su na izmenu vode i čvrste materije između voća i osmotskog rastvora. LF-NMR-om otkrivene su posledice razmene vode i čvrste materije na ćeliju, odnosno vakuole, citoplazmu sa vanćelijskim prostorom i ćelijski zid. Tokom OD, smanjenje vakuole protona bazena, otkrivena je LF-NMR, predložio skupljanja takvog odeljka, potvrđeno LM. Ćelijske zidove spoljne perikarpa su pokazali značajne promene u veličini, strukturi i mrlja uzimanja u toku OD posmatrano na sistem. Predloženi multianalitical pristupi treba da omogući bolji dizajn u kombinaciji obrade tehnologija dozvoljava procenu njihovog uticaja na tkivo odgovor.

Ključne reči*: osmotske dehidratacije, mobilni pregrade, DSC, NMR, TEM.*

INTRODUCTION

Osmotic dehydration (OD) is a partial dewatering impregnation process carried out by the immersion of cellular tissue in hypertonic solution. The difference in water chemical potential between the food and osmotic medium promotes the release of water from the tissue into the osmotic solution with a simultaneous impregnation of the product with the solutes (*Ferrando, Spiess, 2001, Khin et al., 2006*). OD decreases water mobility and availability, promoting the improvement of fresh vegetable tissue stability (*Gianotti et al., 2001*). The use of combining different analytical techniques like Differential Scanning Calorimetry (DSC) and Nuclear Magnetic Resonance (NMR) can offer different but complementary point of view in studying the water status and compartmentalization in several systems (*Cornillon, 2000, Venturi et al., 2007, Tylewicz et al., 2011*). DSC measurement allows to determine the unfrozen water content within the samples, which depends on the presence of small solutes, for example ions, the presence of macromolecules and membranes and viscosity of the solution (*Wolfe et al., 2002*). NMR measurement yields an additional degree of details for the description of the embedded water. The water state and compartmentalization has been studied by NMR techniques in different fruits such as apples (*Hill, Remigerau, 1997*) and strawberries (*Marigheto et al., 2004*), showing different transversal relaxation times (T_2) for the protons located in the cell walls, vacuoles, extracellular spaces and/or cytoplasm. Cellular compartment modification can be more conveniently studied by means of light (LM) and transmission electron microscopy (TEM) techniques, already used to describe cellular organization changes during ripening and/or technological processing of vegetable tissue (*Alandes et al., 2006; Salvatori, Alzamora, 2000; Hallett et al., 1992*). The objective of the present study was to compare the different analytical techniques in a joint laboratory research in order to evaluate the mass transfer phenomena, water state and cellular compartment modifications of the kiwifruit outer pericarp tissue during osmotic dehydration treatment. For this purpose the DSC, LF-NMR, LM, TEM measurements were performed on fresh and osmotic dehydrated kiwifruits.

MATERIAL AND METHODS

Raw Materials

Two species of kiwifruit (*Actinidia deliciosa* var. Hayward and *Actinidia chinensis* var. Hort 16A) were bought on the local market and stored at 4 ± 1 °C until they were processed. The osmotic dehydration treatment was applied on fruit hand peeled and cut into 10 mm thick slices. The fruit had homogeneous size (major axis of 60 ± 5 mm and minor axis of 45 ± 5 mm) and refractometric index of 12.0 ± 0.4 °Brix.

Osmotic dehydration treatment

The osmotic dehydration was carried out by dipping the samples in 61.5 % (w/v) sucrose solution equilibrated at three temperatures (25, 35 and 45 °C) for pre-established contact period of 0, 15, 30, 60 and 300 min. The product/solution ratio was about 1:4 (w/w), to avoid changes in the solution concentration during the treatment. Three slices from the central part of each kiwifruit (about 180 g) were placed in mesh baskets and immersed in osmotic solution. The baskets were continuously stirred with a propeller. After that, the slices were taken from the osmotic solution and each slice face was rinsed with distilled water for 3 s and placed on blotting paper for 2 s.

Analytical determinations

Kiwifruit slices were weighted before and after osmotic dehydration process by means of technical balance (precision 0.01 g). The moisture content of kiwifruit samples was determined gravimetrically by vacuum drying (pressure ≤ 100 mm Hg) at 70 °C until a constant weight was achieved (AOAC 920.15, 2002). Soluble solids content was determined at 20 °C by measuring the refractive index with a digital refractometer (PR1, Atago, Japan).

Mass transfer parameters

Osmotic dehydration kinetics of kiwifruit were evaluated by calculating net change (Δ) of kiwifruit slices total mass (M°), water mass (M^W) and solids mass (M^{ST}) adopting the following equations (Fito and Chiralt, 1997):

$$\Delta M_t^\circ = M_t^\circ - M_0^\circ = \frac{m_t - m_0}{m_0} \quad (1)$$

$$\Delta M_t^W = M_t^W - M_0^W = \frac{m_t x_{wt} - m_0 x_{w0}}{m_0} \quad (2)$$

$$\Delta M_t^{ST} = M_t^{ST} - M_0^{ST} = \frac{m_t x_{STt} - m_0 x_{ST0}}{m_0} \quad (3)$$

where: m_0: initial weight before osmotic treatment (kg); m_t: weight after a time t (kg); x_w: water mass fraction (kg · kg^{-1}), x_{ST}: total solids mass fraction (kg · kg^{-1})

DSC Measurements

DSC analysis was carried out on a Pyris 6 DSC (Perkin-Elmer Corporation, Wellesley, USA). The DSC was equipped with a low-temperature cooling unit Intacooler II (Perkin-Elmer Corporation). Temperature and melting enthalpy calibrations were performed with ion exchanged distilled water (mp 0.0 °C), indium (mp 156.60 °C), and zinc (mp 419.47 °C); heat flow was calibrated using the heat of fusion of indium (ΔH = 28.71 J·g^{-1}). For the calibration, the same heating rate, as used for sample measurements, was applied under a dry nitrogen gas flux of 20 mL · min^{-1}. Samples of about 20-30 mg were encapsulated in 50 μl hermetic aluminium pans prior to measurements. An empty pan was used as a reference. DSC curves were obtained by cooling samples to -60 °C and then heating at 5 °C · min^{-1} to 110 °C after an isothermal hold for 5 min at -60 °C.

NMR Measurements

Samples of about 400 mg of kiwifruit were placed inside 10 mm outer diameter NMR tubes so that they did not exceed the active region of the radio frequency coil, and they were analyzed at 24 °C with the Carr−Purcell−Meiboom−Gill (CPMG) pulse sequence using a Bruker Minispec PC/20 spectrometer operating at 20 MHz. Each measurement comprised 30000 echoes, with a 2τ interpulse spacing of 80 μs and a recycle delay of 3.5 s. The number of scans was varied depending on moisture content, to obtain a S/N ratio in the range 900–1400. The CPMG decays were normalized to the sample weight, and analyzed with the UPEN program, which inverts the CPMG signal using a continuous distribution of exponential curves, according to equation (3):

$$I(2\tau n) = \sum_{i=1}^{M} I_0(T_{2,i}) \exp(-2\tau n / T_{2,i}) \quad (3)$$

where 2τ is the CPMG interpulse spacing, n is the index of a CPMG echo, and $I_0(T_{2,i})$ provides a distribution of signal intensities for each T_2 component extrapolated at τ = 0 (the relaxogram), sampled logarithmically in the interval $T_{2,\min} - T_{2,\max}$ set by the user. Default values for all UPEN parameters were used throughout this work.

Neutral red staining (Light Microscopy – LM)

The kiwifruit juice, obtained by blending the raw kiwifruit in a centrifuge, thermal inactivated and filtered, was used as a medium to which neutral red stain (which penetrates the vacuole of intact protoplast of plant cells) has been added to reach a final concentration of 0.05 % (w/v) (*Mauro et al., 2002*). Slices, 2 mm thick, were cut manually at about 2 mm distance from the peeled kiwifruit (*A. deliciosa*) surface, parallel to its longitudinal axis and stained for 10-20 min. To obtain a real time visualization of the vacuole shrinkage occurring during the osmotic treatment, each stained slice was mounted on a microscope slide and immersed in a 61.5 % (w/v) aqueous sucrose solution drop. The slide was inserted in the microscope and viewed for 60 min at 25 °C. RGB images were acquired under the same conditions (true colour – 24 bit, 300 BPP) using a digital photocamera mod. Camedia C-4040-ZOOM (Olympus, Tokyo, Japan) and stored in JPEG format.

The images obtained using neutral red staining were processed with the software Photoshop® v. 5.0 (Adobe Systems Incorporated, USA), in order to evaluate the retraction of the vacuole after 60 min of OD treatment.

Transmission Electron Microscopy

Samples (1-2 mm cubes) of outer pericarp tissue were removed from the kiwifruit slices (*A.deliciosa*, fresh and OD at 35 °C for 120 min), parallel to the kiwifruit longitudinal axis, at about 2 mm distance from the slice surface. The choice of osmotic conditions was based on the preliminary study. Tissue was fixed in 5 % (w/v) glutaraldehyde in 0.1 M phosphate buffer at pH 7.2. After washing in the buffer, the samples were postfixed in 1% (w/v) osmium tetroxide in 0.1 M phosphate buffer at pH 7.2, for 1 h while gently agitated. All these steps were performed at 4°C. After washing in phosphate buffer and in distilled water, these pieces were block stained in 0.5 % (w/v) aqueous uranyl acetate for 2 h at 4 °C, in the dark. All samples were washed in distilled water, dehydrated in aqueous ethanol series and embedded in Spurr's low viscosity resin (*Spurr, 1969*). The specimens were cut using an LKB Ultramicrotome. The ultrathin sections were double stained with uranyl acetate and lead citrate and examined under a Philips CM10 TEM, at an accelerating voltage of 60 kV. Pictures were taken on Kodak film.

Statistical analysis

Significance of the osmotic dehydration effects was evaluated by means of one-way and two-way analysis of variance (ANOVA, 95 % significance level) using the software STATISTICA 6.0 (Statsoft Inc., Tulsa, UK).

RESULTS AND DISCUSSION

Mass transfer parameters

For both *A. chinensis* and *A. deliciosa* kiwifruit species, the highest water loss rates occurred during the first treatment hour as shown in Figure 1. During that time water loss in *A. chinensis* was 18, 20 and 35 % of the initial fresh weight and in *A. deliciosa* 15, 21 and 29 %, for 25, 35 and 45 °C, respectively. After 300 min of osmotic treatment, the percentage of water loss varied on average close to 38, 45 and 62 % in *A. chinensis* and 27, 50 and 58 % in *A. deliciosa* at 25, 35 and 45 °C (*Tylewicz et al., 2011*). This agrees with the literature; in fact *Kowalska and Lenart* (2001) showed noteworthy water content decreasing during the first 30 min of the osmotic process (30 °C, 61.5 % sugar solution). After this period the dehydration of carrots, apples and pumpkins appears slower.

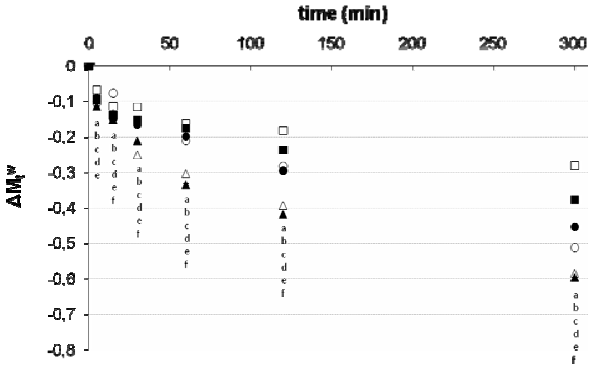

Fig. 1. Water loss during osmotic dehydration of Actinidia chinensis kiwifruit at 25 °C (■), 35 °C (●) and 45 °C (▲) and Actinidia deliciosa kiwifruits at 25°C (□), 35 °C (○) and 45 °C (△). Different letters within the same sampling time indicate statistical differences ($p < 0.01$).

Statistical analysis of the values represented in Figure 1 shows that, for both *A. deliciosa* and *A. chinensis*, the osmotic solution temperature positively influenced the water loss rate. It is well recognized that diffusion is a temperature-dependent phenomenon. Higher process temperatures seem to promote faster water loss through swelling and plasticising of cell membranes, faster water diffusion within the product and better mass (water) transfer characteristics on the surface due to lower viscosity of the osmotic medium (*Lazarides et al., 1995*). Kiwifruits have a porous structure, so high temperature would release trapped air from the tissue structure, resulting in more effective removal of water by osmotic pressure (*Cao et al., 2006*).

The kiwifruits solid gain during the osmotic dehydration is shown in Figure 2. Statistical analysis of the values represented in Figure 2 shows different solid gain behaviors for the two species. The solutes gain of *A. chinensis* seemed to be positively influenced by the temperature less than the one of *A. deliciosa*. *Tylewicz et al.* (2009) also observed a low temperature effect on solute gain of *A. chinensis* slices during osmotic dehydration but, to the contrary, *Cao et al.* (2006) showed a notably enhanced of solute gain, in *A. deliciosa* kiwifruits, by increasing osmotic dehydration temperature and time.

Moreover the Peleg's model was used to fit mass transfer parameter data over processing time ($0.83 < R^2 < 0.99$). This kinetic model confirmed and highlighted that the main response differences between the two kiwifruit species occurred during the initial phase of the osmotic treatment (data not shown).

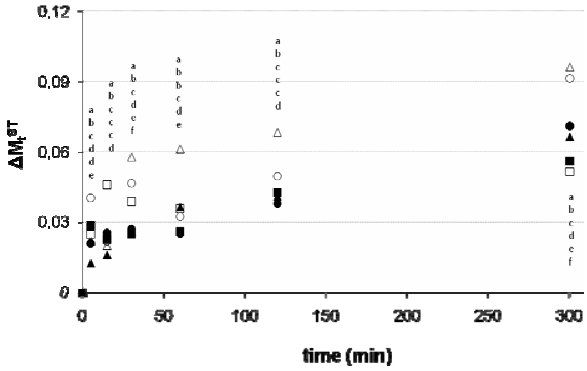

Fig. 2. Solid gain during osmotic dehydration of Actinidia chinensis kiwifruit at 25 °C (■), 35 °C (●) and 45 °C (▲) and Actinidia deliciosa kiwifruits at 25 °C (□), 35 °C (○) and 45 °C (△). Different letters within the same sampling time indicate statistical differences ($p < 0.01$).

Multianalytical approach was used in order to study the water state and compartmentalization in raw and osmotic dehydrated kiwifruit. DSC measurements permitted to evaluate the changes of initial point of ice melting ($T_{f,onset}$) and frozen water content (x^F_w), that are related to product stability. The frozen water is water having enough mobility to freeze, as weakly bound to the macromolecular matrix. During the osmotic treatment, the kiwifruit slices thermo-physical properties ($T_{f,onset}$ and x^F_w) progressively changed as shown in Table 1.

Table 1. $T_{f,onset}$ (initial point of ice melting) and x^F_w (frozen water content) average values obtained during the osmotic dehydration of A. deliciosa and A. chinensis kiwifruit, as reported by Tylewicz et al., 2011. Statistical significance was assessed by one-way ANOVA. Different letters within the same column indicate statistical differences ($p < 0.01$).

Kiwifruit species	Temperature (°C)	Time(min)	$T_{f,onset}$(°C)	X_W^F(g/g_{fw})
Actinidia chinensis	raw	0	- 1.8 ^{a}	0.75 ^{a}
	25	60	- 4.3 ^{bc}	0.61 ^{b}
		120	- 4.4 ^{bc}	0.62 ^{b}
		300	- 4.8 ^{c}	0.60 ^{b}
	35	60	- 4.2 ^{bc}	0.61 ^{b}
		120	- 4.6 ^{bc}	0.60 ^{b}
		300	- 8.7 ^{e}	0.42 ^{d}
	45	60	- 4.1 ^{b}	0.61 ^{b}
		120	- 6.7 ^{d}	0.59 ^{b}
		300	- 9.1 ^{e}	0.47 ^{c}
Actinidia deliciosa	raw	0	- 2.7 ^{a}	0.66 ^{a}
	25	60	- 4.9 ^{b}	0.60 ^{b}
		120	- 4.5 ^{b}	0.67 ^{a}
		300	- 5.4 ^{bc}	0.65 ^{ab}
	35	60	- 4.6 ^{b}	0.60 ^{b}
		120	- 6.6 ^{c}	0.49 ^{c}
		300	- 7.8 ^{c}	0.48 ^{de}
	45	60	- 5.2 ^{b}	0.52 ^{c}
		120	- 7.0 ^{c}	0.42 ^{de}
		300	- 12.6 ^{d}	0.36 ^{e}

In agreement with *Cornillon* (2000) the depletion of the initial ice melting temperature ($T_{f,onset}$) progressively increased along with the proceeding of the osmotic treatment and with the increase of the treatment temperature, following the trend of water loss and solids gain results. With the proceeding of the osmotic treatment tendentially all the samples showed a decrease of frozen water content; this behaviour was particularly evident for samples treated at high temperatures (35, 45 °C). For both $T_{f,onset}$ and x^F_w two-way ANOVA analysis evidenced significant effects of both time ($p < 0.001$) and temperature ($p < 0.01$).

NMR measurements allowed the identification of three proton pools in both kiwifruit species, with T_2 for raw fruits around 40, 300 and 950 ms respectively. Through a comparison with the results obtained on apples and carrots by *Hills* (1997, 1999), such pools were ascribed to cell wall, cytoplasm plus extracellular space and vacuole respectively.

In raw kiwifruits, the protons located inside the vacuole represented the 61 % of the total protons in *A. deliciosa*, and an even greater portion in *A. chinensis* (70 %). During the osmotic treatment the T_2 value and amount of vacuole protons of *A. deliciosa* decreased proportionally to the temperature. The reduction could be observed also in *A. chinensis*, resulting higher than *A. deliciosa* at 45 °C and lower at 25 and 35°C (Fig. 3).

This behaviour can be explained considering that, at 20 MHz radiofrequency, T_2 value (ms) shorter than the one of pure water (≈ 1600 ms) mainly reflects the proton exchange between water and solutes (*Hills and Remigereau, 1997*). Thus the T_2 of the water protons pertaining to a certain compartment can decrease when the (solutes + biopolymers) / water ratio increases. The decreasing of signal values from vacuole protons suggests that this compartment can undergo shrinkage during the dehydration, due to water leakage (*Aguilera et al., 2003*); consequently the solutes concentration caused a shortening of the T_2.

In order to better understand the micro and ultrastructural changes in kiwifruit outer pericarp tissue during OD the LM and TEM measurements were performed.

LM images of neutral red stained cells displayed the vacuole shrinkage subsequent to the OD treatment confirming the results obtained by NMR measurements. Figure 4 shows the outline of a stained kiwifruit vacuole before and after one hour of OD. Comparing these two micrographs, it seems that occupied volume by the fluorescent vacuole qualitatively decreased during the 60 min of the treatment.

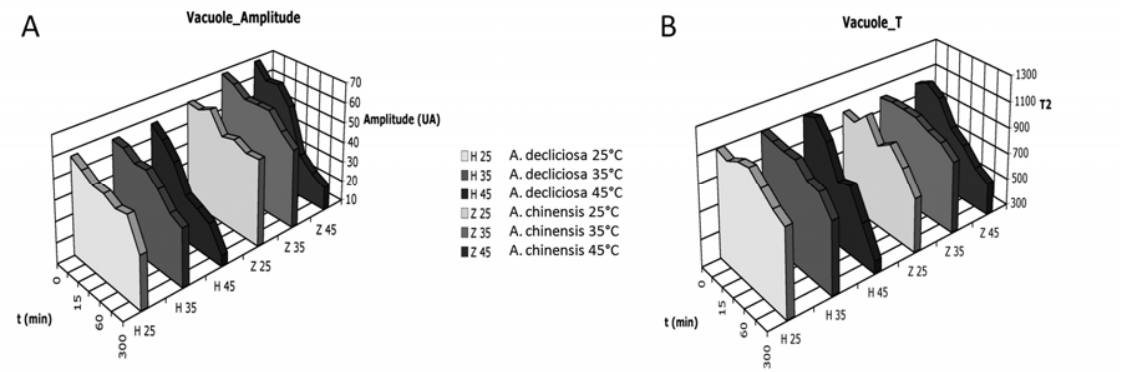

Fig. 3. Intensities (A) and transversal relaxation time (T_2) (B) of vacuole proton pools of both kiwifruit species during the osmotic treatment at 25, 35 and 45 °C.

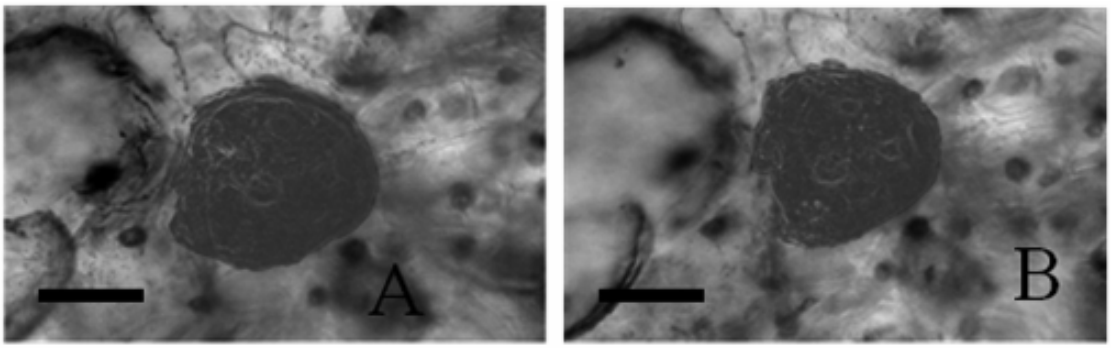

Fig. 4. LM of kiwifruit (A. deliciosa) outer pericarp cells. Highlighted neutral-red stained vacuole after 60 min of OD at 30 °C: (a) processed image of cell prior OD (b) processed image of cell after OD. Bar = 100 μm.

As far as the cytoplasm / extracellular space proton pool is concerned, with the proceeding of the treatment time, the proton pool intensity increased together with a T_2 reduction (data not shown). This could be due to the intracellular space creation filled by vacuole content and osmotic solution, which contribute to the cytoplasm and the extracellular space proton pool.

The treatment seemed to increase the proton pool located in the cell walls, without changing its T_2 (data not shown). Since the NMR signal is not enough sensible to measure with accuracy the proton pools from cell wall the changes of the last were evaluated by TEM observations.

TEM observations marked a decrease of the staining together with a visible swelling of the cell wall and the loss of cell wall fibrous appearance (Figures 5A and 5B). Moreover the decrease of the plasmodesmata region staining was observed (Figures 5C and 5D). The reduction in staining intensity of cell wall material occurred predominantly in the treated kiwifruit tissues and might be partially accounted by wall expansion. The loss of staining probably reflects a change in cell wall structure and composition *in situ*, since it has not been revealed in the raw fruits.

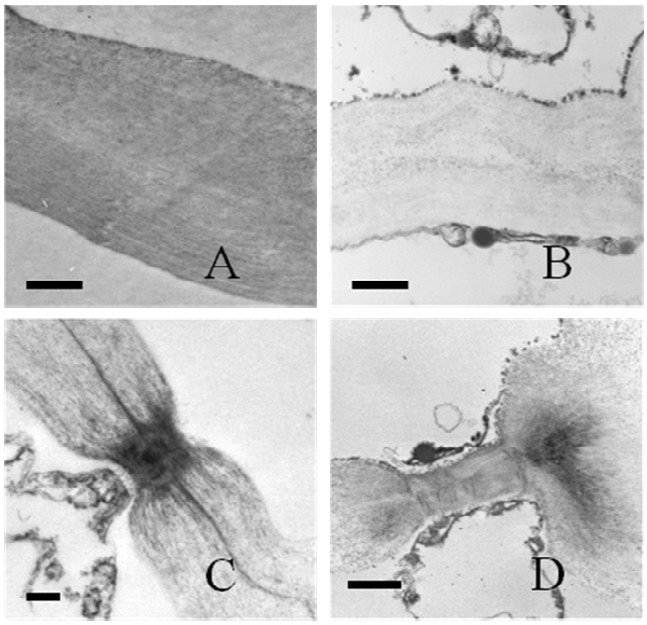

Fig. 5. TEM microscopy of outer pericarp cells from kiwifruit (A.deliciosa). Cell wall of raw kiwifruit (A) and 2 hours after OD-treatment (B); electrondense plasmodesmata complex of raw (C) and two hours OD-treated kiwifruit (D). Scale (A)-(D) 1μm.

CONCLUSIONS

The present work shows the effect of osmotic dehydration on two kiwifruit species, *A. deliciosa* and *A. chinensis*, in terms of mass transfer phenomena, water state behaviours and cellular compartment modification.

Treatment time positively influenced water loss and solid gain of both the studied species, while temperature significantly affected only water loss. Peleg's model highlighted that the main response differences between the two species occurred during the initial phase of osmotic treatment.

Thermal properties and relaxation time measurements offered a complementary view concerning the effects of osmotic dehydration on kiwifruit. DSC parameters appeared to be sensitive to water and solid exchange between fruits and osmotic solution. During the osmotic treatment, the initial freezing temperature and the frozen water content decrease was dependent on treatment time and temperature, showing a similar tendency for both the kiwifruit species.

LF-NMR proton T_2 revealed the consequences of the water-solid exchange on the cell compartments, namely vacuole, cytoplasm plus extracellular space and cell wall. The reduction of the vacuole protons suggested shrinkage of such compartment, confirmed by LM images of neutral red stained cells. Cell walls of outer pericarp showed considerable changes in size, structure and stain uptake during OD observed at TEM.

The multianalytical approach proposed in this study represents a powerful and versatile tool with the potentiality to investigate the behaviour of vegetable tissues towards those subjected to different processing conditions.

REFERENCES

Aguilera, J.M., Chiralt, A., Fito, P. (2003). Food dehydration and product structure. Trends in Food Science Technology, 14, 432-43.

Alandes, L., Hernando, I., Quiles, A., Pérez-Munuera, I., Lluch, M. A. (2006). Cell wall stability of fresh-cut Fuji apples treated with Calcium Lactate. Journal of Food Science, 71*,* 615–620.

Cao, H., Zhang, M., Mujumdar, A., Du, W., Sun J. (2006). Optimization of osmotic dehydration of kiwifruit. Drying Technology, 24 (1), 89-94.

Cornillon, P. (2000). Characterization of Osmotic Dehydrated Apple by NMR and DSC. Lebensm.-Wiss.Technol., 33, 261-267.

Ferrando, M., Spiess, W.E.L. (2001). Cellular response of plant tissue during the osmotic treatment with sucrose, maltose and trehalose solutions. Journal of Food Engineering, 49, 115-127.

Fito, P., Chiralt, A. (1997). An approach to the modeling of solid food-liquid operations: Application to osmotic dehydration. In: Fito P., Ortega E. and Barbosa G. (eds), Food Engineering 2000. New York: Chapman & Hall. 231-252.

Gianotti, A., Sacchetti, G., Guerzoni, M.E., Dalla Rosa, M. (2001). Microbial aspects on short-time osmotic treatment of kiwifruit. Journal of Food Engineering, 49, 265-270.

Hallett, I. C., Macrae, E. A., Wegrzyn, T. F. (1992). Changes in kiwifruit cell wall ultrastructure and cell packing during post-harvest ripening. International Journal of Plant Sciences*,* 154*,* 49-60.

Hills, B.P., Nott, K.P, (1999). NMR studies of water compartmentation in car- rot parenchyma tissue during drying and freezing. Applied Magnetic Resonance, 17, 521-535.

Hills, B.P., Remigereau, B. (1997). NMR studies of changes in subcellular water compartmentation in parenchyma apple tissue during drying and freezing. International Journal of Food Science & Technology, 32 (1), 51-61.

Khin, M.M., Zhou, W., Perera, C.O. (2006). A study of mass transfer in osmotic dehydration of coated potato cubes. Journal of Food Engineering, 77, 84-95.

Kowalska, H., Lenart, A. (2001). Mass exchange during osmotic pretreatment of vegetables. Journal of Food Engineering, 49, 137-140.

Lazarides, H.N., Katsanidis, E., Nickolaidis, A. (1995). Mass transfer kinetics during osmotic preconcentration aiming at minimal solid uptake. Journal of Food Engineering, 25, (2), 151-166.

Marigheto, N., Vial. A., Wright, K., Hills, B. P. (2004). A combined NMR and microstructural study of the effect of highpressure processing on strawberries. Applied Magnetic Resonance 26, 521-531.

Mauro, M. A., Tavares, D., Menegalli, F. C. (2002). Behaviour of plant tissue in osmotic solutions. Journal of Food Engineering*,* 56*,* 1-15.

Salvatori, D., Alzamora, S. M. (2000). Structural changes and mass transfer during glucose infusion of apples as affected by blanching and process variables. Drying Technology, 18*,* 361–382.

Spurr, A.R. (1969). A low viscosity epoxy resin embedding medium for electron microscopy. Journal of Ultrastructural Research*, 26,* 31-43.

Tylewicz, U. , Panarese, V., Laghi, L., Rocculi, P., Nowacka, M., Placucci, G., Dalla Rosa, M. (2011).NMR and DSC Water Study during Osmotic Dehydration of *Actinidia deliciosa* and *A. chinensis* kiwifruit. Food Biophysics, 6, (2), 327.

Tylewicz, U., Rocculi, P., Cocci, E., Dalla Rosa, M. (2009). Fenomeni di trasporto di massa durante la disidratazione osmotica di Actinidia (*Actinidia chienensis* cv. *Hort16A*). Industrie Alimentari, 48, 1-5.

Venturi, L., Rocculi, P., Cavani, C., Placucci, G., Dalla Rosa, M., Cremonini, M.A. (2007). Water absorption of freeze-dried meat at different water activities: a multianalytical approach using sorption isotherm, differential scanning calorimetry and nuclear magnetic resonance. Journal of Agricultural and Food Chemistry, 55, 10572-10578.

Wolfe, J., Bryant, G., Koster, K. L. (2002). What is 'unfreezable water', how unfreezable is it and how much is there? CryoLetters, 23, 157–166.

Received: 14.04.2011. Accepted: 18.10.2011.

Paper III

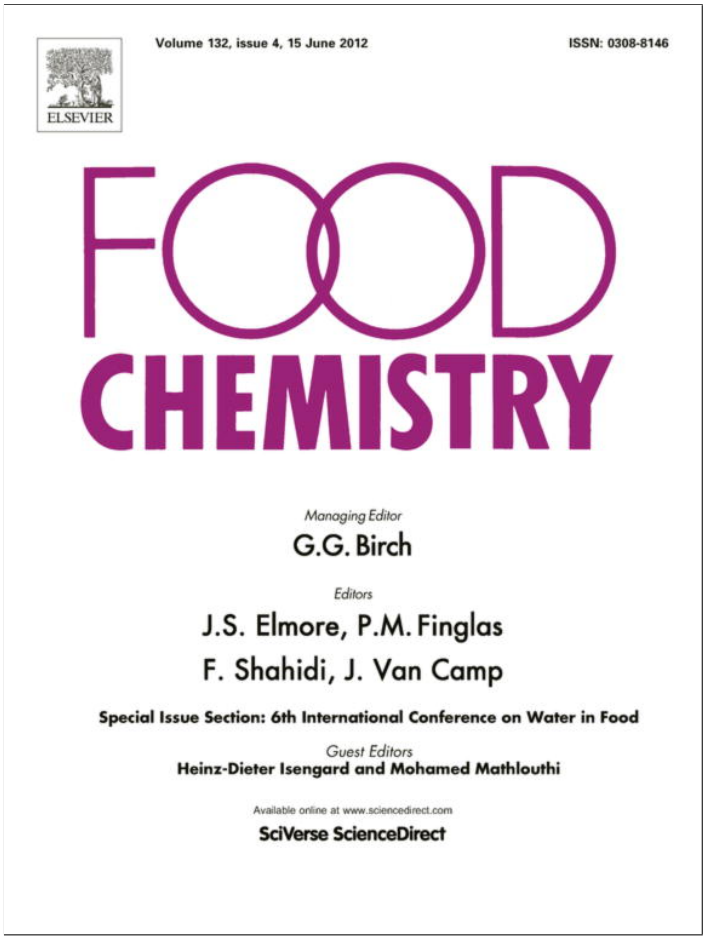

Food Chemistry 132 (2012) 1706–1712

Contents lists available at ScienceDirect

Food Chemistry

journal homepage: www.elsevier.com/locate/foodchem

Effect of osmotic dehydration on *Actinidia deliciosa* kiwifruit: A combined NMR and ultrastructural study

Valentina Panarese [a,*], Luca Laghi [a], Annamaria Pisi [b], Urszula Tylewicz [a], Marco Dalla Rosa [a], Pietro Rocculi [a]

[a] Department of Food Science, University of Bologna, Campus of Food Science, Piazza Goidanich 60, 47521 Cesena (FC), Italy
[b] Department of Agroenvironmental Science and Technologies, University of Bologna, Viale G. Fanin 44, 40127 Bologna, Italy

ARTICLE INFO

Article history:
Available online 1 July 2011

Keywords:
Actinidia deliciosa
Osmosis
Cell compartments
NMR
TEM
LM

ABSTRACT

The effects of individual osmotic dehydration processes (OD) on kiwifruit outer pericarp tissue were studied as reliant on treatment temperature (25, 35 and 45 °C) and extent (0–300 min). Macro (Low Frequency Nuclear Magnetic Resonance, LF-NMR), micro (Light Microscopy, LM) and ultrastructural (Transmission Electron Microscopy, TEM) measurements were performed to evaluate modifications of three cellular compartments, namely vacuole, cytoplasm – extracellular space and cell wall.

Both LF-NMR relaxometry and LM observations highlighted shrinkage of the vacuole compartment along the OD. Intercellular space formations, observed at TEM, were in agreement with LF-NMR results. Cell walls of outer pericarp showed considerable changes in size, structure and stain uptake during OD, at both LM and TEM. Furthermore cell walls showed extensive swelling, which intensity varied from cell to cell and even within the same cell.

The proposed multianalytical approach should enable both better designs of combined processing technologies and estimations of their effects on tissue response.

1. Introduction

The osmotic dehydration treatment (OD) is a partial dewatering process by immersion of cellular tissue in hypertonic solution. The driving force for the water removal is the concentration gradient between the solution and the intracellular fluid (Rahman, 2008). The diffusion of water from the vegetable tissue to the solution is usually accompanied by the simultaneous solutes counter-diffusion into the tissue (Kaymak-Ertekin & Sultanoğlu, 2000; Kowalska & Lenart, 2001). Moreover, the cellular membranes are not perfectly semi-permeable and natural solutes present in the cells (vitamins, organic acids, minerals, pigments, etc.) can be leached into the osmotic medium (Dixon & Jen, 1977; Lerici, Pinnavaia, Dalla Rosa, & Bartolucci, 1985).

In the case of kiwifruit, the OD is employed to increase the product shelf life, but since by itself is not enough adequate, generally it is combined with other stronger stabilizing methods such as freezing or air-, freeze-, vacuum-drying (Rahman, 2008). OD could be also a mild process to improve the fresh-cut product stability and quality along with other preservative technologies (i.e. sanitation, refrigeration, modified atmosphere packaging) (Torreggiani & Bertolo, 2004).

Raw under-ripe products with high firmness and low soluble solid content are required by the fresh-cut industry, in order to mechanically perform peeling and cutting operations on kiwifruit. The obtained final product does not have a sufficient ripening level for consumption, at least during the first part of the storage period. OD could be applied to obtain minimally processed kiwifruits with sufficient firmness and overall quality, as suggested by Bressa, Dalla Rosa, and Mastrocola (1997).

From the surface inward, a kiwifruit is made of skin, outer pericarp, inner pericarp, and core. Small and radially compressed cells can be identified under the skin tissue, made of dead cells. The bulk of outer pericarp tissue is composed by single or small groups of large cells dispersed in a matrix of smaller ones; the walls of such cells are about 2.5 μm thick. Elongated cells characterise the inner pericarp, which contains also the seeds; the core is relatively uniform with spherical/ellipsoidal cells (Hallett, Macrae, & Wegrzyn, 1992).

The natural solutes leaching caused by the OD and the overall loss of water suggest modifications of the native cellular organisation and microstructure of the cell wall, plasmalemma and tonoplast. In addition water naturally located in extracellular spaces, cytoplasm and vacuoles may be redistributed. The latter phenomenon can be conveniently monitored in large tissue samples using non-spatially resolved low frequency nuclear magnetic resonance (LF-NMR) techniques. This is possible because protons in different subcellular organelles are often characterised by different transverse relaxation times (T_2). Indeed LF-NMR techniques have been used to study a number of different physiological conditions in several fruits and vegetables, including changes caused by ripening,

* Corresponding author. Tel.: +39 0547 63 61 20; fax: +39 0547 38 23 48.
E-mail address: valentina.panarese2@unibo.it (V. Panarese).

0308-8146/$ - see front matter © 2011 Elsevier Ltd. All rights reserved.
doi:10.1016/j.foodchem.2011.06.038

bruising, microbial infection, drying, freezing and high pressure processing (Hills & Clark, 2003; Hills & Remigerau, 1997; Marigheto, Vial, Wright, & Hills, 2004).

Cell membranes characteristics can be more conveniently studied by means of Light microscopy (LM) and Transmission Electron Microscopy (TEM) techniques, already used to describe cellular organisation changes during ripening and/or technological processing of vegetable tissues, including kiwifruit (Alandes, Hernando, Quiles, Pérez-Munuera, & Lluch, 2006; Gerschenson, Rojas, & Marangoni, 2001; Hallett et al., 1992; Salvatori & Alzamora, 2000; Sutherland, Hellett, Redgwell, Benhamou, & MacRae, 1999). Structural organisation rather than the presence of single components dictates textural properties (Stanley, 1987). Vegetable tissue texture can be mainly attributed to the structural integrity of the cell walls and middle lamellae, as well as to the turgor pressure generated within cells by osmosis (Jackman & Stanley, 1995).

The objective of the present study has been to combine NMR, microstructural and ultrastructural measurements, to evaluate the cellular compartment modifications of the kiwifruit outer pericarp tissue during the osmosis and verify whether kiwifruit cell wall undergoes degradation during the treatment. For this purpose, the analytical measurements were performed on kiwifruit slices treated for different periods in a 61.5% sucrose solution at different treatment times and temperatures. Knowledge of such changes occurring during processing should enable better design of combined preservation procedures to maintain quality characteristics. This study intends to describe the major structural and ultrastructural changes in cell walls and cell packing that occur in kiwifruit tissue, as a consequence of OD.

2. Materials and methods

2.1. Raw material

Kiwifruits (*Actinidia deliciosa* cultivar "Hayward") were harvested and stored for one month at 4 ± 1 °C until processing. The OD was applied on fruits with homogeneous size and a refractometric index of 12.0 ± 0.4 °Brix.

2.2. Osmotic dehydration treatment

The process was carried out by dipping the samples in 61.5% (w/v) sucrose solution at three temperatures (25, 35 and 45 °C) for pre-established contact period of 0, 5, 15, 30, 60, 120 and 300 min. Product/solution ratio was about 1:4 (w/w), to avoid changes in the concentration of the solution during the treatment. The temperature of the solution was maintained constant by a thermostatically controlled water bath. The kiwifruit were sliced (10 mm thick) transversally to their axis, removing carefully the peel, using a scalpel. Three slices from the central part of each kiwifruit were prepared, placed in mesh baskets and immersed in the osmotic solution. The baskets were continuously stirred with a propeller. The rotational speed was experimentally determined to assure negligible external resistance to mass transfer. After the OD, the slices were removed from the solution, their surface rinsed with distilled water and gently blotted with tissue paper. Determinations for each analysis were made in triplicates.

2.3. NMR measurements

Proton transverse relaxation time (T_2) of the samples was measured in triplicate at each time/temperature condition. From the slices, cylinders of about 400 mg of outer pericarp tissue were cut, parallel to the kiwifruit longitudinal axis, with a core borer at about 2 mm distance from the slice surface. The samples were placed inside 10 mm outer diameter NMR tubes, so that they did not exceed the active region of the radio frequency coil, and analysed at 24 °C with the CPMG pulse sequence using a Bruker Minispec PC/20 spectrometer operating at 20 MHz. Each measurement comprised 30,000 echoes, with a 2τ interpulse spacing of 80 μs and a recycle delay of 3.5 s. The specified τ, chosen to avoid sample and radio frequency coil overheat, allowed the observation of the protons with T_2 higher than a few milliseconds. The number of scans varied depending on moisture content, to obtain a S/N ratio in the range 900–1400. The CPMG decays were analysed with the UPEN (Borgia, Brown, & Fantazzini, 1998) program, which inverts the CPMG signal using a continuous distribution of exponential curves, according to Eq. (1):

$$I(2\tau n) = \sum_{i=1}^{M} I_0(T_{2,i}) \exp(-2\tau n/T_{2,i}) \quad (1)$$

where 2τ is the CPMG interpulse spacing, n is the index of a CPMG echo, and I_0 ($T_{2,i}$) provides a distribution of signal intensities for each T_2 component extrapolated at $\tau = 0$ (the relaxogram), sampled logarithmically. Default values for all UPEN parameters were used throughout this work.

Due to the algorithm UPEN is based on, the relaxograms obtained on several samples showed partially overlapped peaks. To observe them separately, fittings to the sum of an increasing number of exponential curves were performed. An *F*-test showed that the optimum ratio (fitting ability)/(complexity of the model), for most samples with three exponentials, was reached.

To assign some of the peaks of the relaxograms to specific proton pools, a doping experiment was carried out, by placing a cylinder of parenchyma tissue inside an NMR tube, together with a water solution 50 mM $MnCl_2$–200 mM mannitol. The cylinder height and the amount of solution were chosen to have the entire sample in front of the active region of the radio frequency coil.

2.4. Light Microscopy (LM) and Transmission Electron Microscopy (TEM) of fresh and embedded material

2.4.1. Toluidine blue staining

Toluidine blue resolves tissue sections into their components by colouring various types of wall with strikingly different colours. The cell walls stained from reddish purple to green with the increasing of their lignification grade. Hand sections were taken from outer pericarp tissue at about 2 mm distance from the slice surface, parallel to the kiwifruit longitudinal axis. The sections were stained with 0.05% toluidine blue in 0.1 M phosphate buffer at pH 6.8 (O'Brien, Feder, & McCully, 1964).

2.4.2. Neutral red staining

To obtain a qualitative profile of the vacuolar compartment changes during the osmosis, the tissue was stained applying a technique proposed by Mauro, Tavares, and Menegalli (2002). Neutral red is a vital stain of relatively low molecular weight (288.8 g/mol), which penetrates the vacuole of intact protoplast of plant cells. Its molecules have no electric charge, but the low pH inside the vacuoles transforms them to an ionic state incapable of penetrating the tonoplast, where the stain remains confined; neutral red thus accumulates in the vacuole (Thebud & Santarius, 1982), and it has been used to observe the plasmolysis of plant cells in various solutions (Carpita, Sabularse, Montezinos, & Delmer, 1979).

The kiwifruit juice, obtained by blending the raw kiwifruit in a centrifuge, thermal inactivated and filtered, was used as a medium to which neutral red stain has been added to reach a final concentration of 0.05% (Mauro et al., 2002).

The ideal staining time for good definition in photographs was found to be from 10 to 20 min. Slices, 2 mm thick, were cut

manually at about 2 mm distance from the peeled kiwifruit surface, parallel to its longitudinal axis. To obtain a real time visualisation of the vacuole shrinkage occurring during the osmotic treatment, each stained slice was mounted on a microscope slide and immersed in a 61.5% (w/v) aqueous sucrose solution drop. The slide was inserted in the microscope and viewed for 60 min at 25 °C. RGB images were acquired under the same conditions (true colour – 24 bit, 300 BPP) using a digital photocamera mod. Camedia C-4040-ZOOM (Olympus, Tokyo, Japan) and stored in JPEG format.

2.4.3. Image analysis

The images obtained using neutral red staining were processed with the software Photoshop® v. 5.0 (Adobe Systems Incorporated, USA), in order to evaluate the retraction of the vacuole after 60 min of OD treatment. After conversion in grey scale (8BPP), the vacuole areas of fresh and treated kiwifruit samples were selected using the command Magic Wand Tool of the software, with a threshold value of 5. The obtained area of interest has been evidenced using the command Trace Contour filter.

2.4.4. Transmission Electron Microscopy

TEM micrographs of control samples (untreated kiwifruit) were compared with micrographs of kiwifruit slices treated at 35 °C for 120 min. This osmotic condition (35 °C – 120 min) was chosen based on the following considerations. First the treatment temperature of 35 °C was the middle point of the temperature range tested in this study. Secondly LM micrographs, using toluidine blue staining, showed that this osmotic condition caused a weak blue staining of the kiwifruit cell walls but still visible under the microscope. The higher osmotic condition (35 °C – 300 min) caused a critical disruption of the cell walls and a consequent nearly absence of the blue staining in the sample. Finally NMR measurements displayed statistically significant changes in water distribution of the various cellular compartments, comparing treated (35 °C – 120 min) and raw samples.

Samples (1–2 mm cubes) of outer pericarp tissue were removed from the kiwifruit slices, parallel to the kiwifruit longitudinal axis, at about 2 mm distance from the slice surface. Tissue was fixed in 5% glutaraldehyde in 0.1 M phosphate buffer at pH 7.2. After washing in the buffer, the samples were postfixed in 1% osmium tetroxide in 0.1 M phosphate buffer at pH 7.2, for 1 h while gently agitated. All these steps were performed at 4 °C. After washing in phosphate buffer and in distilled water, these pieces were block stained in 0.5% aqueous uranyl acetate for 2 h at 4 °C, in the dark. All samples were washed in distilled water, dehydrated in aqueous ethanol series and embedded in Spurr's low viscosity resin (Spurr, 1969). The specimens were cut using an LKB Ultramicrotome. The ultrathin sections were double stained with uranyl acetate and lead citrate and examined under a Philips CM10 TEM, at an accelerating voltage of 60 kV. Pictures were taken on Kodak film.

3. Results and discussion

3.1. Cellular water compartmentation and osmosis

To have an insight of the major structures of kiwifruit parenchyma tissue, and their modifications due to OD, proton transverse relaxation time spectra were considered first. The T_2 of the protons located in the parenchyma of a fruit is mainly determined by the chemical exchange among water and biopolymers (and solutes), with a T_2 of 1.5 s and microseconds respectively, and by the diffusion through locally generated magnetic field inhomogeneities (Hills & Duce, 1990). Some of the compartments characterising a cell, with different composition, showed a different chemical

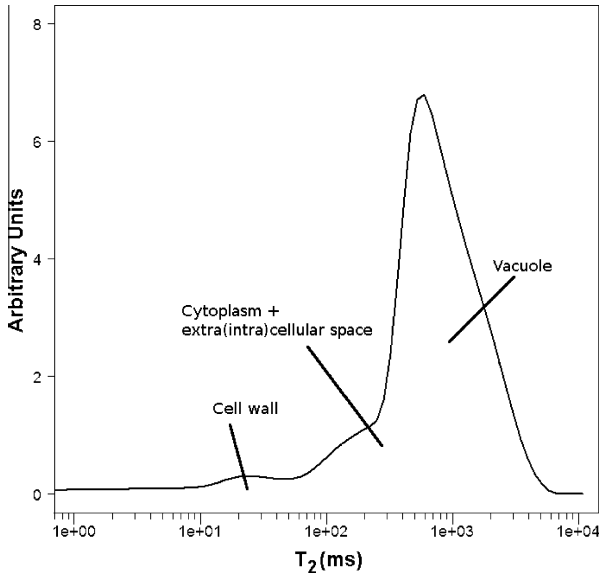

Fig. 1. Example of T_2 spectrum obtained on kiwifruit treated 30 min at 25 °C.

exchange rate. They could thus be observed separately through T_2 spectra, obtained with a CPMG pulse sequence, as evidenced by Fig. 1. Water diffusion among the compartments might make them appear as one, when the cells are too small, and/or τ is too long. Hills and Duce (1990) noticed that zucchini showed a complete diffusive averaging of the proton pools, due to a τ of 25 μs, and a cell diameter of 27.5 μm. Hills and Remigerau (1997) observed three separate pools in apple, due to cells with a diameter of 100 μm. Cornillon (2000) instead, studying apples, observed only two water populations, due to a τ of 500 μs. The complex profile of Fig. 1 shows that the diffusive averaging of the protons populations is far from complete, due to both average cell diameter (0.8–0.1 mm), and chosen τ.

As suggested by Marigheto et al. (2004) for strawberry, the well resolved peak around 30 ms can be assigned to the protons located in the cell walls, while the remaining peaks, due to the protons in the extracellular spaces, vacuoles and cytoplasm, can be univocally assigned through a kinetic doping experiment (Snaar & As Van, 1992). A parenchyma sample was thus immersed in a water Mn^{2+} solution, isotonic to the cell content, and a sequence of T_2 spectra was registered. As this ion is paramagnetic, it lowers the relaxation time of protons to microseconds, causing the progressive disappearance of the peaks due to the protons located in the reached compartments. Fig. 2 shows that the peak with a T_2 of 900 ms decreased during Mn^{2+} penetration at a slower rate than the one at 300 ms, allowing to ascribe the former to the vacuole, and the latter to the remaining compartments, namely cytoplasm and extracellular space. This finding was not unexpected, as the peak at 900 ms represents the majority of the signal of the fresh tissue (around 70%), and indeed in most plant cells the vacuole region can take up from 60% to 95% of the protoplast (Wayne, 2009, chap. 7).

Fig. 3 shows the typical effect of the OD on the intensity and T_2 values of the three peaks, related to the above-mentioned compartments. The values for each treatment temperature, before and after 300 min of OD are summarised in Table 1. In fresh fruit tissue the protons located inside the vacuole represented about 72% of the total. The OD seemed to reduce the vacuolar protons by 30% at 25 °C and 46% at 35 and at 45 °C. The water loss, leading to the shrinkage, caused a concentration of solutes, retained by the tonoplast, making the vacuole T_2 to decrease at each treatment. Again, the effect of the treatment at 35 °C equalled the one at

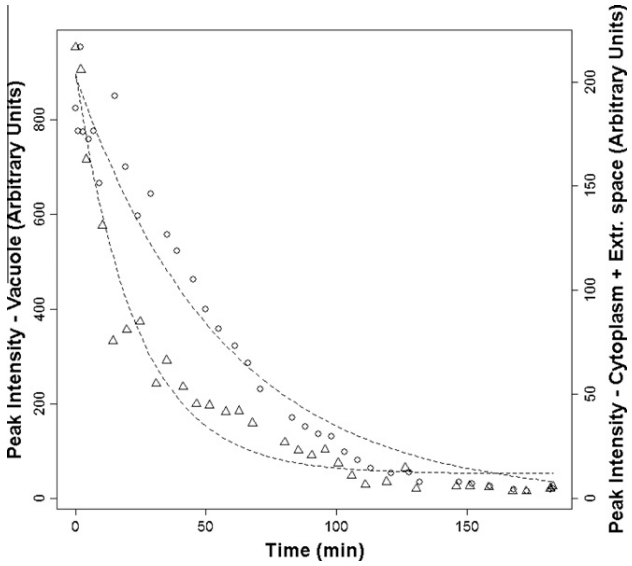

Fig. 2. Peak intensity at 900 ms, assigned to protons in vacuole (circles), and at 300 ms, assigned to protons in cytoplasm and extracellular space (triangles), during a doping experiment with Mn^{2+}.

45 °C Bowtell et al. (1992) showed through NMR microscopy that, during vacuole shrinkage, the cytoplasm sticks to the tonoplast, followed by the cellular membrane. This creates intracellular spaces, filled by vacuole content and osmotic solution, which contribute to the cytoplasm and the extracellular space proton pool.

Table 1
T_2 and intensity values of peaks ascribed to cell compartment proton pools. Raw kiwifruit is compared with 300 min treated kiwifruits at 25, 35 and 45 °C. The intensities are scaled to the raw kiwifruit, set to 100. The errors are expressed as standard deviation among the replicates.

Cell compartment	OD temperature (°C)	T_2 (ms)	Peak intensity (a.u.)
Vacuole	Raw kiwifruit	1091 ± 92	71 ± 4
	25	675 ± 67	50 ± 4
	35	479 ± 137	39 ± 2
	45	450 ± 153	39 ± 3
Cytoplasm/extracellular space	Raw kiwifruit	296 ± 18	20 ± 5
	25	169 ± 10	37 ± 3
	35	154 ± 3	47 ± 2
	45	134 ± 21	51 ± 3
Cell wall	Raw kiwifruit	33 ± 4	6 ± 1
	25	30 ± 5	12 ± 1
	35	29 ± 3	14 ± 1
	45	28 ± 5	11 ± 1

In agreement with Bowtell et al. (1992) findings, Table 1 shows that the cytoplasm and extracellular water proton pool considerably increased during the treatment, almost triplicating after 300 min at 45 °C. In parallel, the transverse relaxation time of the same proton pool decreased, suggesting that the osmotic solutes, with short T_2, gave an important contribution to it. The treatment seemed to increase the proton pool located in the cell walls,

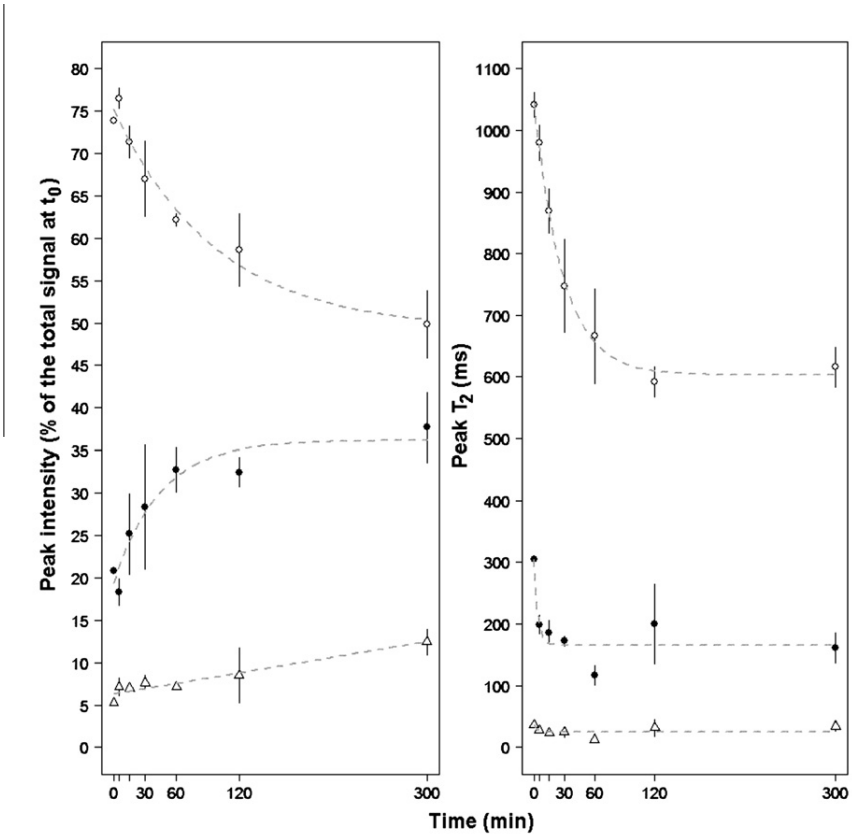

Fig. 3. Intensities and T_2 of kiwifruit tissue proton pools during the OD at 25 °C: vacuole (empty circles), cytoplasm and extracellular space (filled circles), cell wall (empty triangles). To help visualising the trends, the points are fitted to mono-exponential curves (dashed lines).

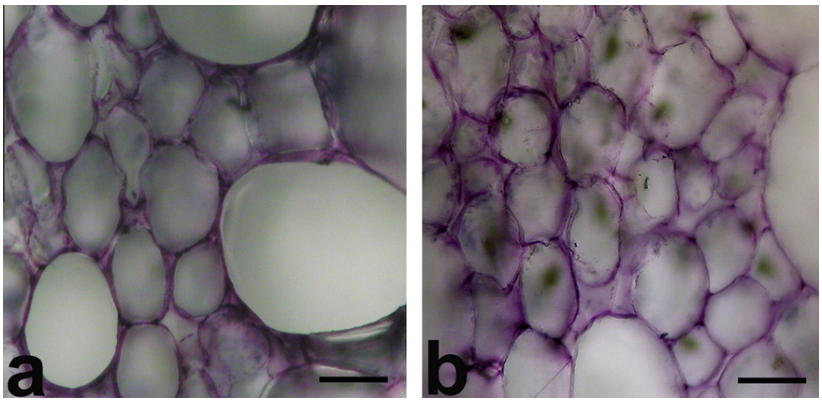

Fig. 4. LM of kiwifruit outer pericarp cells: stained cell walls before (a) and after (b) 120 min of OD at 35 °C. Bar = 100 μm.

without changing its T_2. Unfortunately these last observations are hindered because the cell wall proton population led to only 6% of the total NMR signal and it had a too short T_2. Therefore the cell wall changes, caused by OD, were evaluated through better-suited techniques, as described in the following sections.

3.2. Cell components and osmosis

Cell walls of outer pericarp tissue showed considerable changes in size, structure and stain uptake during the OD process, at both LM and TEM. Moreover cell walls showed extensive swelling,

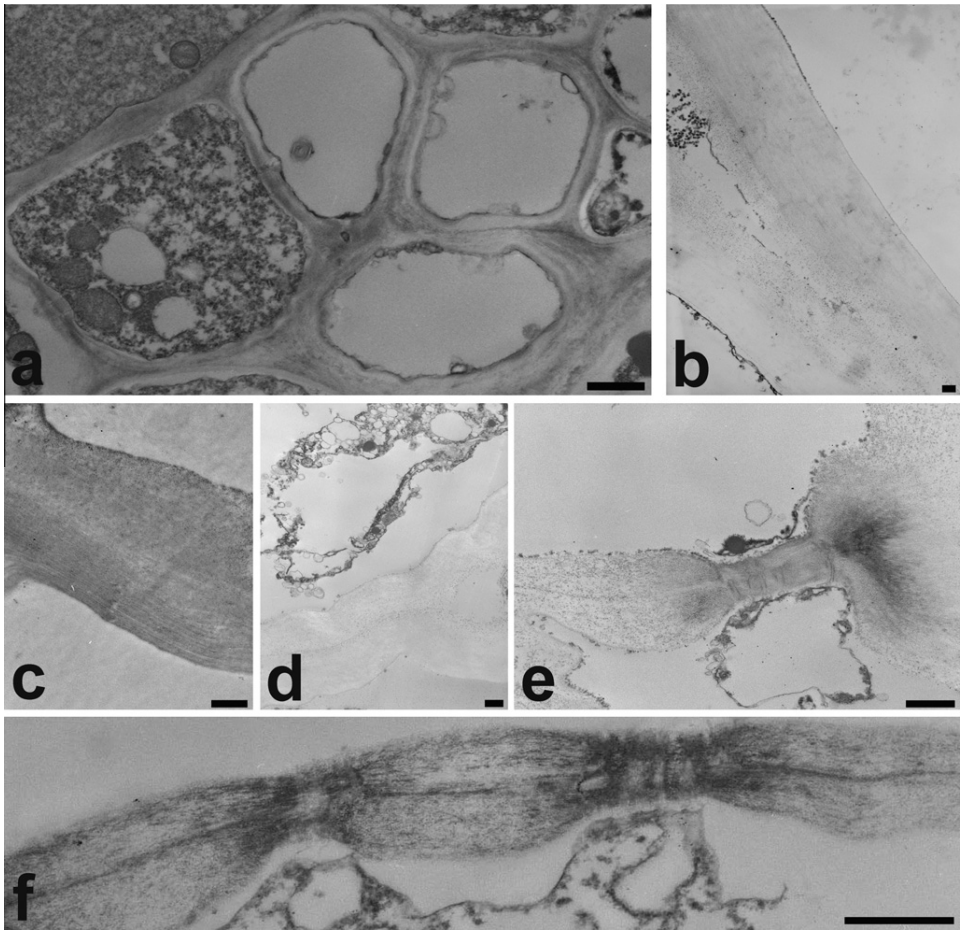

Fig. 5. Transmission electron micrographs of cell wall, plasmodesmata and intercellular spaces of outer pericarp cells of raw and treated fruits. Bar = 1 μm. (a) Section of the raw fruit tissue. The cells are well attached along the contact areas showing a well-preserved structure. (b) Detail of cell wall from treated fruit. Wall swollen and lack of staining are apparent. Electron-dense deposits accumulated in intercellular space region and wall margins. (c) Detail of cell wall from raw fruit. Wall shows intense staining of mainly longitudinal fibres. No swelling detected. (d) Detail of cell wall from treated fruit. Wall is swollen, failed to show any significant staining and little details are visible within the wall. (e) Plasmodesmata in cell wall from treated fruit. Plasmodesmata appear as a distinct constriction of the wall, staining is restricted to this area and there is a sharp difference between the lightly stained cell wall and the plasmodesmatal site. (f) Detail of plasmodesmata in cell wall from raw fruit. Wall shows a constriction in the plasmodesmata region. Staining density is similar in wall and plasmodesmatal regions.

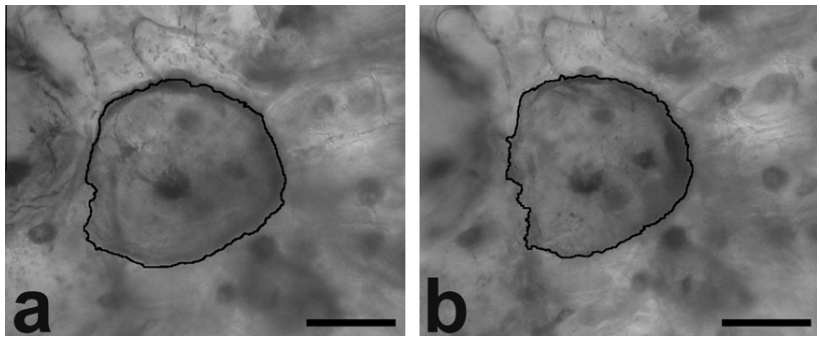

Fig. 6. LM of kiwifruit outer pericarp cells. Highlighted neutral-red stained vacuole after 60 min of OD at 30 °C: (a) processed image of cell prior OD (b) processed image of cell after OD. Bar = 100 μm.

which intensity varied from cell to cell and even within the same cell.

At LM the expansion of the cell walls was detected, as shown in Fig. 4a and b, respectively obtained on raw and treated (35 °C, 120 min).

Tissues of raw kiwifruits observed at TEM showed cells with an apparent well-defined cell wall structure (Fig. 5a). Cells were more or less regular in shape, in general isodiametric, and attached along extended contact areas.

The cell wall stained intensely, exhibiting dense longitudinal fibrous or reticulate staining (Fig. 5c). In treated fruits the stain became much more grainy and light and most wall material failed to stain (Fig. 5d). Furthermore the cell wall showed swelling (Fig. 5d) and accumulation of electron-dense deposits in intercellular spaces and wall margins (Fig. 5b). Outer pericarp cells from raw kiwifruits showed at TEM numerous plasmodesmatal connections densely stained and a slight thinning of the cell wall containing plasmodesmata (Fig. 5f). In treated fruits, the plasmodesmatal region appeared as a distinct constriction of the wall, with the staining restricted to this site with a sharp difference between the lightly stained cell wall and the plasmodesmatal area (Fig. 5e). These structural anomalies could result in connectivity deviations between adjacent cells.

A marked reduction in staining intensity of cell wall material occurred predominantly in the treated kiwifruit tissues and might be partially accounted for by wall expansion. The loss of staining could be due to artifactual losses of cell wall material during sample preparation, but electron micrographs support the idea that loss of staining intensity reflects a change in cell wall structure and composition *in situ*, since it has not been revealed in the raw fruits. Thus either the material was being lost from the cell wall or there occurred chemical modifications, which reduced the reactivity of cell wall materials with the stain. Hemicellulose stains strongly, and it could be that during the OD there was a modification of hemicelluloses molecular size. This change might contribute to a decrease reactivity of hemicelluloses for staining by reducing the number of available staining sites (Redgwell, Melton, & Brasch, 1989, 1991).

LM images of neutral red stained cells displayed the vacuole shrinkage subsequent to the OD treatment, confirming the results obtained by NMR measurements. As an example, Fig. 6a shows the outline of a stained kiwifruit vacuole before the OD; Fig. 6b shows the outline of the same vacuole, after 1 h of immersion in a 61.5% sucrose solution. Comparing these two micrographs, it seems that occupied volume by the fluorescent vacuole qualitatively decreased during the 60 min of the treatment. The observed vacuoles showed a heterogeneous range of shapes and dimensions, suggesting the need of further studies to better investigate the likely multiple mechanisms to which a vacuole can undergo in osmotic conditions.

4. Conclusions

With the present work the consequences of OD on the cell compartments of kiwifruit parenchyma tissue were investigated at macroscopic level, by measuring protons T_2, at microstructural level, by LM and ultrastructural level, by TEM.

LF-NMR observations revealed that OD promoted a redistribution of water among the cell compartments, followed by substantial shrinkage. TEM analysis showed that OD treatment induced intracellular space formations; this observation was confirmed by means of LF-NMR. Cell wall changes promoted by OD, i.e. wall swelling, dissolution of the middle lamella and reduction of overall staining, were similar to those promoted by fruit ripening. The multianalytical approach proposed in this study represents a powerful and versatile tool to investigate the behaviour of vegetable tissues exposed to different processing conditions.

References

Alandes, L., Hernando, I., Quiles, A., Pérez-Munuera, I., & Lluch, M. A. (2006). Cell wall stability of fresh-cut Fuji apples treated with calcium lactate. *Journal of Food Science, 71*, 615–620.

Borgia, G. C., Brown, R. J. S., & Fantazzini, P. (1998). Uniform-penalty inversion of multiexponential decay data. *Journal of Magnetic Resonance, 132*, 65–77.

Bowtell, R., Mansfield, P., Sharp, J. C., Brown, G. D., McJury, M., & Glover, P. M. (1992). NMR microscopy at 500 MHz: Cellular resolution in biosystems. In B. Blümich & W. Kuhn (Eds.), *Magnetic resonance microscopy: Methods and application in materials science, agriculture and biomedicine* (pp. 427–439). New York: VCH Publishers.

Bressa, F., Dalla Rosa, M., & Mastrocola, D. (1997). Use of a direct osmosis treatment to produce minimally processed kiwifruit slices in a continuous pilot plant. *Acta Horticolturae, 444*, 649–654.

Carpita, N., Sabularse, D., Montezinos, D., & Delmer, D. P. (1979). Determination of the pore size of cell walls of living plant cells. *Science, 205*, 1144–1147.

Cornillon, P. (2000). Characterization of osmotic dehydrated apple by NMR and DSC. *Lebensmittel-Wissenschaft und Technologie, 33*, 261–267.

Dixon, G. M., & Jen, J. J. (1977). Changes of sugars and acids of osmovac-dried apple slices. *Journal of Food Science, 42*, 1136–1140.

Gerschenson, L. N., Rojas, A. M., & Marangoni, A. G. (2001). Effects of processing on kiwifruit dynamic rheological behaviour and tissue structure. *Food Research International, 34*, 1–6.

Hallett, I. C., Macrae, E. A., & Wegrzyn, T. F. (1992). Changes in kiwifruit cell wall ultrastructure and cell packing during postharvest ripening. *International Journal of Plant Sciences, 154*, 49–60.

Hills, B. P., & Clark, C. J. (2003). Quality assessment of horticultural products by NMR. *Annual Reports on NMR Spectroscopy, 50*, 75–120.

Hills, B. P., & Duce, S. L. (1990). The influence of chemical and diffusive exchange on water proton transverse relaxation in plant tissue. *Magnetic Resonance Imaging, 8*, 321–331.

Hills, B. P., & Remigerau, B. (1997). NMR studies of changes in subcellular water compartmentation in parenchyma apple tissue during drying and freezing. *International Journal of Food Science and Technology, 32*, 51–61.

Jackman, R. L., & Stanley, D. W. (1995). Creep behaviour of tomato pericarp tissue as influenced by ambient temperature ripening and chilled storage. *Journal of Texture Studies, 26*, 537–552.

Kaymak-Ertekin, F., & Sultanoğlu, M. (2000). Modelling of mass transfer during OD of apples. *Journal of Food Engineering, 46*, 243–250.

Kowalska, H., & Lenart, A. (2001). Mass exchange during osmotic pretreatment of vegetables. *Journal of Food Engineering, 49*, 137–140.

Lerici, C. L., Pinnavaia, G., Dalla Rosa, M., & Bartolucci, L. (1985). OD of fruit: Influence of osmotic agents on drying behaviour and product quality. *Journal of Food Science, 50*, 1217–1219.

Marigheto, N., Vial, A., Wright, K., & Hills, B. (2004). A combined NMR and microstructural study of the effect of high pressure processing on strawberries. *Applied Magnetic Resonance, 26*, 521–531.

Mauro, M. A., Tavares, D., & Menegalli, F. C. (2002). Behaviour of plant tissue in osmotic solutions. *Journal of Food Engineering, 56*, 1–15.

O'Brien, T. P., Feder, N., & McCully, M. E. (1964). Polychromatic staining of plant cell walls by toluidine blue O. *Protoplasma, 59*, 368–373.

Rahman, M. S. (2008). Osmotic dehydration of foods. In M. S. Rahman (Ed.), *Handbook of food preservation* (pp. 403–432). Boca Raton: CRC Press.

Redgwell, R. J., Melton, L. D., & Brasch, D. J. (1991). Cell wall polysaccharides of kiwifruit (*Actinidia deliciosa*): Effect of ripening on the structural features of cell wall materials. *Carbohydrate Research, 209*, 191–202.

Redgwell, R. J., Melton, L. D., & Brasch, D. J. (1989). Cell wall changes in kiwifruit following postharvest ethylene treatment. *Phytochemistry, 29*, 399–407.

Salvatori, D., & Alzamora, S. M. (2000). Structural changes and mass transfer during glucose infusion of apples as affected by blanching and process variables. *Drying Technology, 18*, 361–382.

Snaar, J. E. M., & As Van, H. (1992). Probing water compartments and membrane permeability in plant cells by ^{1}H NMR relaxation measurements. *Biophysical Journal, 63*, 1654–1658.

Spurr, A. R. (1969). A low viscosity epoxy resin embedding medium for electron microscopy. *Journal of Ultrastructural Research, 26*, 31–43.

Stanley, D. W. (1987). Food texture and microstructure. In H. R. Moskow (Ed.), *Food texture instrumental and sensory measurement* (pp. 35–64). New York: Marcel Dekker Inc.

Sutherland, P., Hellett, I., Redgwell, R., Benhamou, N., & MacRae, E. (1999). Localization of cell wall polysaccharides during kiwifruit (*Actinidia deliciosa*) ripening. *International Journal of Plant Sciences, 160*, 1099–1109.

Thebud, R., & Santarius, K. A. (1982). Effects of high-temperature stress on various biomembranes of leaf cells in situ and in vitro. *Plant Physiology, 70*, 200–205.

Torreggiani, D., & Bertolo, G. (2004). Present and future in process control and optimization of osmotic dehydration: From unit operation to innovative combined process: An overview. *Advances in Food and Nutrition Research, 48*, 173–238.

Wayne, R. (2009). *Plant cell biology: From astronomy to zoology*. Burlington: Academic Press.

Paper IV

Innovative Food Science and Emerging Technologies 15 (2012) 66–71

Contents lists available at SciVerse ScienceDirect

Innovative Food Science and Emerging Technologies

journal homepage: www.elsevier.com/locate/ifset

Isothermal and differential scanning calorimetries to evaluate structural and metabolic alterations of osmo-dehydrated kiwifruit as a function of ripening stage

Valentina Panarese [a,*], Urszula Tylewicz [a], Patricio Santagapita [a,b], Pietro Rocculi [a], Marco Dalla Rosa [a]

[a] Alma Mater Studiorum, University of Bologna, Department of Food Science, P.zza Goidanich 60, Cesena (FC), Italy
[b] University of Buenos Aires, Faculty of Exact and Natural Sciences, Industry Department — Member of the National Council of Scientific and Technical Research (CONICET), Buenos Aires, Argentina

ARTICLE INFO

Article history:
Received 27 December 2011
Accepted 1 April 2012

Editor Proof Receive Date 30 April 2012

Keywords:
Kiwifruit
Ripening stage
Osmotic dehydration
DSC
Isothermal calorimetry
Texture
Respiration rate

ABSTRACT

The effects of osmotic dehydration (OD) on kiwifruit outer pericarp tissue as affected by treatment extent (0–300 min) and raw kiwifruit ripening stage (9 and 14 °Bx) were investigated.
Differential scanning calorimetry (DSC) measurements show decomposition of cell wall components (pectins, cellulose and hemi-celluloses). Changes in decomposition parameters (peak temperature lowered and enthalpy increased) were observed related to kiwifruit ripening degree and OD extent increased. Cell wall pectin network disassembly led to the formation of compounds with lower degradation temperature. Raw unripe fruits showed higher firmness values and lower compressibility compared to ripe and OD treated fruits.
Isothermal calorimetry revealed metabolic heat production of unripe fruits decreasing linearly with the OD extent. Ripe fruit heat production sharply decreased during the first treatment hour, probably as a consequence of membrane integrity loss.
Industrial relevance: OD leads to moisture removal and solute uptake in vegetable tissue, providing minimally processed commodities or ingredients for bakery or ice-cream industry. The industrial relevance is the energy-efficiency, since the process does not require water-phase change. OD provokes still unknown collateral alterations on tissue structure and metabolism. The present work applies a new calorimetric approach to evaluate both structure and metabolism changes on kiwifruit as reliant on process extent and raw fruit ripening stage.

1. Introduction

Osmotic dehydration treatment or Dewatering–Impregnation–Soaking (DIS) in concentrated solution increases solid concentration in food. Whole fruits or pieces are immersed in hypertonic solution and once contact takes place, three spontaneous fluxes of mass transfer occur. A major flux of water is accompanied by a minor one composed of those solutes capable of crossing the semipermeable membranes of the food into the solution. In a reverse process, some solutes are transferred from the solution into the food as a third flux (Torregiani & Bertolo, 2001).

Raw kiwifruits used in the fresh-cut industry require high firmness and low soluble solids content (Beaulieu, 2010). As a consequence the final fresh-cut product will not present the sufficient ripening level for the consumption. As suggested by Bressa, Dalla Rosa, and Mastrocola (1997), if the unripe fruit slices were subjected to osmotic dehydration (OD) treatment, a new product ready for the consumption could be obtained. Few minutes of OD in 61.5% (w/v) sucrose solution enable unripe kiwifruit slices to reach soluble solids content comparable with ripe fruit (Tylewicz, Rząca, Rocculi, Romani, & Dalla Rosa, 2010). Panarese et al. (2012) showed in an ultrastructural study that cell wall of kiwifruit tissue subjected to OD decreased the reactivity for staining; similar change was also detected on cell wall of ripe kiwifruit tissue and it was related to the highly branched hemicelluloses characterizing the cell wall of ripe fruit (Hallett, Macrae, & Wegrzyn, 1992). Besides both OD and ripening processes can lead to loss of cell wall integrity and modification of tissue textural properties and carbohydrate content, detectable through texture measurements and differential scanning calorimetry (DSC) on different fruits (Falcão-Rodrigues, Moldão-Martins, & Beirão-da-Costa, 2007; Pereira, Carmello-Guerreiro, & Hubinger, 2009; Yashoda, Prabha, & Tharanathan, 2006). Furthermore osmotic dehydration involves alteration on the fruit metabolism (Castelló, Fito, & Chiralt, 2006). Fruit and vegetables are biological active tissues and produce heat as a result of their metabolism. Calorimetric measurements of heat production rate have been used to provide indications of plant tissue metabolic response such as respiration and reaction to wounding stress (Gómez Galindo, Rocculi, Wadsö, & Sjöholm, 2005; Rocculi et al., 2007; Rocculi et al., 2005; Wadsö, Gomez, Sjöholm, & Rocculi, 2004), to quantify the cell damage occurring during thermal treatments (Gomez, Teledo,

* Corresponding author. Tel.: +39 0547 63 61 20; fax: +39 0547 38 23 48.
E-mail address: valentina.panarese2@unibo.it (V. Panarese).

1466-8564/$ – see front matter © 2012 Elsevier Ltd. All rights reserved.
doi:10.1016/j.ifset.2012.04.001

Wadsö, Gekas, & Sjöholm, 2004; Gómez Galindo, Teledo, & Sjöholm, 2005).

The aim of the present work was to evaluate the effect of the ripening stage on the changes of textural and thermal properties and metabolic response promoted by OD on kiwifruit.

2. Materials and methods

2.1. Raw materials

Kiwifruits (*Actinidia deliciosa* var *deliciosa* cv Hayward) with homogeneous size and refractometric index of 6.9 ± 0.8 °Bx were bought on the local market. Kiwifruits were sorted to eliminate damaged or defective fruit and were partially ripened at 4 ± 1 °C and 90–95% of relative humidity (RH) in air. Along the storage time, two kiwifruit groups were selected with refractometric index values of 9 ± 1 (called as LB, low °Brix) and 14.1 ± 0.9 °Bx (called as HB, high °Brix). The osmotic dehydration treatment was applied on fruit hand peeled and cut into 10 mm thick slices with a sharp knife.

2.2. Osmotic dehydration treatment

Osmotic dehydration (OD) was carried out by dipping the samples in 61.5% (w/v) sucrose solution equilibrated at 25 °C for pre-established contact periods of 0, 30, 60, 180 and 300 min, as reported by Tylewicz et al. (2011). The product/solution ratio was about 1:4 (w/w) and at each OD time, the osmotic solution was changed in order to avoid changes in its concentration. The temperature of the solution was maintained constant by a thermo-controlled water bath (25 °C). Eight OD runs were performed on a total of 240 kiwifruit slices (30 kiwifruit slices for each time–°Brix group condition). Each slice was taken from the central part of each kiwifruit (about 60 g) and was placed in mesh baskets and immersed in osmotic solution. The baskets were constantly stirred at 0.2 *g* with a propeller. The rotational speed was experimentally determined to assure negligible outer resistance to mass transfer. After that, the slices were taken from the osmotic solution and each slice face was rinsed with distilled water for 3 s and placed on blotting paper for 2 s.

2.3. Analytical determinations

2.3.1. Moisture content and soluble solids content

The moisture content of kiwifruit samples was determined gravimetrically by difference in weight before and after drying in vacuum oven (pressure ≤ 100 mm Hg) at 70 °C. The drying was performed until a constant weight was achieved (AOAC International, 2002). Duplicate measurements were conducted for each kiwifruit slice.

The soluble solids content (SSC) was determined at 20 °C by measuring the refractive index with a digital refractometer (PR1, Atago, Japan) calibrated with distilled water. For each sample, the SSC was determined in triplicate on the juice obtained from each kiwifruit slice, after filtering through Whatman #1 filter paper.

For both moisture content and SSC determinations, average values were obtained for 30 kiwifruit slices for each time–°Brix group condition.

2.3.2. Texture analysis

Firmness (N) was evaluated by performing a penetration test on kiwifruit slices' outer pericarp using a TA-HDi500 texture analyzer (Stable Micro Systems, Surrey, UK) with a 5 kg load cell. Experiment was run with a metal probe of 6 mm diameter, and a rate and depth of penetration of 1 mm s^{-1} and 6 mm, respectively (Beirão da Costa, Steiner, Correia, Empis, & Moldão Martins, 2006). Firmness (N) was evaluated as the first peak force value according to other authors (Beirão da Costa et al., 2006). The mean of two replicates of each kiwifruit slice was averaged for each OD condition (n = 30).

2.3.3. Differential scanning calorimetry (DSC)

DSC analysis was carried out on a Pyris 6 DSC (Perkin-Elmer Corporation, Wellesley, USA). The DSC was equipped with a low-temperature cooling unit Intracooler II (Perkin-Elmer Corporation, Wellesley, USA). Temperature calibration was performed with indium (mp 156.60 °C), tin (mp 231.88 °C), and zinc (mp 419.47 °C); heat flow was calibrated using the heat of fusion of indium (ΔH = 28.71 J g^{-1}). For the calibration, the same heating rate, as used for sample measurements, was applied under a dry nitrogen gas flux of 20 ml min^{-1}. About 10 mg of kiwifruit outer pericarp tissue was sampled and placed in 50 μl punctured aluminum pans prior to measurements. An empty pan was used as a reference. DSC curves were obtained by heating samples from 100 to 390 °C with a heating rate of 10 °C min^{-1}. The chosen range of temperatures enabled to evaluate only decomposition transitions, as kiwifruit T_g has been found in the range of −30 to −50 °C (Li et al., 2008). Three replicates for each treatment condition were performed.

2.3.4. Isothermal microcalorimetry

Six cylinders were sampled using a core borer from the outer pericarp tissue of each kiwifruit slice and placed in sealed 20 ml glass ampoule. Four replicates for each treatment condition were performed. The rate of heat production was continuously measured in a TAM air isothermal calorimeter (Thermometric AB, Järfälla, Sweden), with a sensitivity (precision) of ± 10 μW (Wadsö & Gómez Galindo, 2009). This instrument contains eight twin calorimeters. Each calorimeter had its own reference and the measured signal is the difference between the sample signal and the reference signal. The reference is a sample with thermal properties similar to the sample, except that it does not produce any heat; water was chosen as the reference material. By assuming that the heat capacity of kiwifruit dry matter (C_{ST}) is 1 J g^{-1} K^{-1}, the quantity of water in each reference ampoule (M_w) was determined as:

$$M_w = \frac{C_{ST} \cdot M_{ST} + C_W \cdot M_W}{C_W} \quad (1)$$

where M_{ST} is the dry matter content and M_W is the water content of the kiwifruit sample; C_W is the water heat capacity. The measurements were performed at 20 °C for 24 h. Immediately after the ampoules discharging from the calorimeters, the CO_2 percentage was measured in the ampoule headspaces by a gas analyzer (MFA III S/L gas analyzer, Witt-Gasetechnik, Witten, Germany).

2.3.5. Respiration rate

The respiration rate was evaluated on raw and 60 min treated HB kiwifruit, using a static method. Six cylinders were sampled from the outer pericarp tissue of the slice and sealed in 20 ml glass ampoule. O_2 percentage of triplicate specimens was measured in the ampoule headspace by a gas analyzer (MFA III S/L gas analyzer, Witt-Gasetechnik) after 2, 3, 5, 22 and 24 h at 20 °C from the sampling. The respiration rate (RRO_2) was calculated as:

$$RRO_2 = \frac{mm_{O_2} \cdot V_{head} \cdot \frac{(20.8 - \%O_{2,head})}{100} 101.325}{t \cdot m \cdot R \cdot 293} \quad (2)$$

where mm_{O_2} is the oxygen molar mass (g/mol), V_{head} is the ampoule headspace volume (L), $\%O_{2,\ head}$ is the oxygen percentage in the ampoule headspace at time t (h); m is the sample mass (kg); R is the gas constant (L kPa K^{-1} mol^{-1}).

2.4. Statistical analysis

Significance of the osmotic dehydration effects was evaluated by means of one-way analysis of variance using the software STATISTICA 6.0 (Statsoft Inc., Tulsa, UK). The analysis of the means

was performed using the Tukey procedure at $P<0.05$. Correlation analysis was performed using GraphPad Prism v.5 (GraphPad Software, Inc., La Jolla, CA, USA) with two-tailed P values<0.05, assuming that data were sampled from Gaussian distribution.

3. Results and discussion

3.1. Soluble solid content of ripe and unripe OD-kiwifruit

It is well known that osmotic treatment leads to a great water loss from kiwifruit and the simultaneous counter-diffusion of solutes from the concentrated solution into the kiwifruit tissues. The soluble solids content (SSC) increase along osmotic dehydration resulted similar for both kiwifruit groups (LB, low and HB, high °Brix degree), as shown in Fig. 1a. However it is possible to observe that the SSC increase of HB group was lower than that of LB group. This result may be due to the higher sugar content of ripe fruit that, in turn, negatively affects the difference between the osmotic potential of the solution and the fruit, which is the driving force of osmotic transport phenomena (Chiralt & Fito, 2003; Shi & Le Maguer, 2003). Furthermore the decrease of the osmotic pressure difference between solution and fruit over time leads to the decrease of the rate of SCC uptake for both LB and HB kiwifruits, as shown in Fig. 1a. The same trend was observed in previously reported data for kiwifruit slices treated in the same osmotic conditions at 25 °C (Santagapita et al., 2012; Tylewicz et al., 2011). Fig. 1b shows the linear regression between soluble solids content and dry matter. Both parameters increased together during OD with very high correlation coefficient ($r>0.96$) for both LB and HB groups.

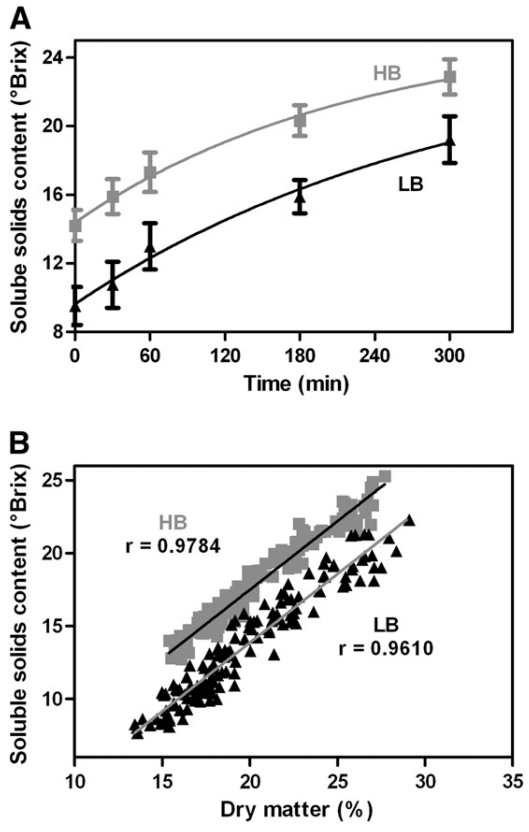

Fig. 1. a) Solid gain expressed as soluble solids content vs. time of dehydration treatment for low (LB) and high (HB) °Brix kiwifruit slices. Each point represents an average of at least 30 kiwifruit slices and bars represent standard deviation values. b) Linear correlation between soluble solids content and dry matter.

3.2. Texture and cell wall integrity of ripe and unripe OD-kiwifruit: texture and DSC measurements

Fig. 2b shows the texture changes of low and high °Brix kiwifruit as a function of osmotic dehydration time. The importance of texture on minimally processed fruits both for technological and qualitative aspects is noteworthy. According to Muntada, Gerschenson, Alzamora, and Castro (1998), firmness is one of the most important parameters since its changes could be related to structural changes. Several structures are affected along OD treatment. Panarese et al. (2012) described that OD induced plasmolysis, shrinkage of the vacuole compartment, changes in size and structure of the cell walls of outer pericarp during OD and dissolution of the middle lamella. The firmness change produced along OD could be partially limited by adding texture-enhancing solutes such as Ca^{2+} and pectinmethylesterase (PME) to the sucrose solution (Van Buggenhout, Grauwet, Van Loey, & Hendrickx, 2008).

The overall shape of the curve obtained by penetration test is shown in Fig. 2a for both HB and LB groups, before and after 300 min of OD. Firmness values showed the expected differences for both LB and HB raw kiwifruits due to the higher ripening on HB samples (Barboni, Cannac, & Chiaramonti, 2010; Beirão da Costa et al., 2006). OD-treated samples of both kiwifruit groups displayed lower firmness and higher compressibility than raw samples. Raw LB revealed the highest firmness values, but the firmness loss along OD was more marked with respect to HB kiwifruit (Fig. 2a). This in turn can be related to the higher capabilities of LB group to increase the SSC (Fig. 1a). The lower firmness values observed after 300 min can be also observed in Fig. 2b, which shows firmness vs. OD time. The major firmness loss occurred during the first hour of OD with different rates for the two kiwifruit groups. LB and HB firmness loss occurring during the first hour of OD resulted respectively four and two times higher than the firmness loss recorded during the following 4 h of treatment.

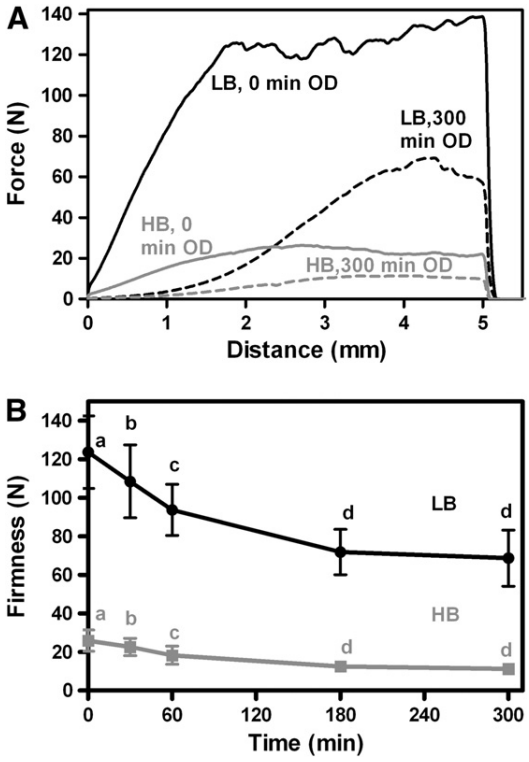

Fig. 2. Overall shape of the penetration curves (a) and firmness (b) of low (LB) and high (HB) °Brix kiwifruit slices as a function of OD duration.

Fig. 2a depicts for the OD-treated samples two very different slopes prior to arrive to the first peak/maximum force (Fig. 2a). Instead, raw samples (especially LB samples) showed a unique slope prior to the first peak. Since the slope of the force deformation curve (N/s) until the first inflection point indicates the point of non-destructive elastic deformation (Beaulieu, 2010), it could be proposed that the LB raw material did not present the non-destructive elastic deformation, but appears slightly with the ripening increase and especially along OD.

DSC measurements were performed to follow the modification promoted by OD on the principal components of the cell wall, which are: pectins (between 40 and 50%), cellulose (between 23 and 35%), hemi-celluloses (between 15 and 25%) and proteins (between 1 and 7%) (Redgwell, Melton, & Brasch, 1991).

Fig. 3 shows the thermograms obtained for LB and HB kiwifruits before and after 300 min of OD. It is worth noting that characteristic decomposition temperatures of sucrose and cell wall principal components are detected in the range 150–350 °C (Abd-Elrahman & Ahmed, 2009; Einhorn-Stoll, Kunzek, & Dongowski, 2007; Ray, Sarkar, Basak, & Rana, 2004).

Peak 1, highlighted in Fig. 3 by a square shape, can be attributed to sucrose, which decomposition temperature was reported between 206 and 232 °C (Abd-Elrahman & Ahmed, 2009). Peak 1 integration has been carried out from 180 to 235 °C; on average the obtained peak temperature value (209 ± 2 °C) was consistent with the decomposition temperature of sucrose found in previous researches (Abd-Elrahman & Ahmed, 2009).

The peak enthalpy values of peak 1 reported in Table 1 appeared higher for HB than for LB kiwifruit, following the sucrose content increase. Enthalpy values increased slowly for LB along OD whereas enthalpy increased up to 3 times after 3 h for HB kiwifruit.

For higher temperature, a complex peak appears (peak 2, pointed out in Fig. 3 through arrows), ascribable to cell wall component (pectins, hemi-celluloses and cellulose) decomposition (Abd-Elrahman & Ahmed, 2009; Einhorn-Stoll et al., 2007; Ray et al., 2004). For the overall evaluation of cell wall component modification, peak 2 integration has been carried out from 180 to 370 °C. To obtain values, the peak 1 enthalpy has been subtracted in order to reduce the integral overestimation caused by peak overlap.

Peak 2 related to raw LB kiwifruit showed a higher heat flow value than the corresponding peak of raw HB kiwifruit, ascribable to the different physiological state of the cell wall in the LB and the HB raw material (Bennett, 2002). Values of peak 2 associated to HB and LB kiwifruits changed similarly along OD. This analogy can be related to cell wall modifications promoted by both fruit ripening and OD, as pre-established by microstructure analysis by Panarese et al. (2012). Actually, even in terms of calorimetric response, the effect of ripening

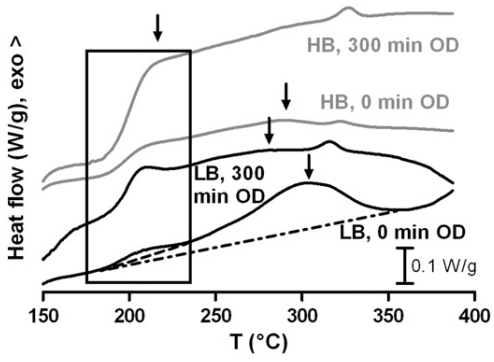

Fig. 3. Thermograms obtained by differential scanning calorimetry (DSC) of low (LB) and high (HB) °Brix kiwifruit slices raw (0 min) and subjected to 300 min of osmotic dehydration. The square indicates the changes that occurred to peak 1 and arrows point out the peak temperature of peak 2. The dashed lines show the two analyzed peaks (values reported in Table 1).

Table 1
Enthalpy values of raw (0 min) and subjected to OD low and high °Brix kiwifruit slices. Peaks 1 and 2 correspond to those evidenced by the dashed lines in Fig. 3.

Kiwifruit ripening (°Brix)	Time (min)	Peak 1 Area (J/g)*	Peak 2 Area (J/g)*
Low °Brix	0	1.6 ± 0.2^{c}	72 ± 4^{b}
	30	4.5 ± 0.5^{a}	84 ± 11^{b}
	60	4.0 ± 0.4^{a}	79 ± 15^{b}
	180	2.7 ± 0.4^{b}	142 ± 26^{a}
	300	4.1 ± 0.4^{a}	105 ± 27^{ab}
High °Brix	0	10 ± 2^{c}	84 ± 6^{b}
	30	11.9 ± 0.4^{c}	62 ± 3^{b}
	60	11 ± 1^{c}	62 ± 21^{b}
	180	27 ± 2^{b}	101 ± 3^{a}
	300	37 ± 3^{a}	107 ± 17^{a}

* Values in the same column followed by different letters differ significantly at $P<0.05$ levels.

and OD seems to be comparable; this is confirmed by the very similar shape of LB 300 min and HB 0 min thermograms, in the temperature range corresponding to cell wall component decomposition.

Peak 2 enthalpy values decreased and increased respectively as a consequence of OD for both kiwifruit groups, mainly for HB kiwifruit (Table 1). Bennett (2002) determined that the softening of vegetal tissues during the first stages of ripening is due to depolymerization of hemi-cellulose. Then, the rupture of the pectin network predominates in the last stages of ripening and during fruit over-ripening. Hemi-cellulose depolymerization and pectin network disassembly lead to the formation of more compounds with minor molecular mass (Bennett, 2002; Lloyd & Wyman, 2003). These compounds depicted lower degradation temperature and overall higher enthalpy values.

OD-treated and ripe samples show a little peak between 320 and 327 °C (Fig. 3) with enthalpy values varying between 1.2 and 1.7 J/g and it could be possibly related to cellulose (Godeck, Kunzek, & Kabbert, 2001). In LB raw kiwifruit this peak is hard to read out because of the decomposition enthalpy of those cell wall components that are affected by both ripening and OD.

Raw LB kiwifruit thermograms showed well separated peaks and higher heat flow value than those corresponding to HB. As a consequence of OD peak temperature attributed to cell wall decomposition diminish and enthalpy values increases. These changes are parallel to firmness loss (Fig. 2b) and once again reveal the relation between firmness changes and cell wall integrity loss.

3.3. Metabolic response of ripe and unripe OD-kiwifruit: respiration and isothermal microcalorimetry measurements

Kiwifruit as well as other fruits and vegetables are metabolic active tissues producing heat as a result of respiration. Fig. 4 depicts an example of heat production profiles of cooked, raw and osmo-dehydrated LB kiwifruit samples during 24 h at 20 °C. Thermal treated (100 °C for 10 min) kiwifruit was used as a control as not producing any metabolic heat. Sample ampoule loading into a calorimeter induced a large initial disturbance lasting for at least 20–30 min. The thermograms evidenced a progressive decrease of the specific thermal power P (mW per gram of kiwifruit sample) by increasing the OD time. A similar behavior was obtained for HB kiwifruit.

The aerobic cell respiration produces about 455 kJ of heat per mol of O_2 consumed or mol of CO_2 produced. Therefore calorimetric measurements on tissue metabolism can give similar information as respiration measurements (Wadsö & Gómez Galindo, 2009). In order to verify this relationship in our experimental conditions, and to confirm the capability of TAM-Air isothermal calorimeter to study the metabolic consequences promoted by osmosis, respiration measurements have been performed on HB raw and 60 min treated kiwifruit samples and compared with the heat production results.

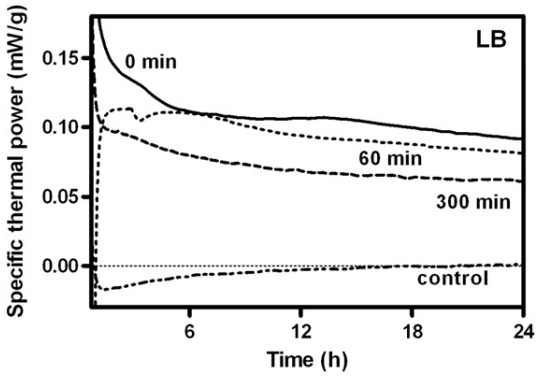

Fig. 4. Specific thermal power profiles of pericarp tissue cylinders of raw, cooked and selected osmo-dehydrated kiwifruits during 24 h of analysis at 20 °C. Each thermogram is an average of four replicates. The initial signal disturbance is a consequence of sample ampoule loading.

The respiration rate RRO_2 ($g\,O_2\,h^{-1}\,kg^{-1}$) was measured using a static method at 2, 3, 5, 22 and 24 h. On the other hand, the thermal power values ($mJ\,s^{-1}\,g^{-1}$) have been integrated at the same measuring time of RRO_2 and expressed as heat of respiration (RRO_2cal) ($g\,O_2\,h^{-1}\,kg^{-1}$). The respiration within the 24 h of analysis was considered aerobic (Iversen, Wilhelmsen, & Criddle, 1989) and the anaerobic metabolism was neglected since the percentage of CO_2 determined by a gas analyzer in the ampoule headspace after 24 h at 20 °C did not exceed the 4–5% for both raw and 60 min treated samples (data not reported). Fig. 5 shows the correlation between RRO_2 values obtained by gas measurement and RRO_2cal values calculated from calorimetric analysis. These parameters appeared strictly and positively correlated for both raw and 60 min treated samples with correlation coefficients higher than 0.98. In order to better understand the effect of OD on the metabolic heat of both LB and HB samples, the thermal power curves have been integrated from 1 to 13 h of analysis. The thermal powers corresponding to the initial disturbance consequent to the sample ampoule loading have been subtracted. Obtained specific heat production (P12h) ($J\,g^{-1}$) results vs. treatment time are reported in Fig. 6. The metabolic heat production of the raw samples was very similar for both the ripening stage investigated and progressively decreased with the increasing of OD time. Gomez et al. (2004) suggested that the decrease in thermal power in carrot tissue is correlated with cell membrane damage as measured by the inactivation of plasma membrane H^+-ATPase. During OD tissue damage progressively occurs. This is induced by osmotic stress and is accompanied by a reduction of the number of viable cells, as reported by Mavroudis, Dejmek, and Sjoholm (2004). The cellular response to osmotic stress depends on the botanical

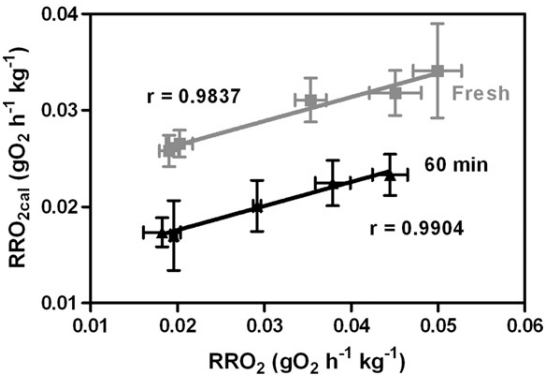

Fig. 5. Linear correlation between respiration rates obtained by O_2 measurement (RRO_2) or calculated from specific thermal power curves (RRO_2cal) for raw and 60 min treated HB samples.

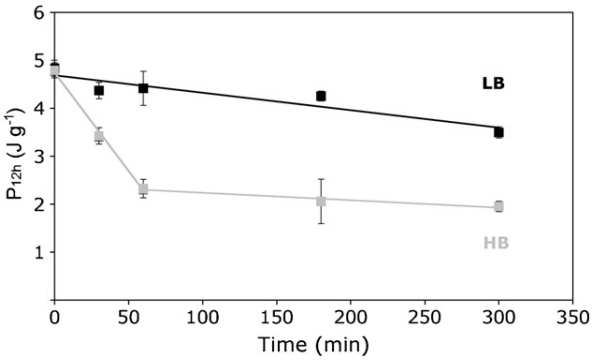

Fig. 6. Specific heat production (P_{12h}) ($J\,g^{-1}$) results vs. osmotic-dehydration treatment time for LB and HB samples.

origin of the observed tissue, i.e. Ferrando and Spiess (2001) observed the reduction of viability of strawberries' cortex cells during OD process, while the protoplast of onion epidermis did not suffer any irreversible changes through the process. Metabolic heat production of LB kiwifruit samples showed a linear decrease with the proceeding of OD; instead, the detected heat production for HB samples sharply decreased along the first 60 min of the treatment. These differences can be explained by the different physiological state of the fruit tissue: cells of more ripe kiwifruit seem to be more sensible to osmotic stress because of the increase of membrane permeability due to the loss of membrane integrity during kiwifruit ripening (Song et al., 2009).

The possibility to highlight how the response to OD treatment was modulated by fruit ripeness suggests that a combined calorimetric approach can represent a powerful and versatile tool to investigate the behavior of vegetable tissues during minimal processing. Then, by knowing the extent of changes on water and solutes during OD, which in turn modified the textural, structural and viability/respiratory characteristics of the final product, it is possible to exploit both raw unripe and ripe kiwifruits from a technological point of view.

4. Conclusions

OD promoted critical changes in the kiwifruit, as pointed out with good agreement by both texture profiles and thermal degradation thermograms. The magnitude of those changes depended on the maturity degree of raw kiwifruits.

DSC revealed hemicellulose degradation and pectin network rupture of kiwifruit cell wall. The measurements showed that the decrease of peak temperature and the increase of enthalpy were both associated with kiwifruit maturity degree and OD extent. These changes seemed to be responsible for the lower force necessary to achieve penetration in the HB kiwifruit.

Isothermal calorimetry confirmed its high potentiality for calorespirometric measurement on fresh vegetable tissues. Metabolic heat production of kiwifruit samples showed a linear decrease with the proceeding of OD, confirming the damage progression on tissue induced by osmotic stress, accompanied by the reduction of the number of viable cells. Ripe kiwifruit metabolic heat reduction was more pronounced, probably as a consequence of the membrane integrity loss occurring within the kiwifruit ripening.

Acknowledgments

Patricio Santagapita acknowledges the EADIC program of Erasmus Mundus External Cooperation Window Lot 16 and the National Council of Scientific and Technical Research (CONICET) for the postdoc scholarships.

References

Abd-Elrahman, M. I., & Ahmed, S. M. (2009). Thermal degradation kinetics and geometrical stability of D-sucrose. *International Journal of Polymeric Materials*, *58*, 322–335.

AOAC International (2002). *Official methods of analysis (OMA) of AOAC International, 17th Edition, USA. Method number: 920.15.* Available at http://www.eoma.aoac.org/

Barboni, T., Cannac, M., & Chiaramonti, N. (2010). Effect of cold storage and ozone treatment on physicochemical parameters, soluble sugars and organic acids in *Actinidia deliciosa*. *Food Chemistry*, *121*, 946–951.

Beaulieu, J. (2010). Factors affecting sensory quality of fresh-cut produce. In O. Martin-Belloso, & R. Soliva-Fortuny (Eds.), *Advances in fresh-cut fruits and vegetables processing* (pp. 115–143). Boca Raton: CRC Press.

Beirão da Costa, S., Steiner, A., Correia, L., Empis, J., & Moldão Martins, M. (2006). Effects of maturity stage and mild heat treatments on quality of minimally processed kiwifruit. *Journal of Food Engineering*, *76*, 616–625.

Bennett, A. B. (2002). Biochemical and genetical determinants of cell wall disassembly in ripening fruit: a general model. *HortScience*, *37*, 3–6.

Bressa, F., Dalla Rosa, M., & Mastrocola, D. (1997). Use of a direct osmosis treatment to produce minimally processed kiwifruit slices in a continuous pilot plant. *Acta Horticulturae (ISHS)*, *444*, 649–654.

Castelló, M. L., Fito, P. J., & Chiralt, A. (2006). Effect of osmotic dehydration and vacuum impregnation on respiration rate of cut strawberries. *Lewensmittel Food Science and Technology*, *39*, 1171–1179.

Chiralt, A., & Fito, P. (2003). Transport mechanisms in osmotic dehydration: The role of the structure. *Food Science and Technology International*, *9*, 179–186.

Einhorn-Stoll, U., Kunzek, H., & Dongowski, G. (2007). Thermal analysis of chemically and mechanically modified pectins. *Food Hydrocolloids*, *21*, 1101–1112.

Falcão-Rodrigues, M. M., Moldão-Martins, M., & Beirão-da-Costa, M. L. (2007). DSC as a tool to assess physiological evolution of apples preserved by edibles coatings. *Food Chemistry*, *102*, 475–480.

Ferrando, M., & Spiess, W. E. L. (2001). Cellular response of plant tissue during the osmotic treatment with sucrose, maltose and trehalose solutions. *Journal of Food Engineering*, *49*, 115–127.

Godeck, R., Kunzek, H., & Kabbert, R. (2001). Thermal analysis of plant cell wall materials depending on the chemical structure and pre-treatment prior to drying. *European Food Research and Technology*, *213*, 395–404.

Gomez, F., Teledo, R., Wadsö, L., Gekas, V., & Sjöholm, I. (2004). Isothermal calorimetry approach to evaluate tissue damage in carrot slices upon thermal processing. *Journal of Food Engineering*, *65*, 165–173.

Gómez Galindo, F., Rocculi, P., Wadsö, L., & Sjöholm, I. (2005). The potential of isothermal calorimetry in monitoring and predicting quality changes during processing and storage of minimally processed fruits and vegetables. *Trends in Food Science & Technology*, *16*, 325–331.

Gómez Galindo, F., Teledo, R., & Sjöholm, I. (2005). Tissue damage in heated carrot slices. Comparing mild hot water blanching and infrared heating. *Journal of Food Engineering*, *67*, 381–385.

Hallett, I. C., Macrae, E. A., & Wegrzyn, T. F. (1992). Changes in kiwifruit cell wall ultrastructure and cell packing during postharvest ripening. *International Journal of Plant Science*, *154*, 49–60.

Iversen, E., Wilhelmsen, E., & Criddle, R. S. (1989). Calorimetric examination of cut fresh pineapple metabolism. *Journal of Food Science*, *54*, 1246–1249.

Li, S., Zhang, M., Song, X., Duan, X., Zhou, L., & Sun, J. (2008). Effect of pretreatments and storage conditions on the quality of frozen kiwifruit slices. *International Journal of Food Properties*, *11*, 68–78.

Lloyd, T., & Wyman, C. E. (2003). Application of a depolymerization model for predicting thermochemical hydrolysis of hemicellulose. *Applied Biochemistry and Biotechnology*, *105–108*, 53–67.

Mavroudis, N. E., Dejmek, P., & Sjoholm, I. (2004). Osmotic-treatment-induced cell death and osmotic processing kinetics of apples with characterised raw material properties. *Journal of Food Engineering*, *63*, 47–56.

Muntada, V., Gerschenson, L. N., Alzamora, S. M., & Castro, M. A. (1998). Solute infusion effects on texture of minimally processed kiwifruit. *Journal of Food Science*, *63*, 616–620.

Panarese, V., Laghi, L., Pisi, A., Tylewicz, U., Dalla Rosa, M., & Rocculi, P. (2012). Effect of osmotic dehydration on *Actinidia deliciosa* kiwifruit: A combined NMR and ultrastructural study. *Food Chemistry*, *132*, 1706–1712.

Pereira, L. M., Carmello-Guerreiro, S. M., & Hubinger, M. D. (2009). Microscopic features, mechanical and thermal properties of osmotically dehydrated guavas. *LWT — Food Science and Technology*, *42*, 378–384.

Ray, D., Sarkar, B. K., Basak, R. K., & Rana, A. K. (2004). Thermal behavior of vinyl ester resin matrix composites reinforced with alkali-treated jute fibers. *Journal of Applied Polymer Science*, *94*, 123–129.

Redgwell, R. J., Melton, L. D., & Brasch, D. J. (1991). Changes to pectic and hemicellulosic polysaccharides of kiwifruit during ripening. *Acta Horticulturae (ISHS)*, *297*, 627–634.

Rocculi, P., Gómez Galindo, F., Mendoza, F., Wadsö, L., Romani, S., Dalla Rosa, M., et al. (2007). Effect of the application of anti-browning substrates on the metabolic activity and sugar composition of fresh-cut potatoes. *Postharvest Biology and Technology*, *43*, 151–157.

Rocculi, P., Romani, S., Dalla Rosa, M., Gómez Galindo, F., Sjöholm, I., & Wadsö, L. (2005). Use of isothermal calorimetry to monitor and predict quality and shelf-life of minimally processed fruits and vegetables. *Industrie Alimentari*, *44*, 841–846.

Santagapita, P., Laghi, L., Panarese, V., Tylewicz, U., Rocculi, P., & Dalla Rosa, M. (2012). Modification of transverse NMR relaxation times and water diffusion coefficients of kiwifruit pericarp tissue subjected to osmotic dehydration. *Food and Bioprocess Technology*. doi:10.1007/s11947-012-0818-5.

Shi, J., & Le Maguer, M. (2003). Mass transfer flux at solid–liquid contacting interface. *Food Science and Technology International*, *9*, 193–199.

Song, L., Gao, H., Chen, H., Mao, J., Zhou, Y., Chen, W., et al. (2009). Effects of short-term anoxic treatment on antioxidant ability and membrane integrity of postharvest kiwifruit during storage. *Food Chemistry*, *114*, 1216–1221.

Torregiani, D., & Bertolo, G. (2001). Osmotic pre-treatments in fruit processing: Chemical, physical and structural effects. *Journal of Food Engineering*, *49*, 247–253.

Tylewicz, U., Panarese, V., Laghi, L., Rocculi, P., Nowacka, M., Placucci, G., et al. (2011). NMR and DSC water study during osmotic dehydration of *Actinidia deliciosa* and *Actinidia chinensis* kiwifruit. *Food Biophysics*, *6*, 327–333.

Tylewicz, U., Rząca, M., Rocculi, P., Romani, S., & Dalla Rosa, M. (2010). Evolution of quality characteristics of Hayward and Hort16A kiwifruit during osmotic dehydration. *Fruit Processing*, *4*, 150–153.

Van Buggenhout, S., Grauwet, T., Van Loey, A., & Hendrickx, M. (2008). Use of pectin-methylesterase and calcium in osmotic dehydration and osmodehydrofreezing of strawberries. *European Food Research and Technology*, *226*, 1145–1154.

Wadsö, L., Gomez, F., Sjöholm, I., & Rocculi, P. (2004). Effect of tissue wounding on the results from calorimetric measurements of vegetable respiration. *Thermochimica Acta*, *422*, 89–93.

Wadsö, L., & Gómez Galindo, F. (2009). Isothermal calorimetry for biological application in food science and technology. *Food Control*, *20*, 956–961.

Yashoda, H. M., Prabha, T. N., & Tharanathan, R. N. (2006). Mango ripening: Changes in cell wall constituents in relation to textural softening. *Journal of the Science of Food and Agriculture*, *86*, 713–721.

Paper V

Modification of Transverse NMR Relaxation Times and Water Diffusion Coefficients of Kiwifruit Pericarp Tissue Subjected to Osmotic Dehydration

Patricio Santagapita, Luca Laghi, Valentina Panarese, Urszula Tylewicz, Pietro Rocculi & Marco Dalla Rosa

Food and Bioprocess Technology
An International Journal

ISSN 1935-5130

Food Bioprocess Technol
DOI 10.1007/s11947-012-0818-5

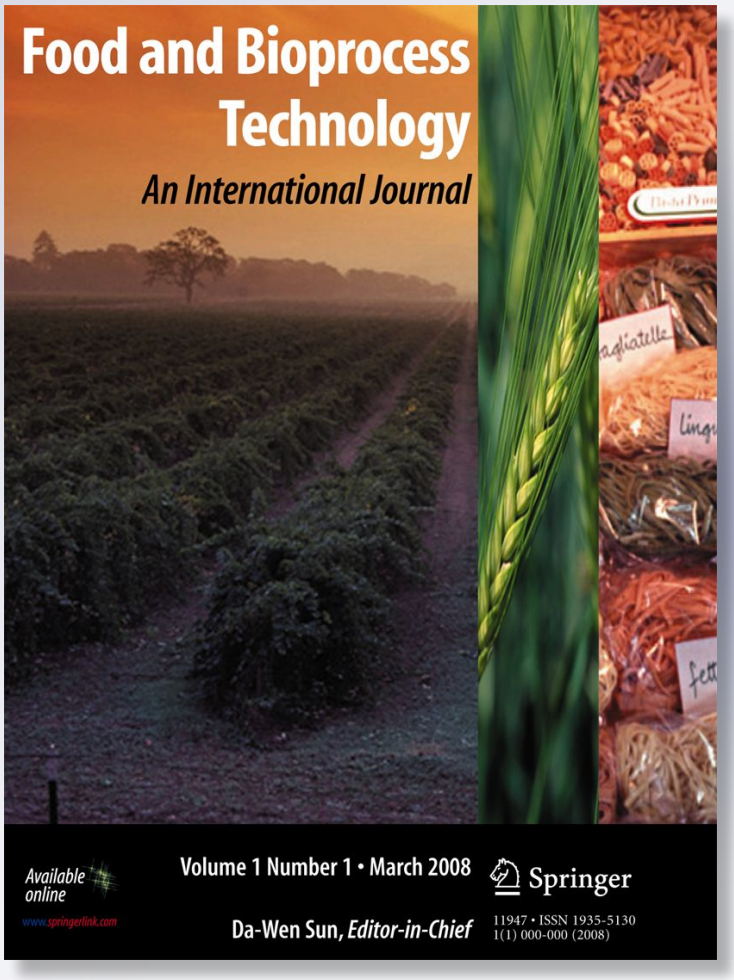

Springer

Food Bioprocess Technol
DOI 10.1007/s11947-012-0818-5

ORIGINAL PAPER

Modification of Transverse NMR Relaxation Times and Water Diffusion Coefficients of Kiwifruit Pericarp Tissue Subjected to Osmotic Dehydration

Patricio Santagapita · Luca Laghi · Valentina Panarese · Urszula Tylewicz · Pietro Rocculi · Marco Dalla Rosa

Received: 1 November 2011 / Accepted: 26 February 2012

Abstract The objective of the present study was to evaluate cellular compartment modifications of kiwifruit (*Actinidia deliciosa*) outer pericarp tissue caused by osmotic treatment in a 61.5 % sucrose solution, through the quantification of transverse relaxation time (T_2) and water self-diffusion coefficient (D_w) obtained by low field nuclear magnetic resonance means. Raw material ripening stage was taken into account as an osmotic dehydration (OD) process variable by analyzing two different kiwifruit groups, low (LB) and high (HB) °Brix. Three T_2 values were obtained of about 20, 310, and 1,250 ms, which could be ascribed to the proton populations, located in the cell walls, in the cytoplasm/extracellular space, and in the vacuoles, respectively. According to T_2 intensity values, vacuole protons represented between 47 and 60 % of the total kiwifruit protons, for LB and HB kiwifruits, respectively. The leakage of water leading to vacuole shrinkage seemed to cause concentration of solutes, retained by the tonoplast, making the vacuole T_2 value decrease along the OD. As expected, the D_w values of raw kiwifruits were lower than the value of the free pure water. The water mobility (and hence D_w), depending on the kiwifruit distinctive cellular structures and solutes, decreased even more during OD due to water loss and sugar gain phenomena. D_w represents an average value of the diffusion coefficient of the whole kiwifruit tissue protons. In order to obtain D_w values specific for each cellular compartment, a multiple component model fitting was also used. According to these results, the vacuole water self-diffusion coefficient ($D_{w,v}$) was much higher than D_w.

Keywords Kiwifruit · Osmotic dehydration · Low field nuclear magnetic resonance (LF-NMR) · Transverse relaxation time · Diffusion coefficient

Nomenclature

m_0	Initial (fresh) weight before osmotic treatment (grams)
m_t	Weight at time t (grams)
$[g_{fw}]$	Grams of fresh weight
x_{w0} x_{wt}	Water mass fraction (g g_{fw}^{-1}) at time 0 and time t, respectively
x_{ST0} x_{STt}	Total solids mass fraction (g g_{fw}^{-1}) at time 0 and time t, respectively
M_t°	Total mass ratio at time t $m_t \cdot m_0^{-1}$
M_0°	Total mass ratio at time 0 $m_0 \cdot m_0^{-1}$
M_t^{W}	Water mass ratio at time t $m_t \cdot x_{wt} \cdot m_0^{-1}$
M_0^{W}	Water mass ratio at time 0 $m_0 \cdot x_{w0} \cdot m_0^{-1}$
M_t^{ST}	Solids mass ratio at time t $m_t \cdot x_{STt} \cdot m_0^{-1}$

P. Santagapita · L. Laghi · V. Panarese · U. Tylewicz · P. Rocculi · M. D. Rosa
Department of Food Science, Alma Mater Studiorum, University of Bologna, Piazza Goidanich 60, Cesena, FC, Italy

P. Santagapita
Industry Department–Member of the National Council of Scientific and Technical Research (CONICET), Faculty of Exact and Natural Sciences, University of Buenos Aires, Buenos Aires, Argentina

P. Santagapita (✉)
Intendente Güiraldes 2160, Ciudad Universitaria, CP 1428, Buenos Aires, Argentina
e-mail: prs@di.fcen.uba.ar

Published online: 10 March 2012

M_0^{ST}	Solids mass ratio at time 0 $m_0 \cdot x_{ST0} \cdot m_0^{-1}$
k_1 k_2	Peleg's constants
k_1^J ($k_1°$ k_1^W, or k_1^{ST}); k_2^J ($k_2°$ k_2^W, or k_2^{ST})	Mass transfer constants
$1/k_1°$	Initial rate of total mass change (1/minute)
$1/k_1^{ST}$	Initial rate of solids mass change (1/minute)
$1/k_1^W$	Initial rate of water mass change (1/minute)
$1/k_2°$	Total mass change at equilibrium (grams/gram)
$1/k_2^{ST}$	Solids mass change at equilibrium (grams/gram)
$1/k_2^W$	Water mass change at equilibrium (grams/gram)

Introduction

Osmotic dehydration (OD) is a partial dewatering-impregnation process usually carried out by immersion of vegetable tissues in hypertonic solution (Ferrando and Spiess 2001). Complex cellular structure of fruit and vegetables could be considered as semipermeable membrane; thus, the mass transfer phenomenon occurs as a consequence of the water chemical potential differences between the tissues and the osmotic medium (Ratti and Mujumdar 2004; Khin et al. 2006). The diffusion of water from cells to the solution is usually accompanied by the simultaneous counterdiffusion of solutes from the concentrated solution into the tissues (Kaymak-Ertekin and Sultanoğlu 2000; Kowalska and Lenart 2001). OD treatments could be useful to increase the shelf life of minimally processed high-moisture content products (Dalla Rosa and Torreggiani 2000).

Technological needs related to mechanically performed peeling and cutting operations require raw unripe kiwifruits with high firmness and low soluble solids content (10–11 ° Bx). Hence the obtained final fresh-cut product does not present a sufficient ripening level for consumption, at least during the first part of the storage period. If unripe slices are subjected to OD, their taste and firmness can be improved (Bressa et al. 1997). Therefore, the output of OD on fresh-cut unripe vegetable tissues would be a product ready for the consumption. In a previous work, Tylewicz et al. (2011) investigated the influence of OD temperature and time on two kiwifruit species. The authors observed that the treatment time positively influenced kiwifruit water loss and solid gain while temperature significantly affected only water loss.

One of the most powerful techniques to study molecular mobility is low field nuclear magnetic resonance (LF-NMR). LF-NMR has the advantage to be a non-destructive technique and do not employ any solvent which can damage the ambient (green technique); the determinations are fast and give information about the structure and about interactions between molecules. Also, LF-NMR can be applied to a variety of biological tissues. For example, it has been applied to obtain information about a number of different physiological conditions in strawberry, carrot, apple, and kiwifruit, including changes caused by ripening, bruising, microbial infection, drying, freezing, high pressure processing, and OD (Tylewicz et al. 2011; Marigheto et al. 2004; Hills and Clark 2003; Hills and Remigereau 1997). In this direction, Panarese et al. (2011) showed that kiwifruit cellular modifications occurring along OD could be efficiently studied by means of LF-NMR. Different subcellular compartments are characterized by specific water–solutes ratio ranges, leading to different transverse relaxation time (T_2) values. These authors evidenced the shrinkage of the vacuole compartment along OD by the use of LF-NMR and light microscopy techniques and the intercellular space formations by TEM, in agreement with LF-NMR results. The measurement of water self-diffusion could enrich such observations allowing the description of barriers, interfaces, and other noteworthy features inside compartmentalized structures (Hills and Clark 2003). However, the relationship between microstructure and the attenuation of a diffusion-weighted signal is often model dependent, which is not easy to extrapolate from one fruit to another.

The information obtained by LF-NMR and its application to the OD process could help in understanding the behavior of water in the cellular tissues and its migration during processing. The purpose of the present work was to evaluate the cellular compartment modifications of kiwifruit's (*Actinidia deliciosa*) outer pericarp tissue caused by osmotic treatment in a 61.5 % (*w*/*v*) sucrose solution through the quantification of T_2 and water self-diffusion coefficient/s (D_w) obtained by LF-NMR. The maturity degree, a key factor to consider for its technological repercussions, was taken into account as an OD process variable, by analyzing two different °Brix kiwifruit groups. Diffusion-weighted LF-NMR signals were also fitted with multiple component models in order to understand the contribution of each cellular compartment to the overall water diffusion.

Materials and Methods

Raw Materials

Kiwifruits (*A. deliciosa* var *deliciosa* cv Hayward) with homogeneous size and refractometric index of 6.9±0.8 °

Bx were bought from the local market. Kiwifruits were sorted to eliminate damaged or defective fruit and were partially ripened at 4±1 °C and 90–95 % of relative humidity in air. Along the storage time, two kiwifruit groups were selected with refractometric index values of 9.5±1.1 (called as LB, low °Brix) and 14.1±0.9 (called as HB, high °Brix) ° Bx. The OD treatment was applied on the fruit, hand peeled and cut into 10-mm thick slices.

Osmotic Dehydration Treatment

OD was carried out by dipping the samples in 61.5 % (*w*/*v*) sucrose solution equilibrated at 25 °C for preestablished contact period of 0, 30, 60, 180, and 300 min, as reported by Tylewicz et al. (2011). The product/solution ratio was about 1:4 (*w*/*w*), to minimize changes in the solution concentration during the treatment as a consequence of water loss from kiwifruit to the solution and simultaneous counter-diffusion of sugar into the kiwifruit tissue. The temperature of the solution was maintained constant by a thermo-controlled water bath. OD was performed eight times on a total of 240 kiwifruit slices (30 kiwifruit slices for each time–°Brix group condition). Each slice was taken from the central part of each kiwifruit (about 60 g) and were placed in mesh baskets and immersed in osmotic solution. The baskets were continuously stirred with a propeller. The rotational speed was experimentally determined to assure negligible resistance to mass transfer. At each OD run, the osmotic solution was changed in order to guarantee the same initial concentration for the eight OD runs. After that, the slices were taken from the osmotic solution and each slice face was rinsed with distilled water for 3 s and placed on blotting paper for 2 s.

Analytical Determinations

Kiwifruit slices were weighted before and after the OD process. The moisture content of kiwifruit samples was determined gravimetrically by difference in weight before and after drying in vacuum oven (pressure ≤100 mmHg) at 70 °C. The drying was performed until a constant weight was achieved (AOAC 920.15, 2002). Duplicate measurements were conducted for each kiwifruit slice.

The soluble solids content (SSC) was determined at 20 °C by measuring the refractive index with a digital refractometer (PR1, Atago, Japan) calibrated with distilled water. For each sample, the SSC was determined in triplicate on the juice obtained from each kiwifruit slice, after filtering through Whatman #1 filter paper. For both moisture content and SSC determinations, the average values were obtained for 30 kiwifruit slices for each time–°Brix group condition.

Mass Transfer Parameters

For each OD treatment performed, total mass change at time t $\left(\Delta M_t^{\circ}\right)$, water mass change at time t $\left(\Delta M_t^{\mathrm{w}}\right)$, and solids mass change at time t $\left(\Delta M_t^{\mathrm{ST}}\right)$ were calculated adopting the following equations (Fito and Chiralt 1997):

$$\Delta M_t^{\circ} = M_t^{\circ} - M_0^{\circ} = \frac{m_t - m_0}{m_0} \tag{1}$$

$$\Delta M_t^{\mathrm{W}} = M_t^{\mathrm{W}} - M_0^{\mathrm{W}} = \frac{m_t x_{\mathrm{w}t} - m_0 x_{\mathrm{w}0}}{m_0} \tag{2}$$

$$\Delta M_t^{\mathrm{ST}} = M_t^{\mathrm{ST}} - M_0^{\mathrm{ST}} = \frac{m_t x_{\mathrm{ST}t} - m_0 x_{\mathrm{ST}0}}{m_0} \tag{3}$$

Kinetic Model

Mass transfer data were modeled according to the equation proposed by Palou et al. (1994) and Sacchetti et al. (2001), using the Peleg's model (Peleg 1988):

$$M_t^{\mathrm{W}} - M_0^{\mathrm{W}} = -\frac{t}{k_1^{\mathrm{W}} + k_2^{\mathrm{W}} \cdot t} \tag{4}$$

$$M_t^{\mathrm{ST}} - M_0^{\mathrm{ST}} = +\frac{t}{k_1^{\mathrm{ST}} + k_2^{\mathrm{ST}} \cdot t} \tag{5}$$

In this work, the same equation rewritten as:

$$M_t^{\circ} - M_0^{\circ} = -\frac{t}{k_1^{\circ} + k_2^{\circ} \cdot t} \tag{6}$$

was also used in order to model total mass change kinetics.

As reported by Sacchetti et al. (2001) at the equilibrium condition ($t \to \infty$) the value for mass change could be calculated as:

$$P_t^{\mathrm{J}} = P_0^{\mathrm{J}} \pm \frac{1}{k_2^{\mathrm{J}}} \tag{7}$$

where P^{J} could be M°, M^{w}, and M^{ST}, respectively.

Similarly, the initial rate (t=0) of mass transfer is:

$$1/k_1^{\mathrm{J}}$$

As shown by Sacchetti et al. (2001), the calculation of the inverse of the kinetic model constants (k_1 and k_2) enables us to obtain both the initial rate values of mass transfer parameters $1/{k_1}^{\mathrm{J}}$ ($1/{k_1}^{\circ}$, $1/{k_1}^{\mathrm{W}}$, or $1/{k_1}^{\mathrm{ST}}$) and the values of mass transfer parameters at the equilibrium condition $1/{k_2}^{\mathrm{J}}$ ($1/{k_2}^{\circ}$, $1/{k_2}^{\mathrm{W}}$ or $1/{k_2}^{\mathrm{ST}}$).

Low Field Nuclear Magnetic Resonance Measurements

One sample cylinder of about 500 mg for each kiwifruit slice was placed inside 10-mm outer diameter tubes so that they did not exceed the active region of the radio frequency coil. The samples were analyzed at 24 °C using a Bruker Minispec PC/20 spectrometer (Bruker Biospin Gmbh, Rheinstetten, Germany) with a 0.47-T magnetic field operating at a resonance frequency of 20 MHz.

Proton Transverse Relaxation Time

Proton transverse relaxation time (T_2) was measured in five samples for each osmotic treatment time by applying the Carr–Purcell–Meiboom–Gill (CPMG) pulse sequence (Meiboom and Gill 1958). Each measurement comprised 30,000 echoes, with a 2τ interpulse spacing of 80 μs and a recycle delay of 3.5 s. By following the procedure setup by Panarese et al. (2011), the CPMG decays were analyzed with the UpenWin software (Borgia et al. 2000), which inverts the CPMG signal by using a continuous distribution of exponential curves, according to Eq. 8,

$$I(2\tau n) = \sum_{i=1}^{M} I_0(T_{2,i}) \exp\left(-\frac{2\tau n}{T_{2,i}}\right) \tag{8}$$

where n is the index of a CPMG echo, and I_0 ($T_{2,i}$) provides a distribution of the signal intensities for each T_2 component extrapolated at τ=0 (the relaxogram) sampled logarithmically. The so obtained relaxograms were characterized by three partially overlapped peaks, with T_2 in the ranges 8–35, 180–250, and 900–1,200 ms, respectively. To observe them separately, fittings were performed to the sum of an increasing number of exponential curves. An F test showed that the lowest ratio between error and degrees of freedom of the model was reached for the 75 % of the samples with three exponentials, as noticed in previous works (Panarese et al. 2011; Tylewicz et al. 2011), while the other samples were best represented by the sum of four exponential curves. To improve the uniformity of the fitting procedure across the samples, the first 80 experimental points were removed from each CPMG curve, as they are known to be subject to noise due to imperfections of the 180° pulses (Le Botlan et al. 1996). Each of the so pruned T_2-weighted signals was now best fit to the sum of four exponential curves. The amplitude and T_2 of the two of them showed that both described the central peak of the relaxogram and were therefore summed.

Water Self-Diffusion Coefficient

Water self-diffusion coefficient measurements were performed through pulsed magnetic field gradient spin echo (PGSE) sequence (Stejskal and Tanner 1965), consisting of a spin echo pulse sequence where two controlled magnetic field gradients are applied respectively between 90° and 180° pulses and between the 180° pulse and the acquisition.

The applied magnetic field gradient intensity (G) was calibrated in the range between 0.04 and 2.0 T/m by employing a 1.25-g/L $CuSO_4 \cdot 5H_2O$ water solution, characterized by a known D_w value ($2.3 \cdot 10^{-9}$ m^2/s at 25 °C (Holz et al. 2000)).

As described below, PGSE sequence was first applied to obtain an overall view of the system under investigation, then to separately observe water located inside the vacuoles and inside the cytoplasm/extracellular space.

Single Component Analysis

Water inside the samples was considered as characterized by a single self-diffusion coefficient, so that D_w could be measured by registering the amplitude (A) of the PGSE signal with ($A_{G(t)}$) and without ($A_{G(0)}$) an applied field gradient (G), according to Eq. 9:

$$\ln\frac{A_{G(t)}}{A_{G(0)}} = -\gamma^2 \cdot D_{w,w} \cdot \delta^2 \cdot \left(\Delta - \frac{1}{3}\delta\right) \cdot G^2 \tag{9}$$

where δ is the gradients length, Δ is the time between the gradients, and γ is the proton gyromagnetic ratio.

The kiwifruit samples were analyzed setting the magnetic field gradient amplitude to 0.7 T/m, τ (the time between 90° and 180° pulses) to 7.5 ms, δ to 0.5 ms, and Δ to 7.5 ms.

Multiple Component Analysis

The amplitude of the PGSE signal was registered for 15 magnetic field gradient values, linearly spaced from 0.04 to 0.6 T/m. To focus on water located in the vacuoles and cytoplasm/extracellular space, τ was set to 15 ms, so to remove the contributions to the signal from cell wall protons, with T_2 lower than a few milliseconds.

Self-diffusion coefficient of the water located in the two considered spaces was then obtained from the Eq. 10,

$$\begin{aligned} Y = \text{offset} &+ P_v \cdot \exp\left(-\left(\Delta \cdot q^2\right) \cdot D_{w,v}\right) \\ &+ P_c \cdot \exp\left(-\left(\Delta \cdot q^2\right) \cdot D_{w,c}\right) \end{aligned} \tag{10}$$

where P_v and P_c identify the fractions of water located inside the vacuole and cytoplasm/extracellular space, respectively; $D_{w,v}$ and $D_{w,c}$ are their corresponding diffusion values and offset is the residual % intensity remaining after the signal decay. To avoid overfitting, P_v and P_c were obtained from the CPMG experiments described above.

Diffusion-Weighted T_2 Curves

In order to double check the results from T_2 and D_w experiments, the merge of the two sources of information was performed by registering diffusion-weighted CPMG curves. For that purpose, a CMPG pulse train was added to the end of the PGSE sequence, as described by Duval et al. (2005). CPMG signals were then registered for the same 15 magnetic field gradients chosen for the multiple component analysis above described. The signals were fitted to a continuous distribution of exponential curves through UpenWin software, thus obtaining relaxograms made up to 100 points each. Finally each point followed through the 15 experiments was fitted to Eq. 9.

Statistical Analysis

Significance of the osmotic dehydration effects on T_2 values was evaluated by means of t test (95 % significance level) using the software STATISTICA 6.0 (Statsoft Inc., Tulsa, UK). In order to estimate the kinetic model constants, nonlinear regression was carried out by means of the quasi-Newton calculus algorithm using STATISTICA 6.0.

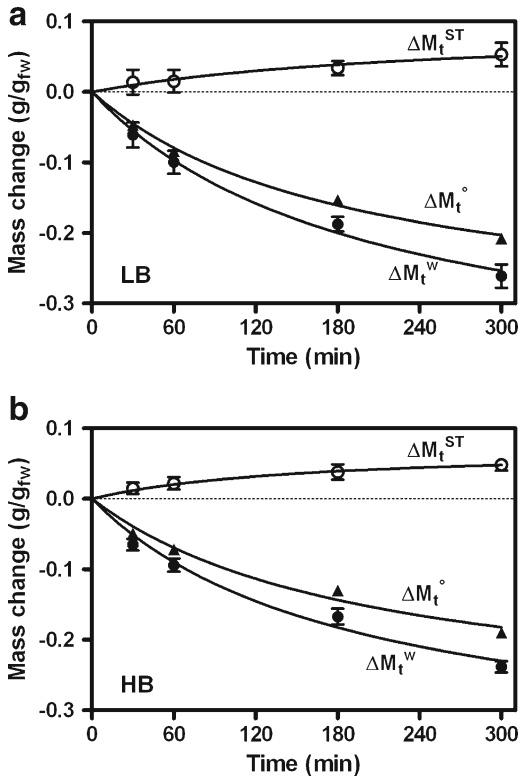

Fig. 1 Application of the Peleg's model to mass transfer data of low (**a**) and high (**b**) °Brix (LB and HB, respectively) kiwifruit subjected to OD at 25 °C. ΔM_t° total mass change, ΔM_t^{W} water mass change, ΔM_t^{ST} soluble solids mass change. Each *point* represents an average of 30 kiwifruit slices and *bars* represent SD values

Results and Discussion

Mass Transfer Parameters

OD leads to a great water loss from kiwifruit and the simultaneous counterdiffusion of solutes from the concentrated solution into the tissues. The kinetic model was used to fit mass transfer parameter data over processing time ($0.82<R^2<0.99$). Figure 1 shows the application of the kinetic model to mass transfer data of LB and HB kiwifruits. Both kiwifruit groups showed similar behavior on mass transfer data (Fig. 1a, b). The highest water loss rates occurred during the first treatment hour, enabling about the 10 and 9 % reduction of the initial fresh weight values for LB and HB kiwifruits, respectively. After 300 min, water loss reached around 26 and 24 % of the fresh weight values for LB and HB, respectively. The water loss rate was the highest at the beginning of the process because the dehydration driving force was the greatest. The observed behavior was similar to previously reported data for kiwifruit (12.0±0.4 °Bx) treated in the same osmotic conditions at 25 °C (Tylewicz et al. 2011) and for other vegetables as carrots, apples, and pumpkins (Kowalska and Lenart 2001).

The reciprocal values of the kinetic model constants (k_1 and k_2) indicating respectively the initial rate values of mass transfer parameters and the mass transfer parameters values at equilibrium condition are displayed in Fig. 2. Both the water loss initial rate value and the water loss value at equilibrium condition of LB kiwifruits are higher than HB samples, as a probable consequence of the lower availability of water in the ripe fruits. Indeed Goñi et al. (2007) found an increase of the unfrozen water along the ripening stages of cherimoya fruits. This increase may indicate a reduction in the amount of water available in the tissues of ripe and overripe fruit associated with the starch conversion and the accumulation of osmolytes. The increase of mass transfer rates from HB to LB kiwifruits is similar to the mass rate increase due to the OD solution temperature increment, reported by Tylewicz et al. (2011). Then, it could be proposed that shorter process time is needed to achieve the same water loss in LB than in HB kiwifruits.

In agreement with Vial's findings (1991), kiwifruit solid gain was minimally influenced by the increase of OD time (Figs. 1 and 2). In fact, during the first hour of OD, the solid gain was about 1.5 and 2.2 % of the fresh weight for LB and HB, respectively, and after 300 min, the percentage of solid gain was 5.3 and 4.8 % for LB and HB, respectively.

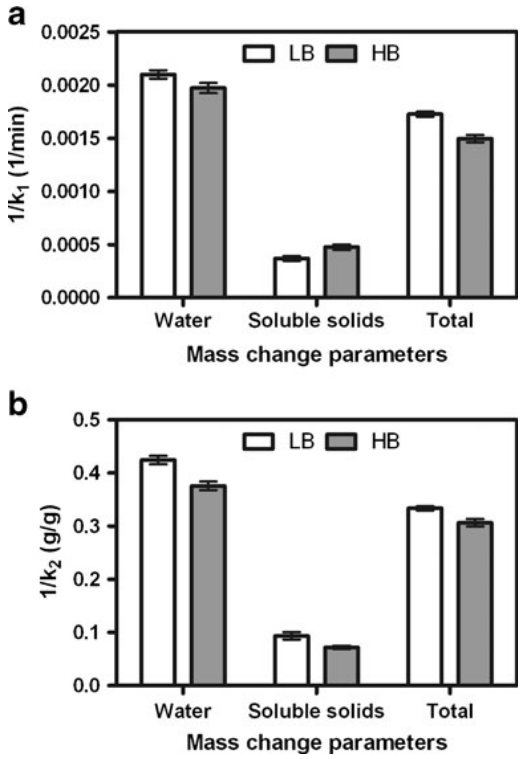

Fig. 2 Mass changes kinetic parameters: **a** initial rate values ($1/k_1$) and **b** values at equilibrium condition ($1/k_2$) of mass change parameters (water mass change, solids mass change and total mass change) during OD in low (*LB*) and high (*HB*) °Brix kiwifruits

Transverse Relaxation Time and Water Self-Diffusion Coefficient

LF-NMR analysis was performed in order to evaluate the changes on kiwifruit water mobility occurring at cellular level during the OD treatment. The kiwifruit water content is considerable high since the 85 % of its fresh weight is water, and CPMG pulse sequence enables to evaluate proton populations with different mobility. Works recently published showed that T_2-weighted curves registered through proton LF-NMR could be successfully employed to gather pieces of information about cellular structures of parenchyma tissue of kiwifruit (Tylewicz et al. 2011; Panarese et al. 2011). This prompted us to employ such technique as a first approach to highlight differences between kiwifruits with high and low °Brix. By fitting the T_2-weighted curves to a continuous and a discrete distribution of exponential curves, three proton pools were observed, with T_2 around 1,250, 310, and 20 ms that were ascribed through the literature to vacuole, cytoplasm plus extracellular space, and cell wall, respectively. Table 1 summarizes their T_2 values and the absolute intensities on raw and 300 min-treated HB and LB kiwifruits. The proton pool separation and assignment agree with Hills and Duce's findings (1990) on different fruits and vegetables.

The absolute intensities allowed to follow the partition of water across cellular structures along kiwifruit ripening groups and OD treatment time. At t_0, the signal from cytoplasm/extracellular space of LB kiwifruits is only slightly lower than the one from vacuole, while in HB kiwifruits the ratio between them is almost 1:2. Also, HB kiwifruits showed higher intensity values for vacuole proton pool than LB kiwifruits. The trends noticed in the signal intensity values seem to be reinforced by T_2 values. LB samples, characterized by a solutes/water ratio lower than HB kiwifruits, showed higher T_2 both in the vacuole and in cytoplasm/extracellular space. The water and solutes transfer promoted by osmosis can modify the original kiwifruit cellular organization and the subcellular structures. OD treatment has the effect of halving vacuole proton pool signal, with slight differences between HB and LB kiwifruits, a probable consequence of water exit from such cellular compartment. The OD shrinks the kiwifruit vacuoles, as reported previously by Panarese et al. (2011). From the decreasing T_2 of the vacuoles, it can be inferred that the water loss leading to the shrinkage of vacuoles causes a concentration of solutes, retained by the tonoplast. Bowtell et al. (1992) showed through NMR microscopy that during OD the cytoplasm sticks to the shrinking tonoplast, followed by the cellular membrane. This

Table 1 T_2 values and absolute intensities of the three proton pools identified through T_2-weighted curves for low (LB) and high (HB) °Brix, raw (t0) and 300-min osmo-treated kiwifruits

		Vacuole		Cytoplasm + extracellular space		Cell wall	
		t_0	300 min	t_0	300 min	t_0	300 min
LB	T_2 (ms)	1,321A±64	1,009 C±14	320A±21	221B±37	19±2	21±5
	Intensity	47b±9	25c±2	41a±5	36a±2	10±3	6±2
HB	T_2 (ms)	1,227B±79	991 C±92	303A±36	259AB±46	21±1	26±6
	Intensity	60a±8	31b±10	33b±3	37a±6	7±2	4±1

The intensities were scaled so that they equaled 100 in the case of raw HB fruits. The letters, capital for T_2 and lowercase for signal intensity, highlight the values which were found to be different with 95% confidence through a *t* test

creates intracellular spaces, filled with water from the vacuoles and osmotic solution, which contribute to the cytoplasm plus extracellular space proton pool. In agreement with Bowtell findings (1992), Table 1 shows that only in the case of HB kiwifruits that the vacuole T_2 decrease is paralleled by an increase of the cytoplasm and extracellular space signal. OD treatment, by removing water from such compartments and increasing their sugar content, causes a marked T_2 decrease in both kiwifruit groups, which show similar values at the end of the treatment.

The phenomena observed through T_2-weighted curves can be followed by determining the water self-diffusion coefficient (D_w) through PGSE sequence. A first overall picture can be obtained by considering the kiwifruit parenchyma tissue as homogeneous from the water distribution point of view. This oversimplification allows to quickly evaluate D_w value through one diffusion-weighted signal only. D_w value obtained through the single component analysis represented an average diffusion value (D_w) comprising the D_w coefficient contribution of each water population (vacuole, cytoplasm plus extracellular space, and cell wall). Figure 3a shows the D_w values evaluated during the OD treatment with the single component analysis.

As displayed in Fig. 3a, D_w values of raw kiwifruit resulted much lower than that of pure water ($2.3 \cdot 10^{-9}$ m^2/s at 25 °C (Holz et al. 2000)). This was not unexpected as cellular structures hinder water diffusion while solutes increase its viscosity. As confirm of such qualitative consideration, LB raw fruits, with a low sugar content, showed higher D_w values than HB ones. This agrees with Goñi's findings (2007), showing the ability of ripe tissues to hold better the water than unripe fruit. Along the OD treatment, the D_w values of both kiwifruit groups decreased (Fig. 3a) as a consequence of tissue water loss and sugar content increase as discussed above. Both kiwifruit groups showed a linear D_w decrease as a function of OD time with similar rates. An inverse correlation with R^2 >0.80 was found between D_w and dry matter for both kiwifruit groups during the OD, as shown in Fig. 3b. This could result especially interesting in view of setting up innovative and not destructive methods to monitor dry matter content in intact fruits.

In order to have a deeper insight into the consequences of the OD treatment on each cell compartment of kiwifruit, the signal from PGSE pulse sequence was analyzed through a multiple component model. Only the diffusion coefficient corresponding to the vacuole and cytoplasm/extracellular space compartments was considered, by properly choosing the PGSE τ. For both kiwifruit °Brix groups, Fig. 4 shows water self-diffusion coefficients obtained respectively for vacuole, major proton population, and cytoplasm/extracellular space. The D_w values previously obtained with the single component model are also included in the figure for comparative purpose.

The D_w values of water in the vacuoles and cytoplasm/extracellular space were respectively higher and lower than the D_w values calculated with the single component model

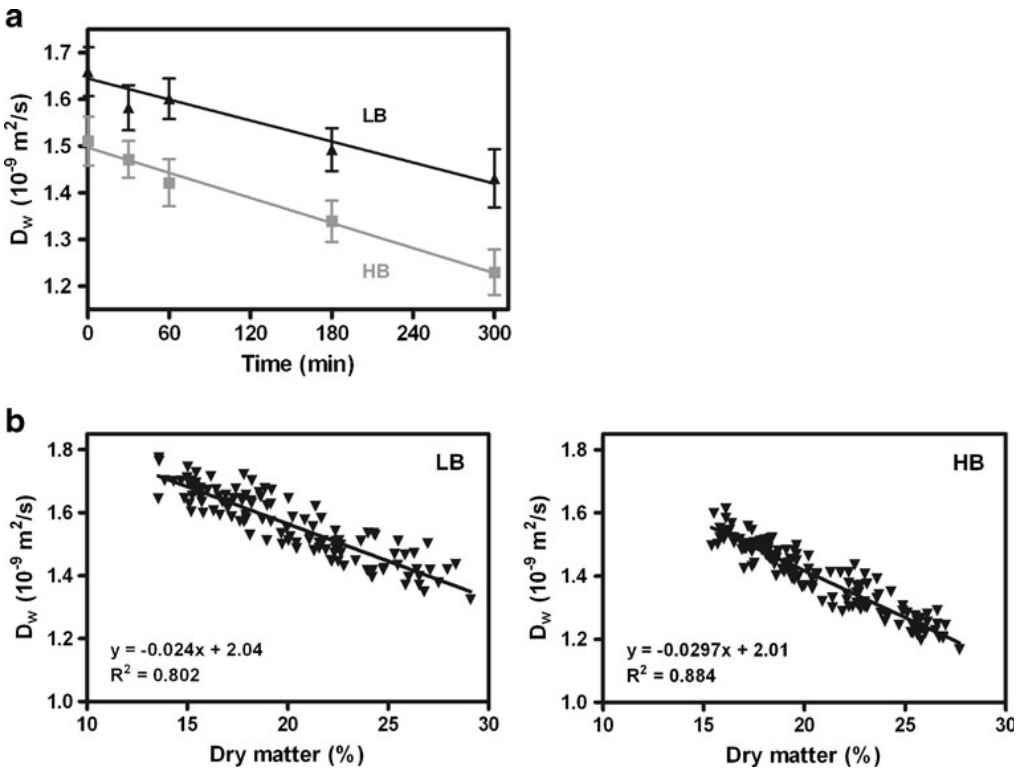

Fig. 3 **a** Average water self-diffusion coefficients of kiwifruit (D_w) as a function of OD time for both low (*LB*) and high (*HB*) °Brix groups. D_w values were obtained by applying the PGSE sequence together with the single component model. Each *point* represents an average of at least 15 kiwifruit slices of each time; *bars* represent SD values. **b** Correlation between D_w and dry matter for both kiwifruit groups

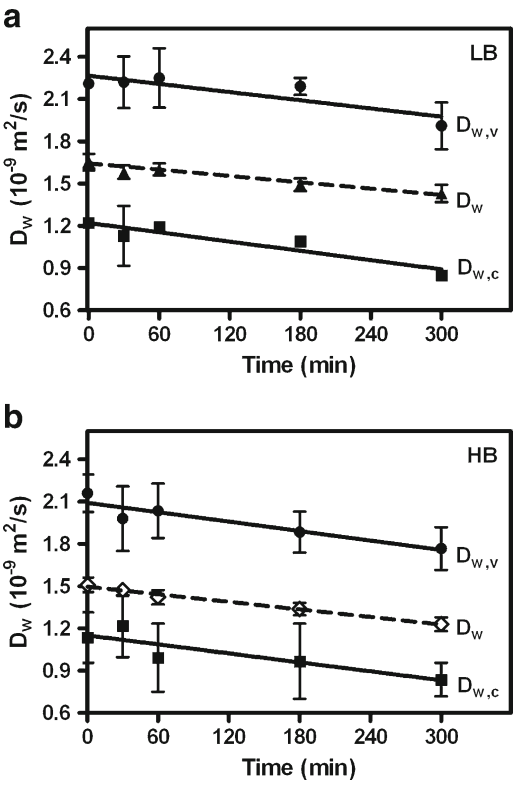

Fig. 4 Water self-diffusion coefficients (D_w) of low (*LB*) (**a**) and high (*HB*) (**b**) kiwifruits as a function of OD time. *Filled symbols* are average values obtained by applying the two components model, leading to two different D_w values for vacuole ($D_{w,v}$) and cytoplasm/extracellular space compartment ($D_{w,c}$). *Open symbols* were obtained by applying the single component model (D_w). *Lines* show the fitting obtained using linear regression. *Bars* represent SD values

for both kiwifruit °Brix groups. This confirms that the D_w obtained through the single component model gives an average value of a more complex situation. D_w value higher in the vacuole than in cytoplasm/extracellular space reflects the lower solutes/water ratio, in agreement with T_2 values. Going into deeper detail, it is possible to notice that the values obtained with the single component model are closer to the D_w values of the cytoplasm/extracellular space than to those from vacuoles. This is a consequence of the 2τ of 15 ms applied to calculate the single component values, instead of the 30 ms applied for the two components model, which does not allow the complete removal of the cell wall component (see Table 1), leading to lower average D_w values.

To have a further confirmation of T_2 and D_w values for the vacuole proton pool and cytoplasm/extracellular space, the PGSE-CPMG sequence was applied to a single sample, a raw kiwifruit pertaining to the HB group, as shown in Fig. 5. This procedure has the advantage to allow the determination of both T_2 and D_w on the same sample at the same moment, giving a 2D LF-NMR spectra (dashed line, Fig. 5). The full line was placed for comparative purposes and corresponds to T_2 spectrum (the relaxogram) of the same sample measured by CPMG, showing the proton kiwifruit populations. Cytoplasm/extracellular space showed a D_w of $1.5 \cdot 10^{-9}$ m^2/s for the considered sample, a value in qualitative agreement with the ones obtained through PGSE sequence. D_w obtained for vacuole proton pool was higher than the one obtained for cytoplasm/extracellular space,

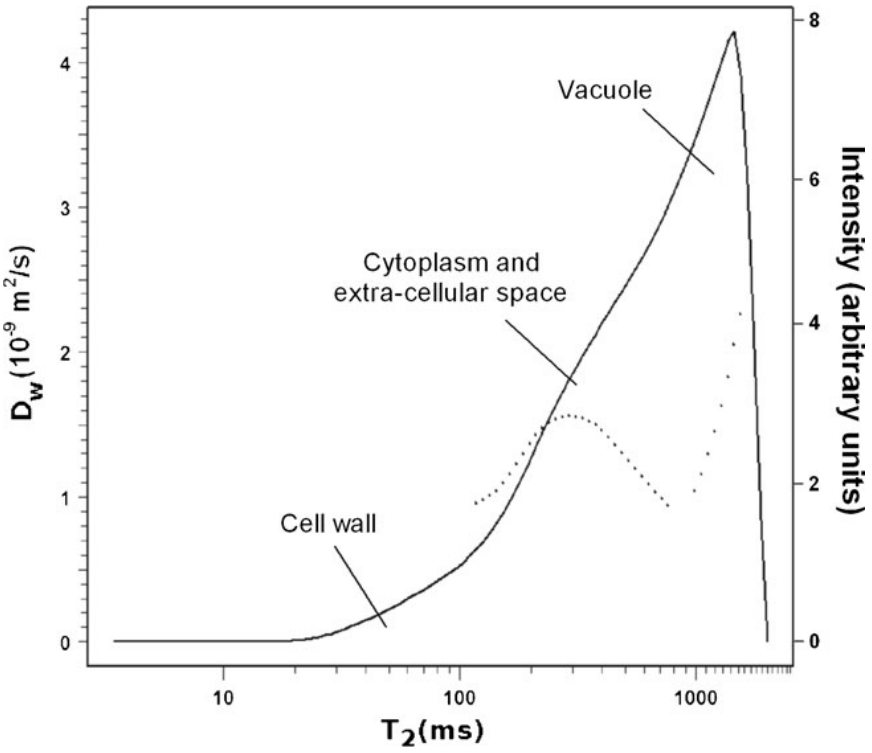

Fig. 5 Diffusion-weighted T_2 curves for HB kiwifruit: water self-diffusion coefficients (D_w) as a function of T_2 values (*left axis, dashed line*). *Full line* corresponds to T_2 spectrum (*right axis*)

again in agreement with PGSE values. Unfortunately vacuole peak appears at the side of the relaxogram, so that D_w values resulted as very noisy and it was not possible to go into deeper detail. However, it is interesting to observe qualitatively the D_w–T_2 dependency and how it is modulated. At the other side of the relaxogram, the low signal hindered the measurement of consistent D_w values for cell wall proton pool.

Conclusions

The combined application of T_2 and water self-diffusion coefficient measurements allowed having an insight of the changes in the cellular compartments of kiwifruit's outer pericarp promoted by OD. T_2 measurements enabled the quantification of the protons located in the three main cell compartments within the mobile water is located: vacuole, cytoplasm plus extracellular space, and cell wall. Water self-diffusion coefficient evaluated through a single component model was found to be a fast technique to follow OD treatment consequences along time and to highlight the different response to the treatment from fruits of different ripeness. D_w evaluated through a two components model allowed a deeper understanding of the changes in each cellular compartment at the expense of both experiment time, in the order of 5 min for each sample, and measurement precision. LF-NMR results showed that the OD process influenced water mobility characteristics within the vacuole and cytoplasm plus extracellular space compartments. The possibility to highlight how the response to OD treatment was modulated by fruit ripeness suggests that LF-NMR can represent a powerful and versatile tool to investigate the behavior of vegetable tissues during minimal processing. Then, by knowing the extent of changes on mass transfer parameters and water behavior during OD, which in turn modified the structural and textural characteristics of the final product, it is possible to exploit both raw unripe and ripe kiwifruits from a technological point of view. Thus, the extent of OD process could be modulated regarding fruit maturity to obtain products that can be used in different food products/processes.

Acknowledgments Patricio Santagapita acknowledges the EADIC program of Erasmus Mundus External Cooperation Window Lot 16 for the postdoc scholarship. We also like to acknowledge Apofruit Italia S.c.a.r.l. for its financial support.

References

AOAC International (2002). Official Methods of Analysis (OMA) of AOAC International, 17th Edition, USA. Method number: 920.15. Available at http://www.eoma.aoac.org/

Borgia, G. C., Brown, R. J. S., & Fantazzini, P. (2000). Uniform-penalty inversion of multiexponential decay data: II. Data spacing, T_2 data, systematic data errors, and diagnostics. *Journal of Magnetic Resonance, 147*(2), 273–285.

Bowtell, R., Mansfield, P., Sharp, J. C., Brown, G. D., McJury, M., & Glover, P. M. (1992). NMR microscopy at 500 MHz: Cellular resolution in biosystems. In B. Blümich & W. Kuhn (Eds.), *Magnetic resonance microscopy (pp 427–439)*. VCH: Weinheim.

Bressa, F., Dalla Rosa, M., & Mastrocola, D. (1997). Use of a direct osmosis treatment to produce minimally processed kiwifruit slices in a continuous pilot plant. *Acta Horticulturae, 444*(2), 649–654.

Dalla Rosa, M., & Torreggiani, D. (2000). Improvement of food quality by application of osmotic treatments. In M. Dalla Rosa & W. E. L. Spiess (Eds.), *Industrial application of osmotic dehydration/treatments of food*. Udine: Forum Editrice Universitaria Udinese. Concerted action FAIR-CT96-1118, pp.

Duval, F. P., Cambert, M., & Mariette, F. (2005). NMR study of tomato pericarp tissue by spin–spin relaxation and water self-diffusion. *Applied Magnetic Resonance, 28*, 29–40.

Ferrando, M., & Spiess, W. E. L. (2001). Cellular response of plant tissue during the osmotic treatment with sucrose, maltose and trehalose solutions. *Journal of Food Engineering, 49*, 115–127.

Fito, P., & Chiralt, A. (1997). An approach to the modelling of solid food-liquid operations: Application to osmotic dehydration. In P. Fito, E. Ortega, & G. Barbosa (Eds.), *Food Engineering 2000* (pp. 231–252). New York: Chapman & Hall.

Goñi, O., Muñoz, M., Ruiz-Cabello, J., Escribano, M. I., & Merodio, C. (2007). Changes in water status of cherimoya fruit during ripening. *Postharvest Biology and Technology, 45*, 147–150.

Hills, B. P., & Clark, C. J. (2003). Quality assessment of horticultural products by NMR. *Annual Reports on NMR Spectroscopy, 50*, 76–117.

Hills, B. P., & Duce, S. L. (1990). The influence of chemical and diffusive exchange on water proton transverse relaxation in plant tissue. *Magnetic Resonance Imaging, 8*, 321–331.

Hills, B., & Remigereau, B. (1997). NMR studies of changes in subcellular water compartmentation in parenchyma apple tissue during drying and freezing. *International Journal of Food Science and Technology, 32*, 51–61.

Holz, M., Heil, S. R., & Sacco, A. (2000). Temperature-dependent self-diffusion coefficients of water and six selected molecular liquids for calibration in accurate 1H NMR PFG measurements. *Physical Chemistry Chemical Physics, 2*, 4740–4742.

Kaymak-Ertekin, F., & Sultanoğlu, M. (2000). Modelling of mass transfer during osmotic dehydration of apples. *Journal of Food Engineering, 46*, 243–250.

Khin, M. M., Zhou, W., & Perera, C. O. (2006). A study of mass transfer in osmotic dehydration of coated potato cubes. *Journal of Food Engineering, 77*, 84–95.

Kowalska, H., & Lenart, A. (2001). Mass exchange during osmotic pretreatment of vegetables. *Journal of Food Engineering, 49*, 137–140.

Le Botlan, D., Rugraff, Y., & Ouguerrm, L. (1996). 180° pulse imperfection effects on fitting of relaxation curves obtained by low field NMR spectroscopy. *Spectroscopy Letters, 29*, 1091–1102.

Marigheto, N., Vial, A., Wright, K., & Hills, B. P. (2004). A combined NMR and microstructural study of the effect of high-pressure processing on strawberries. *Applied Magnetic Resonance, 26*, 521–531.

Meiboom, S., & Gill, D. (1958). Modified spin-echo method for measuring nuclear magnetic relaxation times. *The Review of Scientific Instruments, 29*, 688–691.

Palou, E., Lopez-Malo, A., Argaiz, A., & Welti, J. (1994). Use of Peleg's equation to osmotic concentration of papaya. *Drying Technology, 12*, 965–978.

Panarese, V., Laghi, L., Pisi, A., Tylewicz, U., Dalla Rosa, M., & Rocculi, P. (2011). Effect of osmotic dehydration on *Actinidia deliciosa* kiwifruit: A combined NMR and ultrastructural study. *Food Chemistry, 132*(4), 1706–1712.

Peleg, M. (1988). An empirical model for the description of moisture sorption curves. *Journal of Food Science, 53*, 1216–1217.

Ratti, C., & Mujumdar, A. S. (2004). Drying of fruits. In D. M. Barrett, L. P. Somogyi, & H. S. Ramaswamy (Eds.), *Processing fruits: Science and technology* (2nd ed., pp. 127–159). Boca Raton: CRC Press.

Sacchetti, G., Gianotti, A., & Dalla Rosa, M. (2001). Sucrose-salt combined effects on mass transfer kinetics and product acceptability. Study on apple osmotic treatments. *Journal of Food Engineering, 49*, 163–173.

Stejskal, E. O., & Tanner, J. E. (1965). Spin diffusion measurements: spin echoes in the presence of a time-dependent field gradient. *Journal of Chemical Physics, 42*, 288–292.

Tylewicz, U., Panarese, V., Laghi, L., Rocculi, P., Nowacka, M., Placucci, G., & Dalla Rosa, M. (2011). NMR and DSC water study during osmotic dehydration of *Actinidia deliciosa* and *Actinidia chinensis* kiwifruit. *Food Biophysics, 6*, 327–333.

Vial, C., Guilbert, S., & Cuq, J. L. (1991). Osmotic dehydration of kiwifruits: influence of process variables on the color and ascorbic acid content. *Sciences des Aliments, 11*, 63–84.

Paper VI

Microscopic studies providing insight into the mechanisms of mass transfer in vacuum impregnation

Valentina Panarese, Petr Dejmek, Pietro Rocculi, Federico Gómez Galindo

PII: S1466-8564(13)00024-6
DOI: doi: 10.1016/j.ifset.2013.01.008
Reference: INNFOO 973

To appear in: *Innovative Food Science and Emerging Technologies*

Received date: 11 September 2012
Accepted date: 23 January 2013

Please cite this article as: Panarese, V., Dejmek, P., Rocculi, P. & Galindo, F.G., Microscopic studies providing insight into the mechanisms of mass transfer in vacuum impregnation, *Innovative Food Science and Emerging Technologies* (2013), doi: 10.1016/j.ifset.2013.01.008

MICROSCOPIC STUDIES PROVIDING INSIGHT INTO THE MECHANISMS OF MASS TRANSFER IN VACUUM IMPREGNATION

Panarese, Valentina[a,*]; Dejmek, Petr[b]; Rocculi, Pietro[a]; Gómez Galindo, Federico[b]

[a] *Department of Food Science, Alma Mater Studiorum, University of Bologna, Piazza Goidanich 60, 47521 Cesena (FC), Italy*

[b] *Department of Food Technology, Engineering and Nutrition, Lund University, P.O. Box 124, SE-221 00 Lund, Sweden*

*Corresponding author. Phone: +39 0547 636 120; Fax: +39 0547 382 348;

e-mail: valentina.panarese2@unibo.it

Abstract

A microscopic method was developed to detect pressure thresholds for gas outflow and solution impregnation during vacuum impregnation of plant materials. Raw materials with different porosities (apple and spinach) were impregnated with an isotonic sucrose solution at a minimum pressure of 150 mbar. An automatic vacuum controller system (AVCS) was used to control the pressure during vacuum impregnation. Micrographs of tissues subjected to vacuum impregnation were recorded as the pressure in the treatment chamber was varied. Image analysis allowed the evaluation of the pressure at which gas was released from the pores (seen as bubbles) during the application of vacuum, and the pressure at which tissue impregnation took place during the restoration of atmospheric pressure. Spinach tissues showed gas release at a much lower pressure than apple, and impregnation commenced at a much higher pressure. These differences in pressure threshold could be caused by the narrow pores in spinach and possibly by changes in leaf volume.

Industrial relevance: Vacuum impregnation is considered a promising technology to facilitate the impregnation of vegetable tissues with different solutions containing, e.g., firming, antioxidant or antimicrobial agents.

The mass transfer taking place during vacuum impregnation depends on the characteristics of the tissue pores. Effective vacuum impregnation requires the efficient removal of air from the tissue during vacuum treatment to obtain complete filling of the tissue during the subsequent impregnation step. The findings of this study may allow food manufacturers to optimize vacuum impregnation parameters depending on the porosity characteristics of the raw material.

Keywords: Vacuum impregnation, Porosity, Capillary pressure, Pressure thresholds

Running Title: Microscopic study of vacuum impregnation

1. Introduction

Vacuum impregnation (VI) of a porous tissue involves the removal of the gas or liquid normally contained in open pores and its replacement with a liquid. VI is used in the food industry to facilitate the impregnation of various products with, e.g. firming, antioxidant or antimicrobial agents (Hironaka, Kikuchi, Koaze, Sato, Kojima, Yamamoto, Yasuda, Mori, & Tsuda, 2011; Barrera, Betoret, & Fito, 2004; Gras, Vidal, Betoret, Chiralt, & Fito, 2003). Impregnation takes place due to the action of hydrodynamic mechanisms (HDM) brought about by pressure changes (Fito, 1994; Fito & Pastor, 1994). A model was constructed by regarding the pores of the plant tissue as ideal cylinders of constant diameter, facing the liquid solution. The change in pore volumetric fraction occupied by the liquid was considered to be a function of the internal pressure in the pore (p_i), the capillary pressure (p_c) and the pressure acting on the liquid (p_l) (expressed in Pa). The capillary pressure is related to the characteristics of the pores and is defined by the Young-Laplace equation (Dullien, 1992):

$$p_c = \sigma\left[\frac{1}{r_1}+\frac{1}{r_2}\right]\cos\theta \qquad (1)$$

where σ is the interfacial tension (N m^{-1}), r_1 and r_2 are the principal radii of the pores in (m) and θ is the contact angle (rad).

Vacuum impregnation of a porous material is typically carried out in two steps after immersion of the product in a tank containing the liquid phase. In the first step, vacuum ($p_l < p_{atm}$) is applied to the system for a short time (t_1) in the closed tank, leading to the expansion of the gas contained in the pores ($p_i > p_l + p_c$). Some of the gas leaves the pores, taking with it some of the native liquid. When the pore gas pressure equals the system pressure, capillary effects will promote the penetration of liquid into the pores, as $p_i = p_l$ ($p_l < p_{atm}$). In the second step, atmospheric pressure ($p_l = p_{atm}$) is restored in the tank for a time (t_2). This compression will lead to a considerable reduction in volume of the gas remaining in the pores, resulting in the influx of external liquid into the porous structure (Zhao & Xie, 2004; Fito, Chiralt, Betoret, Gras, Chafer, Martinez-Monzo, Andres, & Vidal, 2001).

VI is significantly affected by the mechanical properties of the biological material (Derossi, De Pilli, La Penna & Severini, 2011), as pressure changes cause not only gas or liquid flow but also solid matrix deformation/relaxation. During the first step of VI the product usually swells

initially, due to the expansion of the gas in the pores. This is followed by a reduction in volume when the solid matrix relaxes as gas is released from the tissue. In the second step, compression causes deformation followed by relaxation, due to the penetration of the external liquid into the pores (Fito, Andrés, Chiralt & Pardo, 1996).

The interaction between air and liquid during the two steps of VI has been studied extensively in single, ideal cylindrical pores (Fito & Pastor, 1994) and in micromodels (Badillo, Segura, & Laurindo, 2011; Lenormand, 1990), however, to the best of our knowledge, it has not been studied directly in plant tissues. We recently performed direct measurements of pressure in apple tissue subjected to VI using gas in scattering media absorption spectroscopy, and found that the pore volume in apple tissue filled with impregnating solution was dependent on the minimum absolute pressure used during the process (Tylewicz, Lundin, Cocola, Dymek, Rocculi, Svanberg, Dejmek & Gómez Galindo, 2012). Impregnation of the sample is also dependent on the raw material characteristics as cell morphology, intercellular forces and pore diameters (Schulze, Peth, Hubbermann & Schwarz, 2012). Thus, tissues with different pore sizes and pore geometry can be expected to show different transport properties during VI. As apple and spinach have different morphological and porosity characteristics these two materials were studied in the present investigation. The average size of a pore in apple is about four times greater than that in spinach (Iwabuchi & Kurata, 2003; Khalloufi & Ratti, 2003). Spinach leaves contain upper and lower epidermis, minor veins and mesophyll tissue, all of which are permeated by an extensive system of intercellular spaces constituting about 40% of the leaf volume (Warmbrodt & Van Der Woude, 1990). The apple cortex is an anisotropic plant tissue with high porosity. Porosity and intercellular space increase from the centre to the periphery of the apple parenchyma (Schulze, Peth, Hubbermann & Schwarz, 2012). The cells of the inner region have an elongated, cylindrical shape and are oriented in a uniform manner, while the spherical cells of the outer region are not uniformly oriented (Chalermchat, Malangone & Dejmek, 2010). It has been estimated that the vascular tissues and intercellular spaces of apple parenchyma constitute about 20% of the total fruit volume (Mavroudis, Dejmek & Sjöholm, 2004).

The aim of the present work was to determine the pressure at which gas was released from the pores (seen as bubbles) during the application of vacuum, and the pressure at which tissue impregnation took place during the restoration of atmospheric pressure. It is hoped that the findings of this study will contribute to the clarification of the mechanisms of mass transfer in

VI will and provide useful information for the optimization of VI based on the characteristics of the pore network of the material.

2 Materials and Methods

2.1 Raw material handling and storage

Baby spinach leaves (*Spinacia oleracea*) grown in southern Sweden were harvested and stored in a packing house storage facility in a normal atmosphere (1-2 °C; 90-95% RH). Within 5 days of harvesting, the leaves were washed, air-dried, packed in 65 g bags, as routinely practiced by the producer, and delivered the same day to our laboratory. During the experimental period the packages were stored at 2 ± 1 °C, and experiments were performed within the product expiration time (7 days). Undamaged leaves (30 ± 3 mm in length x 60 ± 3 mm in width) were manually selected and equilibrated at room temperature before the experiments.

Apples (*Malus domestica cv.* Granny Smith) harvested in northern Italy were bought at a local store in southern Sweden. During the experimental period the apples were stored at 2 ± 1 °C. Experiments were performed within 7 days of purchase. Undamaged fruits (70 ± 5 mm in diameter and 80 ± 5 mm in height) were manually selected and equilibrated at room temperature before the experiments.

2.2 Raw material characterization

Soluble solids content

Four cubes of apple (about 2 g each) were removed about 2 mm from the fruit epidermis. The fruit cubes were ground using a mortar and pestle and the puree obtained was filtered through filter paper (Whatman #1). The soluble solids content was determined at 20 °C by measuring the refractive index of two drops of filtered juice with a refractometer (Abbe refractometer, Bellingham + Stanley Ltd., London).

Porosity

The apparent density (ρ_a) and the real solid-liquid density (ρ_r) of apple and spinach were determined by volume displacement in a pycnometer using appropriate aqueous isotonic sucrose solutions as reference liquid (see below) (Gras, Vidal, Betoret, Chiralt, & Fito, 2003). The real

solid-liquid density was also obtained by volume displacement using sample purees obtained by manually grinding the samples using a mortar and pestle. The purees were placed in a Büchner flask and degasified for 10 min by creating vacuum in the flask. The total porosity of the sample (ε) is the dimensionless ratio of air volume to total volume, and varies between 0 and 1 (Eq. 2) (Lozano, Rotstein & Urbicain, 1980):

$$\varepsilon = 1 - \left(\rho_a / \rho_r \right) \tag{2}$$

2.3 Sample preparation

A rectangular sample of the lamina (length 20 ± 1 mm, width 13 ± 1 mm) was removed from each spinach leaf with a microtome blade, about 2 mm from, and parallel to, the midrib (Fig. 1a).

A sample measuring 15 x 15 x 2 mm was removed from each apple, parallel to the fruit axis, about 2 mm from the epidermis, using a microtome blade (Fig. 1b).

Figure 1a Figure1b

2.4 Isotonic solution determination

Isotonic sucrose solutions for apple and spinach leaves were determined with respect to the cell sap. The isotonic solution concentrations were determined by immersion of three apple samples (40 x 10 x 5 mm) or three spinach leaves (without petioles) in a series of solutions of different sucrose concentrations, according to Tylewicz, Romani, Widell & Gómez Galindo (2011). The variation in tissue weight was recorded every 30 min over a period of 7 h.

2.5 VI chamber

The treatment chamber consisted of a block of plastic (height 7 mm, length 40 mm, depth 40 mm) in which two vacuum pre-chambers and a main opening had been created, as illustrated in Fig. 2. The sample and 4 ml of isotonic solution were inserted through the main opening. The frame was sealed between two glass plates (3 mm x 40 mm x 40 mm, h x l x d) with o-rings and screws. A plastic fastener was used to hold the sample in place on the lower glass plate. The

purpose of the pre-chambers is to collects drops of solution that could adhere to the upper glass slide during the application of vacuum.

Figure 2a Figure 2b

2.6 Automatic vacuum controller system

The automatic vacuum controller system (AVCS, S.I.A., Bologna, Italy) is a programmable device constructed to control the pressure acting on the impregnating solution during the process. The AVCS is connected to the VI chamber by a Teflon tube and includes a number of components: a pressure transmitter, vacuum actuators (valves and vacuum pump), a computer and a programmable logic controller device (PLC, Series 90-30, General Electric, Charlottesville, VA, USA) as illustrated in Fig. 3. The PLC is the core of the AVCS as it manages the vacuum actuators, supervising the value of pressure, time and vacuum release rate by controlling the start and stop of the vacuum pump and the opening and closing of the air inlet and air outlet valves. A software interface (CIMPLICITY® Workbench Version 6.10 Service Pack 3, GE Fanuc Automation Americas, Inc.) allows the working parameters of the AVCS to be set and controlled.

Figure 3

2.7 Vacuum impregnation

Based on preliminary experiments to establish the maximum weight gain of apple and spinach, a minimum absolute pressure of 150 mbar was chosen for both samples. As shown in Fig. 4, pressure was applied in 20 consecutive steps. The chosen pressure profile ensured that cell viability was maintained in both raw materials. Two parameters were set for each pressure step: duration (s) and absolute pressure value (mbar). VI was controlled by the AVCS. As outlined in Figure 4, during the first phase of VI the pressure gradually decreased from the atmospheric value (1000 mbar) to the final reduced pressure value (150 mbar, step 8). During the second

phase, vacuum was released and the pressure progressively returned to the atmospheric value. The chosen duration for each step was: 10 s for step 1 to 4 and step 15 to 20; 20 s for step 5 and steps 12 to 14; 60 s for steps 6, 7 and steps 9 to 11; 120 s for step 8 (Fig. 4). Thus the VI treatment applied had a total duration of 600 s.

Figure 4

2.8 Microscopic observations

The VI chamber containing both the sample and the solution was placed on the specimen stage of an upright microscope (Nikon Eclipse Ti Inverted Microscope, Melville, NY, USA) and was observed during the process with a 4x ocular. The microscope was connected to a computer and a digital camera (Nikon DS Qi1Mc, Melville, NY, USA). The microscope software (Nikon NIS-Elements Advanced Research, Ver. 3.00) controls both the microscope and the camera, enabling images of the specimen to be recorded throughout the process.

2.9 Synchronization of image capture and pressure data recording

The AVCS records pressure values in the VI chamber every 10 s, and images were therefore also recorded at the same frequency. Synchronization between image capture and pressure data recording by the AVCS was performed manually.

2.10 Evaluation of gas outflow and liquid impregnation during VI

Image analysis

A series of images and the corresponding pressures were recorded for each VI experiment. At least six experiments were carried out on both spinach and apple samples. As the tissue was immersed in a solution, the air outflow during the application of vacuum was detected by the formation of bubbles, and liquid impregnation during the restoration of atmospheric pressure through the change in tissue translucency. Pictures were processed using ImageJ software (Image processing and analysis in Java, Ver. 1.45r, National Institutes of Health, Bethesda, MD, USA) to determine the pressure at which gas was released from the pores and tissue impregnation took place.

To determine the pressure at which gas outflow was initiated, the first picture in each experiment exhibiting visible bubbles was inspected. The image type was changed from RGB to 8-bit grey images, sharpening the bubble outlines and modifying the image threshold. One of the largest bubbles in the picture was included in a region of interest (ROI). All the images in the series were adjusted to the same threshold level. In order to remove most of the background while preserving the bubble outlines, the first picture of the series, which was captured at atmospheric pressure and did not exhibit any bubbles, was subtracted from each adjusted picture. The ROI previously defined was analysed in each image and the area of the bubble included in the ROI was determined through 'Analyze particle' by previously performing dilation and erosion operations. The area of the bubbles (in pixels) was plotted *vs.* the corresponding pressure; an increase in area representing bubble formation. The highest pressure at which the measured gas bubble area was nonzero was considered to be the pressure threshold for bubble formation. For each series of images, the area of two bubbles was determined by image analysis. Thus, the pressure threshold leading to gas outflow is the average of at least twelve measurements.

Pressure thresholds leading to impregnation during the restoration of atmospheric pressure were also estimated by image analysis. The image captured at the minimum pressure during VI (Step 8, Fig. 4) was subtracted from each image captured during the restoration of atmospheric pressure using ImageJ. 'Pixel mean grey values' of the images obtained were plotted *vs.* the corresponding pressure. The tissue became more translucent as it became impregnated with liquid. Low mean grey values correspond to low tissue translucency and high values to high translucency (*i.e.* 0 = black, 255 = white). The lowest pressure at which the mean grey value increased was considered to be the pressure threshold for pore impregnation. The pressure threshold for pore impregnation is the average of at least six replicates.

Weight gain

The percentage weight gain (WG) of the impregnated apple and spinach samples was calculated from the following equation:

$$WG = \frac{m - m_0}{m_0} \cdot 100 \qquad (3)$$

where m is the mass of the impregnated samples and m_0 is the initial mass of the samples. WG was determined in triplicate for each material.

3 Results

3.1 Porosity, isotonicity and weight gain after vacuum impregnation

The void phases of apple and spinach were found to be 0.195 ± 0.030 and 0.386 ± 0.026, respectively, in agreement with previous findings (Del Valle, Aránguiz & Díaz, 1998; Warmbrodt & Van Der Woude, 1990),

Isotonic concentration with respect to the cell sap was defined as the solution that provoked a maximum of 2.0 ± 0.5% weight gain in the tissue after 7 h of immersion. Concentrations of 19% and 13% sucrose were found to be isotonic for apple and spinach samples, respectively. The weight gain obtained after VI in isotonic solution was 20.5 ± 0.9% for apple and 38.1 ± 2.5% for spinach.

3.2 Pressure thresholds leading to the outflow of the gas

As the sample was immersed in a solution, the application of vacuum led to the expansion of the gas contained in the pores, seen as the formation of bubbles leaving the tissue. The area of the gas bubbles was determined by image analysis and plotted against the recorded pressure (Fig. 5). At the onset of VI, when the sample was still at atmospheric pressure, no bubbles were detectable for either of the materials. Bubbles were visible in the second image of the series for the apple samples, captured 10 s from the beginning of VI, indicating a pressure threshold for gas outflow of 860 ± 15 mbar (indicated by arrows in Fig. 5a). Spinach tissue, however, showed bubbling at a late stage in vacuum formation. As indicated by arrows in Fig. 5b, pressure threshold for gas outflow resulted in the range of 554 ± 56 mbar. Additional experiments were carried out to observe different regions of the sample under the microscope and the results (not shown) confirmed that the thresholds indicated in Fig. 5 were representative of the whole tissue sample. It can thus be concluded that gas left the pores of spinach tissue later than apple during the application of vacuum, and that at the outflow threshold. Furthermore, the size of the bubbles leaving spinach pores was less than one-hundredth of that of the bubbles leaving the pores in apple tissue, at the respective outflow threshold.

Figure 5a Figure 5b

3.3 Pressure thresholds leading to pore impregnation

Fig. 6 shows images of apple and spinach tissues taken at: (i) 150 mbar, the minimum absolute pressure employed, (ii) during atmospheric pressure restoration, where bright regions appeared in the samples due the impregnation of the tissue, and (iii) at the end of VI (1000 mbar), where the translucency of the sample increased in the whole area, indicating homogeneous impregnation of both the apple and spinach samples.

Figure 6

The results regarding the change in tissue translucency obtained from image analysis are shown in Fig. 7. At the beginning of the period of atmospheric pressure restoration, the mean grey values remained almost constant for both apple and spinach. The pressure thresholds for pore impregnation, were in the range of 220 ± 27 mbar for spinach (dashed lines) and 173 ± 2 mbar for apple (solid lines), as indicated by the arrows in the figure.

Figure 7

Discussion

We have determined pressure thresholds for gas outflow and solution impregnation during VI of spinach and apple. Gas outflow and solution impregnation of spinach samples occurred later than in apple samples. This probably reflects differences in the porous structure of the two materials. Plant tissues are made up of highly interconnected intercellular air spaces forming a complicated network of tortuous paths and clusters contributing to the heterogeneity of the tissue (Mendoza, Verboven, Mebatsion, Kerckhofs, Wevers & Nicolaï, 2007). This complex network is dependent on species, cultivar, tissue structure and functionality (Raven, 1996). The structure of spinach is characterized by interstices within the various layers of mesophyll cells (Warmbrodt & Van Der Woude, 1990). The porosity and intercellular space of apple increase

from the centre to the periphery of the apple parenchyma (Schulze, Peth, Hubbermann & Schwarz, 2012).

The distribution of two immiscible fluids such as liquid and air inside a porous medium has been extensively studied using resin micromodels (Badillo, Segura, & Laurindo, 2011; Lenormand, 1990). These micromodels simulate porous materials and are characterized by the presence of narrow pores (throats) connected to large capillaries (channels). Micromodels have been constructed with fixed characteristics: i.e. channel and pore cross-section geometry was defined, as well as channel depth, the mean curvature of the liquid-air interface, and liquid flow rate. Micromodels allow investigations of how capillarity and viscous pressure control the distribution of two immiscible fluids within the pores. Since we used plant tissues and not micromodels, the values of the tissue porosity parameters were unknown. By using Eq. 4 it can be shown that the air-liquid interface existed in a low Bond number ($Bo<<1$, Eq. 4) (Allen & Hallinan, 2001):

$$Bo = \frac{g \cdot r^2 \cdot \sigma}{\rho} \tag{4}$$

where g is the acceleration due to gravity, r is the pore radius ($5 \cdot 10^{-6}$ and $4 \cdot 10^{-5}$ m for spinach and apple tissue, respectively, Iwabuchi & Kurata, 2003; Khalloufi & Ratti, 2003), and σ and ρ are the interfacial tension and the liquid density ($7.2 \cdot 10^{-2}$ N m^{-1} and 10^3 kg m^{-3}, respectively). As the air-liquid interface existed in a low Bond number, an approximate value of p_c (Eq. 1) can be estimated for spinach and apple tissues, assuming both that the pores were sufficiently narrow with a circular cross section and a contact angle, θ, of 1.05 rad (Carciofi, Prat & Laurindo, 2012). p_c values resulted for apple and spinach of 72 mbar and 580 mbar, respectively.

Fito (1994) and Lenormand (1990) showed that air in a pore is not released to the surrounding solution until the internal air pressure (p_i) exceeds the pressure acting on the liquid (p_l) by a value equal to the capillary pressure (p_c). Thus, gas outflow occurs if:

$$p_i > p_l + p_c \tag{5}$$

If raw plant materials are considered rigid, and the internal pressure (p_i) equal to the initial (atmospheric) pressure, Eq. 5 could be used directly to estimate the threshold capillary pressure, which would depend on the maximum pore size at the surface of the material and on the air-

liquid surface tension. Thus, the lower bubbling pressure of spinach compared to apple could be a consequence of smaller pore sizes in spinach. However, the difference could also be due to the different mechanical properties of the raw materials. Salvatori, Andrés, Chiralt, & Fito (1997) ascribed the small deformation of the solid matrix observed in impregnated apple samples to the large intercellular pores and the rigid cellular structure characterizing apple tissue (Vincent, 1989). Thus, the assumption that the porous material was rigid, used in Eq. 5, could be confirmed for apple tissue. The complex layered tissue morphology and the extensive intercellular space system of spinach might suggest the possible occurrence of leaf expansion during the application of vacuum, leading to the lower observed bubbling pressure.

Fito's HDM model (1994) demonstrated that when the system was at the lowest working pressure for a certain period (e.g. 5 min), an equilibrium condition was reached. During this period, the impregnation of pores by the solution occurred, and p_c was the only driving force, as no pressure gradient was applied. Fito (1994) calculated the volume fraction of the pores occupied by the liquid (x_v) at equilibrium using the expression:

$$x_v = \frac{p_c}{p_l + p_c} \tag{6}$$

where x_v varies between 0 and 1. Our experiments showed no impregnation under the equilibrium conditions at 150 mbar. To verify this, additional experiments were carried out in which the duration of the lowest working pressure was increased to 20 min (step 8 in Fig. 4). No impregnation was observed during this period either. Under the experimental conditions used, sample impregnation was only detectable during the restoration of atmospheric pressure. The discrepancy between our results and those predicted by the HDM model may be due to the fact that it was assumed in the HDM model that the impregnating solution wetted the pores. However, the pores in plant tissue have evolved to allow the diffusion oxygen and carbon dioxide, which is much faster in gas than in water, and it would thus not be surprising to find that the wetting angle was high to avoid the plant from being "drowned".

Impregnation of apple tissue was seen almost as soon as restoration of atmospheric pressure was started, while spinach tissue impregnation occurred later. The difference in pressure between the impregnation of the two materials could be due to the difference in wetting angle and pore size, but impregnation could also be affected by recompression of the expanded leaf.

The results obtained in this study provide important information for the optimization of VI process parameters. Effective VI requires efficient removal of the air from the tissue during the application of the vacuum in order to ensure complete filling of the tissue pores during the subsequent impregnation step. Thus, the threshold pressure leading to gas outflow from the tissue represents the minimum value to which the pressure must be reduced during the vacuum phase to make any infusion possible. Slow release of the vacuum is recommended by Baker & Wicker (1996), so that the liquid can penetrate completely into the tissue. If the increase in pressure is not sufficiently gradual, the reduction in pressure acting on the liquid in the pores may give rise to a positive difference between external pressure and internal air pressure in the centre of the tissue, causing compression. However, if the pore space is hydrophobic and the pores small, compression will be unavoidable.

Conclusions

A microscopic method has been developed to detect pressure thresholds for gas outflow and solution impregnation during VI. Spinach tissue showed incipient bubbling, *i.e.* the release of gas, at a much lower pressure than apple, and impregnation commenced at a much higher pressure. These differences are believed to be the result of the narrow pores and possible changes in volume of the spinach leaves (*i.e.* leaf expansion during the application of vacuum and recompression during the restoration of atmospheric pressure). The findings of the present work might encourage an analytical approach combining different techniques such as microtomography, nuclear magnetic resonance and microscopy to investigate the evolution of the mechanical, structural and volumetric changes in biological tissues subjected to VI.

Acknowledgments The authors would like to thank Norrvidinge Boställe AB, Kävlinge, Sweden for providing the raw materials. V. Panarese acknowledges the Marco Polo Programme, Italy, EU, for financial support. F. Gómez Galindo acknowledges the financial support of the European Community's Seventh Framework Programme (FP7/2007-2013) under grant agreement no. 245280, also known as PRESERF.

References

1. Allen, J. S., & Hallinan, K. P. (2001). Liquid blockage of vapor transport lines in low Bond number systems due to capillary-driven flows in condensed annular films. *International Journal of Heat and Mass Transfer, 44,* 3931-3940.
2. Badillo, G. M., Segura, L. A., & Laurindo, J. B. (2011). Theoretical and experimental aspects of vacuum impregnation of porous media using transparent etched networks. *International Journal of Multiphase Flow*, *37,* 1219–1226.
3. Baker, R. A., & Wicker, L. (1996). Current and potential applications of enzyme infusion in the food industry. *Trends in Food Science and Technology, 7,* 279-284.
4. Barrera, C., Betoret, N., & Fito, P. (2004). Ca^{2+} and Fe^{2+} influence on the osmotic dehydration kinetics of apple slices (var. *Granny Smith*). *Journal of Food Engineering, 65,* 9-14.
5. Carciofi, B. A. M., Prat, M., & Laurindo, J. B. (2012). Dynamics of vacuum impregnation of apples: Experimental data and simulation results using a VOF model. *Journal of Food Engineering, 113,* 337-343.
6. Chalermchat, Y., Malangone, L., & Dejmek, P. (2010) Electropermeabilization of apple tissue: Effect of cell size, cell size distribution and cell orientation. *Biosystems Engineering, 105*, 357 - 366.
7. Del Valle, J. M., Aránguiz, V., & Díaz, L. (1998). Volumetric procedure to assess infiltration kinetics and porosity of fruits by applying a vacuum pulse. *Journal of Food Engineering, 38,* 207-221.
8. Derossi, A., De Pilli, T., La Penna, M. P., & Severini, C. (2011). pH reduction and vegetable tissue structure changes of zucchini slices during pulsed vacuum acidification. *LWT - Food Science and Technology, 44*, 1901-1907.
9. Dullien, F. A. L. (1992). *Porous media: fluid transport and pore structure*. (2^{nd} ed.). USA: Academia Press.
10. Fito, P., & Pastor, R. (1994). Non-diffusional mechanisms occurring during vacuum osmotic dehydration. *Journal of Food Engineering, 21,* 513-519.
11. Fito, P. (1994). Modelling of vacuum osmotic dehydration of food. *Journal of Food Engineering, 22,* 313-328.

12. Fito, P., Andrés, A., Chiralt, A., & Pardo, P. (1996). Coupling of hydrodynamic mechanism and deformation-relaxation phenomena during vacuum treatments in solid porous food-liquid systems. *Journal of Food Engineering, 27*, 229.
13. Fito, P., Chiralt, A., Betoret, N., Gras, M., Chafer, M., Martinez-Monzo, J., Andres, A., & Vidal, D. (2001). Vacuum impregnation and osmotic dehydration in matrix engineering application in functional fresh food development. *Journal of Food Engineering, 49,* 175–183.
14. Gras, M. L., Vidal, D., Betoret, N., Chiralt, A., & Fito, P. (2003). Calcium fortification of vegetables by vacuum impregnation. Interactions with cellular matrix. *Journal of Food Engineering, 56*, 279–284.
15. Hironaka, K., Kikuchi, M., Koaze, H., Sato, T., Kojima, M., Yamamoto, K., Yasuda, K., Mori, M., & Tsuda, S. (2011). Ascorbic acid enrichment of whole potato tuber by vacuum-impregnation. *Food Chemistry, 127*, 1114–1118.
16. Iwabuchi, K., & Kurata, K. (2003). Short-term and long-term effects of low total pressure on gas exchange rates of spinach. *Advanced in Space Research, 31*, 241-244.
17. Khalloufi, S., & Ratti, C. (2003). Quality deterioration of freeze-dried foods as explained by their glass transition temperature and internal structure. *Journal of Food Science*, *68,* 892–902.
18. Lenormand, R. (1990). Liquids in porous media. *Journal of Physics: Condensed Matter, 2,* 79–88.
19. Lozano, J. E., Rotstein, E., & Urbicain, M. J. (1980). Total porosity and open-pore porosity in the drying of fruits. *Journal of Food Science, 45*, 1403–1407.
20. Mavroudis, N. E., Dejmek, P., & Sjöholm, I. (2004) Studies on some raw material characteristics in different Swedish apple varieties. *Journal of Food Engineering, 62,* 121-129.
21. Mendoza, F., P. Verboven, P., Mebatsion, H. K., Kerckhofs, G., Wevers, M., & Nicolaï, B. (2007). Three dimensional pore space quantification of apple tissue using X-ray computed microtomography. *Planta, 226,* 559-570.
22. Raven, J. A. (1996). Into the voids: the distribution, function, development and maintenance of gas spaces in plants. *Annals of Botany, 78,* 137–142.
23. Salvatori, D., Andrés, A., Chiralt, A., & Fito, P. (1997). The response of some properties of fruit to vacuum impregnation. *Journal of Food Process Engineering, 21*: 59–73.

24. Schulze, B., Peth, S., Hubbermann, E. M., & Schwarz, K. (2012). The influence of vacuum impregnation on the fortification of apple parenchyma with quercetin derivatives in combination with pore structures X-ray analysis, *Journal of Food Engineering, 109,* 380-387.
25. Tylewicz, U., Romani, S., Widell, S., & Gómez Galindo, F. (2011). Induction of vesicle Formation by exposing apple tissue to vacuum impregnation. *Food and Bioprocess Technology.* DOI: 10.1007/s11947-011-0644-1.
26. Tylewicz, U., Lundin, P., Cocola, L., Dymek, K., Rocculi, P., Svanberg, S., Dejmek, P., & Gómez Galindo, F. (2012). Gas in scattering media absorption spectroscopy (GASMAS) detected persistent vacuum in apple tissue after vacuum impregnation. *Food Biophysics, 7,* 28-34.
27. Vincent, J. F. V. (1989). Relationship between density and stiffness of apple flesh. *Journal of Science of Food and Agriculture, 47*, 443–462.
28. Warmbrodt, R. D., & Van Der Woude, W. J. (1990). Leaf of *Spinacia oleracea* (spinach): ultrastructure and plasmodesmatal distribution and frequency, in relation to sieve-tube loading. *American Journal of Botany, 77,* 1361-1377.
29. Zhao, Y., & Xie, J. (2004) Practical applications of vacuum impregnation in fruit and vegetable processing. *Trends in Food Science & Technology, 15*, 434-451.

Figure Captions

Figure 1. Sampling of tissues from spinach and apple. (a) Schematic illustration of spinach leaf sampling. (1) midrib; (2); lamina; (3) petiole. Sample size: height 20 ± 1 mm, width 13 ± 1 mm. Excision was performed parallel to the leaf midrib. (b) Schematic illustration of apple sampling. Sample size: height 15 mm, width 2 mm, depth 15 mm. The sample was taken parallel to the fruit axis, about 2 mm from the epidermis.

Figure 2. Schematic of the chamber used for vacuum impregnation. (a) Top view: 1. Vacuum pre-chambers, 2. Main chamber containing sample and impregnating solution, 3. O-ring, 4. Plastic frame; (b) Cross section: 1. Sample, 2. Plastic fastener, 3. Impregnating solution, 4. Upper and lower glass plates sealed to the plastic frame by the O-ring.

Figure 3. Schematic illustration of the AVCS: 1. Treatment chamber, 2. Pressure transmitter, 3. Valve regulating air outlet, 4. Vacuum pump, 5. Valve regulating air inlet, 6. PLC. Arrows indicate the direction of air flow. Solid lines represent pneumatic connections, dashed lines represent electrical connections.

Figure 4. VI of apple and spinach samples with a minimum pressure of 150 mbar. The complete process involved 20 consecutive steps (indicated by numbers from 1 to 20). Each step is defined by two parameters: duration (s) and absolute pressure (mbar).

Figure 5. The areas of gas bubbles in (a) apple and (b) spinach tissue during the application of vacuum. The area of individual bubbles was evaluated by image analysis as described in the text. The arrows indicate the pressure threshold for bubble formation. The results of three replicate measurements are shown.

Figure 6. Examples of microscope images of apple (a, b, c) and spinach (d, e, f) samples during the restoration of atmospheric pressure. Scale bar = 1 mm. (a) and (d) were recorded at the minimum pressure (150 mbar); (b) and (e) at pressures of 330 mbar and 450 mbar, respectively, and (c) and (f) at atmospheric pressure (i.e. at the end of VI).

Figure 7. Pixel mean grey colour values obtained from images of apple (solid lines) and spinach (dashed lines) samples during atmospheric pressure restoration. The results of three replicates are shown. The arrows indicate the pressure threshold for pore impregnation. To better highlight the thresholds, mean grey values are reported in the range 150 mbar to 270 mbar.

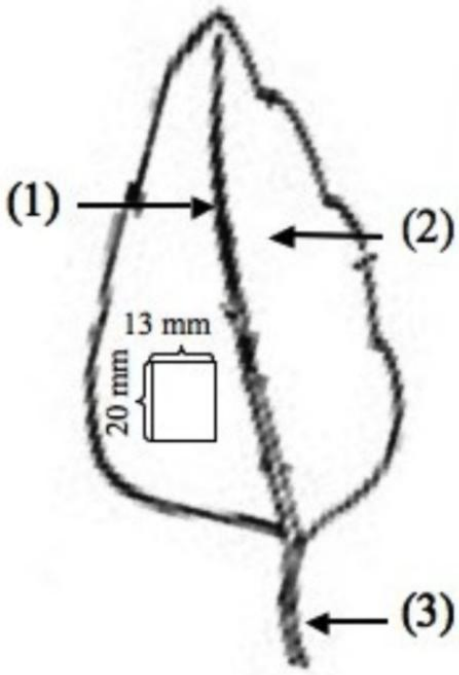

Fig. 1a

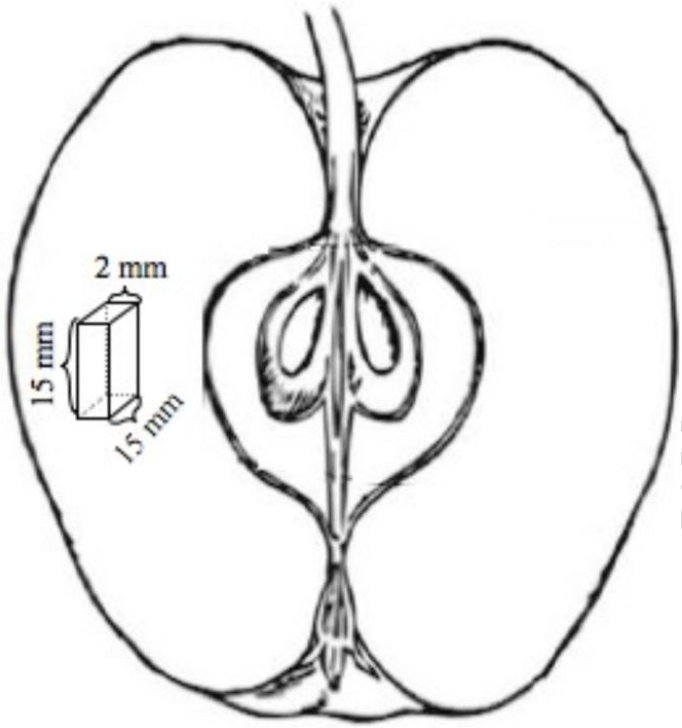

Fig. 1b

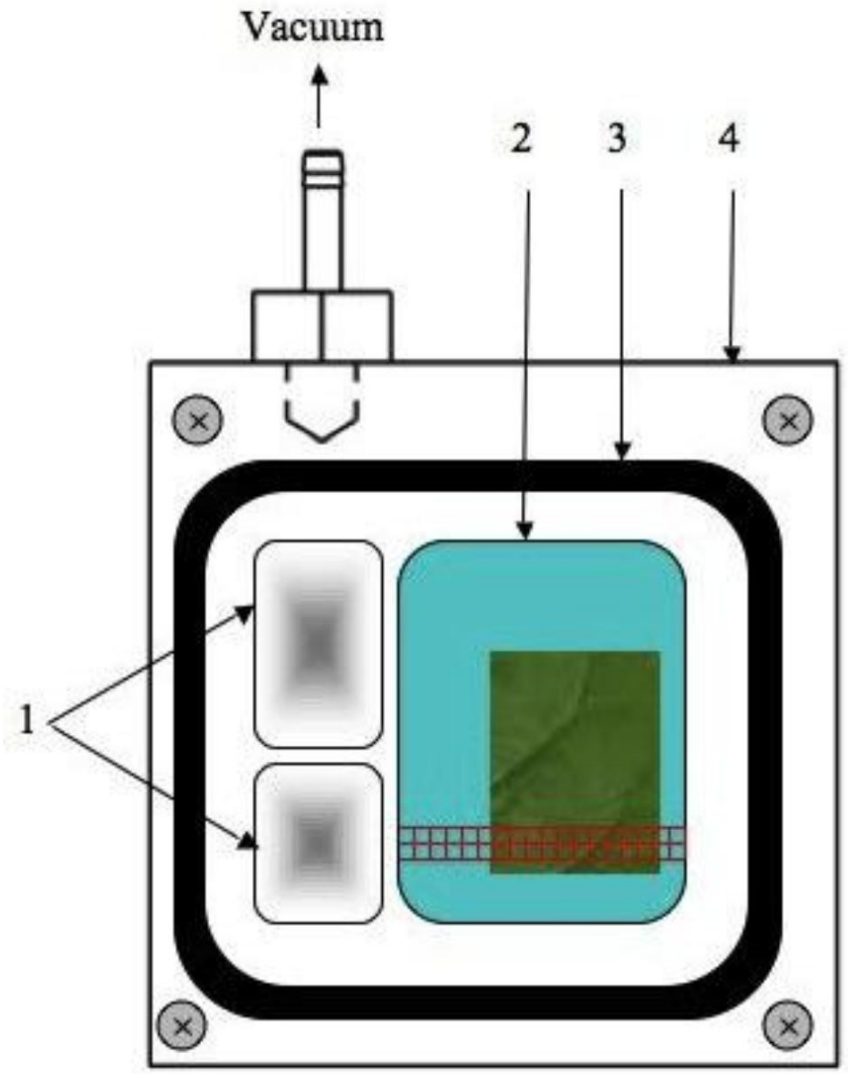

Fig. 2a

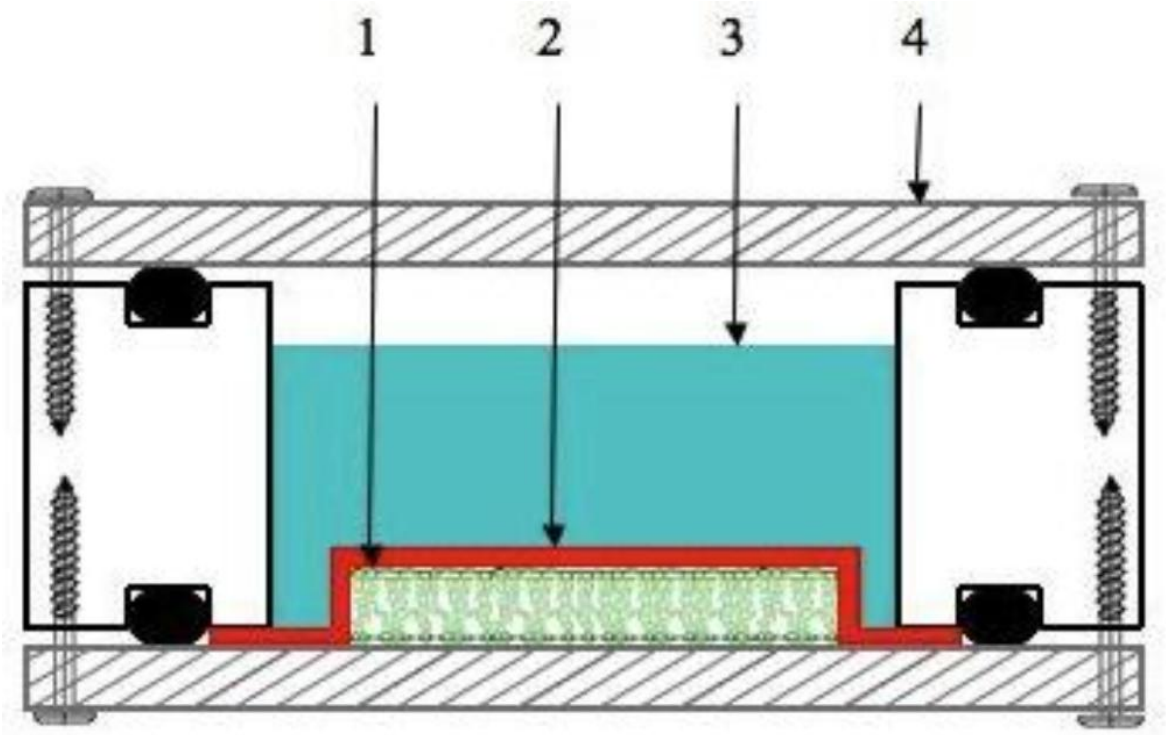

Fig. 2b

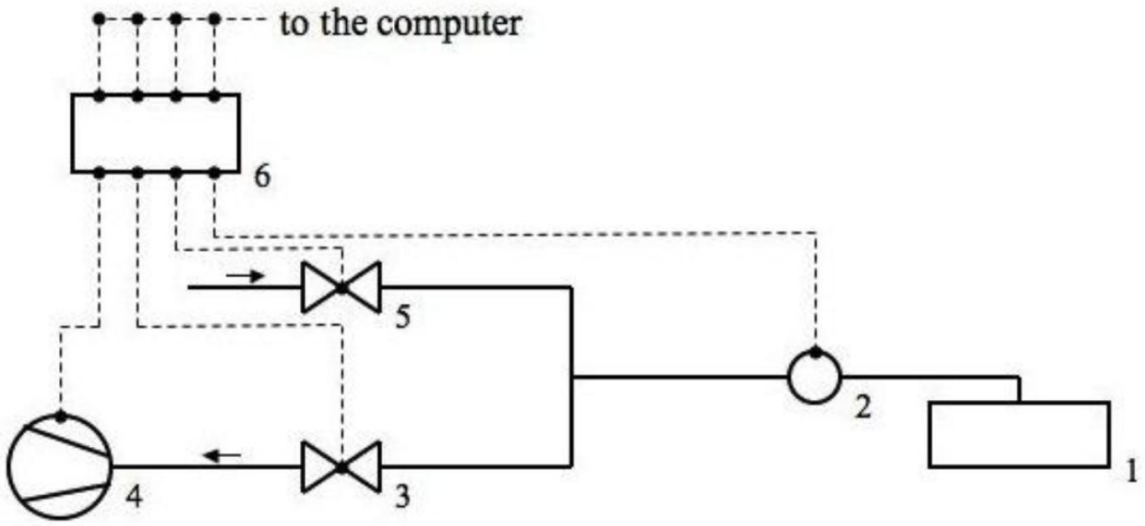

Fig. 3

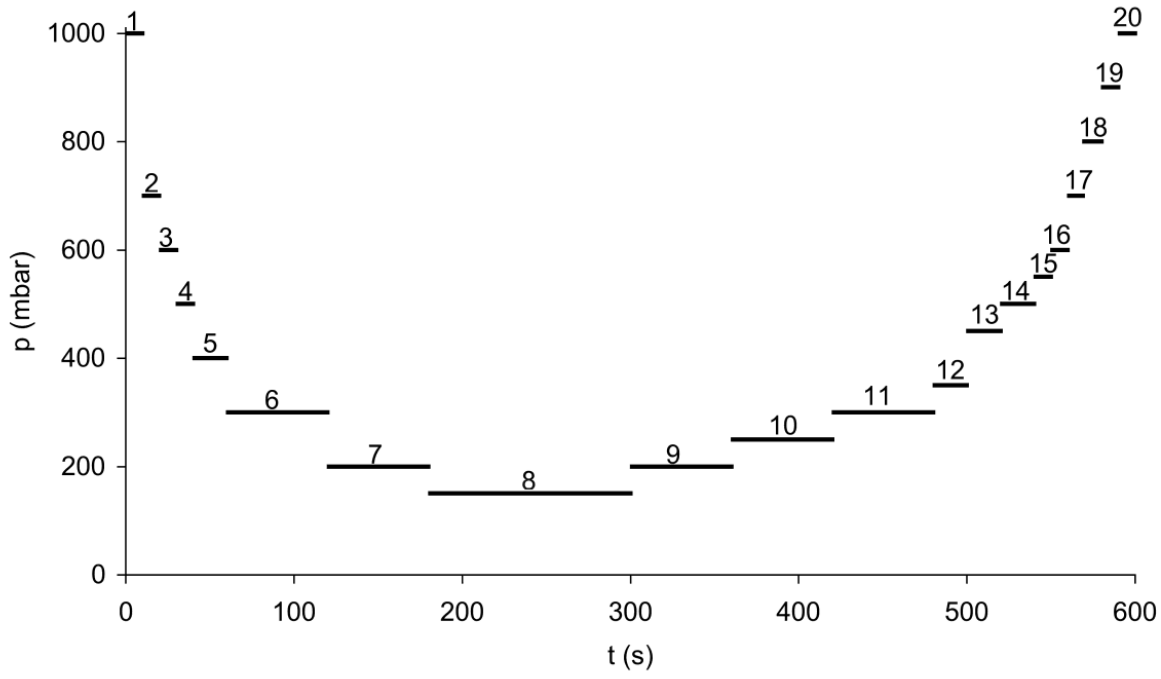

Fig. 4

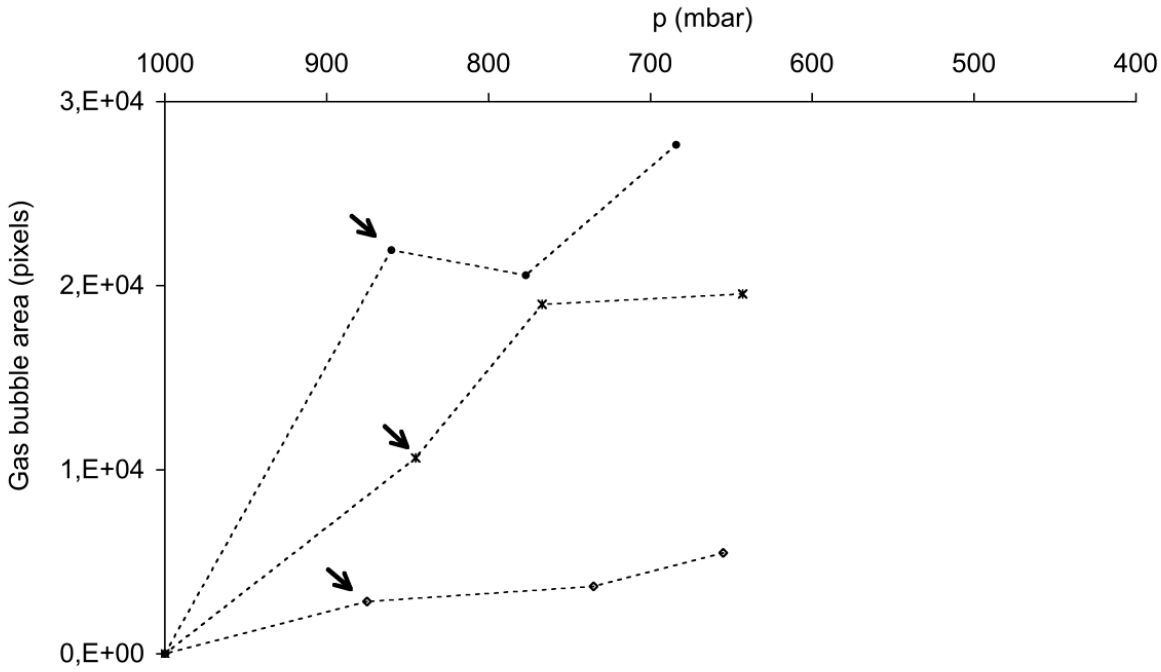

Fig. 5a

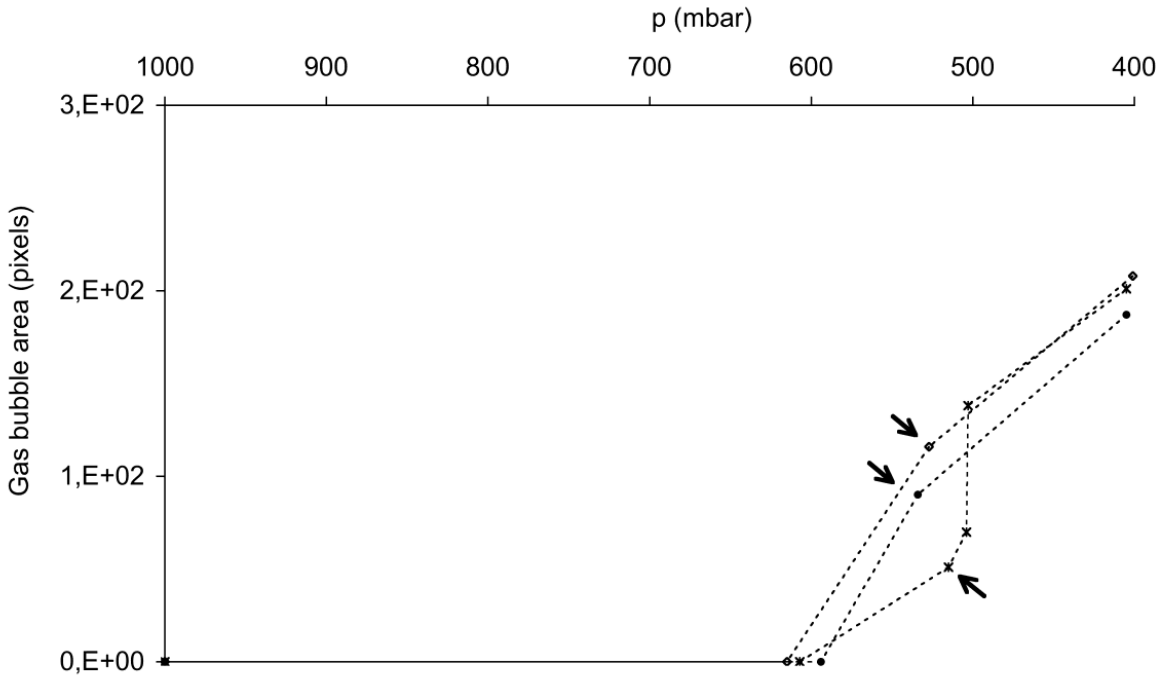

Fig. 5b

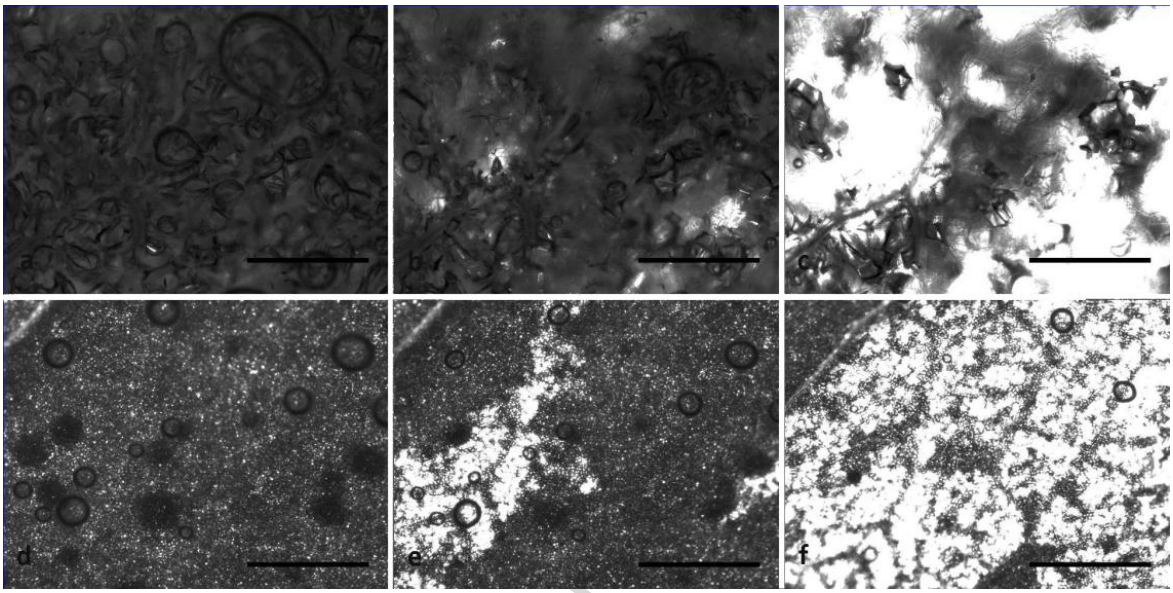

Fig. 6

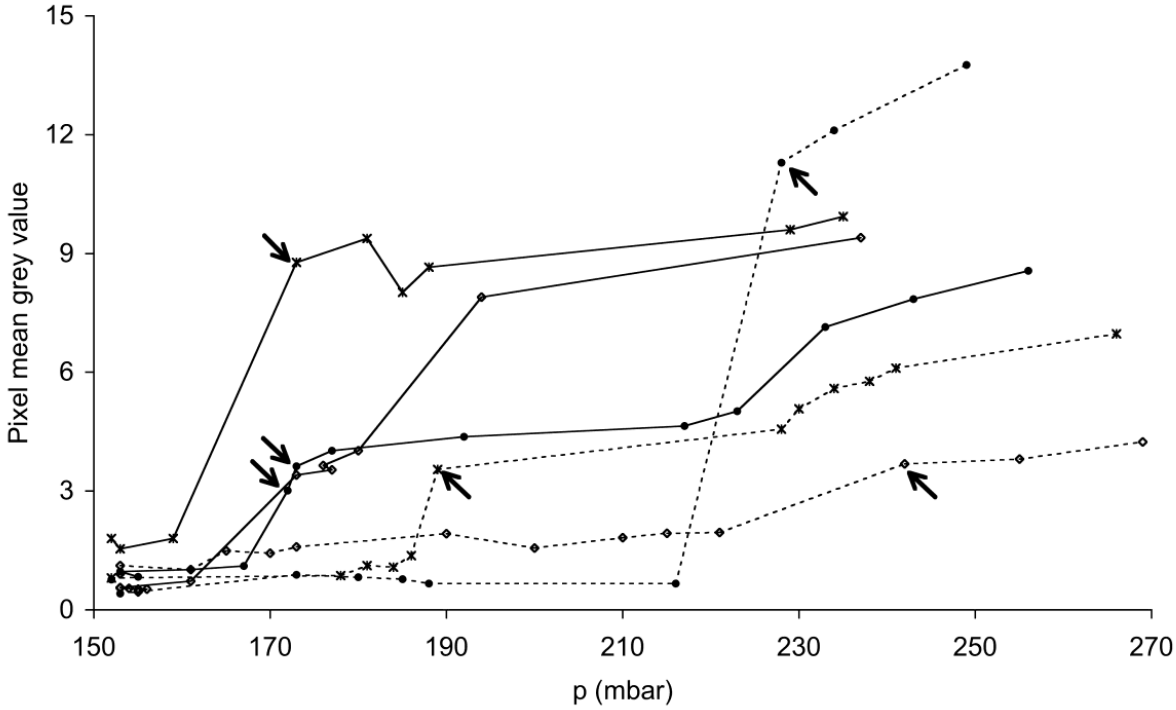

Fig. 7

Highlights:

> Microscopic study of VI on raw materials with different porosities (apple and spinach).

> Gas outflow thresholds in vacuum formation were established: apple 860±15 mbar; spinach 554±27 mbar.

> Gas outflow threshold values could be related to the raw material pore sizes.

> Impregnation thresholds during atm pressure restoration were established: spinach 220±27 mbar; apple 173±2.

> Impregnation threshold values could be related to the raw material wetting angle and pore sizes

Paper VII

EXPLORING METABOLIC RESPONSES OF SPINACH LEAVES INDUCED BY VACUUM IMPREGNATION

Valentina Panarese, Pietro Rocculi, Elena Baldi, Lars Wadsö, Allan G. Rasmusson and Federico Gómez Galindo

Abstract

In this study, calorimetric measurements provided evidence of a drastic increase of spinach leaf gross metabolism as a consequence of vacuum impregnation (VI) at a minimum pressure of 150 mbar with trehalose and sucrose isotonic solutions. With the application of VI, extracellular air is replaced by the impregnation solution, potentially limiting tissue respiration to any remaining volume of air in the tissue. However the fact that the impregnated leaves showed photosynthetic activity strongly suggested that not all air was exhausted during VI. Hence impregnation of spinach tissue appears to reach a maximum with remaining gas filled compartments. Metabolic inhibitors were impregnated together with the sugars showing that the short-term metabolic response responsible for the drastic increase in gross metabolism upon VI depends on the mitochondrial oxygen consuming pathways. Interestingly, the metabolic effect consequent to the impregnation with mannitol was less pronounced and comparable with water impregnation, suggesting that the strong metabolic effect here reported might be influenced by molecules that can be metabolized by the cells (*e.g.* sucrose, trehalose).

Keywords

Vacuum impregnation · metabolism · photosynthesis · spinach

1. Introduction

Vacuum impregnation (VI) is a unit operation in which porous products are immersed in a solution of different compositions and/or concentrations and subjected to a two-step pressure change. The first step (application of vacuum) consists of the reduction of the pressure in a solid-liquid system. During this step, the gas in the product pores is expanded and flows out until mechanical equilibrium is achieved. When the atmospheric pressure (second step) is restored, the residual gas in the pores compresses and the external liquid flows into the pores (Tylewicz *et al.*, 2011). VI is therefore widely used in several processes to incorporate additives in fruit and vegetable tissues, such as anti-browning agents, microbial preservatives or cryoprotectants (Barrera *et al.*, 2009; Phoon *et al.*, 2008). There is a vast amount of literature focused on the effects of the vacuum level and the structure and mechanical properties of the foodstuff on mass transfer phenomena during VI (Chiralt and Fito, 2003; Mujica-Paz, 2003; Fito and Pastor, 1994; Laurindo *et al.*,

2007; Silva Paes *et al.,* 2007; Carciofi *et al.*, 2012) as well as the effects of the impregnating liquid on structure and mechanical properties (Guillemin *et al*., 2008).

Little is known on the metabolic consequences of VI. As it may be expected, the onset of anaerobic metabolism in sucrose solution-impregnated strawberries was demonstrated by Castelló *et al.* (2010) one week after VI. However, to the best of our knowledge, little is known on metabolic responses upon VI that might be provoked by the changes in pressure experienced during the operation, the impregnated substance, structural modifications, and/or anaerobic stress. Recently, we showed the formation of cell membrane vesicles 30 min after the impregnation of apple tissue with different concentrations of sucrose and trehalose, suggesting that the impregnated sugars may not totally remain in the extracellular space, as normally believed, but at least a fraction might be incorporated into the cells (Tylewicz et al., 2011). In this paper, further exploration of short-term metabolic responses is done in spinach using isothermal calorimetry. Calorimetric measures of the heat production rate of a biological tissue is related to its metabolic rate and provides a direct indication of integrated metabolic responses such as respiration and reaction to stress (Gómez Galindo *et al.,* 2008; Criddle et al., 1991).

2. Material and Methods

2.1 Raw material handling and storage

Baby spinach leaves (*Spinacia oleracea*) grown in southern Sweden were harvested and stored in a packing house storage facility in a normal atmosphere (1-2 °C; 90-95% RH). Within 5 days of harvesting, the leaves were washed, air-dried, packed in 65 g bags, as routinely practiced by the producer, and delivered the same day to our laboratory. During the experimental period the packages were stored at 2 ± 1 °C, and experiments were performed within the product expiration time (7 days). Undamaged leaves (30 ± 3 mm in length x 60 ± 3 mm in width) were manually selected.

2.2 Raw material characterization

Porosity

The apparent density (ρ_a) and the real solid-liquid density (ρ_r) of spinach were determined by volume displacement in a pycnometer using appropriate aqueous isotonic sucrose solutions as reference liquid (see below) (Gras *et al.*, 2003). The real solid-liquid density was also obtained by volume displacement using sample purees obtained by manually grinding the samples using a mortar and pestle. The purees were placed in a Büchner flask and degasified for 10 min by creating vacuum in the flask. The total porosity of the sample (ε) is the dimensionless ratio of air volume to total volume, and varies between 0 and 1 (Eq. 1) (Lozano, Rotstein & Urbicain, 1980):

$$\varepsilon = 1 - \left(\rho_a \Big/ \rho_r \right) \tag{1}$$

2.3 Sample preparation

For calorimetric measurements each leaf, placed in a covered Petri dish, was equilibrated in room light at 25 °C for 15 min and each sample (50 ± 1 mm of height x 30 ± 1 mm of length) was obtained using a sharp microtome blade (Figure 1).

For photosynthesis measurements each leaf, placed in a covered Petri dish, was equilibrated in darkness at 25 °C for 15 min and one disc of 36 mm of diameter was removed from each of twelve spinach leaves with a sharp cork borer. Three discs were placed in the dark inside a Petri dish (untreated samples). The remaining nine discs were divided in three 100 ml beakers and flooded with the impregnating solutions. 1 mm thick plastic net allowed the samples to be set apart and submerged during the whole VI treatment. The three beakers were placed in the VI vessel (a desiccator) and subjected to VI.

Figure 1. Sampling of tissues from spinach for calorimetric measurements. Sample size: height 50 ± 1 mm, width 30 ± 1 mm.

2.4 Impregnating solutions

Isotonic solutions in equilibrium with spinach leaves were designed with respect to the cell sap. The isotonic solution concentrations were determined by immersion of three spinach leaves (without petioles) in a series of solutions of different sucrose, trehalose or mannitol concentrations, according to Tylewicz *et al.* (2011). The variation in tissue weight was recorded every 30 min until equilibrium.

When metabolic inhibitors were used, sucrose and trehalose solutions were mixed with inhibitor stock solutions to reach 10 mM salicylhydroxamic acid (SHAM) and 2 mM KCN. KCN and SHAM stocks contained 100 mM in a 20 mM MOPS buffer (pH 7) and 1 M in dimethyl sulfoxide, respectively.

2.5 Automatic vacuum controller system

The automatic vacuum controller system (AVCS, S.I.A., Bologna, Italy) is a programmable device constructed to control the pressure acting on the impregnating solution during the process. The AVCS is connected to the VI chamber by a Teflon tube and includes a number of components: a pressure transmitter,

vacuum actuators (valves and vacuum pump), a computer and a programmable logic controller device (PLC, Series 90-30, General Electric, Charlottesville, VA, USA) as illustrated in Figure 2. The PLC is the core of the AVCS as it manages the vacuum actuators, supervising the value of pressure, time and vacuum release rate by controlling the start and stop of the vacuum pump and the opening and closing of the air inlet and air outlet valves. A software interface (CIMPLICITY® Workbench Version 6.10 Service Pack 3, GE Fanuc Automation Americas, Inc.) allows the working parameters of the AVCS to be set and controlled (Panarese *et al.*, 2013).

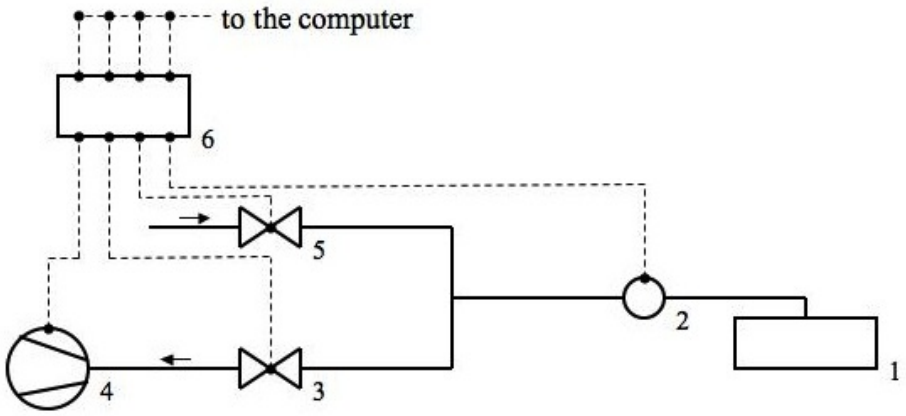

Figure 2. Schematic illustration of the AVCS: 1. Treatment chamber, 2. Pressure transmitter, 3. Valve regulating air outlet, 4. Vacuum pump, 5. Valve regulating air inlet, 6. PLC. Arrows indicate the direction of air flow. Solid lines represent pneumatic connections, dashed lines represent electrical connections.

2.6 Vacuum impregnation

Based on preliminary experiments to establish the maximum weight gain of spinach, a minimum absolute pressure of 150 mbar was chosen. As shown in Figure 3, pressure was applied in 20 consecutive steps. The chosen pressure profile ensured that cell viability was maintained. Two parameters were set for each pressure step: duration (s) and absolute pressure value (mbar). VI was controlled by the AVCS. As outlined in Figure 3, during the first phase of VI the pressure gradually decreased from the atmospheric value (1000 mbar) to the final reduced pressure value (150 mbar, step 8). During the second phase, vacuum was released and the pressure progressively returned to the atmospheric value. The chosen duration for each step was: 10 s for each step 1 to 4 and step 15 to 20; 20 s for step 5 and steps 12 to 14; 60 s for steps 6, 7 and steps 9 to 11; 120 s for step 8. Thus the VI treatment applied had a total duration of 600 s.

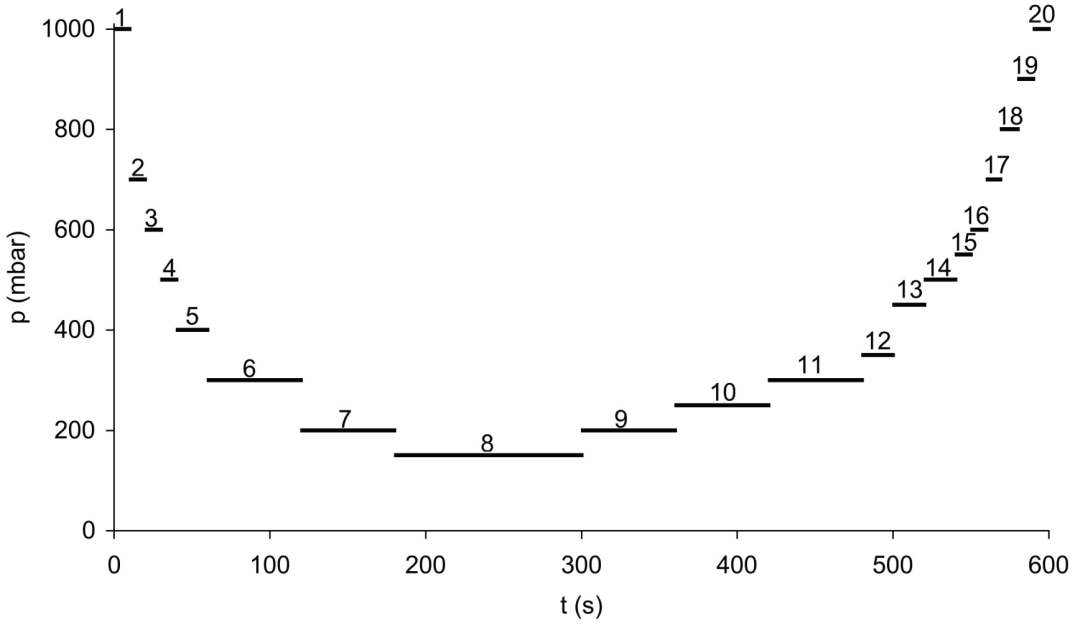

Figure 3. VI of spinach samples with a minimum pressure of 150 mbar. The complete process involved 20 consecutive steps (indicated by numbers from 1 to 20). Each step is defined by two parameters: duration (s) and absolute pressure (mbar).

2.7 Calorimetry: Experimental set-up and heat production measurement

A 20 ml stainless steal ampoule, containing the sample, was closed with a stainless steal screw cap where two openings were made. In each opening, a stainless steal needle was inserted and fixed to the cap with an o-ring. In the outer side of the cap, the ends of the needles were fastened to a 20 ml syringe and to the AVCS, as shown in Figure 4.

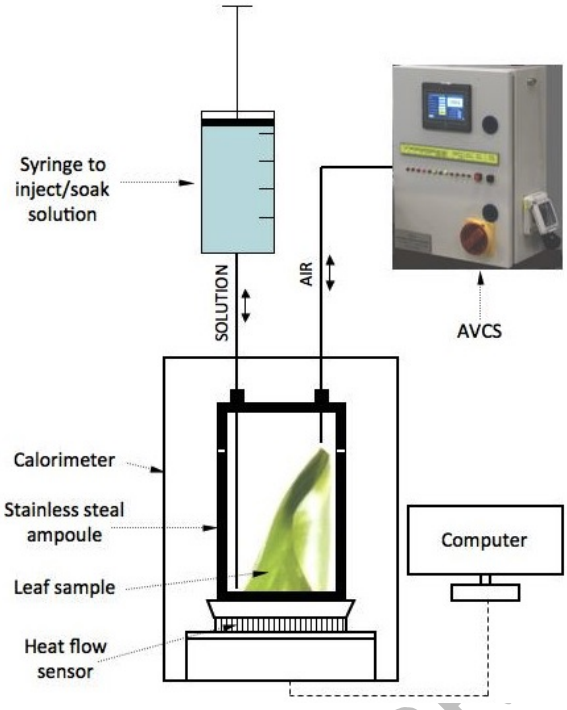

Figure 4. A schematic picture of the experimental set-up (VI and calorimetry).

The sealed stainless steal ampoule containing the sample was placed in the calorimeter at 25 °C. When the sample heat rate was stable, 18 ml of impregnating solution previously thermostatised at 25°C were injected with a syringe in the ampoule and VI treatment was applied. Immediately after VI treatment the solution in the ampoule was drawn back into the syringe, emptying the ampoule. The rate of heat production after VI was continuously measured with a prototype of the TAM Air isothermal**.** Heat is allowed to flow between the reaction vessel containing the sample and a heat sink, the temperature of which is kept essentially constant. The heat transfer takes place through a heat flow sensor that is located between the vessel and the heat sink. The calorimeter had its own reference that consisted of an empty sealed 20 ml volume stainless steal ampoule. The isothermal measurements were performed for periods of about 4 h. Baselines were recorded before or after each measurement. The primary output from the heat flow sensors in the calorimeter (a voltage) was recorded every 10 s by a computer from the digitized output of the calorimeter. The corresponding thermal powers (heat production rates) were calculated (Eq. 2):

$$P = \varepsilon \frac{V_S - V_{BL}}{M} \tag{2}$$

where P (μW g^{-1}) is the specific thermal power of the spinach sample, ε the calibration coefficient of the calorimeter (μW μV^{-1}), V_S the voltage signal from the calorimeter (μV), V_{BL} the corresponding voltage (μV) recorded for the baseline, and M is the mass (g) of the sample. The calibration coefficients were calculated from electrical calibrations made at 20 °C. The heat production measurement was performed on at least three samples for each impregnating solution tested.

2.8 Photosynthesis: Experimental set-up and O_2 production measurement

VI was performed in a darkened chamber. After the treatment the leaf discs were blotted with tissue paper (5 s for each sample side), weighed and kept in darkness for 30 min (at 25 °C). Thereafter the photosynthesis rate was registered for 30 min. The leaf disc photosynthesis, expressed in term of O_2 evolution ($nmolO_2\ min^{-1}\ cm^{-2}$) was determined at 25 °C with an O_2 electrode (S1 O_2 electrode, Hansatech, Norfolk, England). The leaf disc sample and electrodes were both placed in a thermostatised electrode chamber (LD2/3, Gas-Phase Oxygen Electrode Chamber). The electrode was placed at the bottom of the chamber while the leaf disc was placed on a fabric plate soaked with bicarbonate buffer pH 9, a mixture of one part saturated KCl solution, one part 0.4 M borate buffer at pH 9 and two parts 1 M sodium bicarbonate solution, previously adjusted to pH 9 by addition of 1 M equimolar sodium carbonate (Walker, 1987; Delieu & Walker, 1981). Once the chamber was sealed, the leaf disc was irradiated with 1230 $\mu E\ m^{-2}\ s^{-1}$ (LS3 Computer Controlled UV Light Source, Hansatech, Norfolk, England), as natural daylight varies in the range 1200 - 1500 $\mu E\ m^{-2}\ s^{-1}$ (Jifon & Syvertsen, 2003). The light source, designed to be coupled with the electrode chamber, was set on the chamber glass window and the leaf was continuously irradiated through the window during the photosynthesis measurement. O_2 electrodes were calibrated before each measurement with air and N_2 (Glazer *et al.*, 2004). The measurement was repeated at least three times for each impregnating solution tested. Statistical significance of the effect of each impregnating solution on photosynthetic activity was evaluated with one-way analysis of variance using the software STATISTICA 6.0 (Statsoft Inc., Tulsa, UK).

3. Results

3.1 Porosity, isotonicity and weight gain after vacuum impregnation

The void phase of spinach was found to be 0.386 ± 0.026, in agreement with previous findings (Warmbrodt & Van Der Woude, 1990).

Isotonic concentration with respect to the cell sap was defined as the solution that provoked a maximum of 2.0 ± 0.5% weight gain in the tissue after 7 h of immersion. Concentrations of 13% sucrose, 11% trehalose, 8% mannitol were found to be isotonic for spinach samples.

The average weight gain (± SEM, n=23) of the leaf obtained after VI in isotonic solutions was 38.1 ± 2.5%. A further decrease to 40 mbar did not significantly affect the weight gain (40.5 ± 3.8 %, n=5).

3.2 Effect of VI on metabolic activity

Calorimetric Measurements

To assess the metabolic responses upon VI calorimetry measurements (in darkness) were performed and an example of the results from the measurements of an impregnated spinach tissue with trehalose is reported in Figure 5. Each time an ampoule was changed into the calorimeter, there was an initial disturbance lasting about 30 min. After that the true thermal power from the sample was measured. In the untreated samples (dashed line in Figure 5) during the time of the measurement the thermal power showed an average (± SEM) overall decrease of 11.2 ± 3.0 % with respect to the initial values. For the sample to be VI treated (continuous line in Figure 5), vacuum was applied when the thermal power was relatively stable (indicated with an arrow in Figure 5). The VI treatment provoked a disturbance on the recorded thermal power values, resulting in a gap in the measurements lasting about 50 min. Once the thermal power values were back within the detectable range, the disturbance in the calorimeter measurements lasted about 20 more min before the true thermal power from the treated sample was measured. The experiment was interrupted after about 150 min from the application of the VI by taking the sample out from the calorimeter.

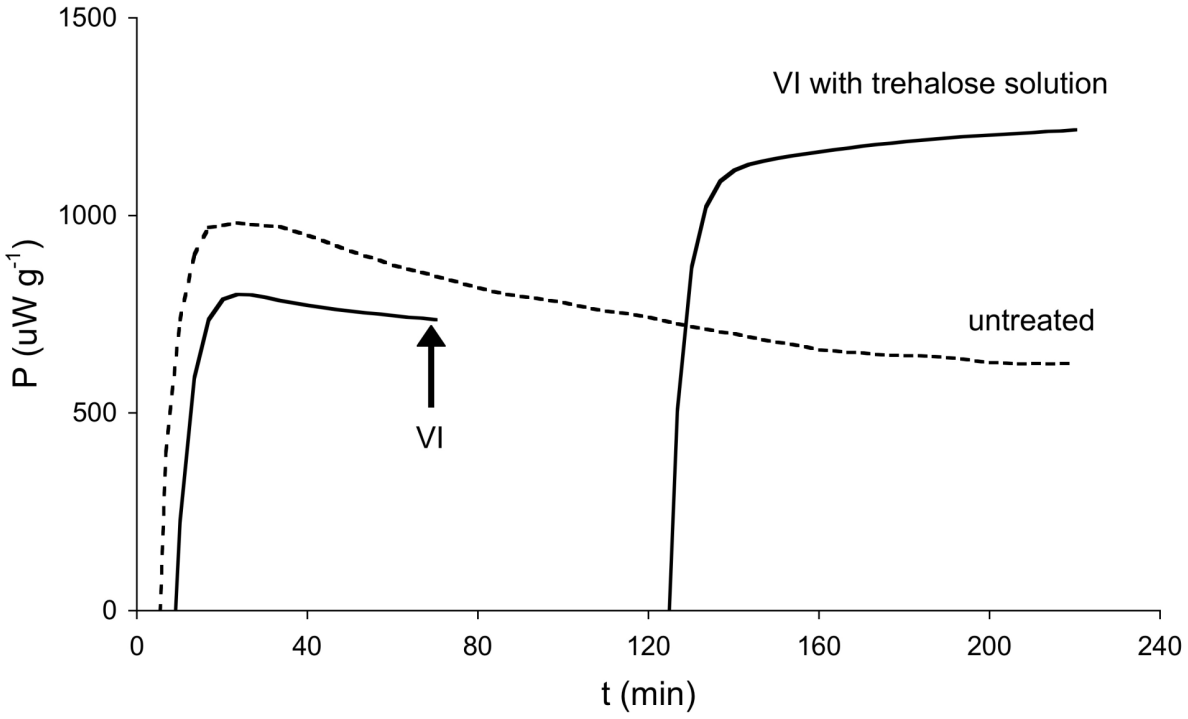

Figure 5. Calorimetric measurements of metabolic heat rates. Typical calorimeter output from untreated spinach (control, dashed line) and spinach tissue subjected to VI with isotonic trehalose solution (continuous line). After an initial disturbance, VI was applied (the time of VI application is indicated with an arrow in the continuous line). Application of vacuum provoked a second disturbance where the thermal power values were outside the detectable range for about 50 min (gap of values in the continuous line) and, once back within the detectable range, the disturbance in the calorimetric measurements lasted about 20 more min before the real thermal power from the impregnated sample was recorded.

Impregnation with sucrose and trehalose drastically increased the metabolic activity of spinach leaves

To facilitate the comparison among VI treatments each heat production rate curve (reported in Figures 6) was normalized by setting the initial sample thermal power value before VI to 100, corresponding to an average (± SEM; n=15) value of 887 ± 71 μW g^{-1}. From the three replicates, average normalised curves are reported. In the x-scale of Figure 6 a variable *m* (min) has been used. The variable *m* is defined by Eq. 3:

$$m = t_1 + t_2 + t_3 \quad (3)$$

where t_1 is the duration of the initial disturbance of the calorimetric measurement; t_2 is the time for the thermal power to relatively stabilise before the application of vacuum; t_3 is the duration of the disturbance provoked by VI. The average values (± SEM; n=15) of t_1, t_2 and t_3 were respectively of 33 ± 1 min, 60 ± 11 min and 72 ± 6 min. Within the time interval described by the variable *m*, Figure 6 reports for each heat production rate curve the initial stable thermal power values normalised to 100.

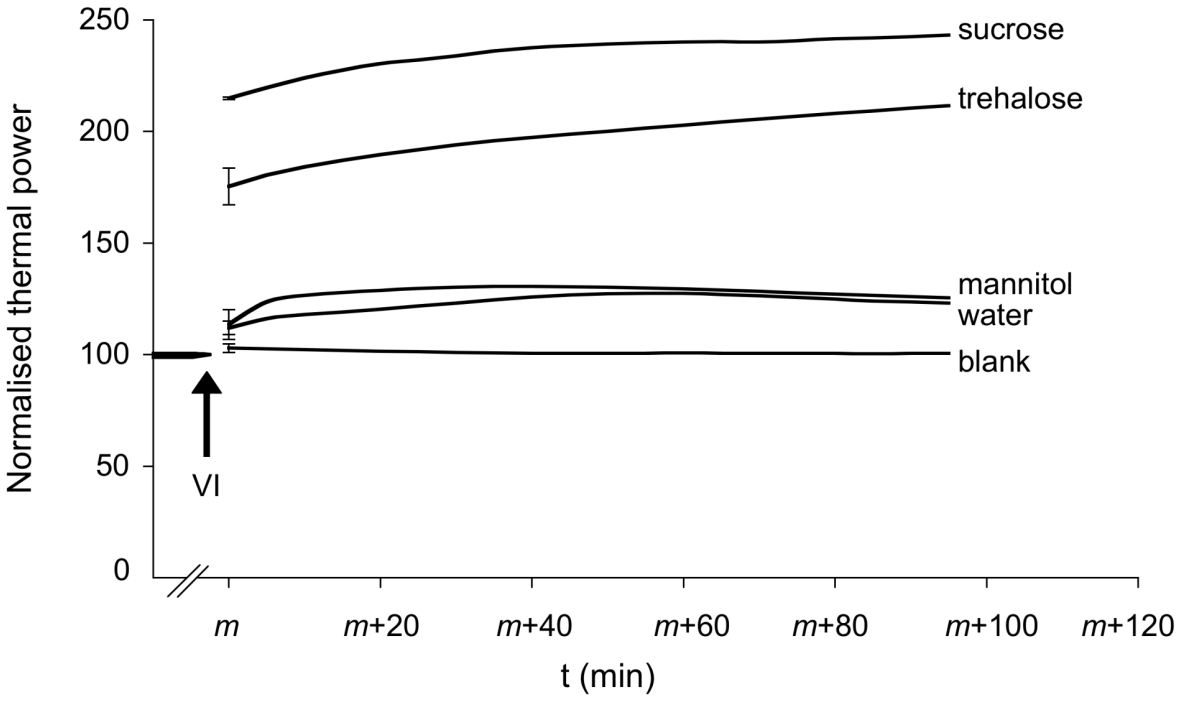

Figure 6. Calorimetric metabolic heat rate measurements of spinach samples subjected to VI. Spinach was impregnated with sucrose solution (13%), trehalose solution (11%), mannitol solution (8%), water or no solution (blank). Average curves from three replicates are shown. The variable *m* (min) in the x-scale is defined by $m = t_1 + t_2 + t_3$, where t_1 is the duration of the initial disturbance of the calorimetric measurement; t_2 is the time for the thermal power to stabilise before the application of vacuum; t_3 is the duration of the disturbance provoked by VI. For each heat production rate curve, within the time interval described by the variable *m*, the initial stable thermal power value normalised to 100 is reported. For each curve is reported the confidence limit (SEM, n=3) of the first heat rate value measured after VI.

Figure 6 shows that impregnation with sucrose and trehalose caused a dramatic increase in the thermal power values with respect to the heat rate before the application of vacuum (indicated with an arrow). The impregnation with both sugars led to a further slow increase in the heat rate during the time of the measurement. The measurement done with a sample subjected to vacuum and atmospheric pressure restoration without the presence of solution (blank, Figure 6) showed no increase of the heat production. By impregnating spinach samples with an isotonic solution of mannitol, a polyol that cannot be metabolized by plant cells (Trip *et al.,* 1964), a slight increase of the heat rate was recorded (Figure 6) and no further increase of the heat rate during the time of the measurement was observed. A comparable metabolic response was recorded by impregnating the sample with water.

Effect of metabolic inhibitors

The effect of impregnating spinach sample with both sucrose and trehalose in combination with KCN (an inhibitor of the cytochrome pathway of mitochondrial electron transport) and SHAM (an inhibitor of the alternative pathway of electron transport in mitochondria) on the metabolic activity of spinach is shown in the example reported in Figure 7. After VI, the recorded thermal power values were close to the baseline of the calorimeter indicating a strong suppression of the metabolic activity.

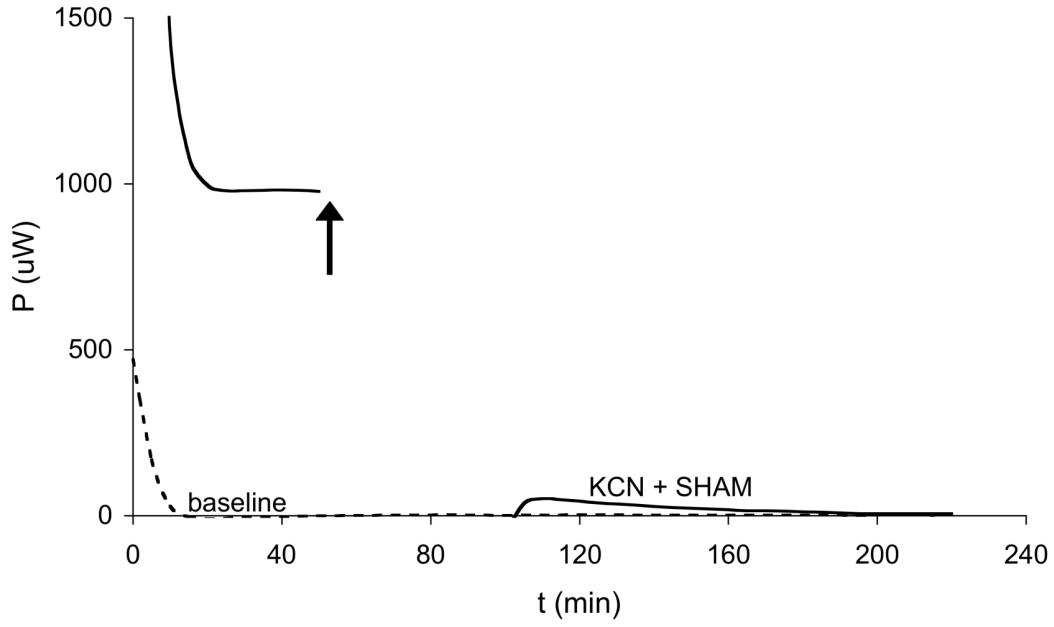

Figure 7. Typical calorimeter output (μW) from spinach tissue subjected to VI with sucrose or trehalose mixed with metabolic inhibitors, as described in the Materials and Methods section (continuous line). VI was applied (the time of VI application is indicated with an arrow in the continuous line). Application of vacuum provoked a second disturbance where the recorded thermal power values were first outside the detectable range for about 50 min (gap of values in the continuous line) and, once back within the detectable range, the disturbance in the calorimetric measurements lasted 20 more min before the real thermal power from the impregnated sample was recorded, which was close to the baseline of the calorimeter (dashed line).

3.3 Impregnated samples show photosynthetic activity

Figure 8a shows the O_2 evolution at saturating light for untreated, sucrose, trehalose and mannitol impregnated samples. Untreated spinach leaves showed the highest photosynthesis. The photosynthetic activity of leaves impregnated with sucrose was significantly lower than the activity of leaves impregnated with mannitol. Leaves impregnated with trehalose displayed a value similar to sucrose impregnation, but not significantly different from either sucrose or mannitol impregnated leaves. Figure 8b shows a negative correlation between photosynthesis values and the first normalised thermal power values measured after VI for untreated, mannitol, sucrose and trehalose impregnated spinach.

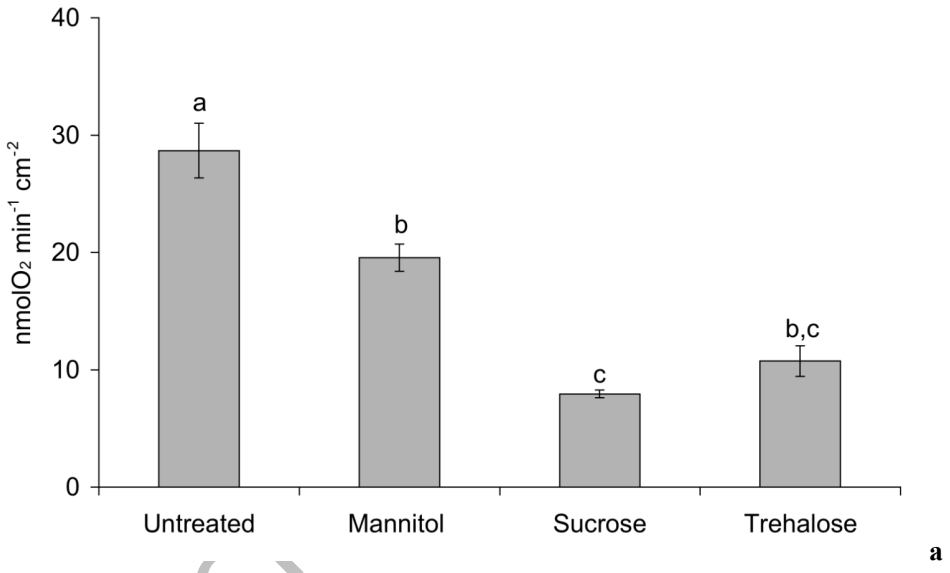

a

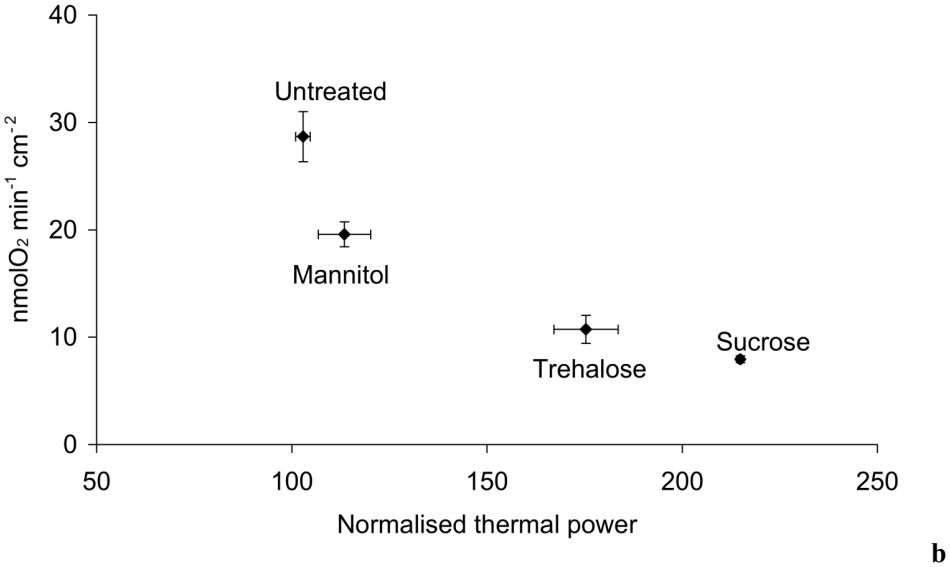

b

Figure 8. **a** Photosynthesis measurements in untreated, mannitol, sucrose and trehalose impregnated spinach. Average and SEM from at least three replicates is reported. Different letters indicate statistical differences (p

< 0.05); **b** Correlation between photosynthesis measurements ($molO_2\ min^{-1}\ cm^{-2}$) and normalised thermal power for untreated, mannitol, sucrose and trehalose impregnated spinach.

4. Discussion

A deeper understanding of the consequences of VI on the metabolism of impregnated plant tissues is a key element for product development, as the product shelf-life is strongly dependent on the tissue metabolic activity. A more active metabolism will induce a faster deterioration of the product, involving loss of acids, sugars and other components which contribute to flavour quality and nutritional value (Cantwell & Suslow, 2002). On the other hand, the addition of a carbohydrate to the leaf interior by VI may compensate for such a loss, so the final effect may depend on the relative magnitude of the treatment and the metabolic effect.

In this study, calorimetric measurements provided evidence of a drastic increase of spinach leaf gross metabolism as a consequence of impregnation with trehalose and sucrose isotonic solutions (Figure 7). The metabolic heat rate of untreated spinach leaves slowly and slightly decreased (Figure 5), possibly upon changes on the rate of respiratory substrate mobilisation or upon either down-regulation or damage of the respiratory pathways (McCutchan & Monson, 2001). However, since the leaves were exposed to light before the calorimetric measurement, a late phase of light-enhanced dark respiration might contribute in decreasing the leaf metabolic activity (Padmasree et al., 2002). With the application of VI, extracellular air is replaced by the impregnation solution, potentially limiting tissue respiration to any remaining volume of air in the tissue. However the fact that the impregnated leaves show photosynthetic activity (Figure 8) strongly suggests that not all air was exhausted during VI. Therefore, in a separate experiment, KCN and SHAM were impregnated together with the sugars (Figure 7). The results clearly demonstrate that the metabolic response responsible for the drastic increase in gross metabolism upon VI depends on the mitochondrial oxygen consuming pathways. Interestingly, the metabolic effect involving mannitol was less pronounced and comparable with water impregnation, suggesting that the strong metabolic effect here reported might be influenced by sugars that can be metabolized by the cells. The inhibition of photosynthesis by sucrose is consistent with Foyer *et al.* (1983) where sucrose strongly decreased CO_2 fixation in protoplast from spinach.

It has been demonstrated that exogenously administrated sucrose to *Urtica dioica* leaves was taken up and metabolized by cells (Möller & Beck, 1992). Further, the respiration in spinach leaves is enhanced by both the exogenous administration of sucrose and by light-induced elevations in endogenous carbohydrate status (Noguchi & Terashima, 1997; Azcon-Bieto *et al.*, 1983). As suggested by Voitsekhovskaya *et al*. (2002), sucrose molecules loaded into the apoplast, can be co-transported with protons into the symplast, leading to the decrease of the membrane potential. Thus, the plasma membrane ATPase is stimulated to pump protons into the apoplast. Proton pumping consumes ATP and, by increasing the ADP symplatic concentration, the respiration consequently increases.

Impregnated trehalose, provoking a drastic increase in the gross metabolic activity of spinach, also suggests the possibility of its uptake and metabolization by the cells. Trehalose and trehalose-6-phosphate (T6P) play a central role in the coordination of the metabolism in plants. Paul *et al.* (2008) reported a possible regulatory function of trehalose and T6P on the size of the cellular pool of uridine diphosphoglucose (UDPG) and hexose phosphates, *i.e.* glucose-1-phosphate (G1P), glucose-6-phosphate (G6P) and fructose-6-phosphate (F6P). UDPG and G6P are two central molecules from which all other cellular functions can be ultimately derived, including glycolysis and respiration. A possible role of trehalose on plant metabolism was also shown by Müller *et al.* (1998), reporting that the invertase activity and sucrose catabolism were stimulated in soybean seedlings either grown in the presence of trehalose or inoculated with a symbiotic microrganism producing trehalose.

The complex layered tissue morphology and the extensive intercellular space of spinach (Warmbrodt & Van Der Woude, 1990) might suggest possible leaf volume changes during VI, *e.g.* leaf expansion during vacuum formation and volume recompression during atmospheric pressure restoration. During the two phases of VI, tissue volume deformation might imply an accumulation of mechanical stress in the cell-cell bonding zones and the subsequent stress relaxation through either volume recovery or rupture response (Chiralt & Fito, 2003). Knight *et al.* (1991) showed that tissue mechanical deformation might increase intracellular calcium concentration. Calcium is a dynamic signalling molecule, which acts to transduce numerous signals in plant tissues (Trewavas & Knight, 1994) and calcium signalling might trigger a more rapid oxygen consumption (Manzoor *et al.*, 2012). The slight increase of spinach heat rate consequent to impregnation with either water or mannitol isotonic solution might possibly be related to calcium signalling promoted by tissue deformation occurring during VI treatment. Mechanical signalling related to the tissue deformation may also contribute to the metabolic response detected upon impregnation with sucrose and trehalose solutions.

5. Concluding remarks

This study, exploring metabolic responses of spinach tissue upon the application of VI, presented important findings. The following remarks underline the main results:

(1) The short-term metabolic response of spinach tissue to the application of VI involves mitochondrial oxygen consuming pathways;

(2) The increase of spinach metabolism upon VI is related to the impregnated molecule. Metabolizable molecules (*e.g.* sucrose, trehalose) seem the main stimulants of metabolic activity. The direct effects of the mechanical treatment instead appear quite low;

(3) Impregnation appear to reach a maximum with remaining gas-filled compartments.

This study shows that calorimetry is a simple and powerful method to provide information on metabolic responses provoked by unit operations such as VI, which drastically changes tissue properties.

Acknowledgments The authors would like to thank the company 'Norrvidinge Boställe AB', Kävlinge, Sweden for providing the raw material. V. Panarese acknowledges the Marco Polo Programme, Italy, EU, that financially supported this research. F Gómez Galindo acknowledges financial support from The Swedish Research Council for Environment, Agricultural Sciences and Spatial Planning, FORMAS and the European Community's Seventh Framework Programme (FP7/2007-2013) under grant agreement no. 245280, also known as PRESERF.

References

Azcon-Bieto, J., Lambers, H. & Day, D. A. (1983) Effect of photosynthesis and carbohydrate status on respiratory rates and the involvement of the alternative pathway in leaf respiration. Plant Physiology, 72: 598-603

Bae, H., Herman, E., Bailey, B., Bae, H.-J. and Sicher, R. (2005), Exogenous trehalose alters Arabidopsis transcripts involved in cell wall modification, abiotic stress, nitrogen metabolism, and plant defense. Physiologia Plantarum, 125: 114–126.

Barrera, C., Betoret, N., Corell, P., & Fito, P. (2009). Effect of osmotic dehydration on the stabilization of calcium-fortified apple slices (var. Granny Smith): Influence of operating variables on process kinetics and compositional changes. Journal of Food Engineering, 92, 416–424.

Cantwell M. & Suslow T. Postharvest handling systems: minimally processed fruits and vegetables. A.K. Kader (Ed.), Postharvest Technology of Horticultural Crops (3rd ed.), Univ. California (2002), pp. 445–463 Special Publ. 3311, Chapter 32.

Carciofi, B. A. M., Prat, M., Laurindo, J. B. (2012) Dynamics of vacuum impregnation of apples: Experimental data and simulation results using a VOF model. Journal of Food Engineering 113: 337 - 343.

Castelló, M.L., P.J. Fito, A. Chiralt, Changes in respiration rate and physical properties of strawberries due to osmotic dehydration and storage, Journal of Food Engineering, Volume 97, Issue 1, March 2010, Pages 64-71

Chiralt, A., & Fito, P. (2003). Transport mechanisms in osmotic dehydration: The role of the structure. *Food Science and Technology International,* 9, 179–186.

Criddle R.S., Breindenbach R.W., Hansen L.D. (1991) Plant calorimetry: How to quantitatively compare apples and oranges, Thermochim. Acta 193, 67-90.

DELIEU, T. and WALKER, D. A. (1981), POLAROGRAPHIC MEASUREMENT OF PHOTOSYNTHETIC OXYGEN EVOLUTION BY LEAF DISCS. New Phytologist, 89: 165–178.

Fito, P., & Pastor, R. (1994). Non-diffusional mechanisms occurring during vacuum osmotic dehydration. Journal of Food Engineering, 21, 513-519.

Foyer, CH, Rowell, J & Walker, D (1983). The effect of sucrose on the rate of de novo sucrose biosynthesis in leaf protoplasts from spinach, wheat and barley. Arch. Biochem. Biophys. 220: 232-238.

Francis GA, Gallone A, Nychas GJ, Sofos JN, Colelli G, Amodio ML, Spano G (2012) .Factors affecting quality and safety of fresh-cut produce. Crit Rev Food Sci Nutr. 52:595-610.

Glazer, B T., Adam G. Marsh, Kevin Stierhoff, George W. Luther III, The dynamic response of optical oxygen sensors and voltammetric electrodes to temporal changes in dissolved oxygen concentrations, Analytica Chimica Acta, Volume 518, Issues 1–2, 2 August 2004, Pages 93-100.

Gómez Galindo, F., Wadsö, L., Vicente, A. A., Dejmek, P. (2008) Exploring metabolic responses of potato tissue induced by electric pulses, Food Biophysics, 3: 352–360.

Gras, M. L., Vidal, D., Betoret, N., Chiralt, A., & Fito, P. (2003). Calcium fortification of vegetables by vacuum impregnation. Interactions with cellular matrix. Journal of Food Engineering, 56, 279–284.

Guillemin, A., Guillon, F., Degraeve, P., Rondeau, C., Devaux, M., Huber, F., et al. (2008). Firming of fruit tissues by vacuuminfusion of pectin methylesterase: visualisation of enzyme action. Food Chemistry, 109, 368–378.

Jifon JL, Syvertsen JP. Moderate shade can increase net gas exchange and reduce photoinhibition in citrus leaves. Tree Physiol. 2003 Feb;23(2):119-27.

Knight MR, Campbell AK, Smith SM, Trewavas A. J. (1991) Transgenic plant aequorin reports the effects of touch and cold-shock and elicitors on cytoplasmic calcium. Nature, 352: 524-6.

Laurindo, J.B., Stringari, G.B., Paes, S.S. and Carciofi, B.A.M. (2007), Experimental Determination of the Dynamics of Vacuum Impregnation of Apples. Journal of Food Science, 72: 470–475.

Lozano, J. E., Rotstein, E., & Urbicain, M. J. (1980). Total porosity and open-pore porosity in the drying of fruits. Journal of Food Science, 45, 1403–1407.

McCutchan, C. L. and Monson, R. K. (2001), Night-time respiration rate and leaf carbohydrate concentrations are not coupled in two alpine perennial species. New Phytologist, 149: 419–430. doi: 10.1046/j.1469-8137.2001.00039.x

Manzoor H, Chiltz A, Madani S, Vatsa P, Schoefs B, Pugin A, Garcia-Brugger A (2012) Calcium signatures and signaling in cytosol and organelles of tobacco cells induced by plant defense elicitors. Cell Calcium, 51: 434-444.

Mujica-Paz, H., Valdez-Fragoso, A., Lopez-Maolo, A., Palou, E., & Welti-Chanes, J. (2003). Impregnation and osmotic dehydration of some fruits: effect of the vacuum pressure and syrup concentration. Journal of Food Engineering, 57,305-314.

Möller I, Beck E (1992) The fate of apoplastic sucrose in sink and source leaves of *Urtica dioica*. Physiologia Plantarum 85 : 1399-3054

Müller, J., Thomas Boller, Andres Wiemken, Trehalose affects sucrose synthase and invertase activities in soybean (Glycine max [L.] Merr.) roots, Journal of Plant Physiology, Volume 153, Issues 1–2.

Noguchi Ko, Terashima Ichiro (1997) Different regulation of leaf respiration between Spinacia oleracea, a sun species, and Alocasia odora, a shade species. Physiologia Plantarum 101: 1399-3054.

Panarese V, Dejmek P, Rocculi P, & Gómez Galindo F (2013) Microscopic study providing insight into the mechanisms of mass transfer phenomena in vacuum impregnation. *Innovative Food Science and Emerging Technologies*, http://dx.doi.org/10.1016/j.ifset.2013.01.008.

Paul M. J., Primavesi L F, Jhurreea D & Zhang Y (2008) Trehalose Metabolism and Signaling. *Annual Review of Plant Biology*, 59: 417-441

Phoon, P. Y., Gómez, G. F., Vicente, A., & Dejmek, P. (2008). Pulsed electric field in combination with vacuum impregnation with trehalose improves the freezing tolerance of spinach leaves. Journal of Food Engineering, 88, 144–148.

Padmasree K., Padmavathi L., & Raghavendra A.S. (2002) Essentiality of Mitochondrial Oxidative Metabolism for Photosynthesis: Optimization of Carbon Assimilation and Protection Against Photoinhibition. Critical Reviews in Biochemistry and Molecular Biology, 37:71–119.

Silva Paes, S., Stringari, G. B. & Laurindo, J. B. (2006) Effect of vacuum impregnation-dehydration on the mechanical properties of Apples. Drying Technology 24:1649 - 1656.

Trewavas, A., & Knight, M. (1994) Mechanical signalling, calcium and plant form. *Plant Molecular Biology*, 26: 1329-1341.

Tylewicz, U Romani, S Widell, S Gómez Galindo, F (2011) Induction of Vesicle Formation by Exposing Apple Tissue to Vacuum Impregnation Food and Bioprocess Technology In press.

Voitsekhovskaya, O.V. Heber, U. Wiese, C. Lohaus, G. Heldt, H.-W. Gamalei, Yu.V. (2002) Energized Uptake of Sugars from the Apoplast of Leaves: A Study of Some Plants Possessing Different Minor Vein Anatomy. Russian Journal of Plant Physiology, 49: 1021-4437

Walker DA (1987) The use of the oxygen electrode and fluorescence probes in simple measurements of photosynthesis. pp 1-145 Oxygraphics Limited, Sheffield,U.K.

Warmbrodt R. D. and Van Der Woude W.J. Leaf of *spinacia oleracea* (spinach): ultrastructure, and plasmodesmatal distribution and frequency, in relation to sieve-tube loading' Amer. J. Bot. 77(10): 1361-1377. 1990.